GEOINFORMATICS IN EVALUATING MORPHOTECTONICS OF INDO-BURMAN FRONTAL FOLD BELT

A THESIS

Submitted in partial fulfilment of the requirements for the award of the degree of

DOCTOR OF PHILOSOPHY

in

EARTH SCIENCES

by

YAZDANA SHUJAT

DEPARTMENT OF EARTH SCIENCES
INDIAN INSTITUTE OF TECHNOLOGY ROORKEE
ROORKEE-247 667 (INDIA)

JULY, 2011

INDIAN INSTITUTE OF TECHNOLOGY ROORKEE

CANDIDATE'S DECLARATION

I hereby certify that the work which is being presented in the thesis entitled **GEOINFORMATICS IN EVALUATING MORPHOTECTONICS OF INDO-BURMAN FRONTAL FOLD BELT**, in partial fulfilment of the requirements for the award of the degree of Doctor of Philosophy and submitted in the Department of Earth Sciences of the Indian Institute of Technology Roorkee, Roorkee is an authentic record of my own work carried out during a period from January 2008 to June 2011 under the supervision of Dr. Arun K. Saraf, Professor, Department of Earth Sciences, and Dr. Josodhir Das, Scientific Officer, Department of Earthquake Engineering, Indian Institute of Technology Roorkee, Roorkee.

The matter presented in this thesis has not been submitted by me for the award of any other degree of this or any other Institute.

Yazdana Shujat

(YAZDANA SHUJAT)

This is to certify that the above statement made by the candidate is correct to the best of our knowledge.

(Josodhir Das)
Supervisor

(Arun K. Saraf)
Supervisor

Date: 04/07/11

The Ph.D. Viva-Voce Examination of **Yazdana Shujat**, Research Scholar, has been held on 15th Oct 2011

Signature of Supervisors

Jayant Kumar Pati

Signature of External Examiner

ABSTRACT

Morphotectonics combines topography and tectonic activity to explain landforms and allows studying the direct effect of earth movements on landform evolution. A valuable means in evaluating the morphotectonics of a region is to characterize the assemblage of landforms present. Concerned landforms are those produced by tectonic processes, such as faulting, folding, tilting, uplift, or subsidence. The earth's land surface exists in a sensitive balance between tectonic and erosional forces. Wherever the tectonic uplift and deformation are absent, erosional processes often predominate. After a sufficiently long period of time, the result is a subdued landscape with low elevation and modest relief. If uplift and deformation predominate over erosion then there is increase in elevation and relief. This competition between the tectonic processes liable to built up the topography and surface processes shredding them is easily manifested by the morphometric indices.

A small part of the earth's surface falling in northeastern India and partly in Bangladesh represents unique rock deformations in the form of westerly convexing north-south oriented alternating anticlines and synclines. This fold belt is the outcome of E-W oriented compressional tectonic forces that prevailed in the region during the eastward subduction of the Indian plate beneath the Burmese plate and still experiencing tectonic events. Owing to such process the westerly laying sedimentary wedge got deformed into such folded features and now represents fold-and-thrust belt. Intensity of folding gradually increases eastward in the Tertiary sedimentary sequence (sandstones and shales). These folds are also affected by several longitudinal and transverse faulting. Considering the tectonic significance of the region morphotectonic study of frontal part of Indo-Burman fold belt, northeast India encompassing Surma Basin has been attempted employing geoinformatics comprising mainly integrated approach of Remote Sensing-GIS and digital elevation modeling to bring out for the first time the pertaining morphotectonic characteristics.

The objective of the present research work is to derive morphotectonic parameters by fold geometry analysis towards understanding the complexity of fold pattern and associated faulting and thrusting, detection of drainage anomalies, change detection analysis and estimation of several morphometric indices.

Remote sensing and GIS techniques provide information of landforms and surface geological structures convincingly and efficiently. Satellite images acquired by Indian Remote Sensing Satellite (e.g. LISS-III, PAN) and Landsat-MSS, TM, ETM+, PAN provided very important information with regard to the several deformational features present in the study area. Digital elevation models (DEMs) proven to be a significant platform in morphological and tectonics studies. DEMs can also be used for identification of tectonic features such as faults, folds easily besides satellite images. All the processing steps were carried out using ArcGIS-9.3 and ERDAS-Imagine-9.3 software packages.

Since DEMs were used intensively, DEMs of the Bhuban anticlinal hills of the study area have been generated from topographic maps (named Contour-DEM) with contour interval of 20m and Cartosat-1 stereo orthokit images (named Cartosat-DEM) forming an important component of the thesis. As DEM accuracy and quality are two major requirements for their applicability therefore, these generated DEMs have been analyzed for accuracy and compared with the available SRTM-DEM and ASTER-DEMs. Both vertical and horizontal accuracies have been calculated, along with topographic and drainage derivatives. A detailed comparative analysis has been carried out for all the DEMs. Cartosat-DEM emerged as the most reliable DEM and show least horizontal and vertical discrepancies. Cartosat-DEM also shows greater details about the topographic and drainage parameters. Based on overall analysis it could be assessed that for regional studies low resolution SRTM-DEM can be used but for the drainage analysis and hydrological studies high resolution Cartosat-DEM is more preferable.

Satellite images and DEMs are capable of displaying prominently the geometry and morphology of the folds especially when these have large spatial extent. Frontal part of the Indo-Burman fold belt falling in parts of Bangladesh and Northeast India have developed into exemplary linear N-S oriented doubly plunging folds in Late-Tertiary

sedimentary rock sequences and are arranged in a set of alternating ridge forming anticlines and valley forming synclines. Fold types present in the area although appear to be simple but the existing fold geometrical arrangement reveal some interesting features. Digital processing of satellite images and DEMs enhancement were performed to understand better the geometry and morphology of the folds covering considerably large area. Morphotectonic information gathered in this study are: identification of multi-folds within the visibly single entity; fold overlapping nature and interrelation between the anticlines; geometry of fold noses; fault affected fold limbs causing bulging; anticline bifurcation and formation of elliptical and cuspate synclines, effect of deformation and faulting etc. Derived morphometric parameters are: drainage basin symmetry, basin elongation ratio, river sinuosity, stream length gradient index (SL-Index), slope gradient index (S-Index) and hypsometric integral (I_{hyp}).

It has been observed that the Bhuban anticlinal hills represent highly deformed and deviated topography from a normal anticline. This N-S trending curved ridge displays very steep scarp on the western side and gentle slope on the east and is affected by several transverse and longitudinal faults. This anticlinal hill has been identified as typical example of fault propagation folding. Different morphotectonic units (six in number) have been identified which are marked by the transverse faults. The northern segment comprising three morphotectonic units (MU1 to MU3) is unique in the sense that this part exhibits effect of both the longitudinal and transverse faulting, uplifted narrow ridge with downthrown eastern side (MU2). Fourth morphotectonic unit MU4 shows normal anticlinal topography with the upliftment. The fifth morphotectonic unit (MU5) is subsided part and bounded by transverse faults TF3 and TF4, whereas, the sixth unit (MU6) exhibit bulging effect as this part experienced differential fault movements. Stream profiles, longitudinal and transverse topographic profiles extracted from various DEMs also seems to support the topographic variations and deformation of the Bhuban Hills.

Rivers are sensitive to intensity of tectonic deformation, adjusting over different periods of time depending on the physical properties of the host rocks, climatic effects and tectonic activity. Thus, the drainage system of a region records the evolution of tectonic deformation. Barak is the major river of the study area and is highly meandering

and changed its course with time at various places along with anomalous behavior at some places. Change detection analysis of Barak, Kushiara river and Surma rivers have been carried out using satellite images and topographic maps of different years spanning from 1955 to 2000. Major tributaries of Barak river have also been investigated for their responses to active tectonics. It has been observed that majority of them are active rivers and shows various meandering loops and also crossing various faulted anticlines through the wind gaps.

The western most part of Tripura (India) region adjoining to Bangladesh has been investigated in the light of its geomorphological characteristics. Quantitative parameters such as stream sinuosity, drainage basin asymmetry, basin elongation ratio have been computed. Main rivers of this part, namely the Gomti and Khowai follows extremely meandering path and crosses through the transversely faulted anticlinal ridges. Fluvial anomalies viz. shift in stream channel and the abandoned meandering loops have been inferred and mapped. Development of drainage system towards north and south from the drainage divide along the latitude $23^{\circ}45'$N indicated up arching of the region which is also corroborated by the extracted topographic profiles. Derived morphometric parameters of Agartala slope and adjoining synclines remained useful to understand the nature of topographical modification attributed to the possible tectonic activity.

A detailed morphometric study of the Lengpui region has also been carried out to understand the morphotectonics. This area lies near Aizwal in the central part of the Indo-Burman frontal fold belt. This area is marked by anomalous topographic expressions which are manifested through several gently sloping large surfaces. Dhaleshwari river is the major stream of the area and is highly active and shows intense down cutting, resulting into a deep V-shape valley also revealed by topographic profiles. Drainage basins show deviation from the normal concave morphometry and slopes are flatter with a tilting which indicate that area is under tectonic influence. Computed morphometric indices also corroborate the above facts.

ACKNOWLEDGEMENT

I bow in reverence to almighty Allah the most merciful who showered his gracious blessings upon me. Showed me the path of righteousness and enable me to achieve this target.

I feel privileged in expressing profound sense of gratitude and indebtedness to my supervisors, **Prof. Arun Kumar Saraf** and **Dr. Josodhir Das** for their generous and keenwitted guidance, incessant encouragement, constructive criticism, excellent supervision that enabled me to complete my work successfully. It has been an honor to be their student. I appreciate all their contributions of time, ideas to make my PhD experience productive and stimulating. The joy and enthusiasm they have for their research was contagious and motivational for me, even during tough times in the PhD pursuit. I am also thankful to them for their friendly behavior during my stay. I will always be thankful to them for supporting me in every front and indeed I am very happy to have such supportive supervisors. I really appreciate their patience for answering my all queries which I have encountered during my thesis. It is my pleasure to express my gratitude wholeheartedly to the families of my supervisor.

I take an opportunity to offer my sincere thanks to the Heads of the Department of Earth Sciences, IIT Roorkee, during the tenure of my research, namely: Dr. R. P. Gupta and Dr. P. K. Gupta for extending the necessary help and facilities whenever I needed during my work.

I wish to sincerely acknowledge the critical financial support by the Ministry of Human Resource Development (MHRD), Council of Scientific and Industrial Research (CSIR), Govt. of India, without which it would have become difficult to take up and complete this research.

I would also like to thank my seniors and lab-mates **Vineeta Rawat**, **Kanika Sharma**, and **Riyaz Mir** for their friendly behavior and for maintaining the academic environment during my stay, without which it could not have been possible to attain the desired results.

I am thankful to the members of the non-teaching staff at the Department of Earth Sciences, IIT Roorkee, especially **Nair ji**, **Rakesh ji** and **Saini ji** for their open-hearted support and administrative help during the course of stay at Roorkee. A special place

holds for **Rahil ji**. His constant round the clock lab support and our tea-breaks will always be part of my fond memories.

I also thank my friends **Archana, Talat, Neha, Shivangi, Rashmi, Neshat, Saima** and **Nahid** for their love, affection and concern toward me. They definitely make my stay in Roorkee memorable.

Words fail to express appreciation to my parents who have taken painstaking efforts to bring me up this level. I solemnly place off all the credit of this work for them. I would also like to thank my sisters **Faiza, Afshan, Aghna**, and brother **Khizar** for their belief, support and love which has been always with me. They deserve special mention for their inseparable support and prayers. Special thanks to my husband **Fishan Ur Rehman** who always remain a source of inspiration and provide me emotional and mental support during the difficult situations. I also thank my in-laws who have helped and support me during my work.

Finally, I would like to thank everybody who was important to the successful realization of thesis as well as expressing my apology that I could not mention personally one by one.

YAZDANA SHUJAT

CONTENTS

LIST OF FIGURES

LIST OF TABLES

CHAPTER-I

Introduction

1.1 Preamble

Morphotectonics refers to the study of short and long-term surficial evidences of tectonic activity. The surface manifestation of endogenous mechanism resulting out of the tectonic activity is always represented by relative movements such as uplifting, subsidence and translation of the parts of the crust. Continuous processes of weathering and erosion leads to formation of landforms manifesting the control of tectonics. Morphotectonics combines geometry and tectonic activity to explain landforms mainly at continental, sub-continental as well as local scales, whereas structural geomorphology considers the passive influence of geologic structure on landforms. Morphotectonics bring out the impact of earth movements on landform evolution. It includes the study of origin of mountains, erosion surfaces, drainage patterns, and sediments on land and offshore. The contrast between active and passive plate margins is one way to subdivide the study of morphotectonics. Along many active margins, plates converge, leading to subduction, uplift, and formation of mountains such as the Indo-Burman fold belt, Himalayas and Andes. Such existing and newly developed morphotectonic features can be examined by employing geoinformatics comprising topographic maps, multi-sensor and multi-date remotely sensed data, digital elevation models (DEMs), GIS and advanced digital image processing techniques.

The orogenic (mountain-building) processes such as thrusting and folding of rocks are very different from the vertical uplift that provides the elevation for erosional development of mountains. When large areas are uplifted high enough, plateaus or mountains are formed; for example, Shillong Plateau (Northeast India) which has been

block uplifted to its present height and the Himalayas, Indo-Burman fold belt and Andes, appear to have formed by folding and thrusting followed by intense erosion during the latter half of the Tertiary. Vertical uplift and warping of large areas are also features of the Himalayas, demonstrated by convex river terraces along the major rivers. The fact that the same major rivers rise on the Tibetan Plateau and flow through the highest mountain range on Earth is important morphotectonic evidence that the rivers existed before uplift of the Himalayas and may reach or pass the warp axis. Exotic terrains have important morphotectonic implications, because they bring together continental fragments that have very different geomorphic histories. Morphotectonics can make an important contribution to theories of continental evolution by placing constraints of age and processes on models developed using geology and geophysics.

In areas where rate of present day tectonism is considerable, several field indications can be directly observed. However, in other cases where rate of tectonism is mild or very slow, evidences mainly comes from morphotectonic investigations based on morphometric indices. Streams and drainages are able to record even minor tectonic deformation. Tectonic activities are often manifested by characteristic geomorphological features such as linear valleys, ridgelines, erosional surfaces, slope-breaks, regional anisotropy and tilt of terrain. Analysis of digital elevation models, by means of numerical geomorphology, provides a means for recognizing fractures and faults and characterizing the tectonics of an area in a quantitative way. Morphometric parameters like drainage basin asymmetry, River sinuosity, bifurcation ratio, hypsometry, slope gradient index, stream length gradient index etc. are key indicators of neotectonic activities prevailing in a region.

During the past few decades, the development of new techniques for determining the ages of landscape features for assessing the mechanisms and rates of geomorphic processes, and for determining rates of crustal movements, has helped revitalize the field of morphotectonics. It is now possible to quantify how rapidly a given site is deforming with respect to another and how those rates of relative convergence or divergence are partitioned among various faults and folds. Similarly it is now possible to quantify how rapidly rivers and glaciers are incising into bedrock and the rate at which landslides are

stripping mountain slopes. Geoinformatics can serve the above purposes efficiently. Satellite imageries of successive years can provide the overview of the deformational changes occurred in the region. Clearly, the merger of such data sets can underpin a new understanding of the balance between the rates at which crustal material is added at a given site and the rates at which this material is eroded away. Defining this balance and interpreting the landscape that results from this competition represents a major component of modern morphotectonic studies.

Indo-Burman fold belt especially the frontal part which has been subjected to folding and faulting and other geomorphological modifications resulted mainly due to the plate tectonic activities serves as an important area for the study of various geomorphological signatures. Incidentally, the region is presently supposed to be undergoing slow deformation processes as the east-west compressional tectonics are accommodated by translational tectonic movements occurring east of Indo-Burman fold belt. In this research work detailed analyses on morphotectonics and morphometry of the frontal Indo-Burman fold belt has been brought out mainly based on Remote sensing and GIS techniques. These techniques have been tested in various regions of the world for morphotectonic analysis but no such work has been attempted for the frontal Indo-Burman fold belt earlier to this work. The significant contribution of this thesis comprises the use of advanced different remote sensing datasets, methodologies, and GIS technique for understanding and carrying out quantitative analysis of various tectonically deformed landforms. The present thesis also provides a regional as well as detailed morphotectonic overview of the region.

1.2 Concept of morphotectonic analysis

In morphotectonic study the relationship between geomorphology and tectonics is fundamental to the understanding of landscape evolution. Stressing, mainly the interpretation of various surface expressions of associated tectonic features. These observations compare the morphological structure of geomorphic markers, drainage systems, river courses, glacial forms, volcanic landscapes and mass movements with joint orientations and fault movements. The latter are indicative of the neo-tectonic stresses, and thus inferences on the genesis of the morphological forms can be drawn.

Remote sensing can be very effective tool in estimation of various morphotectonic parameters. Satellite images provide a synoptic view and capable of generating information regarding the areas which are inaccessible and unreachable for the field investigations due to topographic factors, climatic factors or due to presence of dense vegetation. Availability of high resolution satellite images exhibiting even different minor features distinctly provide opportunity to look into details of occurred modification if any. Remote sensing data products can be easily interpreted on the basis of photographic elements (tone, texture, pattern, shape, size etc.) and geotechnical elements (vegetation, land use, land cover, drainage etc.). Change detection studies can also be done by analyzing data of various successive years. Remote sensing provides us the data product and GIS techniques make it workable. Thus, these two techniques are complementary for each other. Various maps like geological, geomorphological, structural, drainage etc. can be easily prepared by GIS for morphotectonic evaluation of any region. GIS technology is digital as well as spatial, that means all the information have geographic (latitude-longitude) information. Modern GIS have a unique capability of 'Overlay Analysis' by superimposing various layers in a single map. This is very helpful in comparative studies and in analyzing the impact of one parameter on another. For example river morphology and drainage are very sensitive to neo-tectonic activities, and both can be easily traced by remote sensing and GIS approach.

Successful studies of morphotectonics of any region require blending of appropriate data from various specialized disciplines like structural geology, stratigraphy, geomorphology etc. Geomorphic landforms can be studied to track phases of deformation suffered by a region. Faulting and folding can subsequently deform such markers. Documentation of any departure from their unperturbed shape can serve to define the magnitude of deformation. On the basis of all these parameters using Remote Sensing and GIS techniques in combination with ground checks final inferences about any region can be made, whether it is highly active, moderately active or stable. This information can be used as a base for further analysis of that area, and its proneness to various hazards associated with tectonic movements. A conceptual model depicting tectonic setup along with geomorphological processes and various parameters is shown in figure 1.1.

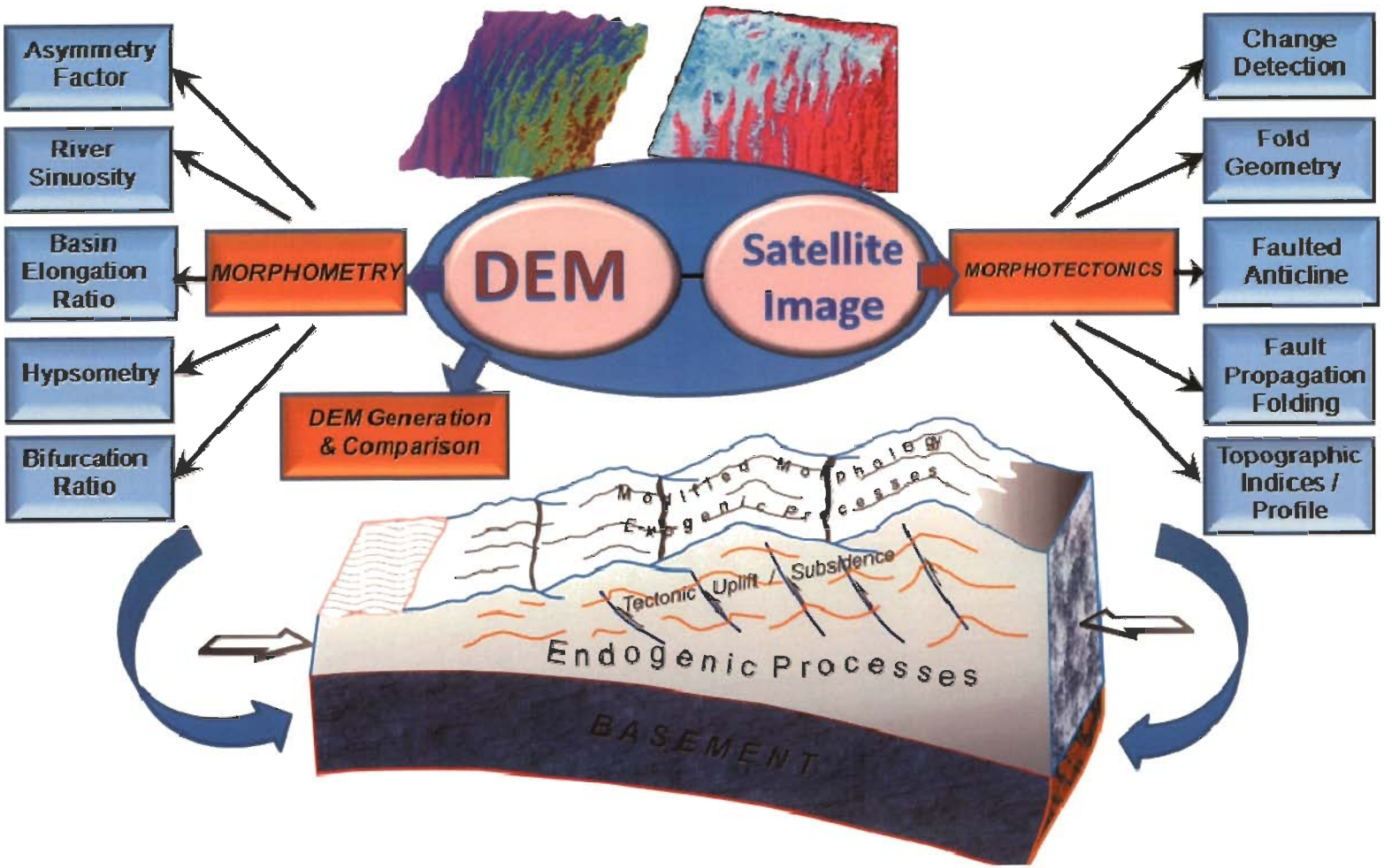

Figure 1.1 Conceptual schematic for a tectonically affected fold belt region and its morphotectonic and morphometrical studies based on satellite images and DEMs.

1.3 Objectives

Remote sensing and GIS techniques have immense importance in understanding the deformation caused by various tectonic processes. Morphotectonic including morphometric analysis of any region is a multidisciplinary approach. The present study employs advanced spatial techniques for morphotectonic study of Indo-Burman frontal fold belt region for the first time. The present work has been carried out with the following major objectives.

- Study of tectonic activities prevailed over the region, delineation and interpretation of various tectonic features like anticlinal ridge and synclinal basin pattern.

- Identification of the areas of major deformation, fold geometry analysis towards understanding the complexity of fold pattern and associated faulting and thrusting.

- Detection of drainage anomalies, change detection analysis and impact of tectonic activities on stream pattern.

- Morphometric analysis of drainage basins and co-relation of various parameters.

- Generation of digital elevation models using different approach and comparative analysis of all DEMs on the basis of topographic indices. Extraction of various morphotectonic parameters and indices from the DEMs.

- Integration of Remote Sensing and GIS techniques and blending of gathered information.

- Interpreting and inferring the morphotectonic scenario for the study area.

The objectives of this work have been achieved through systematic approaches and methodologies as enumerated in the flowchart (Figure 1.2).

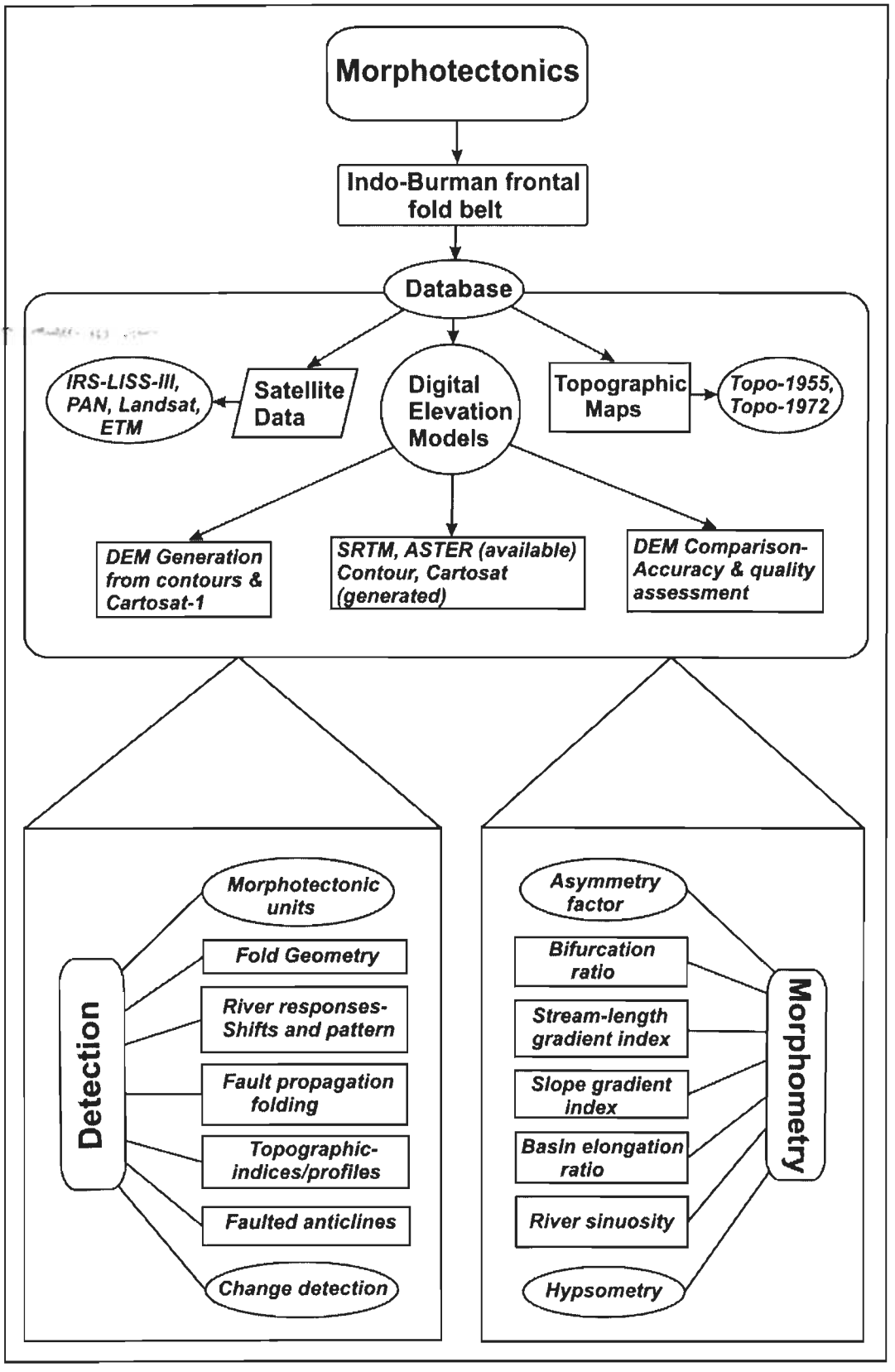

Figure 1.2 Flow chart enumerating the data base, morphotectonic and morphometric characteristics.

1.4 Study area

Study area of the present research work comprises frontal part of the Indo-Burman fold belt forming the Surma Basin and occupies areas of south Assam, Tripura and parts of Bangladesh, Mizoram and Manipur, N-E India. This fold belt is the outcome of E-W oriented compressional tectonic forces that prevailed in the region during the eastward subduction of the Indian plate below the Burmese plate. Owing to this process the westerly laying sedimentary wedge got deformed into a series of N-S oriented alternating anticlines and synclines. Intensity of folding gradually increases eastward in the sedimentary sequence. These folds are also affected by several longitudinal and transverse faults (Nandy, 2001). Figure 1.3 shows study area exhibiting the unique fold patterns present in the Indo-Burman frontal fold belt and adjoining regions. Figure 1.3 also demonstrates the regional plate tectonic set up.

1.5 Data used

Topographic maps of Survey of India (SOI): Topographic maps of 1: 50000 published in 1955 and 1972 were used for the drainage comparison and analysis of Barak river pattern. A few of them were used for the purpose of DEM generation.

Geological maps: Published geological map (Nandy, 2001) as well as geological information from the Seismotectonic Atlas of Northeast India and its Environs (GSI, 2000) were used for understanding the geology of the region. Few of these were regenerated for better representation.

Tectonic maps: Tectonic features were extracted from the Seismotectonic Atlas of Northeast India and its Environs (GSI, 2000).

Resourcesat-LISS-III: Resourcesat-1 (also known as IRS-P6) is an advanced remote sensing satellite built by Indian Space Research Organization (http://www.nrsc.gov.in/). LISS-III data in visible and short wave infrared (SWIR) spectral bands with 23.5 meter spatial resolution of January, February-2005 and January-2006 were procured for this work.

IRS-ID-PAN: The Indian Remote Sensing Satellite IRS-1D was designed to image earth in panchromatic spectral range. It has resolution of 5.8m (http://www.nrsc.gov.in/). IRS-1D PAN data of January, February and December-1999; Januray, February, March and November-2000; January, February-2002 covering Surma Basin were procured for this work.

CARTOSAT-1 Stereo Orthokit data: CARTOSAT-1 is a stereoscopic earth observation sun-synchronous satellite was built, launched and maintained by the Indian Space Research Organization. It has a payload consisting of two cameras – one near nadir looking (-5 deg) and the other forward looking (+26 deg) providing the real time stereo data along the track with spatial resolution of 2.5m. This kind of mounting of cameras on the satellite provides near simultaneous imaging of the same area from two different angles, which facilitates the generation of accurate three-dimensional maps (http://www.nrsc.gov.in/). Three stereo pairs of Cartosat-1 data of December, 2006 covering Bhuban anticlinal hills were procured for generation of DEM.

LANDSAT: Landsat Multi-Spectral Scanner (MSS), Thematic Mapper (TM) and Enhanced Thematic Mapper (ETM) are multispectral scanning radiometer that was carried on board Landsats 4, 5 and 7. All these sensors provided nearly continuous coverage from July 1975 to present. MSS data covers visible and infrared electromagnetic spectrum. TM and ETM data cover electromagnetic spectrum of visible, infrared (near, mid and thermal) having 30 meter resolution and pan with 15 meter resolution. Landsat's global survey mission provides repetitive acquisition of observations over the earth's land mass (http://glcfapp.glcf.umd.edu: 8080/esdi/index.jsp).

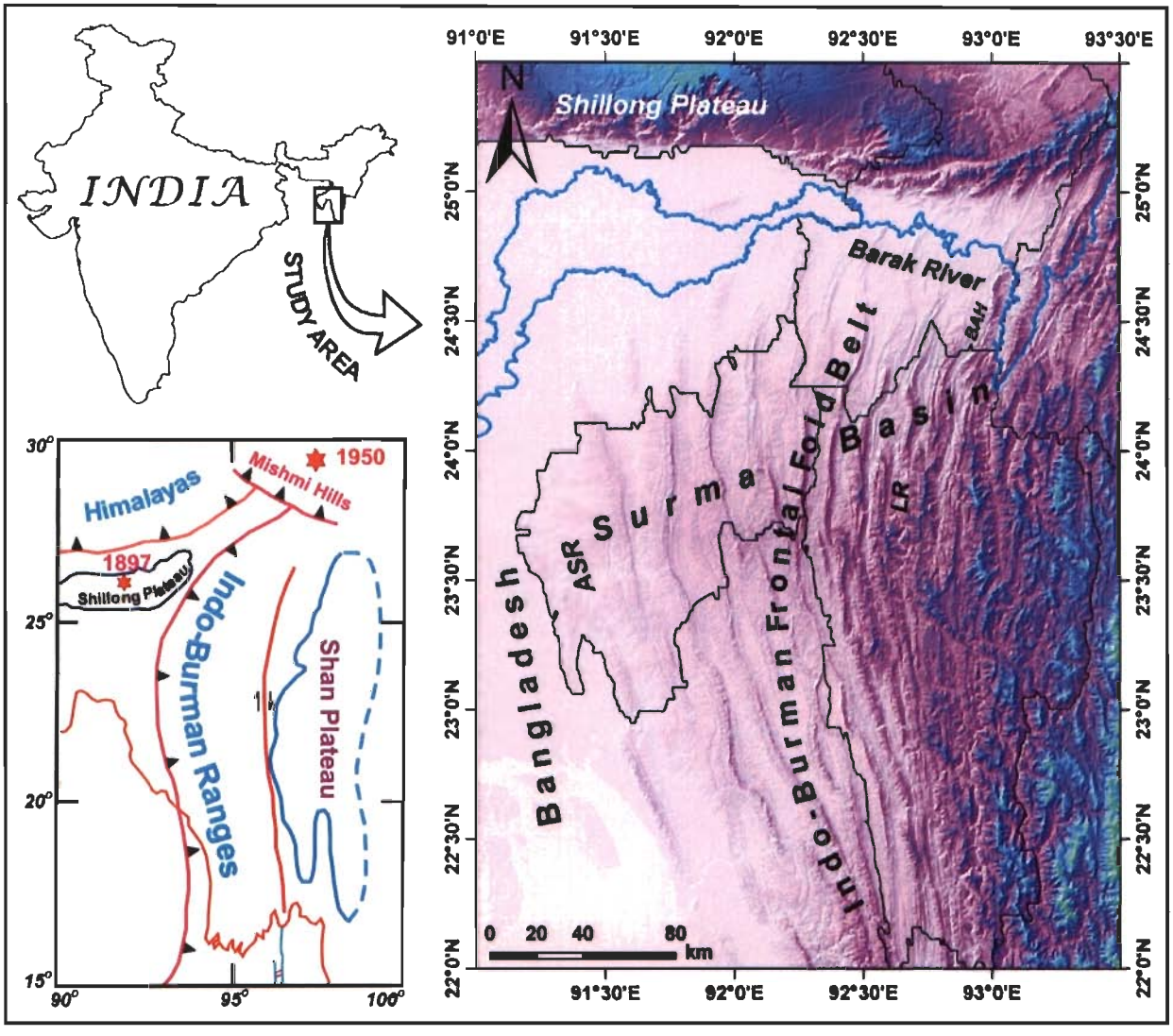

Figure 1.3 Study area showing the Indo-Burman frontal fold belt and adjoining regions along with the regional tectonic perspective. Color coded shaded relief model of SRTM-DEM has been used to exhibit the folded topography. BAH-Bhuban Anticlinal Hills, ASR-Agartala Slope Region, LR-Lengpui Region.

SRTM-DEM: The Shuttle Radar Topography Mission (SRTM) obtained elevation data on a near-global scale to generate the most complete high-resolution digital topographic database of Earth. SRTM consisted of a specially modified radar system that flew onboard the Space Shuttle Endeavour during an 11-day mission in February of 2000. This SRTM digital elevation data, is a major breakthrough in digital mapping of the world, and provides a major advance in the accessibility of high quality elevation data for large portions of the tropics and other areas of the developing world (Bammler, 1999). The global SRTM data is available as 3 arc second (approx. 90m resolution) DEMs. The data is projected in a Geographic (Lat/Long) projection, with the WGS84 horizontal datum and the EGM96 vertical datum (Internet: http://srtm.csi.cgiar.org/I). These are available in both ArcInfo, ASCII and GeoTiff formats to facilitate their ease of use in a variety of image processing and GIS applications.

ASTER-DEM: The Advanced Spaceborne Thermal Emission and Reflection Radiometer (ASTER) GDEM product is generated using bands 3N (nadir-viewing) and 3B (backward-viewing) of an ASTER Level-1A imaging system. The Visible Near Infrared (VNIR) sensor subsystem includes two independent telescope assemblies that facilitate the generation of stereoscopic data. The Band-3 stereo pair is acquired in the spectral range of 0.78 and 0.86 microns with a base-to-height ratio of 0.6 and an intersection angle of about 27.7. The new ASTER-GDEM is a single-band product with 30-meters spatial resolution that is geodetically referenced to the UTM coordinate system, and referenced to the Earth's geoid using the EGM96 geopotential model (http://www.gdem.aster.ersdac.or.jp/search.jsp).

1.6 Software used

Highly capable and efficient software packages were necessary to process and handle various types of data sets viz., satellite images, digital elevation models, topographic maps and for extraction of various important morphotectonic and morphometric parameters to achieve desired results for this research work. Various modules of robust software such as ArcGIS 9.3 and ERDAS-Imagine 9.3 were

extensively used. Further, other commonly available software were also used intensively for computational as well as data presentation purposes.

1.7 Organization of Chapters

Chapter 1 contains the general description of morphotectonic parameters and applications of geoinformatics (RS, GIS and DEMs) in understanding tectonic deformation on the basis of topographic and geomorphological studies. This chapter also enumerates the research objectives, study area and data used for this research work.

Chapter 2 is the review of the research work already done in the context of international and national scenario on morphotectonic studies. Various indices which are widely used by the researchers all over the world for understanding morphotectonics such as tectonics, geomorphology, structures, geomorphic markers etc. have been discussed in detail. This chapter also enumerates significance of geoinformatics in various applications including morphotectonic analysis.

Chapter 3 presents the review of the geotectonic evolution of the Indo-Burman fold belt including Surma Basin and its seismic behavior. Major deformational patterns identified by various workers are highlighted in this chapter.

Chapter 4 deals with the regional morphotectonic perspectives of Surma Basin. It incorporates synthesis of geometry of various folds and tectonic deformation associated with them. Anomalous behavior of Barak, Kushiara and Surma River through the topographic maps and satellite datasets of different years has been analysed. Changes in the morphology of major tributaries of Barak river also been investigated and discussed along with geomorphological parameters through different blocks.

Chapter 5 covers the detailed description, calculation and interpretation of morphometric indices for all the major synclinal valleys of the Surma Basin. Morphometric characteristics of the western Tripura and Lengpui regions have been discussed in detail to understand the morphotectonics. Western Tripura region comprises Agartala slope and

adjacent Baramura and Atharamura anticlines along with intervening Khowai and Ampi Bazar synclines. Drainage networks and stream behaviours have been used as proxy indicator for understanding the morphotectonic scenario of this region. Similarly, Lengpui area located near Aizwal shows anomalous topographic appearance on satellite images and DEMs. This area also exhibits interesting topographic and slope variation. Various computed morphometric indices have been discussed in this chapter.

Chapter 6 includes detailed description of methodology for generation of DEMs from different data sources viz. topographic contours and Cartosat-1 stereo orthokit data. A detailed comparative analysis of the generated Contour and Cartosat-DEMs with the available SRTM and ASTER-DEMs has also been carried out. This chapter demonstrates comparative analysis of various parameters for the accuracy and quality assessment of all the DEMs.

Chapter 7 describes DEM based morphotectonic analysis of Bhuban anticlinal hills. A detailed morphotectonic study of the Bhuban anticlinal hills has been discussed in this chapter. Morphometric analysis was also carried out using various indices.

Chapter 8 summarizes preceding chapters in the light of morphotectonic and morphometric scenario of the study area. Conclusions describe significant findings and contributions of this work on the basis of research outcomes from different observations. It also highlights the future prospect of this work.

CHAPTER-II

Morphotectonic studies : A review

2.1 Introduction

Morphotectonic amalgamates topography and tectonic activity to explain landforms mainly at continental, sub-continental and even at local scales. It includes the study of mountains, erosion surfaces, drainage patterns, and sediments on land and offshore. Significant advances have been made in the fields of morphotectonics, and neotectonics in recent years especially with the advent of remote sensing technique. Further, the development of satellite geodesy and improvements in geophysical tools for dating Quaternary materials combined with widespread availability of high-resolution digital topography have improved our ability to resolve the impacts of active tectonics and surface processes on sculpting the Earth's surface. In recent years, many earth scientists have shifted emphasis from classical geologic, structural and tectonic explorations to investigations of neotectonics and landscape evolution, further accelerating our understanding of surface kinematics and the consequent surficial change expressed as the land surface morphology.

Before the 1960s, morphotectonics focused on, for example, the influence of faulting on landforms, and uplift as a mechanism for raising large areas, which then eroded to form erosion surfaces. These have now been combined by studies of the relationships between global tectonics and geomorphic evolution. The morphotectonic development of landforms takes place on the same timescale as plate tectonics. Ollier (1981) has proposed the term 'evolutionary geomorphology' for this part of earth-science. Morphotectonics requires input from at least three branches of earth-science: geology, geomorphology and geophysics. Until the 1980s, tectonics was largely dependent on the first two, and directly observable evidence of landforms was neglected. Landforms are,

however, much easier and economical to study than the deeper parts, as observations are direct and not made by interpretation of distant geophysical signals. Later with the advancements in the fields of remote sensing and GIS, researchers emphasized mainly on the deformed landforms for morphotectonics. With the availability of high resolution satellite data, digital elevation model and topographical maps it becomes viable to extract minute variations.

2.2 Geomorphic constraints on the active tectonics

The impulse towards the development of quantitative geomorphology in the last decades has shown the way from improved statistical and mathematical models to describe different geomorphic processes (Scheidegger, 1961; Evans, 1972; Anhert, 1973; Mark, 1975). A wide range of work has outlined the usefulness of quantitative geomorphic estimations in interpreting morpho-evolutionary processes in the tectonically active regions (Avena et al., 1967; Buonasorte et al., 1991; Pike, 1993; Lupia Palmeiri et al., 1995, 1998, 2001; Centamore et al., 1996). Quantitative approaches have shown their usefulness in detecting neotectonic influence on geomorphic processes through the application of statistical parameters (Keller et al., 1982; Ciccacci et al., 1986, 1988; Mayer, 1990; Cox, 1994; Merritts et al., 1994; Belisario et al., 1999; Currado and Fredi, 2000).

Study of interior tectonic forces that shape the topography of the earth surface is very difficult. Therefore, most of the researchers have used digital topography to look for indications of active deformation preserved in the local geomorphology. Ramsay et al. (2007) have studied the active tectonics and landscape evolution of the southern Taiwan on the basis of drainage anomalies and deviation of major river systems. Active normal faults evolution in Greece is revealed by geomorphology and drainage pattern (Goldsworthy and Jackson, 2000). Walker and Jackson (2002) have identified 3 km horizontal fault offset of Gowk fault, a major intra-continental strike slip system in SE Iran from well preserved geomorphology.

2.3 Tectonic features and neotectonics

Morphotectonic analysis using different techniques and parameters have been carried out all over the world. As tectonics is the major dimension of morphotectonic, therefore, study on intensity of tectonic activities prevailing in any region becomes important. Hantke & Scheidegger (1998) carried out morphotectonic study of Massacre Island in Indian Ocean on the basis of orientation (strike, trend) of joints, faults, valleys, ridges, and lineaments. Jain et al. (1998) investigated the neotectonics of western India by the evidence from deformed quaternary fluvial sequences of Mahi River in Gujarat. A morphotectonic interpretation of the relief of Iberian Peninsula (IP) is presented by Cotilla and Cordoba (2004) based on several geological–geophysical and geomorphological methods in order to build up a morphostructural sketch. From their study they explained that earthquake occurrence in the Iberian Peninsula is principally due to stress concentrations around morphotectonic zones and maximum seismic activity is found near the first and second rank lineaments. Devi and Singh (2006) analyzed the morphotectonics of the Arunachal Himalaya on the basis of neotectonic deformation of Ganga Lake located in Itanagar capital complex.

Cotilla et al. (2007), from their study, explained that earthquake occurrence in Hispaniola is related with the stress concentrations in the vicinity of morphotectonic zones. Kimura (2004) gives a comparative morphotectonics in the Himalayan foreland and the fore-arc of southwest Japan. Mukherji and Iyer (1999) analyzed morphotectonics and volcanics of the central Indian Ocean and described that a distinct relationship occurs between the morphotectonic forms and the volcanics and perceived two types of volcanic activities. Tsimi et al. (2007) conducted morphotectonic study of Psathopyrgos active fault, located at the western end of Corinth Rift, Greece. Their observations suggest that these areas have experienced very recent uplift and intense down-cutting as a result of bi-directional fault growth. Neotectonics studies of different regions have demonstrated that tectonism has been a major controlling mechanism for topographic and landscape development (Garcia-Melendez et al., 2003; Dumont et al., 2005).

2.4 Geomorphic markers and associated deformation

Geomorphic markers are identifiable landforms, surfaces or linear features that provide a reference frame for deformational history. They can be easily compared with their modern counterparts for variation in morphological parameters (Marshall and Anderson, 1995). Reconstruction of deformed markers is important for reliable results.

River terraces are frequently used as geomorphic markers to document faulting and folding (Molnar et al., 1994; Rockwell et al., 1984). River terraces are very helpful in assessing the vertical as well as horizontal deformation. In many years of Alpine glaciation fluvial terraces have been used to correlate with moraines associated with glacial advances or still stand (Penck and Bruckner, 1909). Potentially complex nature of terrace formation is illustrated by the terrace crossing the San Andreas Fault in California near Cajon pass (Weldon, 1986). When the terrace surface is compared with the modern day stream gradient, it appears to have been warped more than 30m, although it is not physically disrupted along fault. Dating of sediments shows that both the initiation of aggradation and incision are diachronous. River terraces which are similar to alluvial fans do not instantaneously or uniformly changes in controlling parameters like discharge, sediment supply, rock uplift rate and base level lowering (Humphrey and Heller, 1995). Surface processes may tend to modify the appearance of alluvial fans (McFadden et al., 1982; Ritter et al., 1993). Many arid alluvial fans are dominated by deposition from debris flows (Whipple and Dunne, 1992). Even surfaces with considerable roughness, can be used as successful markers, because despite its irregularities the average surface gradient can be defined (Avouac and Peltzer, 1993), and offset of the gradient by faulting can be readily recognized. Lava flows, debris flows, landslides, and erosional surfaces can provide excellent markers (Weldon, 1986; Small and Anderson, 1998). Tien Shan in central Asia is regionally extensive erosion surface which was beveled across Paleozoic rocks and buried by Cenozoic sedimentary rocks (Chediya, 1986; Sadybakasov, 1990). It provides an excellent marker for recording folding and faulting of ranges that rise above the surrounding terrain (Burbank et al., 1999). Not only erosional surface but unconformable surfaces itself forms a reference for calibrating the amount of erosion that has encountered beneath it (Small and Anderson, 1998). The courses of river and ridge

crests that are displaced across strike-slip faults can clearly record lateral offsets (Beanland and Clark, 1994).

2.5 Rate of erosion and upliftment

Studies that define rate of erosion and upliftment lie at the heart of morphotectonics. Landscape evolution is the result of combined effect of tectonic upliftment, subsidence and surface processes. Much current debate revolves around whether climate and tectonics is responsible for change in rate of erosion and reshaping of landscapes (Masek et al., 1994; Molnar and England, 1990; Whipple et al., 1999). Burbank and Pinter (1999) provide a detailed view of the last decade's topographic variation by taking into consideration the views of earlier workers. They tried to outline the landscape evolutionary history of any region under different tectonic, climatic and topographic conditions and introduced the numerical modeling of landscapes. A dynamic equilibrium or steady state topography (Hack, 1960) may develop when rate of tectonic forcing are high and when tectonism sustained for long intervals (>1 Myr). Rate of erosion increases with increasing altitude (Anhert, 1984), and when rate of erosional processes controls longitudinal valley profiles (river incision or glacial erosion) then the hillslopes are likely to be at threshold angle (Schmidt and Montgomery 1995; Burbank et al., 1996; Whipple et al., 1999). In most of the situations, removal of mass from a region will be isostatically compensated by crustal rebound (at regional rates). Consequently, altitude of the peaks could increase at the same time that the mean height of the region is decreasing (Burbank, 1992; Molnar and England, 1990; Small and Anderson, 1995).

2.6 River responses to the active tectonics

Alluvial rivers are very sensitive to variation of slope gradient of a region. Streams respond to vertical displacement along fault by aggradation or degradation. Horst and graben combine two different types of vertical displacements. There will be aggradations on the upstream from the horst and degradation on the downstream part of the horst (Cartier and Alt, 1982). The type of folding will affect a river similar to the various type of faulting, but changes will probably be less abrupt. However, sometimes it is remarkable if

associated with active fold-thrust belt. The effects of tilting will depend upon the amount, but in the simplest case steepening of a valley will cause degradation and a reverse tilt will cause deposition. Lateral tilting will cause channel shift downdip or avulsions (Schumm et al., 2002). Slow rates of uplift can cause more channel adjustment by widening and meandering (Ouchi, 1985).

Responses of both modern and ancient fluvial depositional systems to growing folds can be interpreted in terms of interactions among competing controlling variables which can be incorporated into simple conceptual models. Stream power is the rate of expenditure of potential energy per unit length of the stream. Changes in the stream power have significant effects on the behavior of the river i.e. whether it is aggrading or degrading (Whipple and Tucker, 1999). The balance between stream power and rates of upstream deposition versus bedrock resistance and rates of crestal uplift and fold widening determines whether an antecedent stream maintains its course or is defeated by a growing structure (Burbank et al., 1996). In highly tectonic regions rivers incises through the bed rock at extremely high rates. Burbank et al. (1996) correlate the rate of bedrock incision of Indus River to rock uplift and threshold hillslopes of the north-eastern Himalaya. Reinfelds et al. (2003) assessed downstream trends in channel gradient, total and specific stream power, using a GIS approach. Modeling of downstream trends in channel gradient, total and specific stream power from catchment-wide DEMs have potential to provide a framework with which to investigate conceptual and empirical models between channel gradient, stream power and the form and dynamics of river systems. The pattern changes takes place at critical values of stream power, gradient, and sediment load (Schumm and Khan, 1972). Hooke (1995) has studied the adjustment to meander cut-offs on the River Bollin and River Dane, NW England.

2.7 Drainages and stream networks anomalies

Neotectonic activity of a region with quite young and weakly consolidated sediments can be understood by analyzing the drainage basin asymmetry (Cox, 1994) in spite the drainage system is sensitive indicator of active tectonics (Jackson and Leeder, 1994). Tectonic deformation causes change in channel slope, shift in river channel

position, and variation in channel morphology, fluvial processes and hydrological characteristics of a river system. Local variation in regional slope can cause anomalous drainage. Experimental studies showed that parallel drainage pattern form on the slopes greater than 2.5 percent, whereas dendritic pattern forms on the gentler slopes (Philips and Schumm, 1987). Changes of entire drainage network, with the effect of tilting, are described by Sparling (1967). Topography and drainage patterns in regions of active deformation reveal aspects of faults and anticline growth (Medwedeff, 1992; Mueller and Talling, 1997; Delcaillau et al., 1998; Tate et al., 2002; Burbank and Anderson, 2001; Husson and Mugnier, 2003; Delcaillau, 2004; Gupta and Ellis, 2004). Nucleation, growth and lateral propagation of thrusts faults interact with erosion to create the long term drainage patterns (Elliot, 1976; Gupta, 1997; Champel et al., 2002). Tectonic geomorphology of active folds over buried reverse faults or blind thrusts can be inferred using anomalous drainage and ridge morphology (Delcaillau et al., 2006).

Geomorphic indices are capable in detecting landform responses to recent tectonic and deformational processes and therefore have been broadly used as a recognition tool to characterize sectors deformed by active faults (e.g., Seeber and Gornitz, 1983; Brookfield,1998; Keller and Pinter, 2002; Chen et al., 2003; Kobor and Roering, 2004). Morphometric indices are the proxy indicator of active tectonic prevailing in the regions where the changes are gradual and drainage anomalies are not prominent (Pedrera et al., 2009). Some geomorphic indices have been developed as basic reconnaissance tools to identify areas experiencing rapid tectonic deformation. The most useful in studies of active tectonics are the stream sinuosity, hypsometric integral, drainage basin asymmetry, stream-gradient index, slope gradient index, basin elongation ratio, mountain front sinuosity and ratio of valley floor width to valley height (Keller and Pinter, 1996). Channel sinuosity, proposed by Muller (1968) helps in understanding the nature of active tectonism of a region (Susan, 1993). The stream-gradient reflects the slope change of a stream longitudinal profile, which may reflect tectonic activities (Merritts and Vincent, 1989; Rhea, 1989; Marple and Talwani, 1993; Brookfield, 1998). Hypsometry is the relative portion of an area at different elevations within a river basin and may be sensitive to various forcing factors such as tectonics, lithology and climate (Lifton and Chase, 1992). The stream length-gradient index (SL index) has been commonly used to highlight

gradient change of a stream longitudinal profile and is believed to reflect stream power or competence (Hack, 1973). Usually, it is very sensitive to changes in channel slope and is applied to evaluate relationships between possible tectonic activity, rock resistance and topography (Keller and Pinter, 1996). Basin elongation ratio is proposed by Bull and McFadden (1977) is one of the proxy indicators of recent tectonic activity (Cuong and Zuchiewicz, 2001).

2.8 Remote Sensing and GIS approach in morphotectonic analysis

Remote sensing images are extremely useful for understanding the geomorphology and landform characteristics. The information about the tectonic history can be derived from morphotectonic indices after obtaining the necessary information from topographic maps, aerial photographs, and satellite data (Keller, 1986). Significant improvement in resolution of satellite data and advancement in GIS resources has enabled the investigators to carry out quantitative and more precise analysis of various landforms. Many workers have carried out morphotectonic analysis using remote sensing and GIS techniques. Cuong and Zuchiewicz (2001) studied the morphotectonic characteristics of Lo River fault near the Tam Dao in North Vietnam. Verrios et al. (2004) carried out morphotectonic analysis in Eliki fault zone to correlate active tectonics and erosional processes using topographic maps and aerial photographs. Jain and Verma (2006) used integrated remote sensing and GIS, geomorphology, slope, vegetation index, and morphotectonic information to assess neotectonic potential in Bundi-Indergarh sector of Rajasthan. Remote sensing based study of river migration and active tectonics of the Karjan river basin in western India were carried out by Ramasamy, et al., (1991) and Raj, et al., (2003). Morphotectonics of Anandpur Sahib area of Rupnagar district (Punjab) was investigated by Bhatt et al. (2007) using remote sensing and GIS approach. Based on remote sensing analysis of two panchromatic SPOT scenes covering the western and eastern part of the Crimea, Saintot et al. (1999) determined the geometry of the major structures (folds and fractures). Novak and Soulakellis (2000) combined the digital satellite, Landsat-Thematic Mapper (TM), data with field evidences to delineate the geomorphic features of the island of Lesvos, Greece. Formento-Trigilio et al. (2003) have studied the river response to an active fold and thrust belt in a convergent margin setting,

North Island, New Zealand. Using Remote Sensing data products, Dalati (1994) has studied the tectonic of El-Rouge Depression, NW of Syrian Arab Republics. Ramasamy (2006) and Ramasamy et al., (2011) studied mega drainage characteristics, tectonic, geomorphic, and hydrological anomalies based on satellite images and detected series of N–S trending extensional, NE–SW sinistral and NW–SE dextral strike slip faults with well defined morphology in whole peninsular India.

Morphological analysis of topographic features, in particular lineaments, has long been applied in structural and tectonic studies (Hobbs, 1912; Frisch, 1997). Satellite images show great promise as a tool for mapping and correlation of alluvial geomorphic surfaces (Gillespie et al., 1984; Kahle et al., 1984; Anderson and Beratan, 1993, 1994). Beratan and Anderson (1998) used Landsat-TM data for mapping and correlation of Quaternary geomorphic surfaces in the southern Whipple Mountains, California.

2.9 DEM based morphotectonic studies

DEMs are one of the important products of satellite data having several applications. The potential of DEMs for solving a wide spectrum of theoretical and applied problems has long been known (Evans, 1972). Its simple data structure and widespread availability have made it a popular tool for land characterization. DEMs derived from the Shuttle Radar Topographic Mission (SRTM) and ASTER (Advanced Spaceborne Thermal Emission and Reflection Radiometer) stereo data (GDEM) is now freely available for whole world with a resolution of 3 arc and 1 arc seconds. These products can be very useful for research purposes as well as to supply basic topographic mapping data for poorly mapped areas (Rabus et al., 2003). Accuracy assessment for SRTM-DEM is carried out by various workers using different approaches (Sun et al., 2003; Miliaresis et al., 2005; Kocak et al., 2005).

A number of DEM generation methods have been adopted by researchers. Generating DEM from contour lines is now a main method to get grid DEM because of its low cost and the convenience to get contour maps. One of the most important parts of DEM building is interpolation. The best known methods for interpolation were described

and discussed by Watson (1992), Rognant et al. (2001), Wang and Ellis (2005). Comparative analysis of contour derived DEMs have also been carried out by numerous researchers. Wood and Fisher (1993), Wood (1994), Li (1994), Carrara et al. (1997) and Sharma et al. (2009) compared different algorithms of interpolation. TIN models generated from contours are used to provide better control over terrain slope, aspect, surface areas, volumetric and cut-fill analysis and generating contours (Lee, 1991).

One powerful technique for generating digital elevation is using the digital image correlation method. It implies two optical images acquired with different angles taken from the same pass of an airplane or an Earth Observation Satellites (Buyuksalih et al., 2003; Buyuksalih and Jacobsen, 2008). Habib et al. (2004) have generated DEM from high resolution satellite imagery using parallel projection model. Jacobsen (2004) has studied DEM generation methods from different satellite and photographic products like SPOT, MOMS, IRS-1C / 1D, ASTER, TK350, IKONOS, QUICKBIRD, CORONA and analyzed their quality. Poon et al. (2005) assessed the quality of digital surface models generated from IKONOS imagery. Cartosat-1 stereo image data have been used successfully by Gianinetto (2008) and Rao et al. (2007) for DEM generation. Rao et al. (2007) used DEM generated from Cartosat-1 image for the updating of topographic maps of Goa city of India.

Comparative analysis of DEMs and the impact of DEM error on derived parameters have been investigated by various workers. Gallant and Hutchinson (1996) suggested about the grid resolution of DEMs which can profoundly influence the spatial patterns of attributes derived from them, and also influence models built from these attributes. Sharma et al., (2009) have measured the accuracy of contour interpolated DEMs of differing resolution. Warren et al. (2004) compared slopes measured in the field with those derived from DEMs, and found that higher resolution DEMs (1m) produced much better results than lower resolution DEMs (12m). Sorensen and Seibert (2007) reported the effect of DEM resolution on the basis of Topographic Index. Fisher (1991) evaluated the impact of DEM error on view-shed analyses. Hunter and Goodchild (1997) investigated the effect of simulated changes in elevation at different levels of spatial autocorrelation on slope and aspect calculations. Lee et al. (1992), Lee (1996) and

Holmes et al. (2000) simulated errors in a grid DEM and determined that small errors introduced into the database significantly affected the quality of extracted hydrologic features. Liu (1994) simulated errors in DEMs to evaluate uncertainty in a forest-harvesting model. Ehlschlaeger and Shortridge (1996) evaluated the impact of DEM uncertainty on a least-cost-path application. Holmes et al. (2000) used GPS data to quantify errors in a USGS 30-m DEM and found that these errors had a significant impact on derived terrain attributes.

DEM quality selection is mostly application dependant. For example, high spatial resolution and topographic quality DEM is not a requirement for regional, small scale analyses and for calculating average altitudes. However, topographic accuracy is more sensitive for analyses that use algorithms based on derivatives like slope, aspect, drainage, path simulation, etc. In distributed hydrological modeling, the output is affected to a large extent by model input and researchers have found that DEM quality and resolution significantly affect the accuracy of any extracted hydrological features (Kenward et al., 2000).

DEM plays a vital role in morphotectonic analysis as they are most widely used datasets for representing topography. Furthermore, DEM also displays the tectonically affected topography in better way. Most of the tectonic studies applying DEM use shaded relief models in combination with remotely sensed data products on a regional scale (Florinsky, 1998; Chorowicz et al., 1999). Three dimensional view with image drape (Le Turdu et al., 1995) and digital cross sections (Chorowicz et al., 1998) have been used for morphotectonic investigations. Chorowicz et al. (1991) used DEM to calculate dip and strike from geological maps. Koike et al. (1998) calculated fault plane geometries from digital elevation models. Florinsky (1998) studied the relationship between fault type and landform and used curvature maps to recognize and characterize fault line. Onorati et al. (1992) used slope and aspect calculations in a regional morphotectonic investigation. Riley and Moore (1993) used elevation histogram to identify horizontal pediments on mountain slopes associated with normal faulting. Trend analysis has been used to study tectonically induced tilt (Doornkamp, 1972; Fraser et al., 1995; Guth, 1997). Chorowicz et al. (1989, 1995) studied strike ridge morphology and used profile geometry for its

recognition in DEM. Jordan et al. (2005) gives a procedure for the consistent application of digital terrain analysis methods to identify tectonic phenomenon from geomorphological parameters in Hungary and NW Greece. Zizioli (2008) studied the DEM-based morphotectonics analysis of Western Ligurian Alps exhibiting a peculiar drainage network related to the geological events. They have used GIS based approach to extract the morphotectonic lineament, drainage characteristic and neotectonics of the Lingurian Alps. Development and interpretation of morphometric maps prepared using DEMs are important tools in studies related to neotectonics and geomorphology. Geographic Information System (GIS) allows speed and precision to this process.

CHAPTER-III

Geotectonic evolution of Indo-Burman fold belt including Surma Basin

3.1 Introduction

The Indo-Burman mobile belt is represented by high intensity folding and freely westward migrated fold belt comprising frontal part which also constitutes the Surma Basin. The frontal fold belt have developed in a relatively open basin lying south of the Shillong Plateau. The westerly convex arcuate Indo-Burman fold belt formed at the leading edge of the eastward subducting Indian plate (Nandy, 2001). This chapter deals with geotectonic evolution of the Indo-Burman fold belt as a whole towards understanding deformation pattern and generating knowledge base to carry out morphotectonic and morphometric studies. Figure 3.1 shows regional perspective view of Indo-Burman fold belt and Surma Basin in context of adjoining geotectonic units such as Shillong Plateau, Himalayan belt and Mishmi Hills massif.

3.2 Frontal fold belt (Surma Basin)

The frontal fold belt (Surma Basin) covers part of southern Assam, states of Tripura and Mizoram, western part of Manipur (Northeast India), Sylhet and Chittagong districts of Bangladesh and Arakan coastal zone of Myanmar. Surma Basin is bounded on the north by the Shillong Plateau, to the east of this fold belt lies the intricately folded and faulted Paleogene outer arc complex of the Indo-Burman mobile belt, whereas to the west occurs the alluvium covered gently dipping, homoclinal Tertiary sedimentary succession of Bagladesh (Bengal basin). This assumed a "bell shaped" form having constant southerly and south-westerly paleoslope, and was connected to the open sea to the south.

Neogene Surma basin marked by the post-Barail unconformity, subsequently faulted by the Kaladan thrust (Ganguly, 1993) to the east; the E-W Dauki fault and NE-SW Disang thrust to the north and north-east; the NE-SW Sylhet fault (Nandy et al., 1983 and a structural high concealed below the alluvium of Bangladesh (Sengupta, 1996) to the west and north-west. Within this vast terrain the Surma Group and the younger sediments occur as westerly convex N-S fold belt for a strike length of about 550 km, having a maximum width of 200 km. The thickness of the late Mesozoic and Cenozoic strata in the Surma Basin range from about 13 to 17 km (Evans, 1964; Hiller and Elahi, 1984) and much of these strata are Neogene in age. The Bouger anomaly map shows gradually higher values (negative) towards the center of the basin (Alam et al., 1990). An aeromagnetic interpretation map by Hunting (1980) indicates a gradual deepening of the basement towards the center of the basin and also reveal subsurface synclinal features and faults within the basin. The geology and the hydrocarbon potential of the Surma Basin have been investigated by many workers (Holtrop and Keizer, 1970; Lietz and Kabir, 1982; Hiller and Elahi, 1984; Khan et al., 1988; Johnson and Alam, 1991).

3.3 Geology and Stratigraphy of Surma Basin

The general depositional events in Surma Basin consist of a repetitive succession of mainly Neogene arenaceous and argillaceous sediments, known as rhythmites, with thinning upward sequence. The rhythmites of marine origin were followed later by continental type fluvial deposits of Dupitila and Quaternary-Recent river deposits (Miocene-Pleistocene age) in the topographic and structural lows. They were originally classified into the Surma, Tipam and Dupitila Series (Evans, 1932; Mathur and Evans, 1964; Das Gupta, 1977) on the basis of scattered fossil occurrences. Extensive work carried out in the regions south Assam, Tripura, Mizoram, west Manipur by the Geological Survey of India (GSI) and Oil and Natural Gas Commission (ONGC), India and in Bangladesh part by the geologist of Bangladesh brought out a wealth of information regarding Surma Basin. Figure 3.2 depicts geological information of the Surma Basin and adjoining regions.

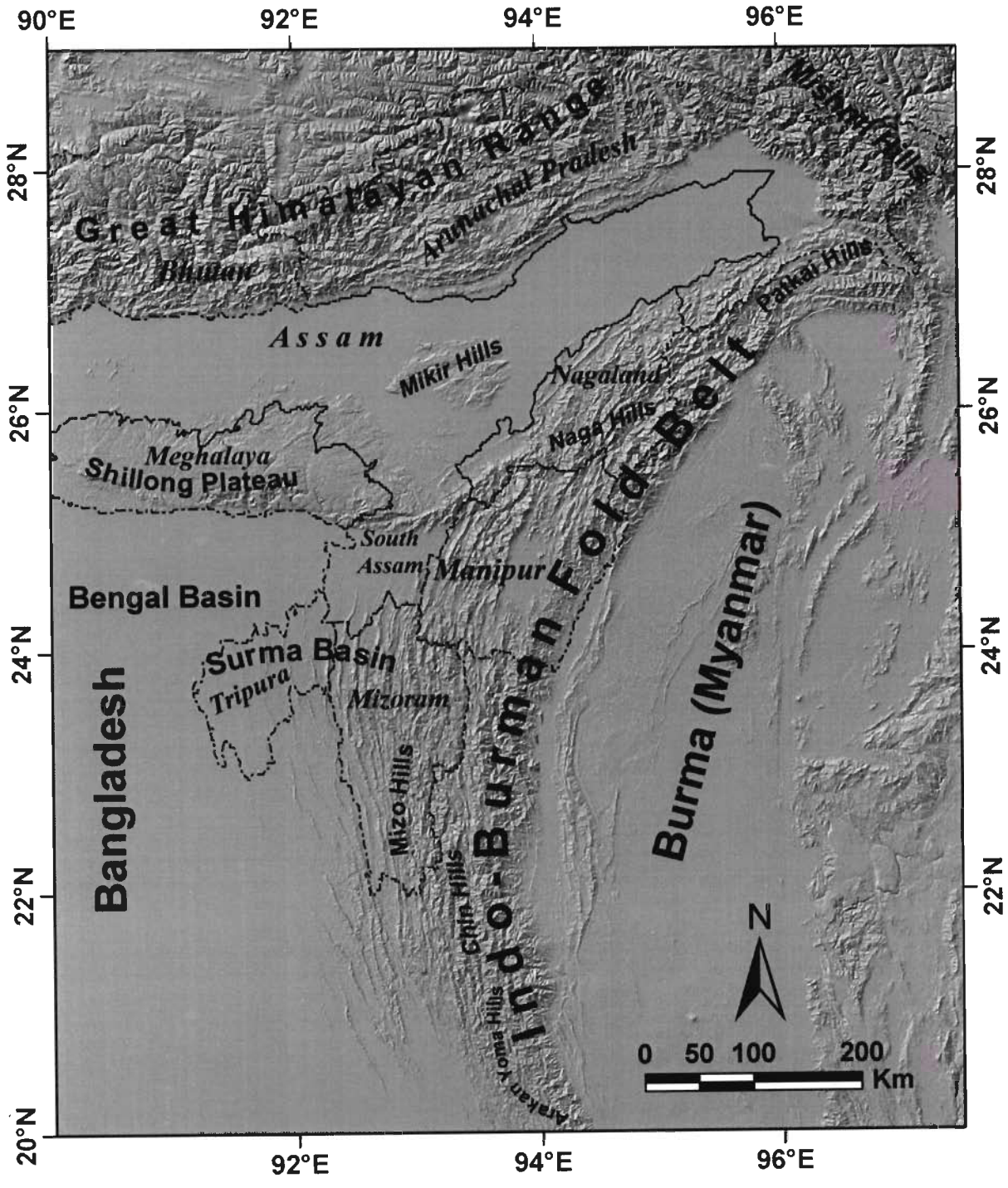

Figure 3.1 Regional perspectives of Indo-Burman fold belt and adjoining geotectonic units on the backdrop of shaded relief model of SRTM-DEM.

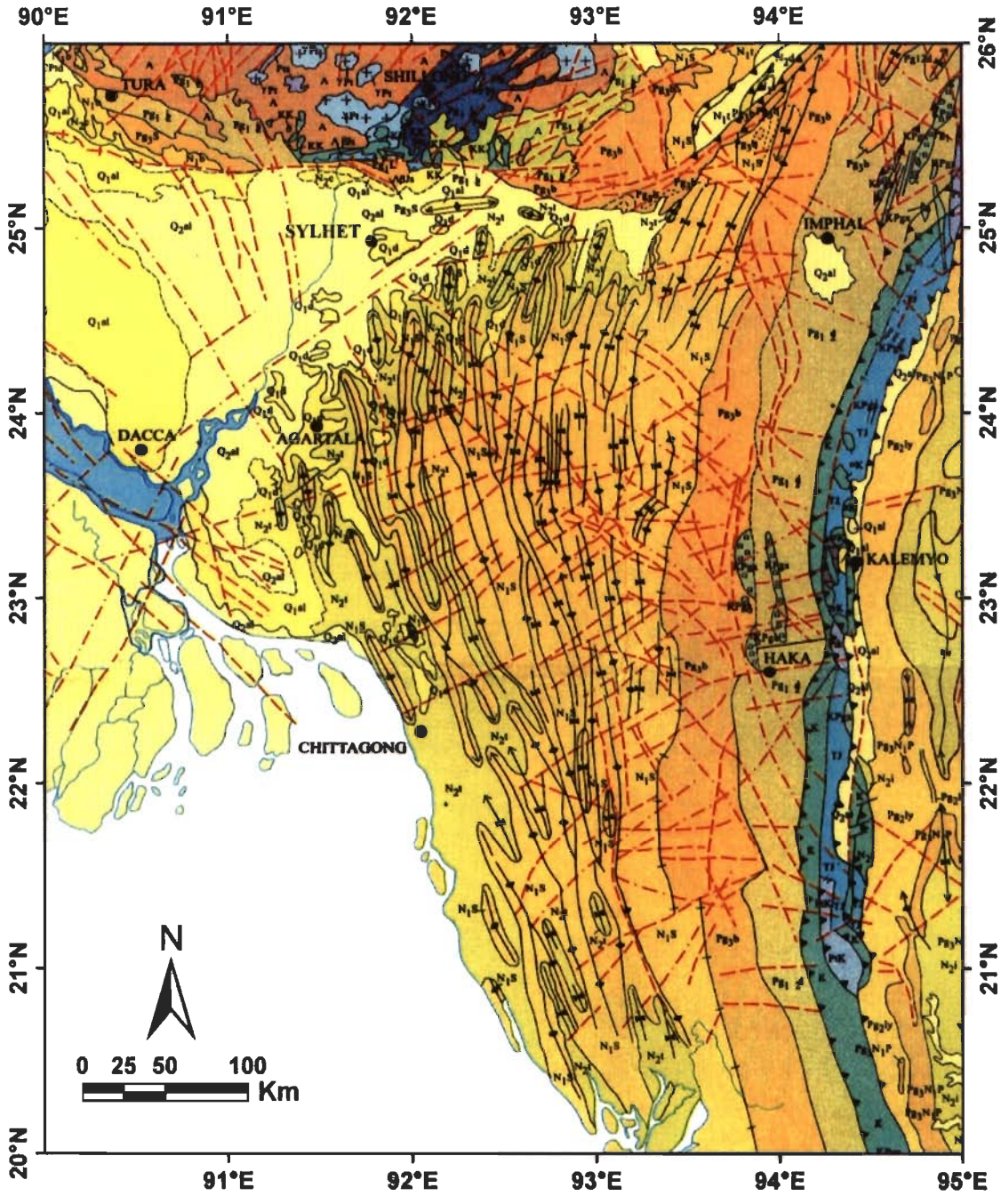

Figure 3.2 Geology and structures of the Surma Basin and adjoining region. (Source: Nandy, 2001). Q_2Al-Older alluvium, Q_1Al-Younger Alluvium, Q_1d-Dupitila formation, N_2C-Chengpara formation, N_1B-Bagmara Formation, Pg_3b= Barail group, Pg_1d - Disang group, Pg_1j-Jaintia group, Pg_1l-Langpur formation, KK-Khasi Group, AβJs=Sylhet Trap, CPtd= Gondwana Super group (Talchir & Damuda Formations), N_2T-Tipam Group, N_1S= Surma Group, N_2D=Dihing Group, TJ Sandstone and shale, KPgx-Exotics [Limest., grit, conglomerate, basalt, serpentinite (σK), dunite (σK), peridotite (sK), spilite], $\Lambda\beta$N2, $\Lambda\rho$N2, $\Lambda\alpha$N2, + βN2= Basic intermediate, acid volcanics and intrusives, Pg_3N_1P=Pegu Stage, NQ_S= Siwalik Group, $\Lambda\beta$=Abor volcanics, γPt- Myllium granite.

The Surma Group named after its type locality in Surma Basin by Evans (1932) is diachronous unit consisting of a succession of alternating shales, sandstones, siltstones and sandy shales with occasional thin conglomerates, indicative of repetitive deposition from pro–delta, delta front and paralic facies with intermittent, wholly marine facies (Holtrop and Kaizer, 1970). Surma Group is divided into the Bhuban (Lower, Middle and Upper) and the Boka Bil Formations, based on differences in their gross lithologies (Mathur and Evans, 1964).

The Bhuban Subgroup has been named after its type area of Bhuban range in the western Manipur hills and is well developed in Mizoram, Tripura, south Assam, West Manipur, Chittagong Hills and Arakan Coastal area, occurring mainly in the cores of the anticlines. Boka Bil Formation named after its type area near Boka Bil village in south Assam and gives rise to characteristic broad swampy valley features and is extensively exposed in the anticlinal cores of western Tripura and in synclinal flanks and cores of eastern Tripura, south Assam, Chittagong and coastal Arakan areas and along the synclinal cores of Mizoram and western Manipur. This is dominantly argillaceous formation and comprises soft, grey, laminated claystone, siltstone/shale alterations, locally interbedded with discoidal hard calcareous siltstone. The formation is characterized by large scale facies variations from shale/claystone to fine sandstone. Thickness of formation varies from 1000m-1500m over the entire basin, maximum thickness (1800m) reported from Chittagong area (Khan, 1980).

The succession of sandstone and mottled clay overlying the Boka Bils, named as the Tipam Series after the name of Tipam river in the type area (Mallet, 1876; Pascoe, 1973) occurs only on the northern and western part of the Surma Basin. This lithounit is predominantly arenaceous succession, comprising massive, soft, friable, highly cross-bedded, medium coarse grained, ill-sorted, ferruginous sandy rock with pebbly layers occurs mostly in the cores of the shallow anticlines and domal structures along the western part of the basin and along the synclinal troughs in the eastern Tripura-south Assam, northwest Mizoram and Chittagong fold belts. The Tipam sequence appears to coincide with the synclinal troughs where the sequence has attained a maximum thickness of over 2000m in Sylhet area of Bangladesh and adjoining areas of Tripura. The

upper contact of the Tipam Group with the overlying Dupi Tila Formation is believed to be a regionally developed erosional unconformity.

3.4 Structures of Surma Basin

Structures of Surma Basin are characterized by the series of continuous and discontinuous N-S, N15°E - S15°W, sub-parallel doubly plunging, enechelon regional anticlinal ridges and synclinal valleys formed of rocks belonging to the Surmas, the Tipams and the Dupi Tilas. The axes of the folds show gentle convexity towards west in the middle part of the fold belt. The eastern contact of these rocks with the Oligocene Barails consists of a series of marginal faults (marginal to the basin) belonging to the Surma Basin which have obliterated the post Barail unconformity in this area (Sarkar and Nandy, 1977). The eastern boundary or the hinge zone of the basin in Mizoram is also supposed to be marked by the Kaladan fault which might have acted as the crustal wrenching for the structural evolution of the Surma Basin. There are also lower amplitude domal structures within the wide synclinal areas. Many of the wider anticlines bifurcate to form two anticlinal ridges with sub-parallel axial trends. In some cases such split axes merge again to enclose synclinal valleys, a common feature in a Chittagong Hills, giving rise to flattened structural domes and basins. There are more than one axial plane culminations and depressions in each long structure with regional plunge varying from 5°-25°. Width of the syncline gradually diminishes from west to east with the increase in intensity of folding and exposing the older rocks. The fold belt is narrowed down to the south and gradually widens to the north (Nandy et al., 1983).

The anticlines range in size from short, oval structures, about 20-30km long (Tichna and Rokhia in western Tripura) to large linear periclinal folds extending for 200 km in length in central Mizoram; the width of the folds varies between 10 and 30km. The intensity of folding, complexity, and also intensity of deformation increase from west to east. To the east, the folds are much compressed, overturned and isoclinal involving older rocks of the basin. Outcrop patterns have been made complicated by the number of strike fault, thrusts and transverse faults. In the west, folds are open and canoe shaped showing broad and less intricate outcrop pattern (Nandy et al., 1983). Accordingly, the folds vary

from gently brachy-anticlines in the western most part of the Tripura to cuspate, box like folds with flat crests and steep limbs in central and eastern Tripura and highly compressed ridge like folds in the central and eastern part of the Mizoram and in the eastern Chittagong Hills. However, intermingling of all these are also seen. The anticlines in Tripura are flat crested and box-shaped (e.g. Baramura, Longtarai) whereas the other anticlines in the neighborhood are sharp crested. Though all the synclines are broad and wide in the central and western Tripura, the synclines in east Tripura is apressed and steeply plunging (Nandy et al., 1983). Thus, it is very clear that the sedimentation and tectonic activities were initiated from the eastern part of the basin and gradually migrated toward west.

The mesoscopic folds of the area are varied in style. They are preserved mostly in thinly laminated multi layers of silt shale alternations. The wavelengths of these folds are greater than their amplitudes. Two types of folds are common viz. sharp crested and disharmonic folds. Parallel concentric folds are also seen in Upper Bhubans. Overturned, recumbent and box folds are noted in the areas bordering Tripura and Mizoram (Nandy et al., 1983). The anticlines are usually bound on one (mainly eastern) or from both the flanks by longitudinal reverse fault which runs close and sub-parallel to the crest of the anticlines. The magnitude of the faulting increases towards the east with the increase in intensity of folding (Ganguly, 1993). These faults have vertical throw of the order of 700-1700m producing many drag folds at higher level (Nandy et al., 1983). The individual structures are segmented by the cross faults and conjugate oblique faults, some of which have strike-slip component and have offset anticlinal axis and flank faults. Sikder and Alam (2003) suggested a 2-D modeling of the anticlinal structures and structural development of the eastern fold belt of the Bengal Basin, Bangladesh. The 2-D models presented in their study illustrate that the anticlinal structures within the eastern fold belt have been developed on a folded detachment or decollement at depth as a result of the combined effects of initial buckling and subsequent fault-propagation folding with increased compression, which is a common structural style in fold-and-thrust belts and accretionary wedges in subduction-related orogenic setting. The morphotectonic lineament as studied on Landsat images revealed bimodal pattern the major population falling between N50°E and N60°E and minor one falling between N43°W and N60°W.

Therefore, these conjugate sets of fractures have their acute bisectrix orthogonal to the regional fold axes (Nandy, 1981; Nandy et al., 1983).

Geophysical surveys carried out by the ONGC indicate presence of subsidiary folds and faults and other structural complications at deeper levels; even underneath the superficially undisturbed folds, and of disharmonic flattening of dips under tight steeply dipping surface folds. Deep wells drilled in Tripura and south Assam into the anticlinal cores have indicated the anomalous zones of steeply dipping beds and formations in the subsurface. These observations as well as vertical seismic profiling surveys conducted in deep wells in Tripura and south Assam have lent support to the concept of 'thin skin tectonics' in Tripura and south Assam areas (Ganguly, 1993). It has been postulated that the fold belt of the Surma Basin has been evolved by compressive forces and their subsequent accentuation by shale/mud flowage due to diapirism or incipient diapirism (Ganguly, 1984). Das Gupta (1977) attributed the increase of deformation in the eastward direction to the change in competence of strata due to increase in argillaceous content and thickness of sediment to that direction. The increasing intensity of deformation from west to east has also been interpreted due to increasing proximity of the plate edge to the east (Nandy et al., 1983; Ganguly, 1984).

3.5 Indo-Burman fold belt

The Indo-Burman tectonic belt forms a N-S trending arc of mountain ridges extending from Mishmi Hills through the Patkai, Naga, Manipur, Mizoram, Chin and Arakan-Yoma Hills and is genetically linked with the Andaman-Nicobar ridge and Sunda belt. In the Patkai region the ranges have northward convex E-W trend swinging to SSW in Naga Hills and then to SSE along the Arakan Yoma. The maximum width of the range is about 230km and the average elevation increases from 1000m to about 3000m from south to north.

Geologically, the hill ranges of this tectonic belt are mainly formed of thick turbiditic Cretaceous to upper Eocene shales and sandstones (Brunnschweiler, 1966). This belt has been folded more intricately in Nagaland and the NE-SW trending Naga Thrust

traverses the whole of Nagaland and then verges with the Dauki Fault after taking a swing towards southwest to west near Haflong. This zone has undergone large dislocation, as is indicated by enormous variation in lithotectonic associations and attributes on either side of the Naga Thrust.

3.6 Geotectonic evolution of Indo-Burman fold belt

The Indo-Burman mobile belt was developed during the Cenozoic in response to the subduction of Indian lithosphere below the Burmese plate (Figure 3.3). A linear arcuate deep basin was developed along the leading edge of the subducting Indian plate during the Paleocene - Eocene time that was filled up by Eocene Disang-Chin-Arakan Yoma flysch and Oligocene Barail subflysch or by their equivalents. At the close of Oligocene, the flysch trough was completely closed and uplifted forming the backbone of Indo-Burma fold belt Palaeogene outer arc ridge or the accretionary prism. On the eastern side of this uplifted outer arc ridge sedimentation continued in the central Burma basin during Mio-Pliocene time after a marked hiatus, whereas to the west two separate Neogene basins were formed on either side of the Shillong Plateau in front of this raised outer arc ridge viz. the Tipam Basin of Upper Assam and the Surma Basin to the south designated as Neogene outer arc. Continued subduction of the Indian Plate resulted in intense and intricate fold-thrust belt along the outer ridge including those in the Neogene outer arc complex of the Upper Assam and Surma Basin to the west. The sediments of the central Myanmar basin were folded due to overall east-west compressive stress regime. Major thrusting also occurs along the contact of the outer arc ridge and fore-arc basin (Eastern Boundary Thrust, Nandy, 1980). The elements of forearc trough including the oceanic crust were overthrust to the west upon the accretionary prism.

3.7 Seismotectonics of Indo-Burman fold belt

The 1100km long Indo-Burman arc has been experiencing innumerable earthquakes. Utilizing seismic data for different periods and from various agencies, several authors have tried to draw correlation of seismicity to tectonics of this N-S trending arcuate belt (Fitch, 1972; Chandra, 1975; Verma et al., 1980; Le Dain et al., 1984; Mukhopadhyay and Das Gupta, 1988; Das Gupta et al., 2003; Satyabala, 2003). Shallow and intermediate earthquakes are very frequent in this region, but earthquakes more than 180km deep are also reported. Mukhopadhyay (1984), Biswas and Das Gupta (1986) and Mukhopadhyay and Das Gupta (1988) have suggested subduction of the Indian plate below Burmese arc, which extends up to 180km deep below the central lowlands east of the Arakan-Yomas. Figure 3.4 shows tectonic features and earthquake activities in the Indo-Burman Fold Belt and adjoining regions.

In this fold belt, a different rate of subduction of the Indian Plate may be occurring, depending on the tectonic settings (Mukhopadhyay and Dasgupta, 1988). Chen and Molnar (1990) document a NNE-SSW regional compression within the subducted Indian Plate and most of the earthquakes are occurring only within the Indian Plate. Strike-slip fault mechanism probably indicate that the northward movement of Indian Plate still continues to drag its east-dipping slab beneath the Indo-Burman ranges northward through the asthenosphere. Moreover, northward translation of Indian Plate is largely accommodated by strike-slip movement along the Sagaing Fault (Le Dain et al., 1984). Dasgupta et al. (2003) suggests definite variations in the subduction zone geometry along and across the arc affected by several transverse faults dissecting the subducting lithosphere. According to Biswas and Dasgupta (1986), extensional stress was in NW-SE direction in Manipur-Burma region with shallow focus earthquakes revealing normal faulting as a major element in this region. But, Molnar et al. (1973), Chandra (1975) and Verma et al. (1980) have suggested earthquakes with normal as well as thrust-type faulting in this region. From fault mechanism solutions for earthquakes below the Tripura Fold Belt, Mukhopadhyay and Dasgupta (1988) have observed E-W compression along the N-S faulting.

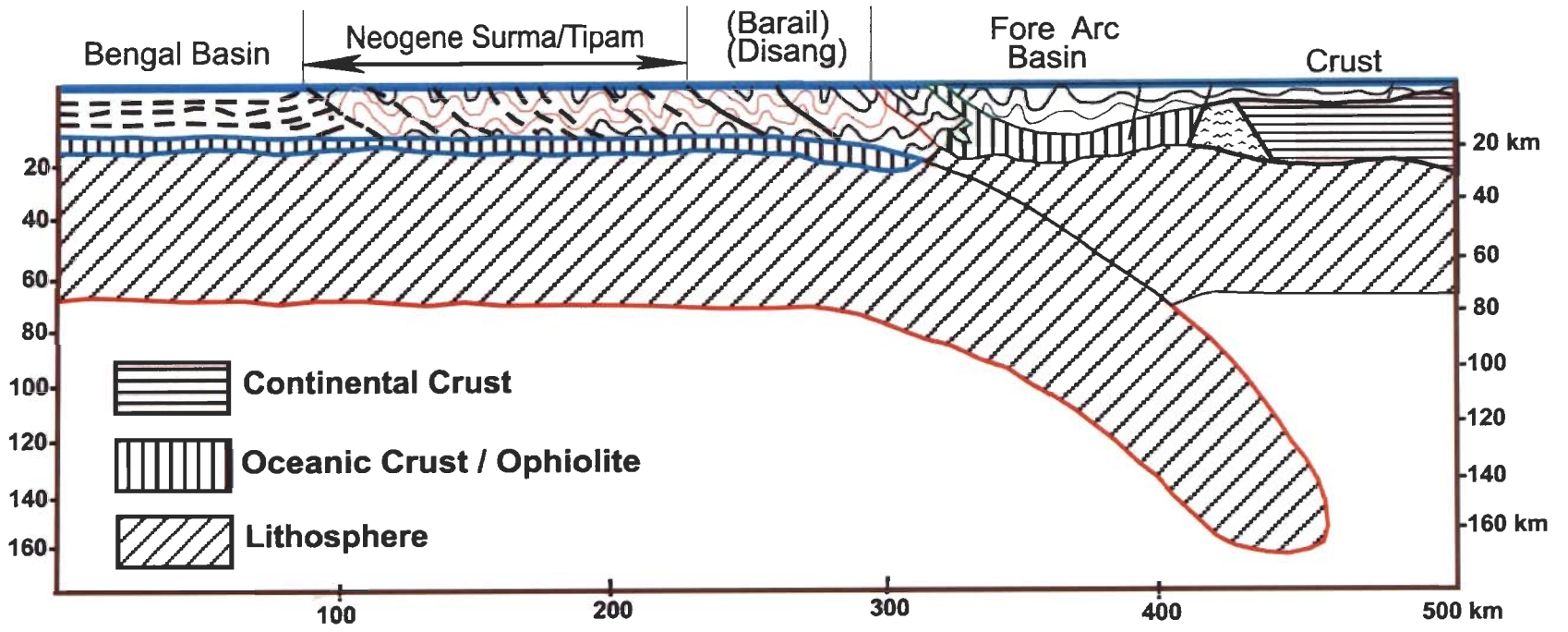

Figure 3.3 Structural set up of the Surma Basin in the plate tectonic perspective. (Source: Nandy, 2001)

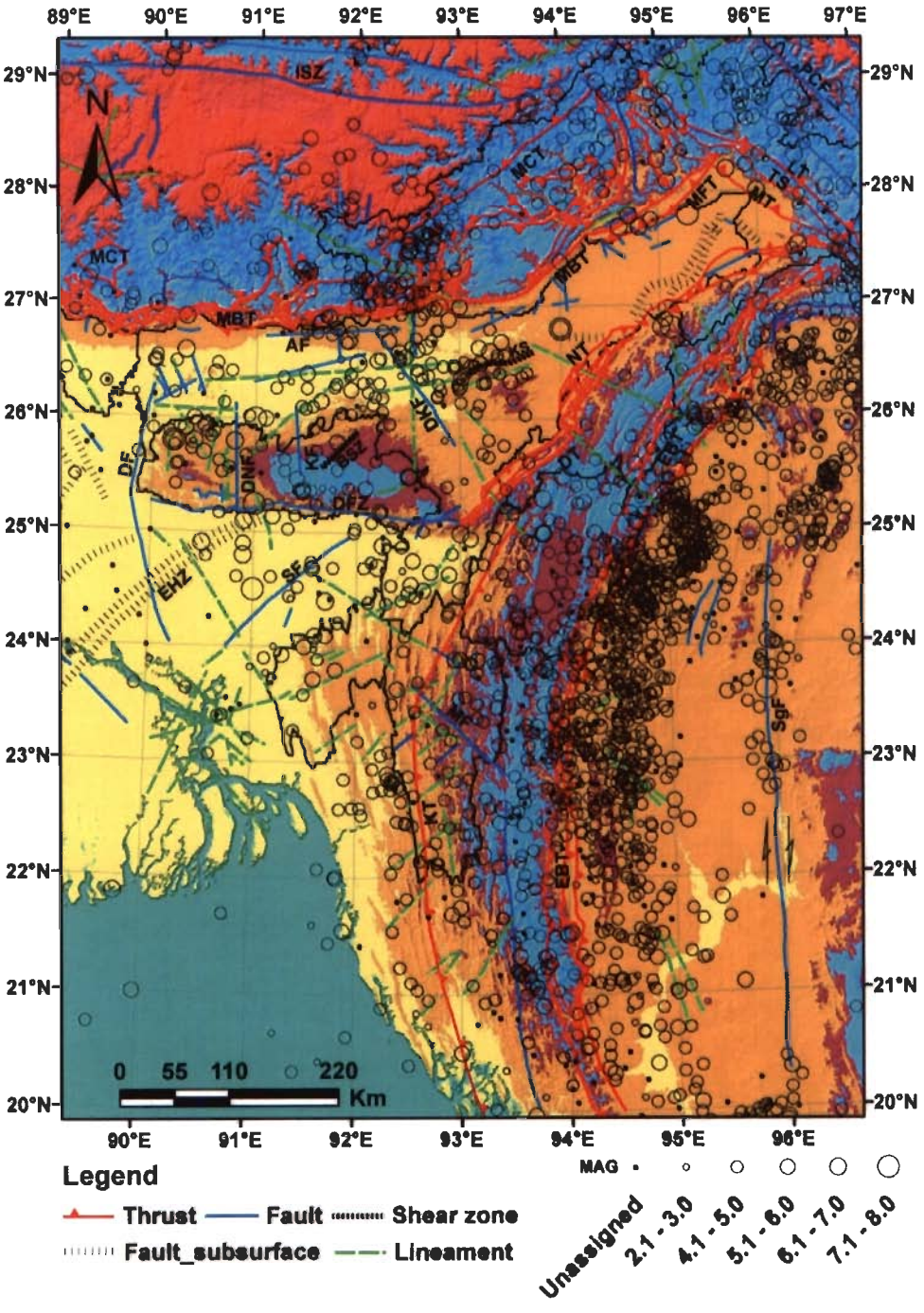

Figure 3.4 Seismotectonic set up of the frontal Indo-Buraman fold belt and adjoining regions shown on color coded shaded relief model of GTOPO DEM. MCT- Main Central Thrust, MBT-Main Boundary Thrust, MFT-Main Frontal Thrust, AF-Atherkheit Fault, KS-Kalyani Shear, DKF-Dhansiri Kopili Fault, NT-Naga Thrust, DT-Disang Thrust, DFZ-Dauki Fault Zone, BS-Barapani Shear, KF-Kulsi Fault, DNF-Dudhnoi Fault, DHF-Dhubri Fault, EHZ-Eocene Hinge Zone, MF-Mat Fault, KT-Kaladan Thrust, EBT-Eastern Boundary Fault, SgF-Sagaing Fault. Earthquakes data (source USGS) plotted from 1737-2010 belonging to all magnitude range. Tectonic features are taken from Seismotectonic Atlas of India and its Environs (GSI, 2000).

CHAPTER-IV

Fold morphology and river channel change detection

4.1 Introduction

The frontal Indo-Burman fold belt is formed by several elongated folds revealing a significant structural pattern. This pattern has been analyzed using satellite images and digital elevation models (DEMs) and discussed in this chapter. In a tectonically affected region the formation of folds, faults and basins are the manifestation of deformation processes that the area has undergone. Under the operating tectonic activities the region is supposed to undergo deformational changes which may either be rapid, fast, slow and gradual. Morphometric indices of such a region can play an important role in indicating changes, if any, which occurred silently. Areas of major fold deformation and cases of fault propagation folding have been studied on the basis of fold geometry and morphology.

Further, any region experiencing tectonic deformation should affect the river channel as the rivers response is very prompt to such action. In view of this, a detailed channel pattern analysis of the Barak, Kushiara, Surma rivers including Barak river tributaries have been carried out and are also discussed in this chapter. Anomalous pattern of the river channel at different places were examined to study the channel shift through temporal analysis.

4.2 Folding and Faulting

The frontal Indo-Burman fold belt comprises of a series of north–south-trending westerly convexing curvilinear anticlines and synclines representing a fold-and-thrust belt (Figure 4.1). Folding of rocks extended westward for maximum distance up to the

longitude 91°N and the geometry of the fold appear to have undergone rotational movements which can especially be seen in case of Sylhet anticline and the folds in the northern part of Barak river basin. In the Surma Basin intensity of folding increased eastward and low amplitude folds in the western part exhibit interesting pattern. Smaller anticlines have developed on the western part and large linear periclinal folds as long as 200km in length formed in the central Mizoram (Nandy, 2001). Some anticlines bifurcate to form two anticlinal ridges and at some place these merge again to enclose an elliptical or cuspate synclinal valley. Sharp crested and disharmonic folds are commonly present in the area. Overturned, recumbent, box folds and also parallel concentric folds are present.

The folded belt has suffered compressional stress resulting in development of thrusts/faults. The anticlines of this basin have been affected by longitudinal faults either on one or both flanks. Near the surface these faults are steep and flatten with depth and gently sloping faults are also present near the surface (Nandy, 2001). It is suggested that the anticlinal structures which are hybrid and superposed in character have developed on the folded detachment due to the combined effects of buckling and fault propagation (Sikder and Alam, 2003). Due to the propagation of thrust progressive tightening of the fold hinge occurs and front limb becomes steeper (Mitra, 1990). Structural information from seismic sections indicate presence of a zone of folded detachment or decollement which developed due to the east-west directed tectonic compression of under-compacted pressured shale sequence involving thin skinned tectonics (Sikder and Alam, 2003). In such a case the surface folding becomes non-representative of the deeper structures (Prost, 1990). The folded sedimentary layers have been segmented by cross faults and conjugate oblique faults through later phases of deformations. Some of these faults have strike slip components and are responsible for offsetting the anticlinal axes and flank fault. The eastern part of the basin is far more complicated than the southern and western portions. The relief and complexity of folding strata increases towards the east. Figure 4.1 is showing the ridge traces of major anticlinal and synclinal structures extracted from ASTER-DEM and IRS PAN-D Images. A normal anticlinal-synclinal pattern is found in the western part but towards east the intermingling of ridges has occurred. Consequently, the structures of the eastern part are tightly folded, faulted and thrusted with narrower synclines between them.

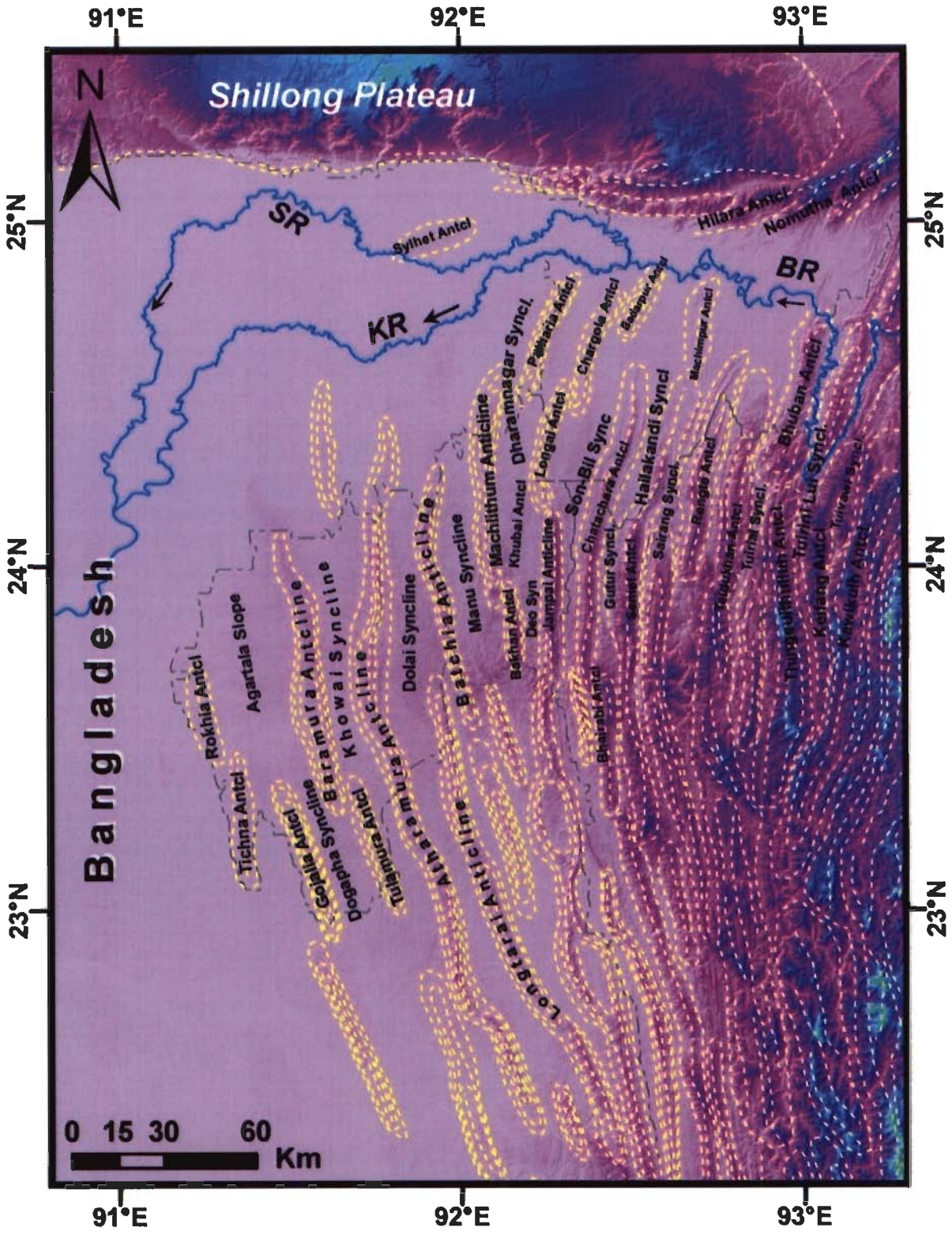

Figure 4.1 Folded Surma Basin and part of Indo-Burman fold belt as shown by color coded shaded relief model of ASTER-DEM along with ridge traces and nomenclatures for anticlines (antcl) and synclines (syncl). BR-Barak River, SR-Surma River, KR-Kushiara River.

4.3 Areas of major deformation

4.3.1 Fault propagation folding

The anticlines of Surma Basin are affected by faulting and thrusting at various places and fault propagation folding could be observed at several places. Fault-propagation folds form at the tip of a thrust fault where propagation along the decollement has ceased but displacement on the thrust behind the fault tip is continuing. The continuing displacement is accommodated by formation of an asymmetric anticline-syncline fold pair. As displacement continues the thrust tip starts to propagate along the axis of the syncline. When the folded belt is examined carefully integrating satellite images and digital elevation models a few cases of fault propagation folding could be identified and delineated. Bhuban anticlinal hill located on the east of Barak river valley shows the fault propagation folding prominently in northern side and to some extent in the southern side also. Figure 4.2 shows a few cases of fault propagation folding in Rengte anticline near the Kolasib area, Chatachara and Serkhan anticlines in the central part of Surma Basin and Kalanaga anticline in the NE of Bhuban anticlinal hill.

4.3.2 River responses

Generally, the river's response to operating tectonic activity is very prompt and even the mild tectonic deformation can be recorded by the stream behavior and pattern. In the Surma Basin many anticlial ridges are affected by transverse faulting. At several places incidence of river crossing the ridges following the faulted part have been identified and marked. Further, severe deflection and turn in river course could also be observed. For example, the Barak river takes a hair pin bend near Tipaimukh by changing its southward flow into northward flow (Figure 4.3A). Similarly the Barak river also crosses two anticlinal ridges at the locations near Doltang and Senvon (Figures 4.3B and C). Another river the Tlabung flowing in the western part of Surma Basin also crosses three different anticlinal ridges near Lungsen, Lungei, and Barkal regions through transverse fault zones (Figures 4.4A, B and C). In the central part of Surma Basin Deo river also crosses three different anticlinal ridges in areas near the Marpara, Kumarghat and Kukichara (Figures 4.5A, B and C). Such effect of anticlinal ridge crossing by the rivers in

case of western Tripura region, Gomti, Khowai and Dhaleshwari also has been identified and are discussed in Chapter 5.

4.4 Tectonic constraints on fold geometry

Geometry and morphology of the folds are very prominently displayed on satellite images especially in case of large scale folds. In the study area outcrop of anticlines and synclines of different length, width and shape are exposed that appears to be simple folds. But, studying these features on satellite images makes it possible to pull out interesting geometry. Several areas of interest (Figure 4.6) exhibiting specific folding pattern have been selected for detailed studies. These fold patterns have been studied in view of their arrangement, geometry and morphology using DEM, satellite images, image processing and GIS technique. Also this study helped in revealing the nature of deformation that the area has experienced.

4.5 Image processing

4.5.1 Principal Component Analysis (PCA): This technique is useful for image data spectral compression, image enhancement, change detection and image fusion. In this process all of the information contained in an original n-band data set gets compressed into fewer new bands or components. Statistical process of PCA transforms a multivariate data set of inter-correlated variables into a data set of new un-correlated linear combinations of the original variables. The PCA images then become linearly uncorrelated with other because these n-components are orthogonal. The total variance of original images is mapped into new components. The first principal component (PC1) has the greatest percentage of the total variance and succeeding components (PC2, PC3, ... PCn) each contains a decreasing percentage of the total variance. In this study PCA has been carried out using image processing software in following steps; first all the Landsat ETM+ bands (except thermal ones) were stacked forming an input file for PCA, and then multilayer output containing PC elements were generated. Bright and different color coding than the FCC (False Colour Composite) image makes the ridges and surrounding features more contrasting.

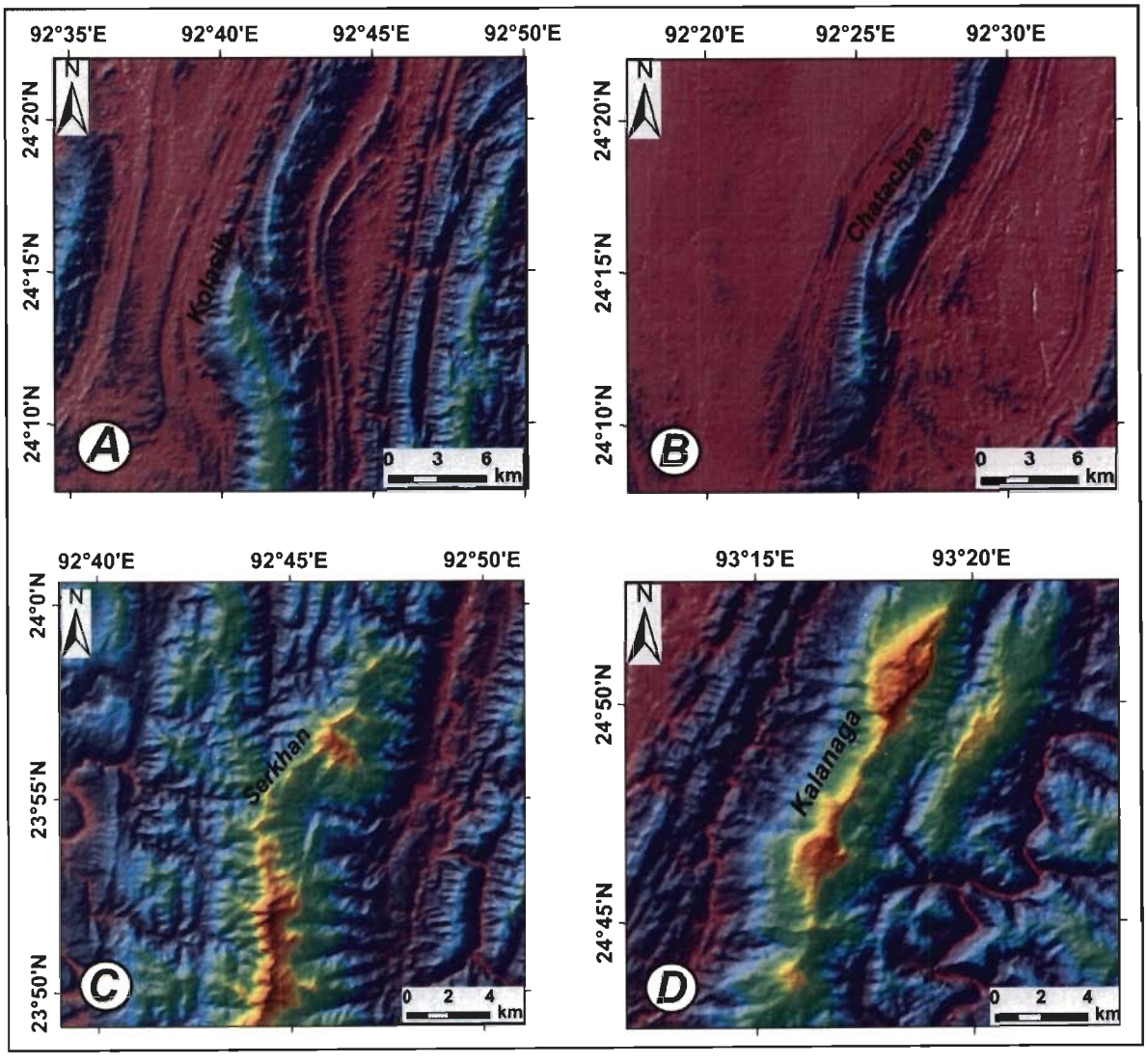

Figure 4.2 Fault propagation folding in Rengte (A), Chatachara (B) Serkhan (C) and Kalanaga areas (D) shown on color coded shaded relief model of ASTER-DEM.

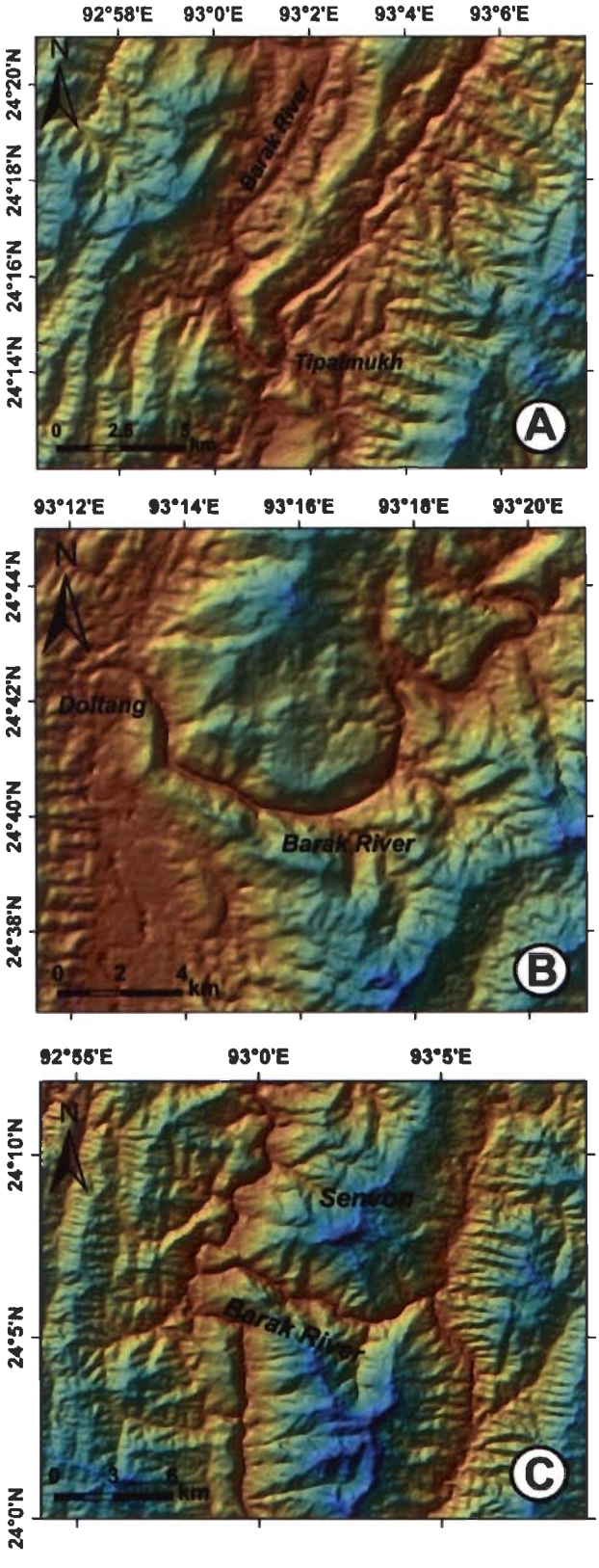

Figure 4.3 Barak river showing hair pin bend (A), and crossing the anticlinal ridges (B and C). Terrain is shown by color coded shaded relief model of ASTER-DEM.

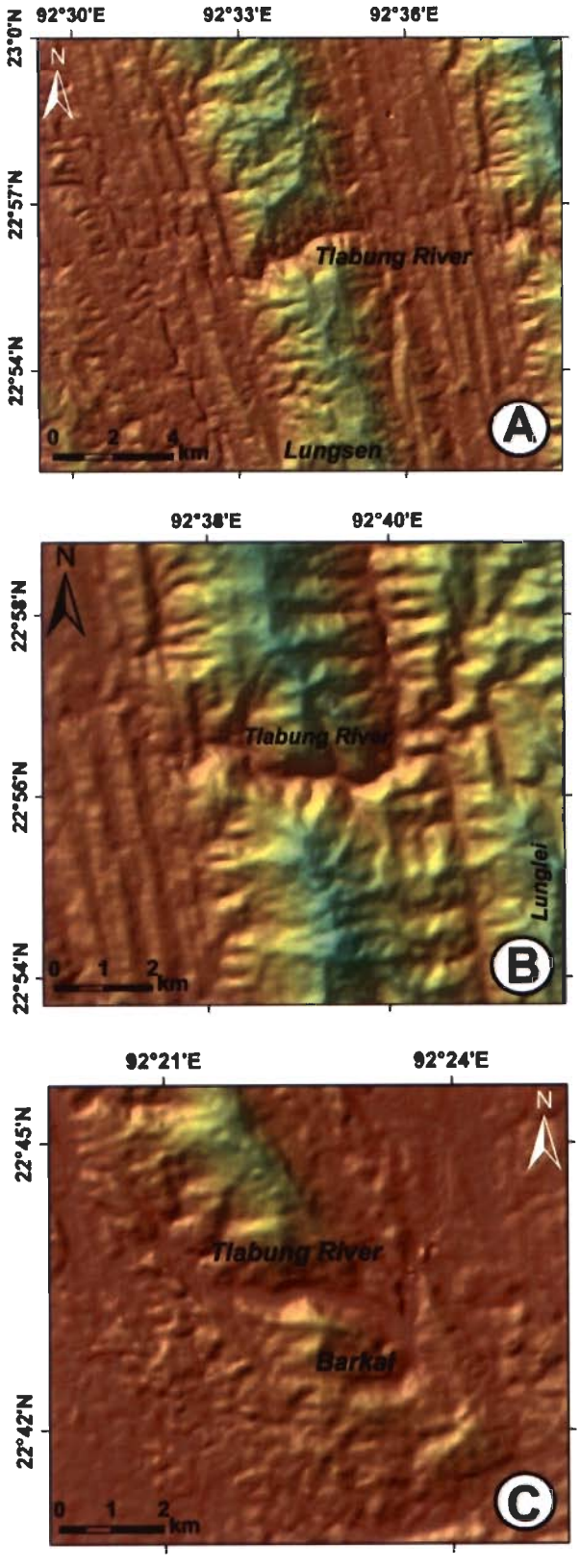

Figure 4.4 Tlabung river crossing the anticlinal ridges (A, B and C) at different locations. Terrain is shown by color coded shaded relief model of ASTER-DEM.

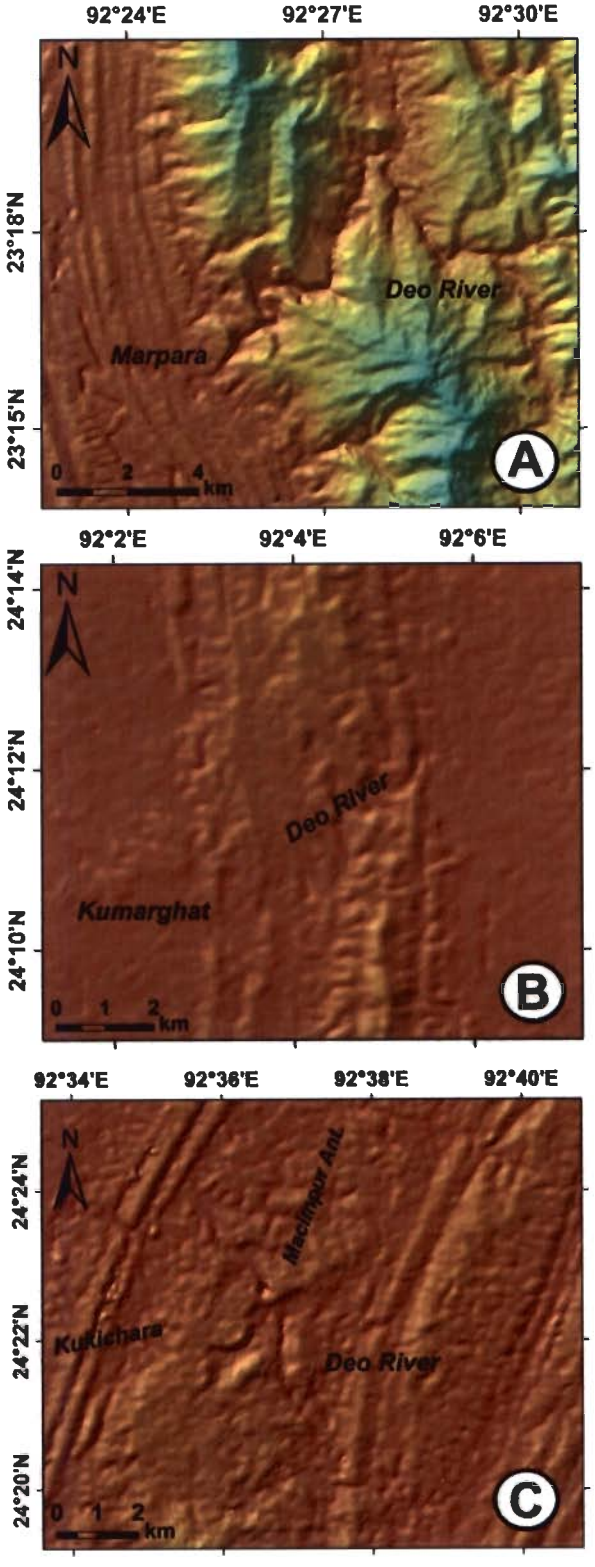

Figure 4.5 Deo river crossing the anticlinal ridges (A, B and C) at different locations. Terrain is shown by color coded shaded relief model of ASTER-DEM.

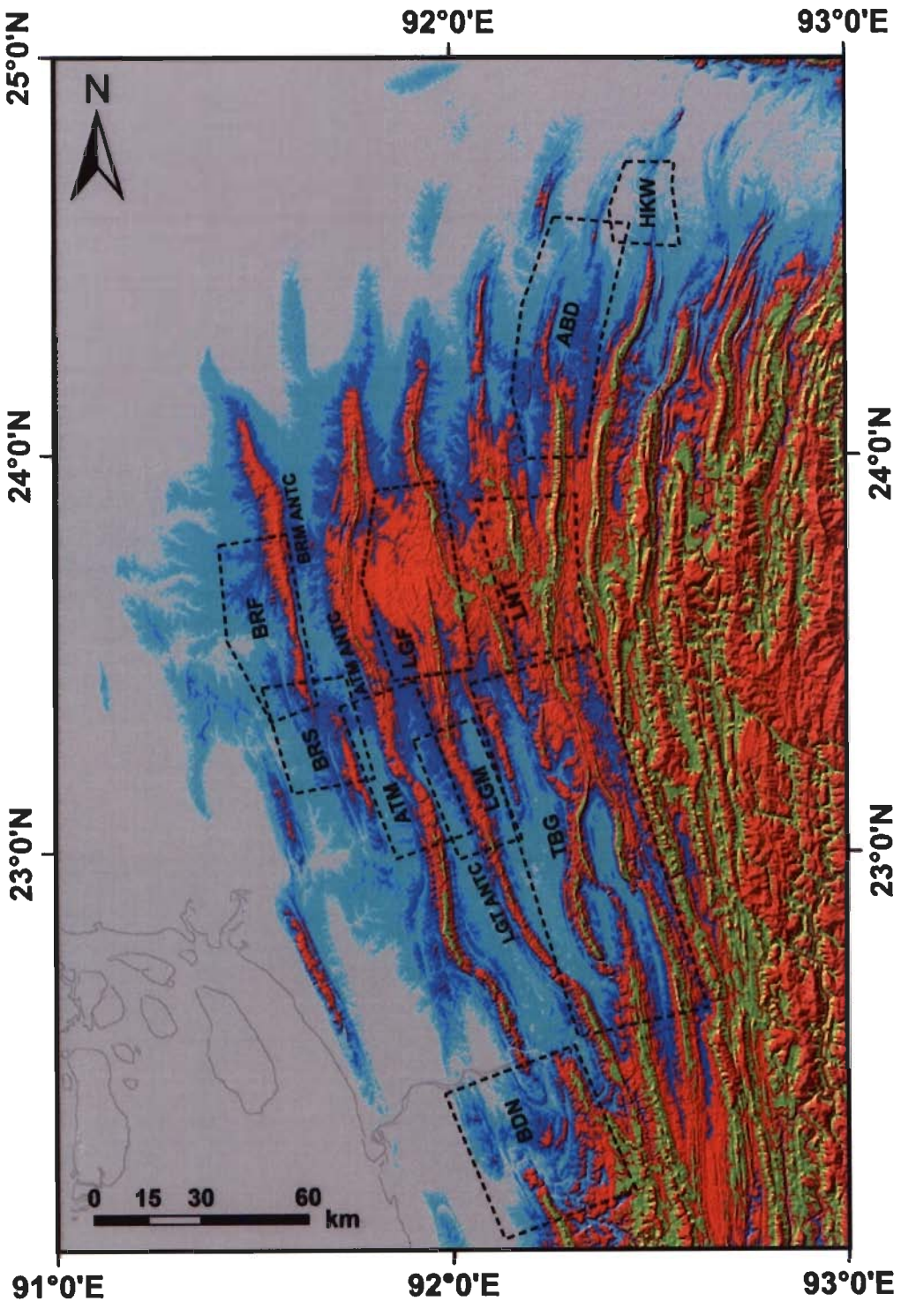

Figure 4.6 Colour coded shaded relief model of 90m-SRTM-DEM of the study area showing N-S trending linear fold ridges with westward curvature. ATM-ANTC-Atharamura Anticline, BRM-ANTC-Baramura Anticline, LGT-ANTC-Langtarat Anticline, HKW-Hailakandi-west overlap, ABD-Abdullapur overlap, BRF-Baramura west limb fault, LGF-Langtarat west limb fault, BRS-Baramura south overlap ATM-Atharamura Middle, LGM-Langtarat Middle, TBG-Tuibangadam synclines, BDN-Bandarban Nose.

4.5.2 Image fusion: For improved visual and effective image interpretation multi sensor data are integrated and this technique has been used successfully by Cliche et al. 1985; Welch and Ehlers 1987; Chavez et al 1991; Pohl and Van Genderen 1998; Saraf, 1999; Zang 1999. Data fusion is the combination of multi sensor data which have different characteristics such as spatial, spectral and radiometric to acquire high quality image. Low and high resolution merged images are applicable for many remote sensing applications such as geology, topographic mapping, land cover and land use mapping etc.

Several techniques are available to combine images from different sensors however, in this study the image fusion techniques has been used which preserve spectral characteristics whilst increasing spatial resolution to provide images of greater quality. Landsat ETM+ FCC (bands 4 to red, 3 to green and 2 to blue) and Landsat PAN data were fused by employing Modified Intensity Hue Saturation merge technique. Bilinear interpolation resampling technique has been chosen for this purpose. Although, other techniques viz. Principal Component, Brovery Transform, Multiplicative, etc for fusing multisensor data are available it is found that IHS technique is most suitable for the set of data used in this work.

4.6 Geometry and geomorphology of folds

Satellite images and DEM of the study area exhibit outcrops of doubly plunging anticlines and synclines having different pattern, shape, size and arrangements. Generally, anticlines are forming linear higher ridges having well defined geometry exhibiting the effect of deformational processes that the region has experienced. Top layers of the anticlinal folds have been removed due to erosional processes of natural agents exposing fold limbs and plunging noses which are identifiable on satellite images. Fold limbs belonging to either anticline or syncline are recognized based on nature of erosional surfaces, geometrical arrangement, the nature of exposed elongated beds and the bedding arrangement pattern as displayed on satellite images (Figure 4.7). It is observed that some features such as extent and size and bulged out limbs of folds are better depicted on DEM than FCC. For the purpose of detailed analysis, some areas with

interesting geomorphological features have been selected. Areas of interest have been picked up from 90m-SRTM-DEM, PC-FCC (FCC generated using first three PC elements of Landsat ETM+ bands) and FCC-PAN merged (FCC generated from Landsat ETM+ bands 4, 3 & 2 fused with Landsat PAN) and several subsets were prepared. Nature of all the features became more obvious on satellite images enabling for better visual interpretation. It is also noted that false topographic perception plays a role when viewed the features on image (Saraf et al., 1996) and in order to nullify this effect images were rotated suitably.

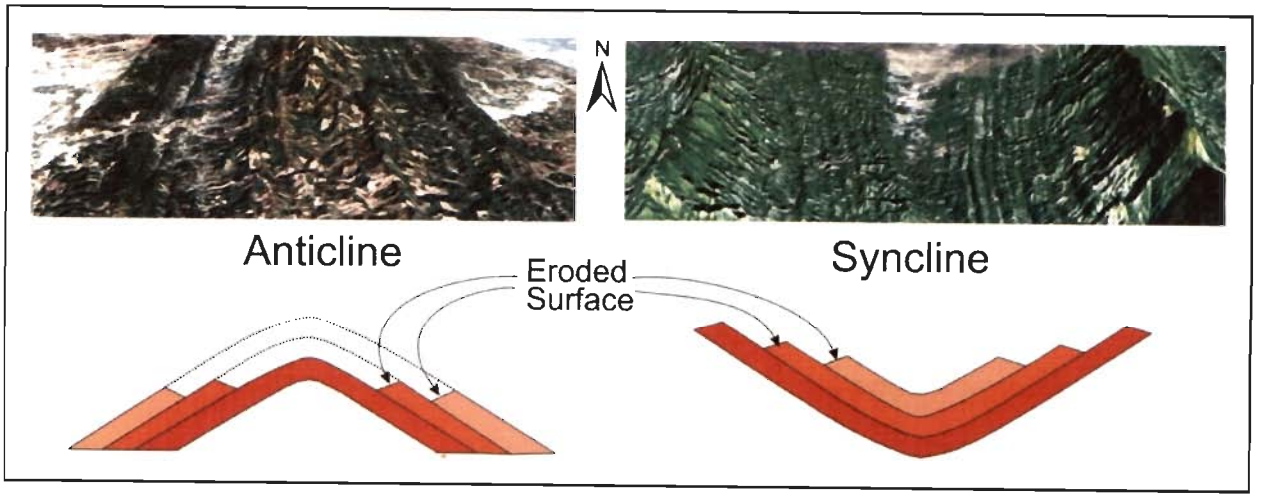

Figure 4.7 Arrangement of anticlinal and synclinal bedding. Upper pictures are satellite images (grabbed from Google Earth) show the 3D perspective view of bedding arrangement in case of anticline and syncline. Nature of eroded bedding surfaces is marked in the lower sketches.

Prominent westernmost individual anticlinal ridges encountered are Baramura, Atharamura, Langtarat etc. (Figure 4.6). All these anticlines occur partly in Bangladesh and Northeast India (Tripura). The Baramura anticline is a doubly plunging anticline with curved fold axis and bulged out western fold limbs and westward bending in the northern part. This anticline extends for about 94km with maximum width 245m and maximum bulge in the anticline occurs at latitude 28°35′ with a water gap through which a river cross over the anticline transversely. The westward bend in the upper part of this anticline is probably due to transverse faulting. The Atharamura and Langtarat anticlines appear as

single continuous long fold ridge with several longitudinal curves and bends with overall westward curvature. But, closer examination reveals that these anticlines are constituted by three doubly plunging anticlines. However, these anticlines are bordered by the outer continuous sedimentary layers providing continuity of the fold ridge. The southernmost part of Atharamura anticline possessing the clearer exposure of plunging nose exposing maximum number of detectable folded layers. The length and maximum width of the northernmost, middle and southern Atharamura anticlines are about 112km, 53km, 36km and 400m, 490m, 405m respectively. Whereas, the length and maximum width of the northernmost, middle and southern Langtarat anticlines are 54km, 62km, 35km and 315m, 320m, 550m respectively.

4.6.1 Plunging anticlines

A few cases of plunging fold noses delineated based on geometry and bedding arrangement are presented in this section. These are Atharamura-middle (ATM of figure 4.6) and Langtarat-middle (LGM of figure 4.6). It may be seen that in all these cases the outermost sedimentary layer shows continuity however, the inner layers become rounded to form closers. The upper plunging fold nose of the Atharamura middle part are more prominent on color coded DEM and FCC-PAN (Figures 4.8a and c). Although both the fold noses have same trend slight bending (towards each other) occurred in the linked region. The Langtarat middle part although show quite smooth continuity of the fold but, the upper and lower plunging fold noses are very prominent and distinct in all the three images (Figures 4.9a, b & c).

4.6.2 Faulted anticlines

It is to be observed that the western limb of the Baramura anticline bulges out (BRF of figure 4.6) considerably as shown in Figure 4.10. Several limbs, at least four, show bulging with maximum effect on the outer limb which could have happened due to the faulting. A gravity/growth faulting along the western limb (F_L in figure 4.10b) can cause such lateral bulging. Due to westward down throw mechanism, the limbs moved away causing the bulging effect. Substantial gap has also been created between the

limbs and a linear river valley has developed along the contact of two fold limbs. At this place the fold ridge also faulted transversely (F_T in figure 4.10b) creating first a gap through which a river could cross over. These effects are especially very clearly seen in figures 4.10b and c. Another example of such fault affected western limb and bulging can be seen in the north Langtarat anticline (Figure 4.11) located just east of the Baramura anticline bulge across the Atharamura anticline (LGF of figure 4.6). Westward bulging effect can be seen very clearly on DEM (Figure 4.11a) which happened due to similar faulting effect as described above. Several limbs are involved in this process which got bulged out for about 9km. It may be seen that due to this bulging the Atharamura anticline became curved westward to accommodate the expansion. These bulged out limbs got terminated against another adjacent anticline to the northeast. This morphology is the result of faulting and further deformation.

4.6.3 Enechelon anticlines

There are several instances of en-echelon (overlapping) anticlines occurring in the study area (Figures 4.12 - 4.15). Intricate overlaps are seen at two places i.e. Abdullapur (ABD) and Hailakandi-west (HKW). In the overlapping part of HKW, the limbs of the upper and lower anticlines got pressed against each other so much that the limbs got merged (Figure 4.12). The western side limbs (four) of the lower anticline show the continuity after a kink at the overlapping part. This might have caused by reverse faulting as marked in figure and subsequent movement.

Baramura-south anticlinal overlap (BRS of figure 4.6) shows a simple contact with slight compression on the limbs of eastern anticline (Figure 4.13). However, it appears that the folds contact is affected by faulting. In case of Abdullapur overlap three anticlines are involved (Figure 4.14). The fold nose of the southern Jampai Anticline (JA) pressed against the middle anticline. But, it may be observed that the northernmost anticline extends much southward although it appears not to be. The eastern middle ridge although exhibit outcrop of bedding but the complete geometry is not preserved (Figure 4.13). In another case (down south of the area in figure 4.15) the specific arrangement of the anticlinal ridges (LNT of figure 4.6) gave appearance of fork shape (Figure 4.15). The

anticlines involved in this are Jampai Anticline (JA) and Bakhan Anticline (BA). In fact the Jampai anticline has got faulted transversely in the area marked by F_T and shifted diagonally (Figure 4.15b). Whereas, the western anticline is individual one but placed closer to the JA.

4.6.4 Cuspate and elliptical geometry

A very interesting feature developed in the study area due to specific arrangement of the anticlines (TBG of figure 4.6) is cuspate and elliptical geometry (Figures 4.16 and 4.17). It may be seen that the southern part of Jampai anticline (marked as JA in figure 4.16b) gets bifurcated into two sided limbs (EL1 & WL1) at geographical coordinates 23°22′N and 92°15′E and again reunites at 23°07′N and 92°19′E to form an elliptical syncline (about 25 km long with maximum width about 8.5 km, marked as ES in figure 4.16b) occupied by harder rocks with circular exposures. Just at the lower east side of the elliptical valley the eastern limbs again bifurcate into two sided limbs (EL2 & WL2) giving rise to a cuspate shaped syncline (about 26km long with maximum width 10 km, marked as CS in figure 4.16). The cuspate valley is bounded by very high ridges with very steep inner slopes which should have formed due to reverse faulting and during this process the eastern limbs upthrusted along the side of the syncline (Figure 4.17). The west bounding ridge of the cuspate valley extends up to a river whereas, the anticlinal limbs on the eastern side continue further south. Another minor elliptical valley bounded by the curved anticline on the west could be seen formed to the southwest of the cuspate valley. This specific configuration could have resulted due to fault related folding and later stage of deformation processes. The morphological trends of folded beds formed around the elliptical and cuspate synclines and cross profile of cuspate syncline are shown by sketch (Figure 4.17). The sections C-C′ across the cuspate syncline shows the transverse topography revealing the high ridge and steep inner slopes (elevation information has been derived from DEM using topographic profiles).

4.6.5 Anticlinal co-noses

Anticlinal plunging co-noses (BDN of figure 4.6) occur at the southernmost tip of the Atharamura Anticline (AASN). In this area, referred to as Bandarban (a place in Bangladesh), one wide fold nose (marked as BFN) and three other fold noses can be seen (Figure 4.18). These folds are NNW-SSW trending fold ridges with one very wide fold nose which is partially preserved. The wide nose represents early stage of open anticline. During the later stage of deformation other anticline has developed at the core of wide anticline with slight westward axial shift. The anticlines marked as AASN and BFN are not same as the fold axes are different having different fold geometry. A sketch (Figure 4.18d) shows the morphology of the folds. This sketch has been prepared after rotating the image by 180° for the purpose of better conceiving of the feature.

Some of the plunging noses of anticlinal folds show several folded limbs that are preserved. From the weathered outcrop of the anticline closer to the low plunging nose it is possible to identify on the satellite image, the number of sedimentary layers those got eroded away. In case of one such anticline (marked as AASN in Figure 4.18) having its bedding (weathered) geometry well preserved that are well recorded on satellite image (Figure 4.18e). In all, eight (8) bedding layers could be identified. Nature of the some plunged folded layers is shown by a sketch which is rotated for 180° (Figures 4.18d-f). Length of this particular anticline is about 35km having central width of 7.32km with maximum elevation of about 400 meter.

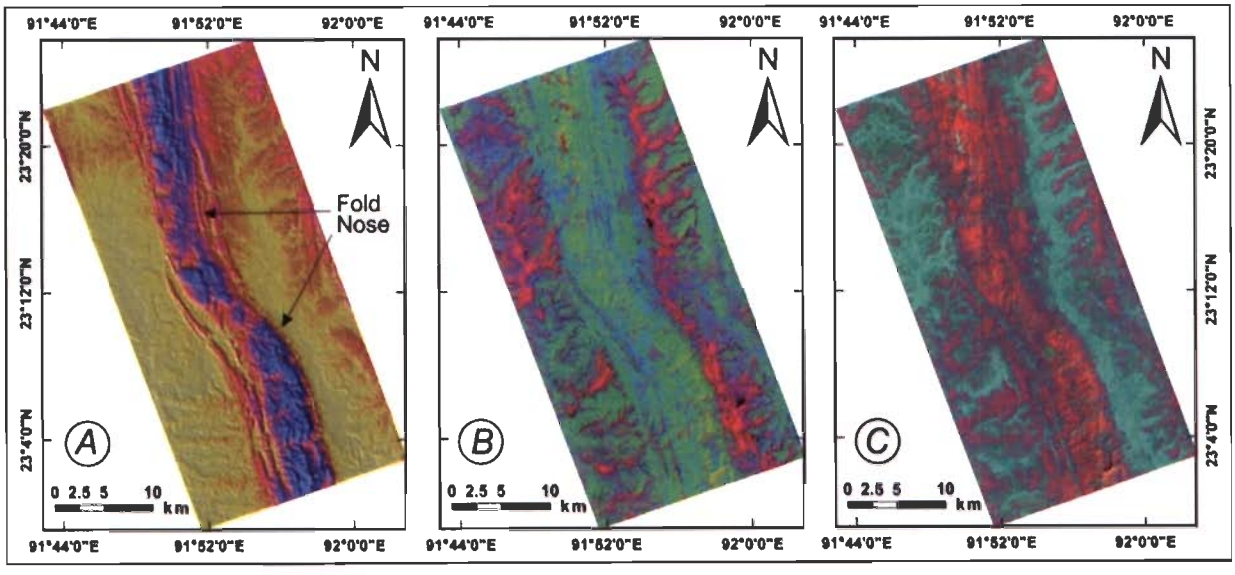

Figure 4.8 Plunging middle Atharamura anticline noses (ATM in Figure 4.6). (a) 90m-SRTM-DEM (colour coded shaded relief model), (b) FCC of first three principal component images obtained from Landsat ETM+ multi band data, (c) Fused Landsat ETM+ FCC (bands 4, 3 & 2 as R, G, B) and Landsat PAN image.

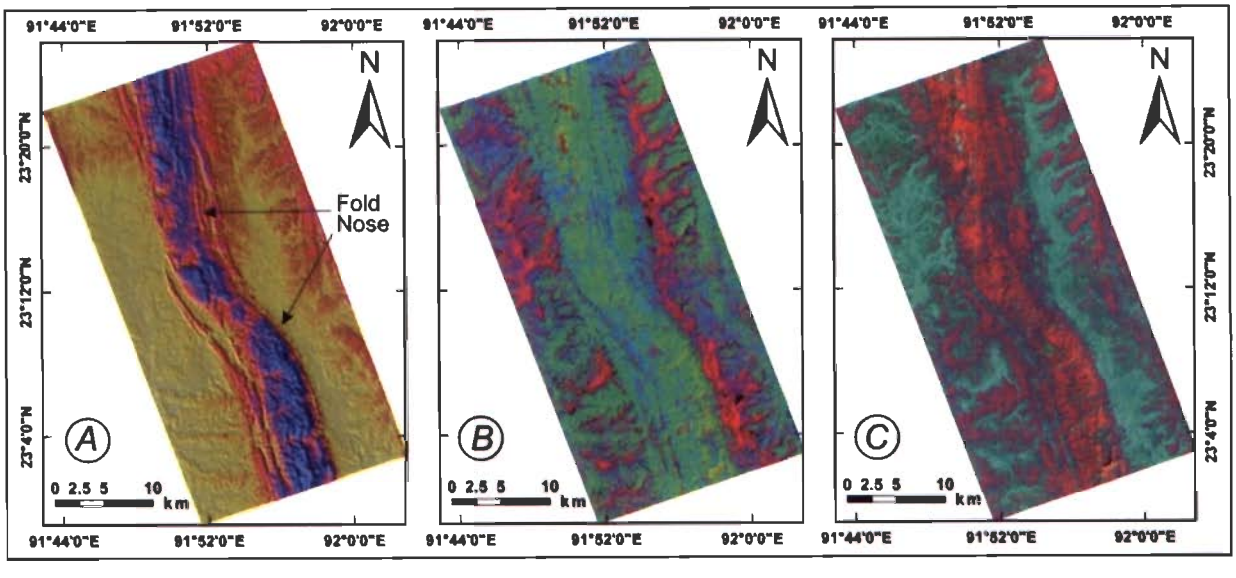

Figure 4.9 Plunging middle Langtarat anticline noses (LGM in figure 4.6). (a) 90m-SRTM-DEM (colour coded shaded relief model), (b) FCC of first three principal component images obtained from Landsat ETM+ multi band data, (c) Fused Landsat ETM+ FCC (bands 4, 3 & 2 as R, G, B) and Landsat PAN image.

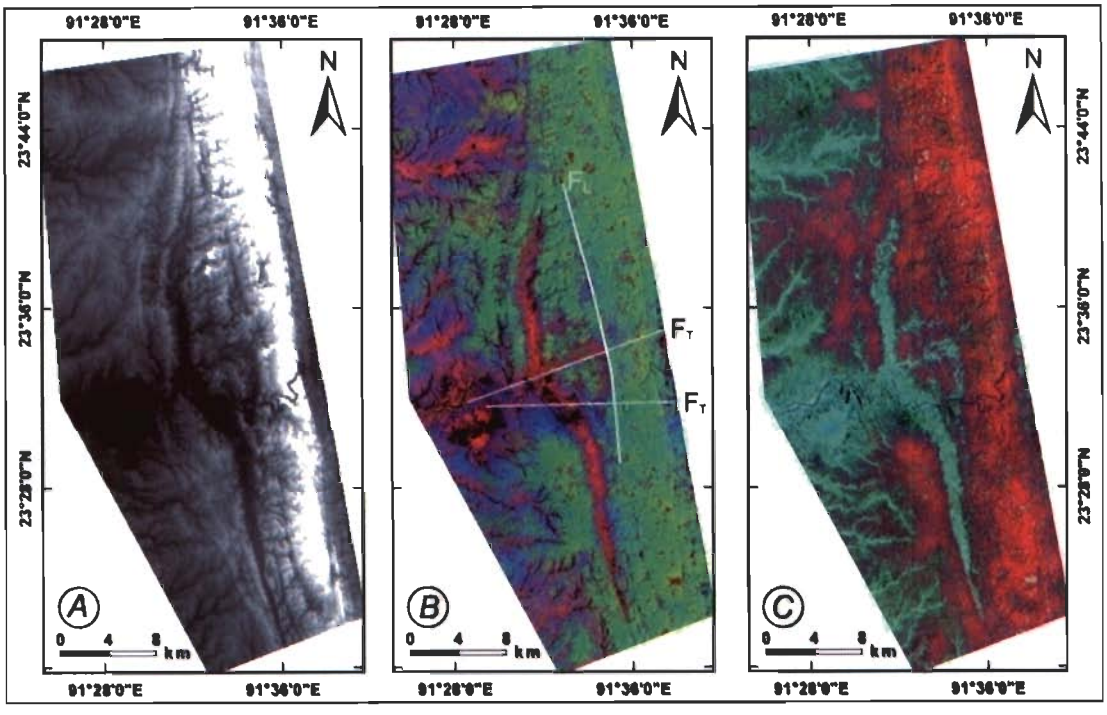

Figure 4.10 Faulted western limb of the Baramura anticline (BRF in Figure 4.6). (a) 90m-SRTM-DEM, (b) FCC of first three principal component images obtained from Landsat ETM+ multi band data, (c) Fused Landsat ETM+ FCC (bands 4, 3 & 2 as R, G, B) and Landsat PAN image. F_T and F_L are transverse and longitudinal faults.

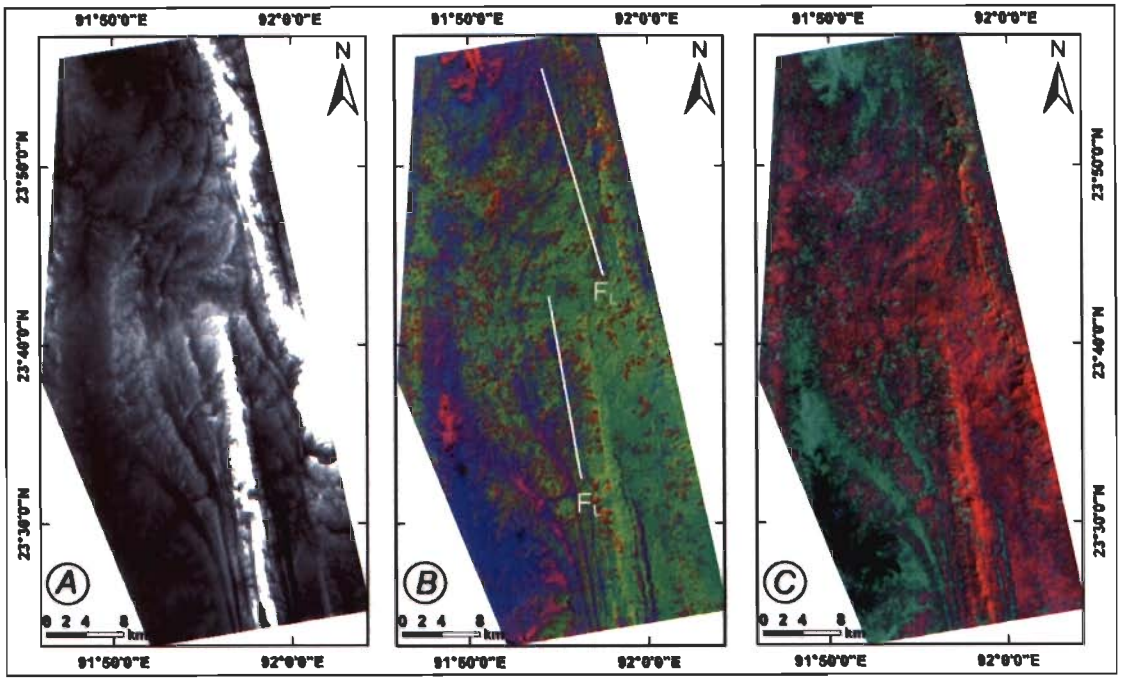

Figure 4.11 Faulted western limb of the Langtarat anticline (LGF in figure 4.6). (a) 90m-SRTM-DEM, (b) FCC of first three principal component images obtained from Landsat ETM+ multi band data, (c) Fused Landsat ETM+ FCC (bands 4, 3 & 2 as R, G, B) and Landsat PAN image. F_L –Longitudinal fault.

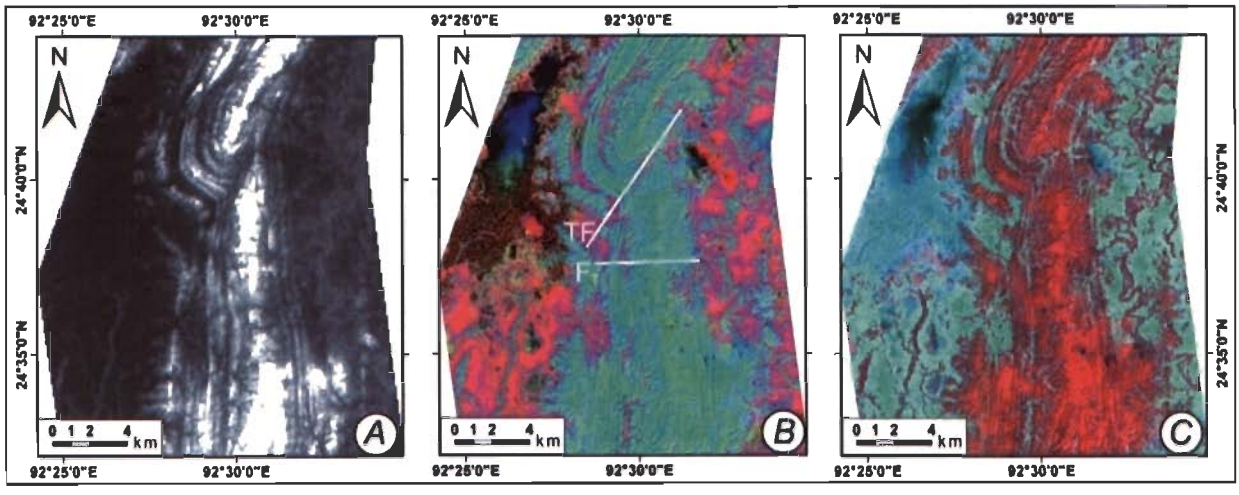

Figure 4.12 Overlapping anticlines in Hailakandi-west area (HKW in Figure 4.6). (a) 90m-SRTM-DEM, (b) FCC of first three principal component images obtained from Landsat ETM+ multi band data, (c) Fused Landsat ETM+ FCC (bands 4, 3 & 2 as R, G, B) and Landsat PAN image. TF-Thrust Fault, F_T – Transverse Fault.

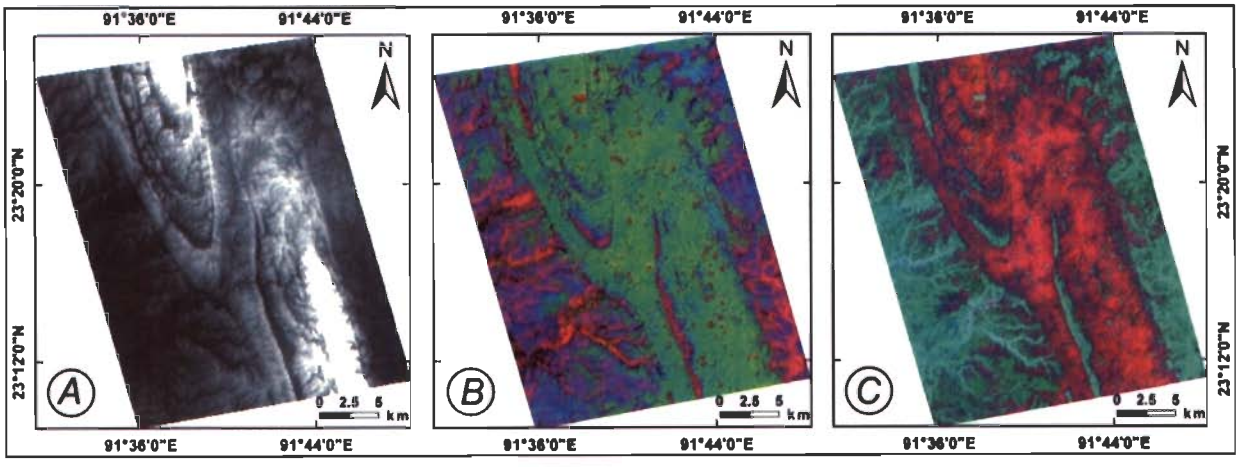

Figure 4.13 Overlapping anticlines in Baramura south anticline (BRS in Figure 4.6). (a) 90m-SRTM-DEM, (b) FCC of first three principal component images obtained from Landsat ETM+ multi band data, (c) Fused Landsat ETM+ FCC (bands 4, 3 & 2 as R, G, B) and Landsat PAN image.

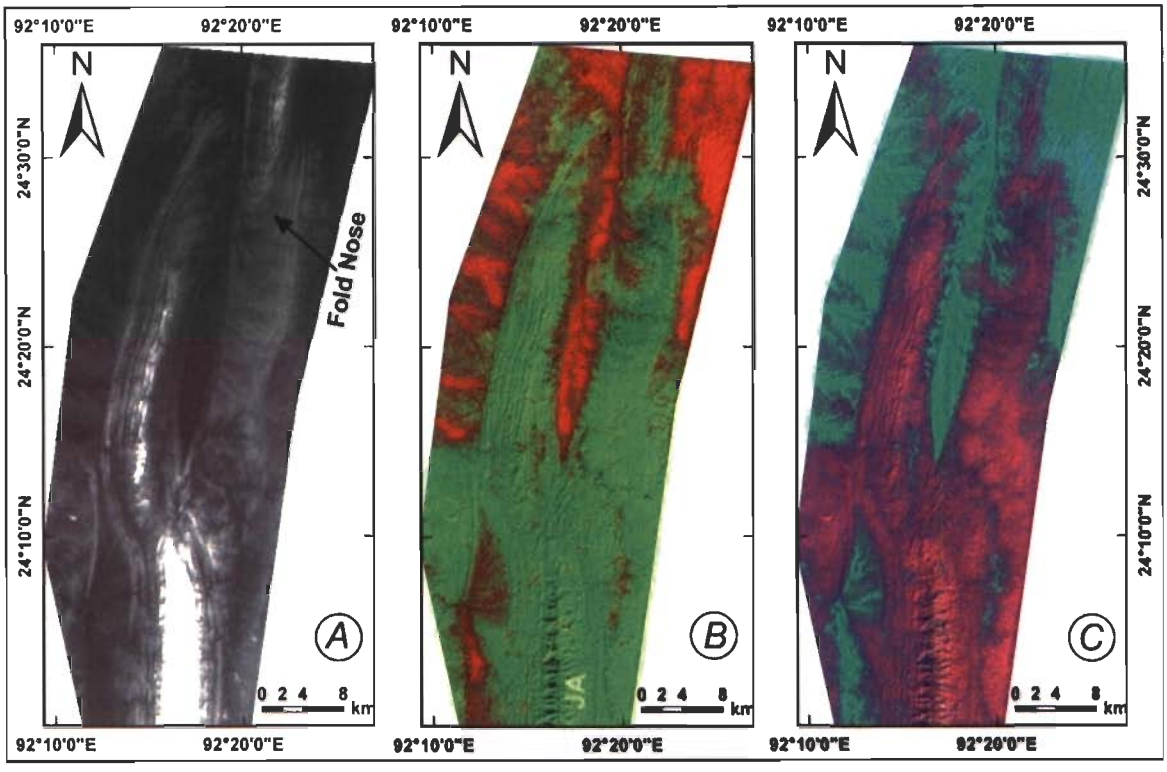

Figure 4.14 Overlapping and linked anticlines in Abdullapur area (ABD in Figure 4.6). (a) 90m-SRTM-DEM, (b) FCC of first three principal component images obtained from Landsat ETM+ multi band data, (c) Fused Landsat ETM+ FCC (bands 4, 3 & 2 as R, G, B) and Landsat PAN image. JA-Jampai Anticline.

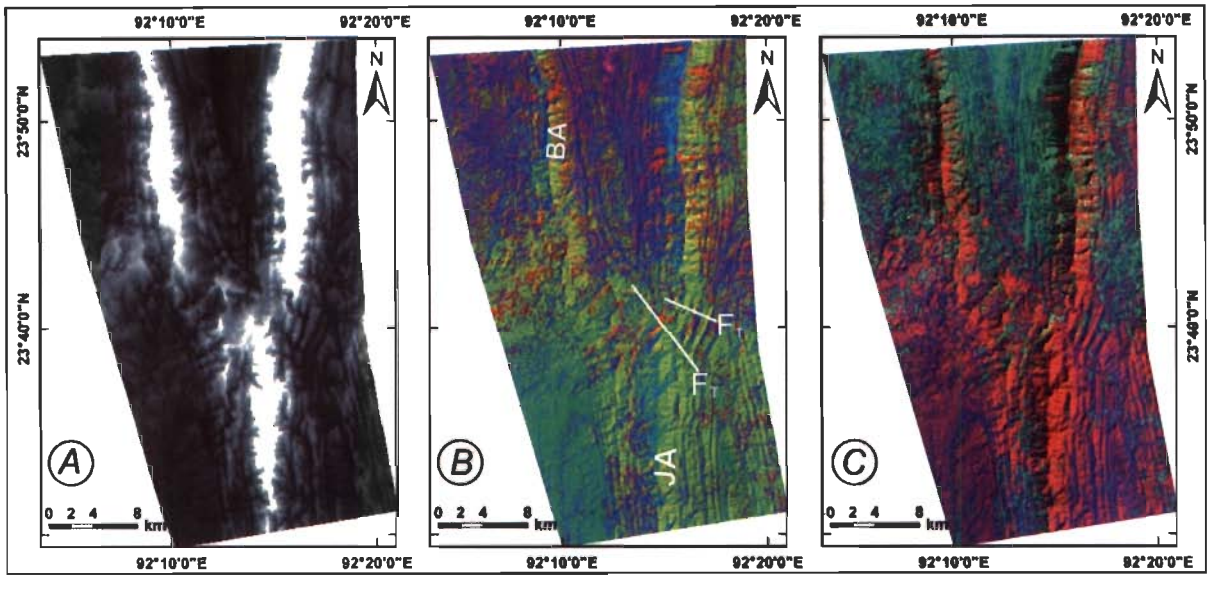

Figure 4.15 Anticlines arrangement giving appearance of fork (LNT in Figure 4.6). (a) 90m-SRTM-DEM, (b) FCC of first three principal component images obtained from Landsat ETM+ multi band data, (c) Fused Landsat ETM+ FCC (bands 4, 3 & 2 as R, G, B) and Landsat PAN image. F_T – Transverse Fault. JA-Jampai Anticline and BA-Bakhan Anticline.

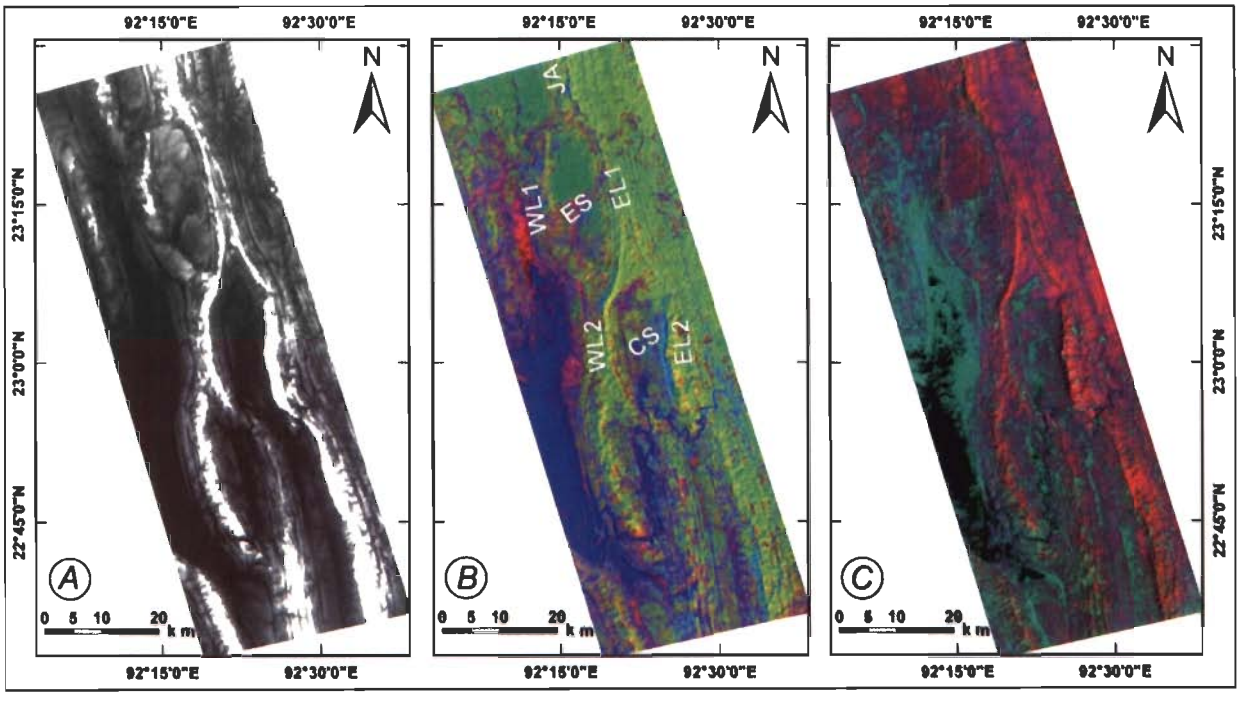

Figure 4.16 Anticline bifurcation, elliptical and cuspate valleys in Tuibangadam area (TBG in Figure 4.6). (a) 90m-SRTM-DEM. (b) FCC of first three principal component images obtained from Landsat ETM+ multi band data, (c) Fused Landsat ETM+ FCC (bands 4, 3 & 2 as R, G, B) and Landsat PAN image. JA-Jampai Anticline, EL and WL-Eastern and western limb, ES-Elliptical Syncline, CS-Cuspate Syncline.

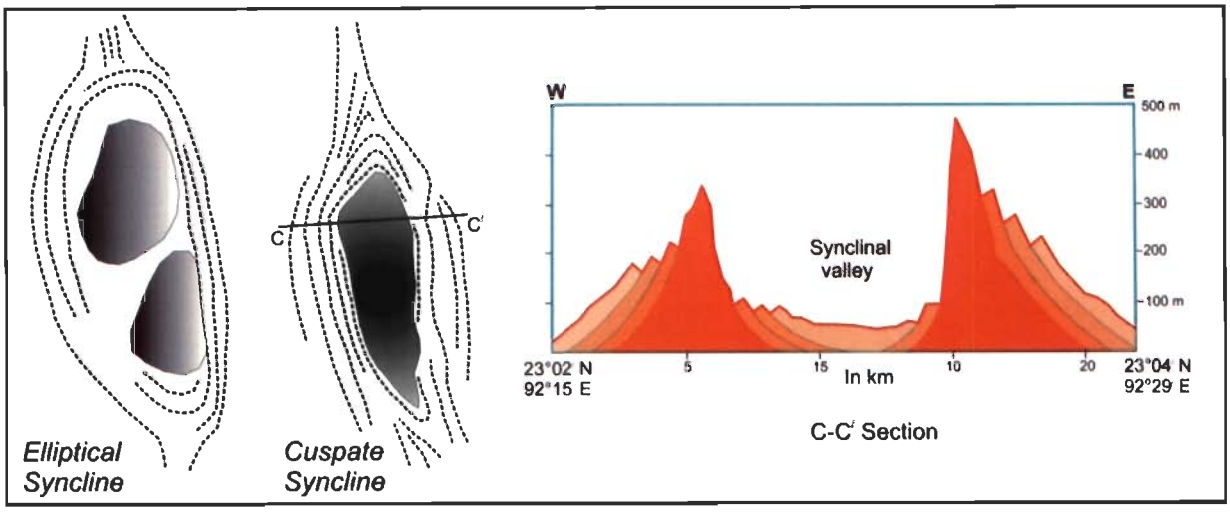

Figure 4.17 Schematic drawing of morphological traces of the elliptical and cuspate synclines and a cross profile section along C-C′ of cuspate syncline. The elevation values across the cuspate syncline are obtained through topographic profiling from 90m-SRTM-DEM.

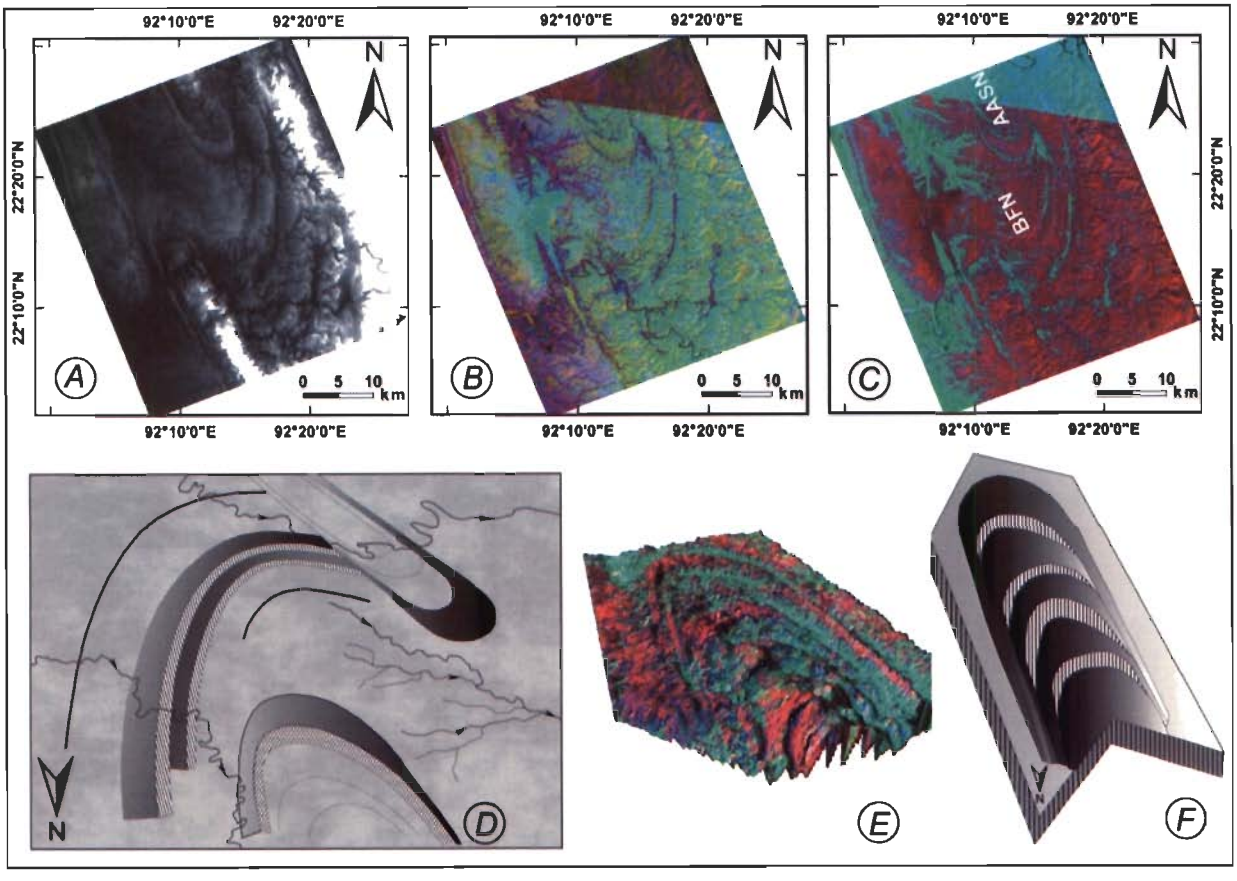

Figure 4.18 Plunging anticline co-noses in southernmost Atharamura anticline and Bandarban area (BDN in Figure 4.6). (a) 90m-SRTM-DEM, (b) FCC of first three principal component images obtained from Landsat ETM+ multi band data, (c) Fused Landsat ETM+ FCC (bands 4, 3 & 2 as R, G, B) and Landsat PAN image. (d) Sketch showing interrelation of anticlinal fold noses as in the above figure. (e) Image showing the individual plunging fold noses (rotated for 180°) which is generated by draping Landsat FCC on DEM with 7 times exaggeration using virtual GIS. (f) Sketch showing the example of folded limbs as exposed. AASN - Atharamura Anticline Southern Nose, BFN-Bandarban Fold Nose.

4.7 River channel pattern and change detection analysis

Active tectonics can modify the behavior of alluvial rivers. Deformation of the valley floor by active tectonics can influence alluvial river and every rivers respond differently to the active tectonic forces. In case of meandering rivers if upliftment occurs than there will be a sinuosity increase on the downstream side of the uplift as the valley side steepened. The Barak river and its tributaries show high channel sinuosity. Streams have changed their course rapidly and also show several abandoned meandering loops at different locations. Major tributaries of Barak river were also investigated for their response to the tectonics prevailing in the region.

4.7.1 Barak River

Barak is one of the major rivers of study area and is a part of Meghna river system. Barak river originates from the hills of Nagaland and enters onto the plains near the Lakhipur after draining the hills of Manipur. Downstream of Silchar town and before entering into Bangladesh Barak river bifurcates into Surma and Kushiara rivers. The Barak river valley is represented by a narrow E-W trending elongated alluvial filled basin and is located at the northern edge of N-S trending fold ridges of the Indo-Burman frontal fold belt. Several tributaries join the Barak from north and south.The principal tributaries of the Barak river are Dhaleshwari, Katakhal, Madhura, Singla, Chari, Jiri, Longai and Sonai. Figure 4.19a is showing the Barak river and basin along with all major tributaries. Perspective three dimensional view of Barak river basin is shown in figure 4.19b.

The river appears to have changed its course at several places through space and time. Eight places of the river channel have been investigated for change detection analysis. All these places have been defined as Blocks 1 - 8 (Figure 4.19a). A detailed change detection study has been carried out from the available data set of 1955 to 2000 spreading over time span of 45 years. In order to make out the amount of shift of the river channel, data of 7 different years have been investigated. Toposheets of 1955 (1:250,000), 1972 (1:50,000), digital satellite data of Landsat MSS of 1975, TM of 1988, IRS-LISS III of 1995, ETM+PAN of 1999 and IRS PAN-D data of 2000 have been used to

detect and delineate the shifting in river channel as well as analysing the variation in channel morphology. All the datasets used in the study were georeferenced on the basis of available geographical coordinate information which made the data comparable at the same scale for the analysis purpose. Later, areas of major variation have been identified on the different datasets, and a detailed change detection study was carried out.

4.7.1.1 Block 1

This block is located in the eastern most part of the selected area near Lakhipur region. Here Barak river enters onto the low relief area and flows from east to west making a large northward curvature with two abandoned meandering loops both on north as well as south of the main channel. Large abandoned loop (on the south) with respect to the present river channel, indicate large-scale northward shift in the river course. Figures 4.20 A-G exhibit shift in channel course from the datasets 1955 to 2000. Further, a small meandering lost channel is also present on the northern side.

The geomorphological features of this part are mainly vegetation (arranged linearly with very coarse texture), agricultural fields, barren land, abandoned loops and striation marks (Figure 4.20-H). Linearly arranged vegetation and abandoned river loops indicate position of the past river channel and provides evidence for reconstruction of past position of the channel. Some striation marks are seen on the image, which might have caused due to the water receding flow after the flood. Various natural and man-made ponds are also present. Three GCP's are selected and plotted to quantify the shift of the river channel in space and time (Figure 4.20-I). Distances of the river banks from three GCP's have also been shown graphically (Figure 4.21)

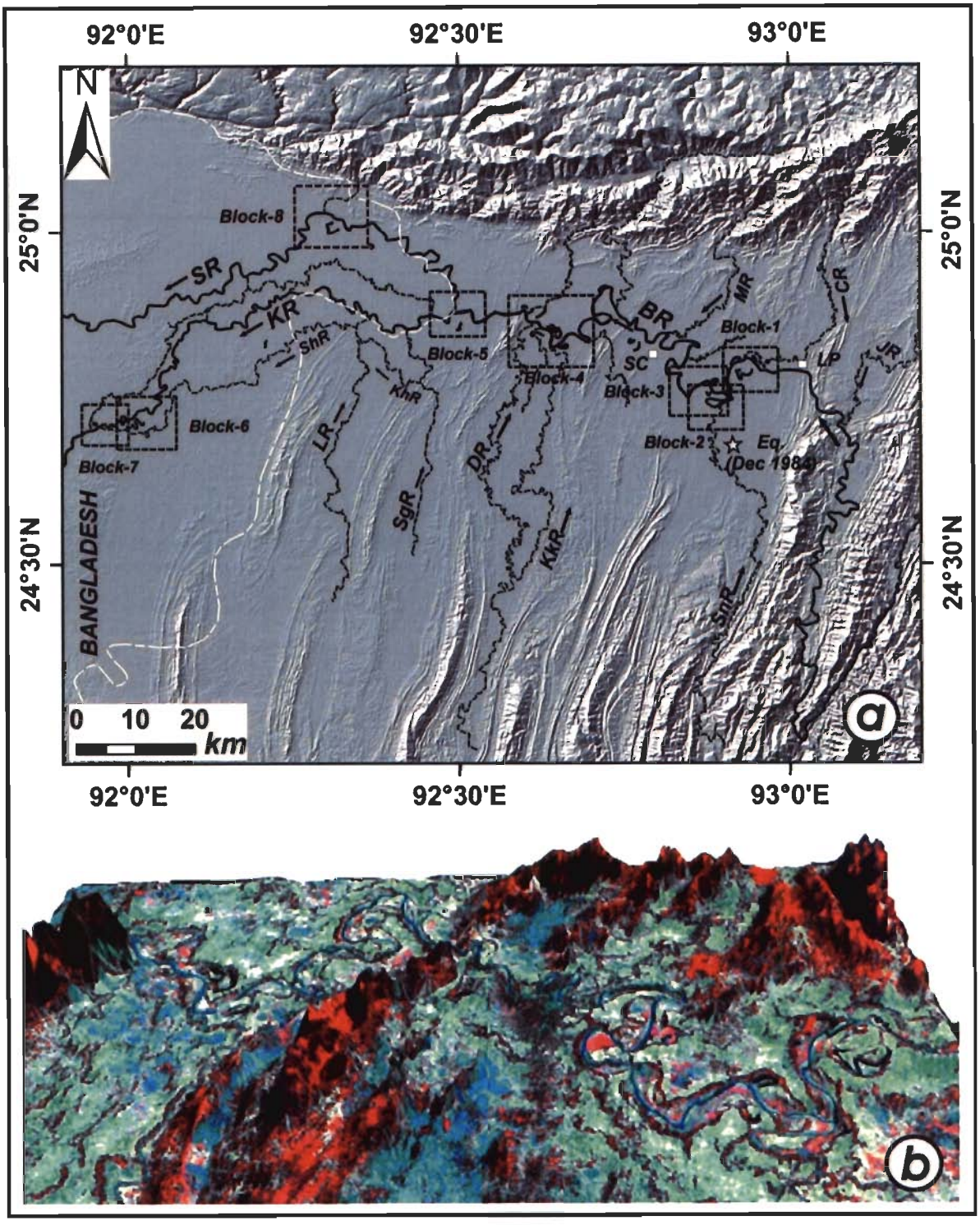

Figure 4.19 (a) Barak river and major tributaries shown on shaded relief model of ASTER-DEM. BR-Barak River, JR-Jiri River, CR-Chari river, SR-Sonai River, MR-Madhura River, KkR-Katakhal River, DR-Dhaleshwari River, SR-Singla River, KhR-Khakra River, LR-Longai River, ShR- Shunai River, KR-Kushiyara River, SR-Surma River, SC-Silchar, LP-Lakhipur. Star mark shows occurrence of an earthquake. (b) Perspective view (3d) of Barak river and surroundings between the longitudes 92.5° to 93°E.

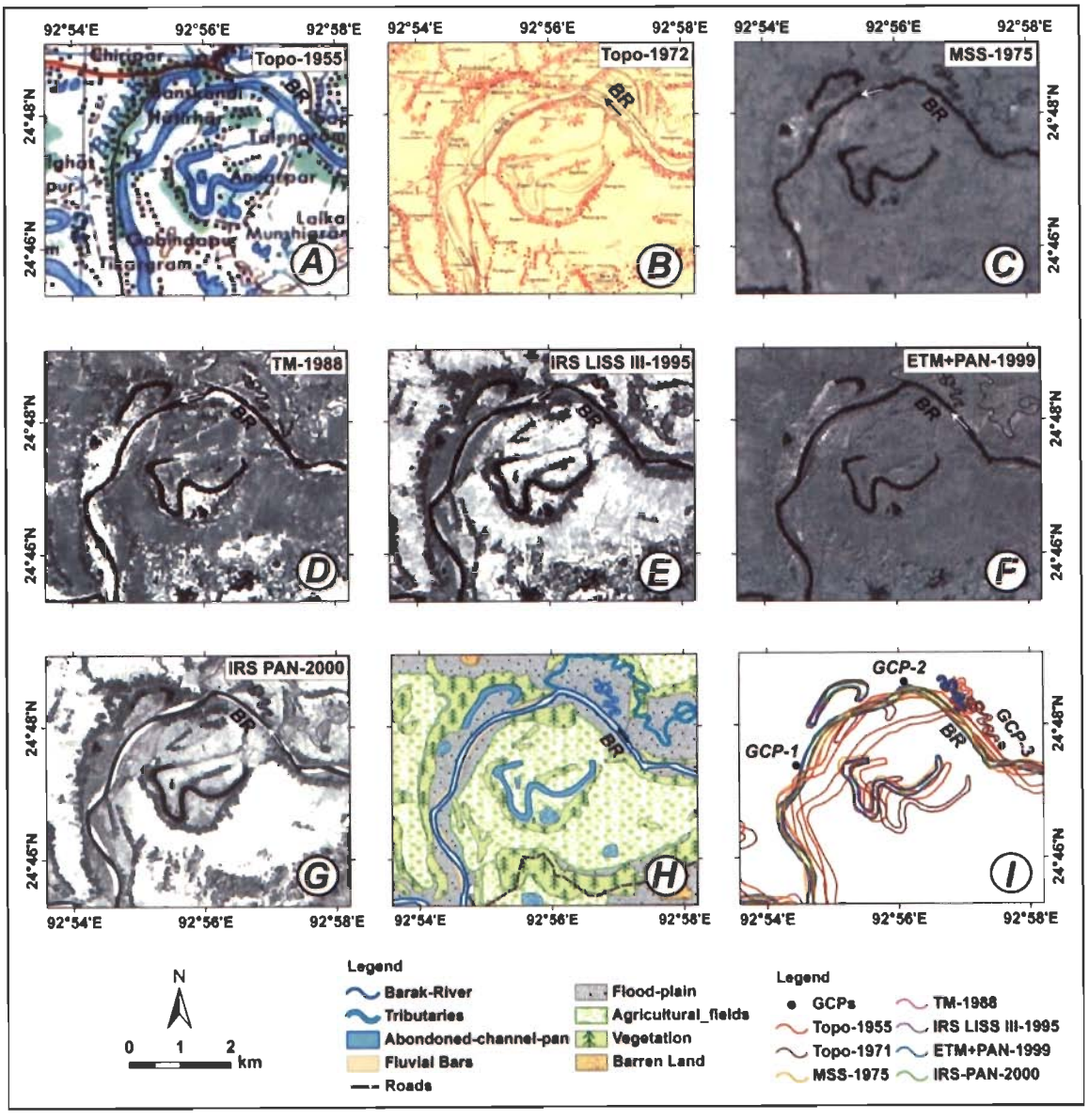

Figure 4.20 Block-1 of Barak river through different years, geomorphology and vectorised river morphology from different datasets along with GCPs.

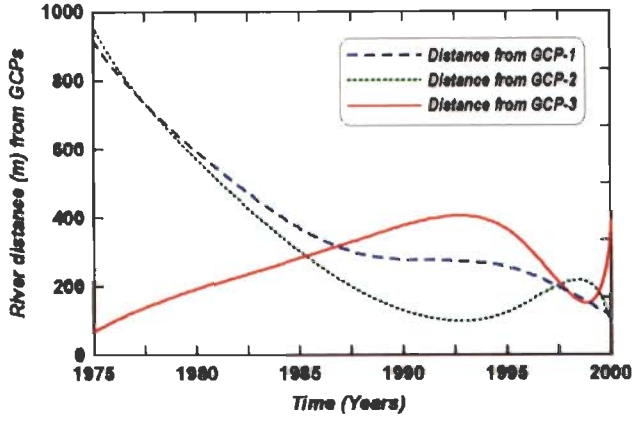

Figure 4.21 River channel positions from GCPs in different years for Block-1.

4.7.1.2 Block 2

The block 2 is the adjacent one of first block and lies just southwest in the downstream direction. A huge meandering loop was developed in the region which is very much evident from the datasets of up to 1988. After that this loop became abandoned due to neck cut off as can be seen on the image of 1995 onwards. Now the river flows through considerably shortened course. Cut off of meandering loop has occurred sometime in between 1988 and 1995. Actually the neck-cut-off took place on 16-10-1992 as reported by local authority.

Figures 4.22 A-G showing the variation of river channel occurring from the 1955 to 2000 through different datasets. IRS PAN-D is high resolution data of 5m which shows the geomorphology of the area in much detail. Various channel bars are developed along the banks of the river indicating the depositional and erosional sites. Cultivated lands along with various ponds and depression can be seen. The Sonai river, a major tributary of the Barak river can be seen joined the southern part of the Barak river loop up to the year 1988 before the neck cut off occurred. Channel overlays of different years (Figure 4.22-I) are describing variation of river channel. Vegetation is found to be linearly arranged even along with abandoned channel (Figure 4.22-H).

Figure 4.24 shows nature of abandoned river loop and filled up river bed. A large difference has been reported with respect to GCP-3 during the 1995 to 1997 which is due to shorter river course developed due to meandering cut-off (Figure 4.23). Incidentally an earthquake (Mb=5.5) occurred in 1984 south of the recently abandoned river loop as shown in the figure 4.19a might have contributed towards this river shift.

4.7.1.3 Block 3

At this place, the river channel shows substantial changes in its pattern. A large rounded curvature has been formed exhibiting small narrow notches at both the ends. With time one of eastward notch gets separated and forms a small rounded loop. On the other hand westward notch disappear slowly with time as readjustment of the channel has occurred. Similarly it is also evident from the datasets that during the time span of 1988 to 1995 the rounded southward curvature of the river also transformed into angular notch. Figures 4.25 A-G show channel position through different years along with geomorphological interpretation (Figure 4.25-H) and channel overlays of different years (Figure 4.25-I).

In this block the river forms wide flood plains and characterized by angular flow. The vegetations are seen to be arranges in a linear fashion away from the present river channel. There is also an oxbow lake in the north-eastern part of this block and the wide flood plain is marked by striation marks. Geomorphological features like abandoned loops, bank line and vegetation provide information on wide flood plain and earlier path of channel flow.

Three GCP's are plotted to quantify the shift of river channel (Figure 4.26). Measurements of distance of river bank from three GCP's indicate the western sharp bend of the river became closer to the GCP1 indicating westward shift. At the location of GCP2 the river show southward shift as the distance between GCP and river has gradually decreased. Whereas, in case of GCP3 the distance has increased through time indicating westward shift. In general, the river channel exhibits wide flood plain. From graphical presentation (Figure 4.26) river bank distances from GCP's through different years clearly indicate gradual closeness of river towards the GCP1 and GCP2 and gradual increase in distance of river from GCP3.

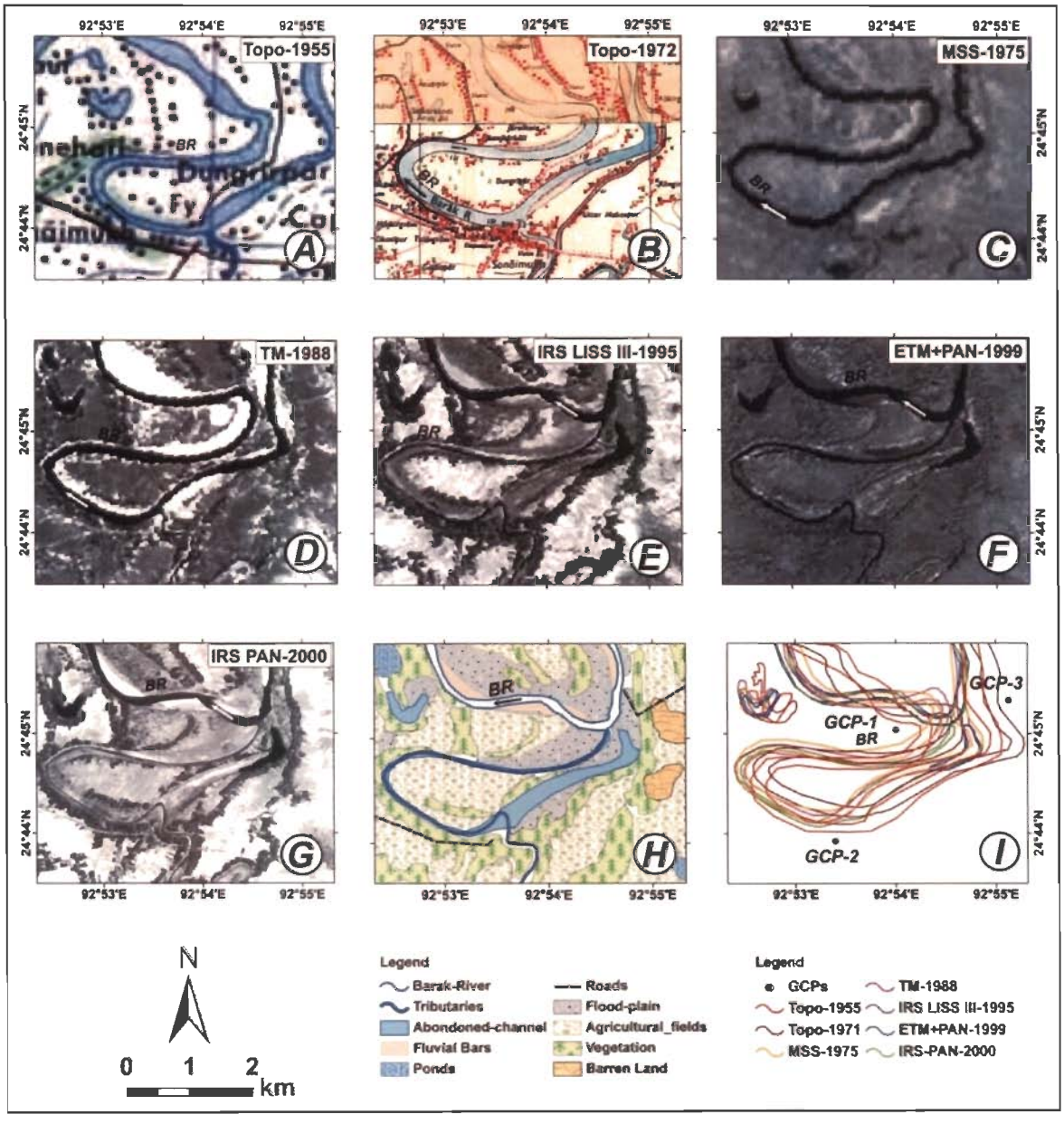

Figure 4.22 Block-2 of Barak river through different years, geomorphology and vectorised river morphology from different datasets along with GCPs.

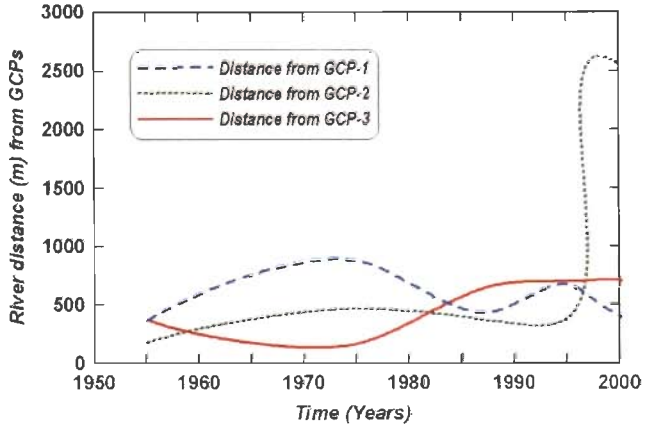

Figure 4.23 River channel positions from GCPs in different years for Block-2.

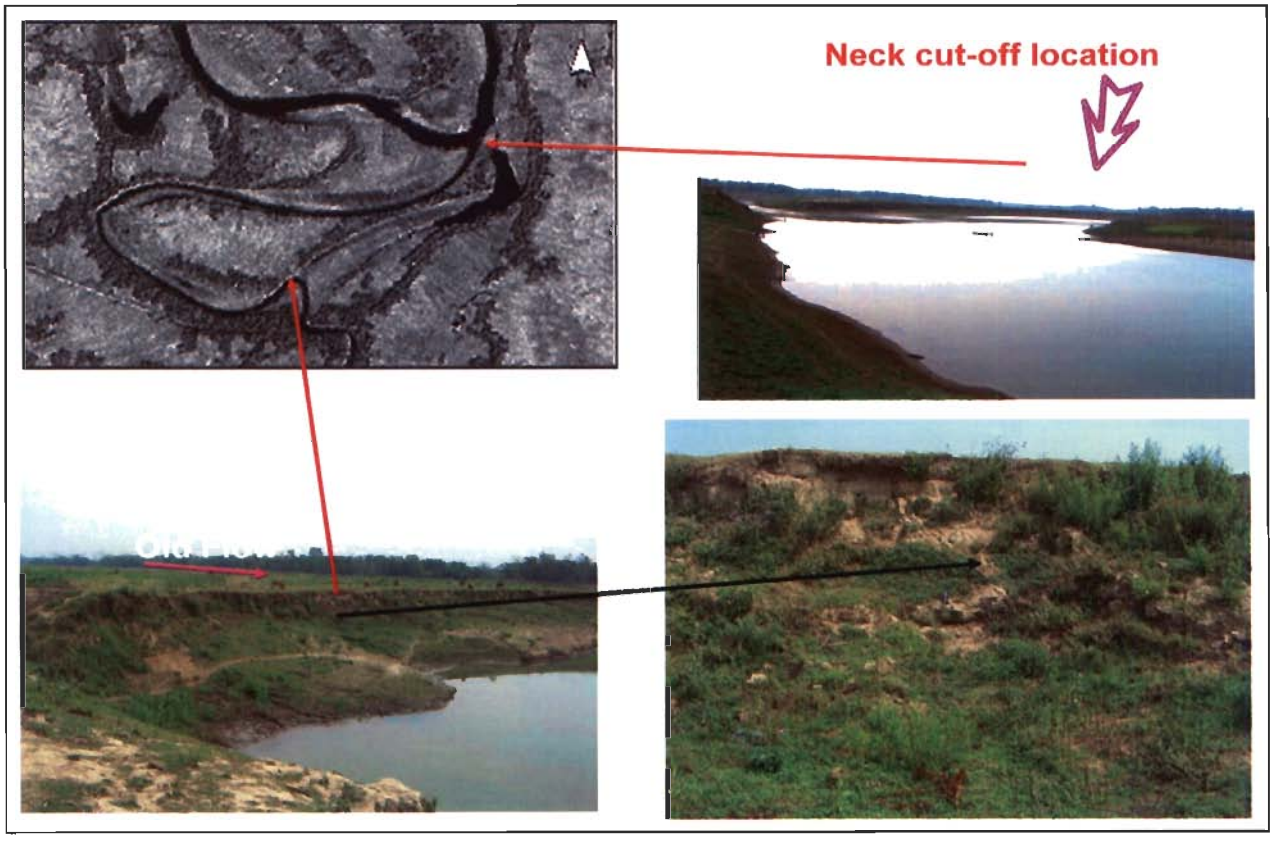

Figure 4.24 Abandoned river loop as seen on satellite image and field photographs.

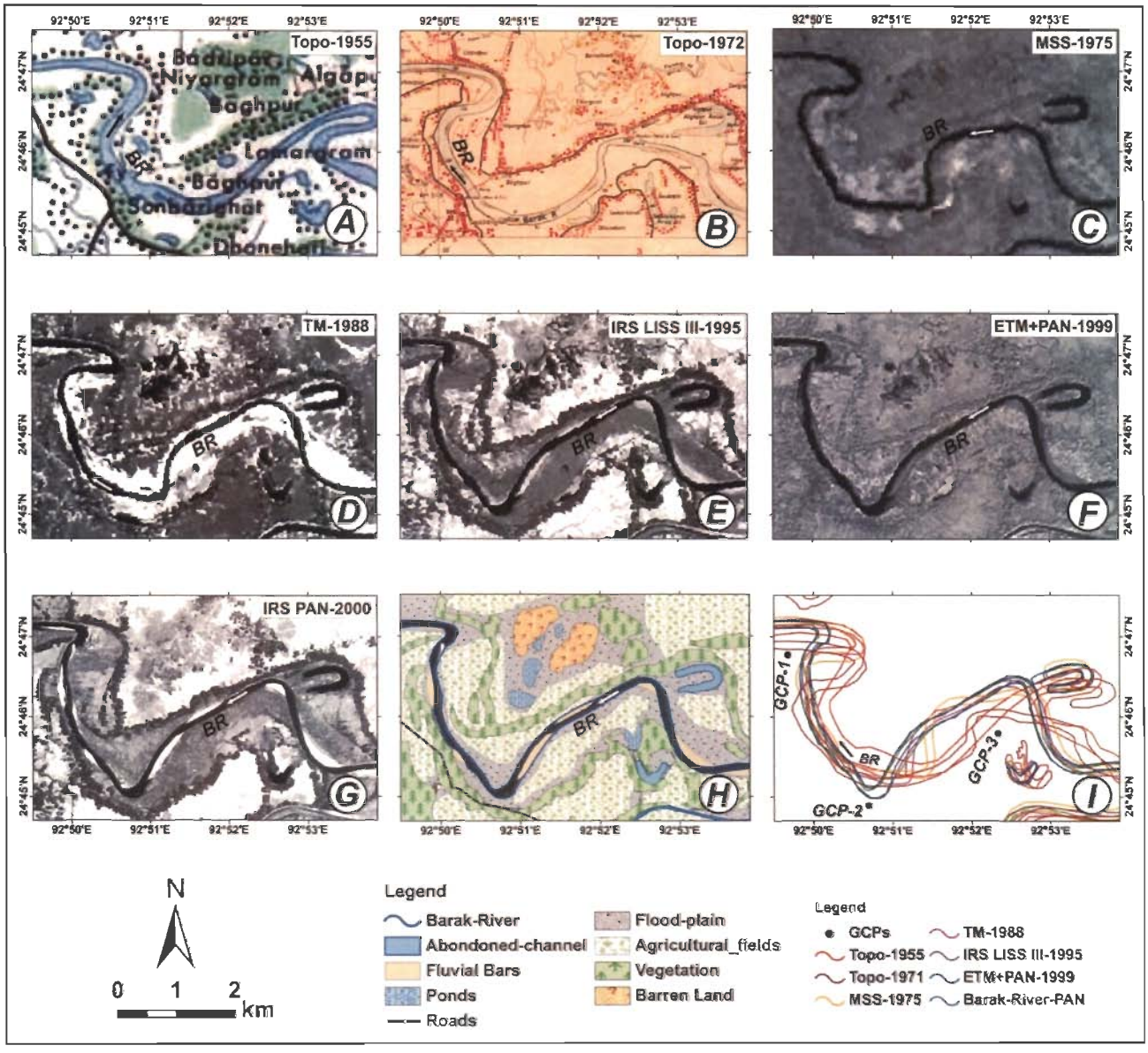

Figure 4.25 Block-3 of Barak river through different years, geomorphology and vectorised river morphology from different datasets along with GCPs.

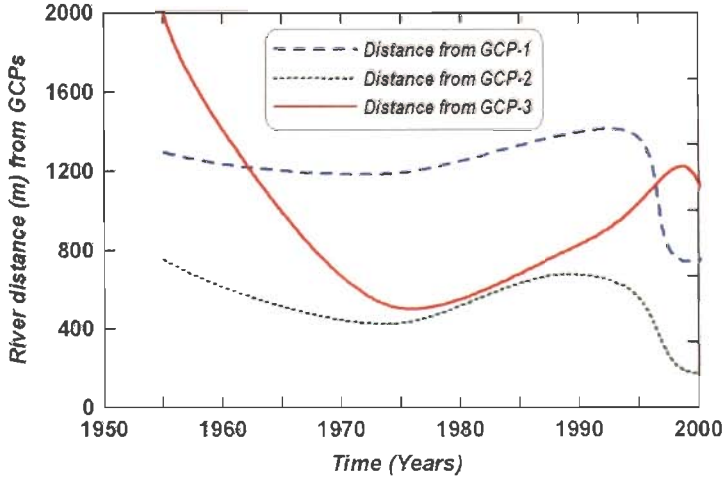

Figure 4.26 River channel positions from GCPs in different years for Block-3.

4.7.1.4 Block 4

This block lies in the central region of Barak basin and maximum variation in morphology of the river has been detected in this block. River has shown seven abandoned meandering loops and channels of varied dimensions. After abandoning the loops river has changed its course from EW to SW and NW direction. One loop on the southern bank has been separated between time span of 1955 to 1972 apparent from the figures 4.27 A-G.

Geomorphologically, a fold ridge and several meandering loops mark this block. The ridge has very low altitude on the southern side of the river and the valley is slighter narrow in this region. This block falls near the Silchar town therefore, nearby area is highly urbanised having a number of man-made structures like buildings, roads and canals. Similarly due to rapid shifting of course linearly arranged vegetation has been developed on the older traces of the river. Flood plain is wide which has been transformed into the cultivation land. Graphical representation of the river channels from various dataset also reflects oscillatory change in the river course (Figure 4.28).

4.7.1.5 Block-5

This block is located in the western part of Barak valley near the Badarpur town of Karimganj district. At this place Barak river enters into Bangladesh and bifurcates into Surma and Kushiara rivers at the Haritikar place. A rectangular loop is developed at this place and through which Surma river gets bifurcated. On the southern side a large abandoned loop is formed which indicate the northward shift of the river (Figure 4.29). Vegetation is intense and scattered and not in linear pattern as it is found in the upstream course of river. Ridge traces are also found in the eastern area. Numerous ponds, natural depression and marshes are developed on the northern side of the river bank. Agricultural fields have developed but are intervened by the barren lands and vegetation.

In this block Barak river abandoned one loop prior to the 1955 as shown in toposheet. But a narrow notch is visible in the toposheet of 1955, which later transforms into a normal bend in the images from 1975 onwards. Analysis of all the datasets indicate that although time of abandoning of loop cannot be established from the available data but the variation of river course and readjustment can be understood. Figure 4.30 showing that from the year 1955 to 2000 river has shifted its course about 700m northward from the place of notch. The Barak River from northeast India bifurcates at the India-Bangladesh border into the Surma and the Kushiara rivers.

4.7.2 Kushiara River

Kushiara river is one of the bifurcated rivers originated from the Barak river. Kushiara river flows southward from the bifurcation place and appears to follow the natural course of the Barak river. Kushiara river flow sluggishly following the meandering path through the plains of Bangladesh.

4.7.2.1 Block-6

Block 6 is located near the Manik Kuna area. At this place two abandoned loops are present. Initially in 1955 only one loop is visible and river course seems to look almost straight (Figure 4.31-A). But in the MSS image it can be seen that a large curve is developed and river has shifted northward, which is prominent in other datasets also (Figure 4.31-C). From the GCPs it can be analyzed that Kushiara river shifted towards north for about 400m in the western side and about 100m towards south in the eastern side in block 6 (Figure 4.32). This block falls into a natural depression and flood plain covering a large area. Vegetation is linear near the banks but scattered away from the banks. A large lake area is found in southern part of the river valley known as Hakaloki haor (Lake) near Killaura, Sylhet. This lake is one of the largest lakes of the Bangladesh. Large ponds and water logged areas have formed in the region (Figure 4.31-G).

4.7.2.2 Block-7

This block is the westernmost block lies adjacent to the block 6 and fall near Islampur village of Fenchuganj town. It can be observed in the toposheet of 1955 that in this block river has developed a small meandering loop towards north (Figure 4.33-A). Later this loop becomes abandoned in between 1955 and 1975 and river has shortened its course and starts flowing straight (Figures 4.33-B, C). An overall northward shift was reported in the river course with the slight southward shifts in the eastern side in datasets of IRS LISS III (1995) afterwards (Figures 4.33-D-G). This shift is also evident from the GCPs (Figure 4.34). Larger ponds are developed in this block like block 6. A major tributary of Kushiara river known as Shunai river joined it in the block 7.

4.7.3 Surma River

The Surma is the other branched out river from the Barak River. Surma river enters into the Sylhet depression (or trough) which forms in the Surma Basin (Figure 4.19a). The Surma is fed by tributaries from the Meghalaya Hills.

4.7.3.1 Block-8

Surma River flows northwestward towards the Shillong Plateau then again flow back southward following a meandering path. A large meandering cut-off towards southern bank near the Kanaighat area has been identified (Figures 4.35A-E). A tributary from Meghalaya hills also joins at this location. The channel morphology of this river is characterized by a U-turn joining with the Barak River resulting in oppositely directed water flow. Also at this place the Surma River flows northward initially and then northwest-ward flowing closer to the southern edge of the Shillong Plateau. Incidentally this area suffered large scale subsidence along the Dauki fault marking the southern edge of the Shillong Plateau and resulting in formation of several depressions now occupied by water bodies and marshy land. It seems that the Surma river has undergone significant modifications due to operating tectonic disturbance in the area. Large flood plain of the

region has been converted into the cultivated land and vegetation is sparse and scattered in this region (Figure 4.35G).

Channel shift of Surma river is shown graphically in figure 4.36. Due to limited data availability channel shift could only be analyzed for 25 years from 1975 to 2000. It may be observed that a gradual shifting has occurred towards the north as evident from all the GCPs (Figure 4.36).

4.8 Major tributaries of Barak River

4.8.1 Longai and Singla River

Longai river originates in the Jampui Hills of Tripura. Longai river joins the Barak river with high sinuosity in the lower reaches. A channel known as Shunai river can be observed to have developed in this area flowing nearly parallel to the Kushiara river for about 12kms linking Longai river and the Barak river near Fenchuganj (Block 7 of Kushiara river).

The Singla river originates in Mizoram and flows through the Sonbil synclinal valley. River shows intense meandering and eastward shifting exhibiting a large curvature near the Kaliganj area. At this place when it enters onto the wide valley, Singla river bifurcates to form Khakra river and later joins Longai river. Singla river has lesser amount of water in it and remains dry for longer period of year.

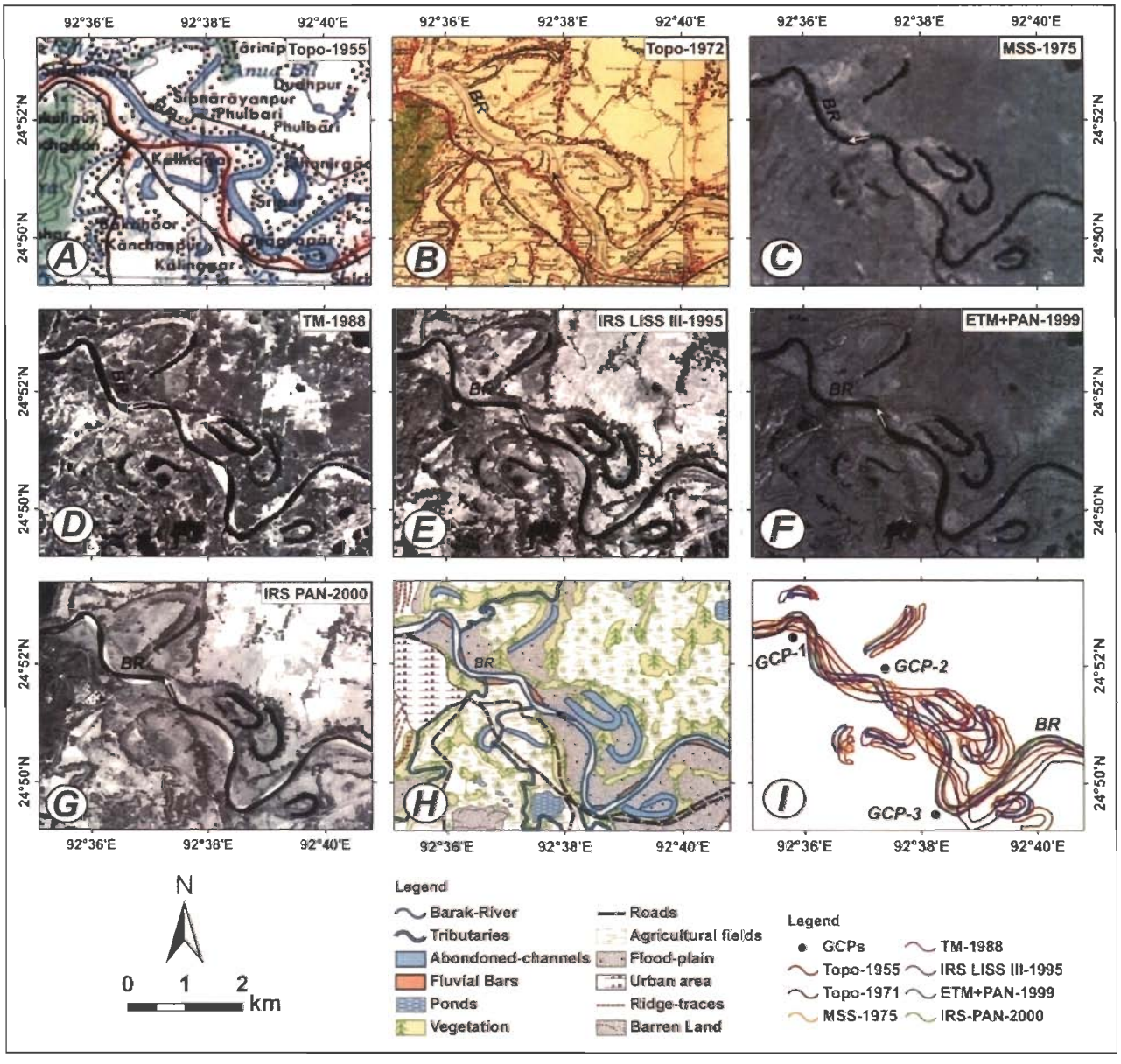

Figure 4.27 Block-4 of Barak river through different years, geomorphology and vectorised river morphology from different datasets along with GCPs.

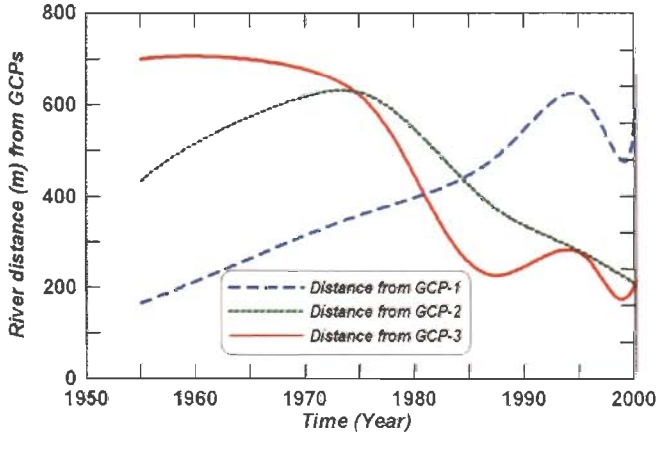

Figure 4.28 River channel positions from GCPs in different years for Block-4.

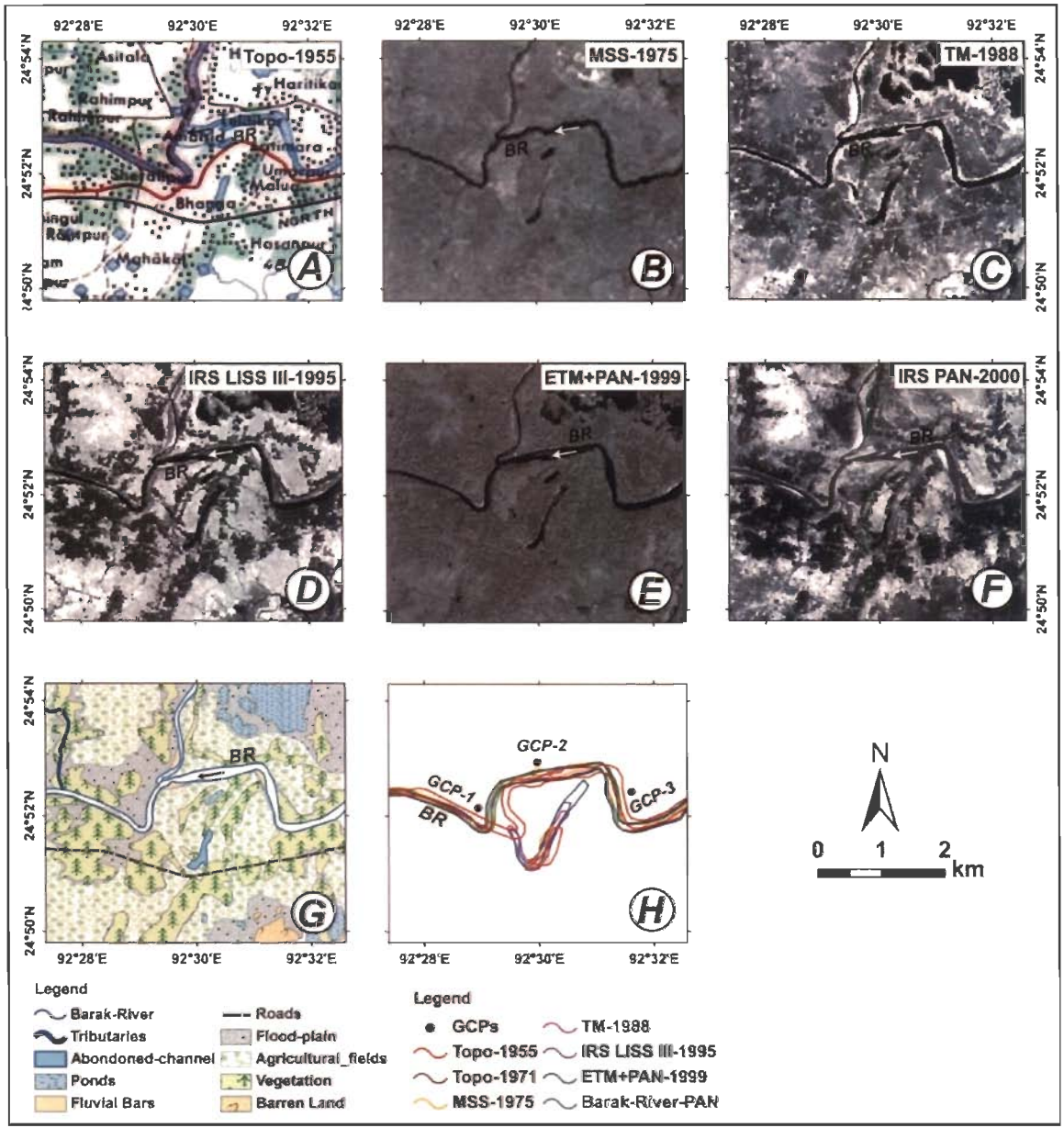

Figure 4.29 Block-5 of Barak river through different years, geomorphology and vectorised river morphology from different datasets along with GCPs.

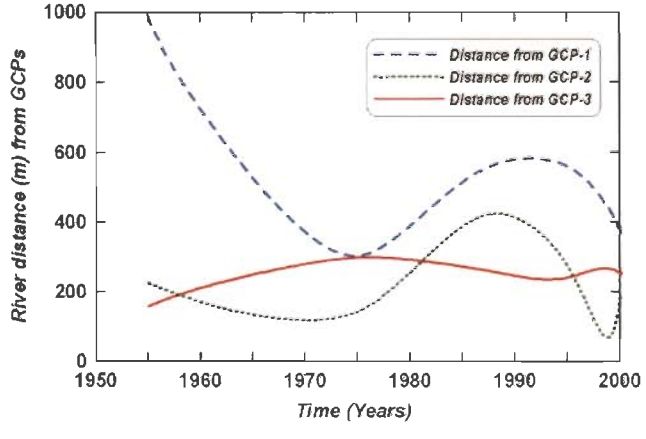

Figure 4.30 River channel positions from GCPs in different years for Block-5.

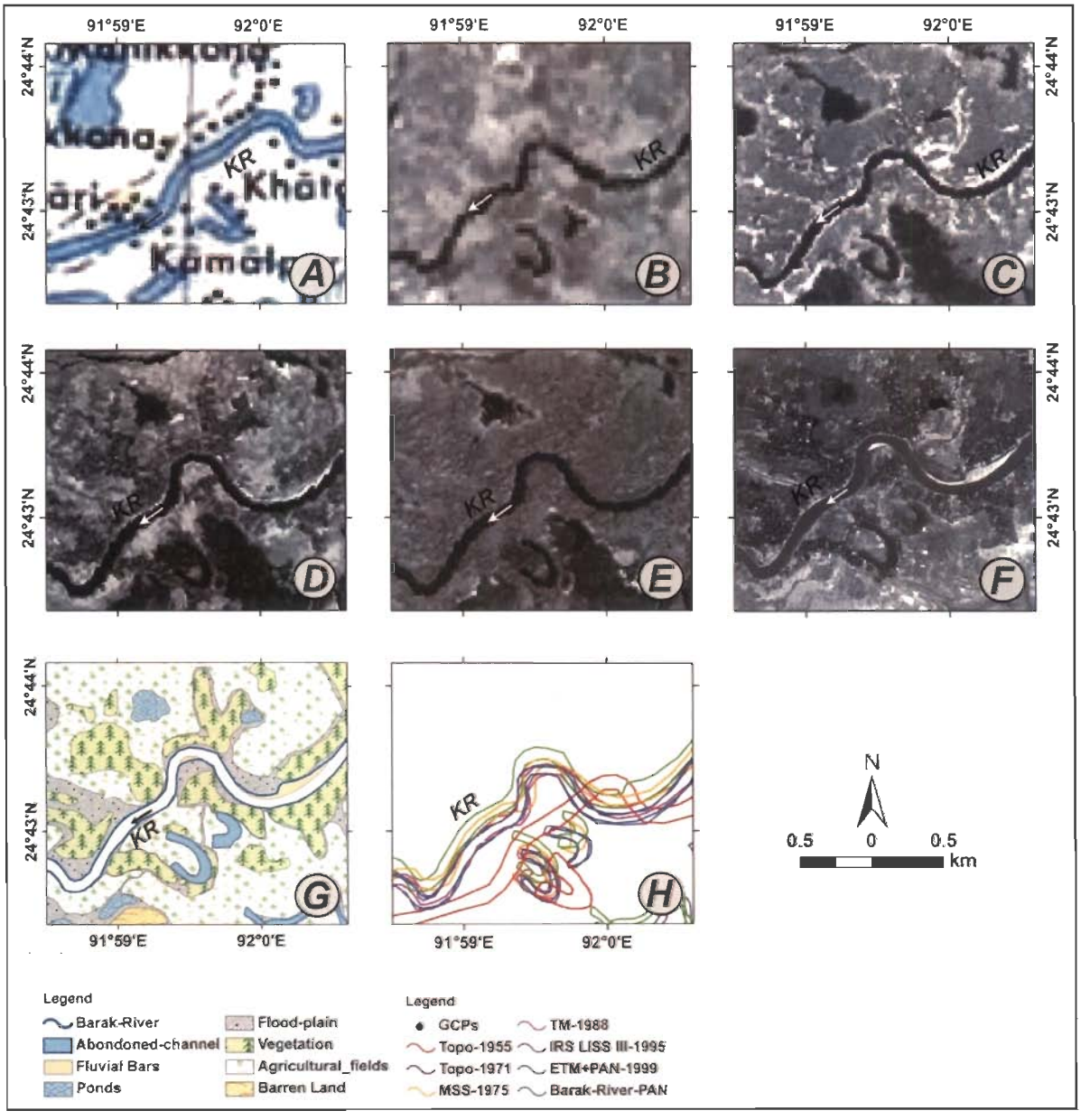

Figure 4.31 Block-6 showing Kushiara river through different years, geomorphology and vectorised river morphology from different datasets along with GCPs.

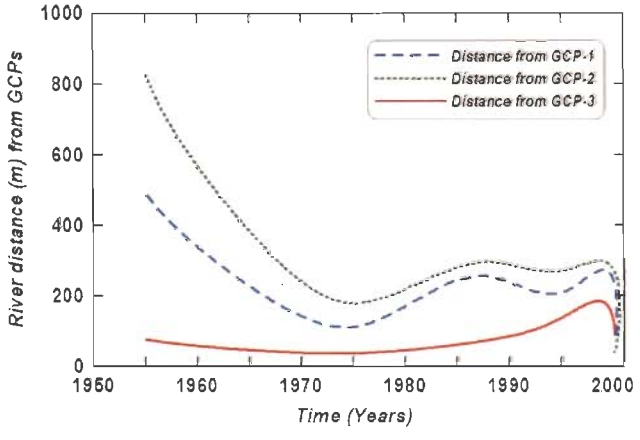

Figure 4.32 River channel positions from GCPs in different years for Block-6.

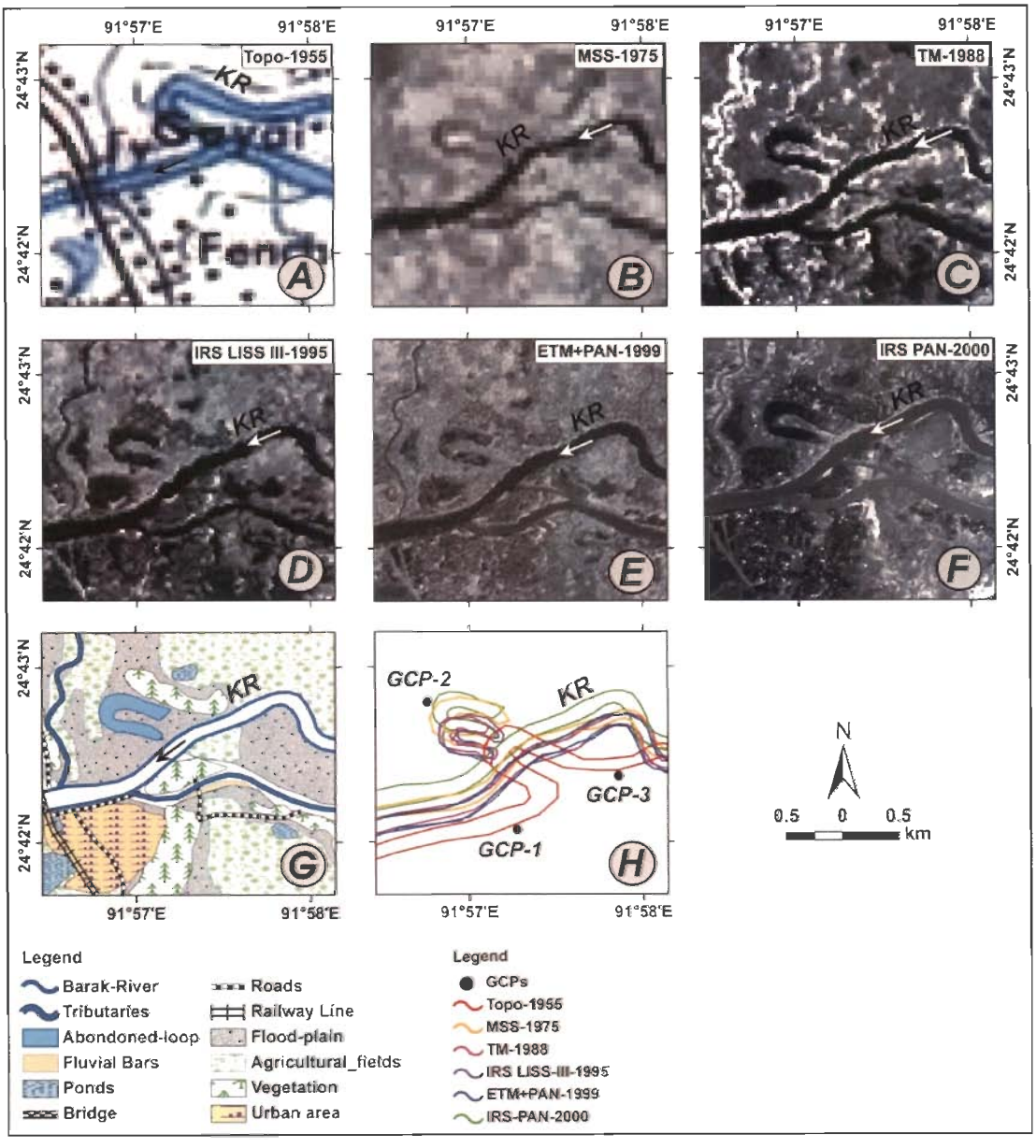

Figure 4.33 Block-7 showing Kushiara river through different years, geomorphology and vectorised river morphology from different datasets along with GCPs.

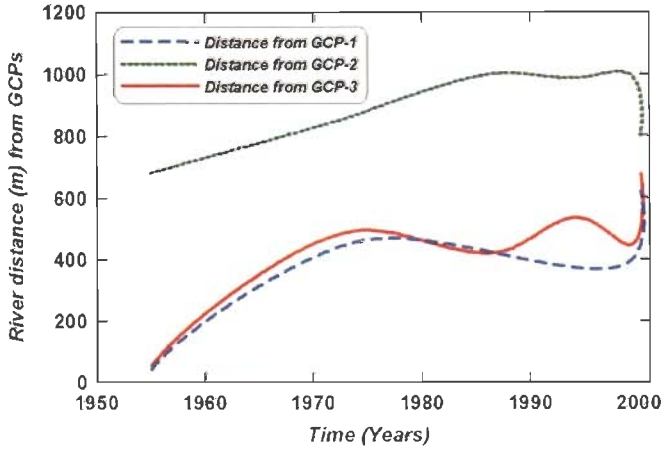

Figure 4.34 River channel positions from GCPs in different years for Block-7.

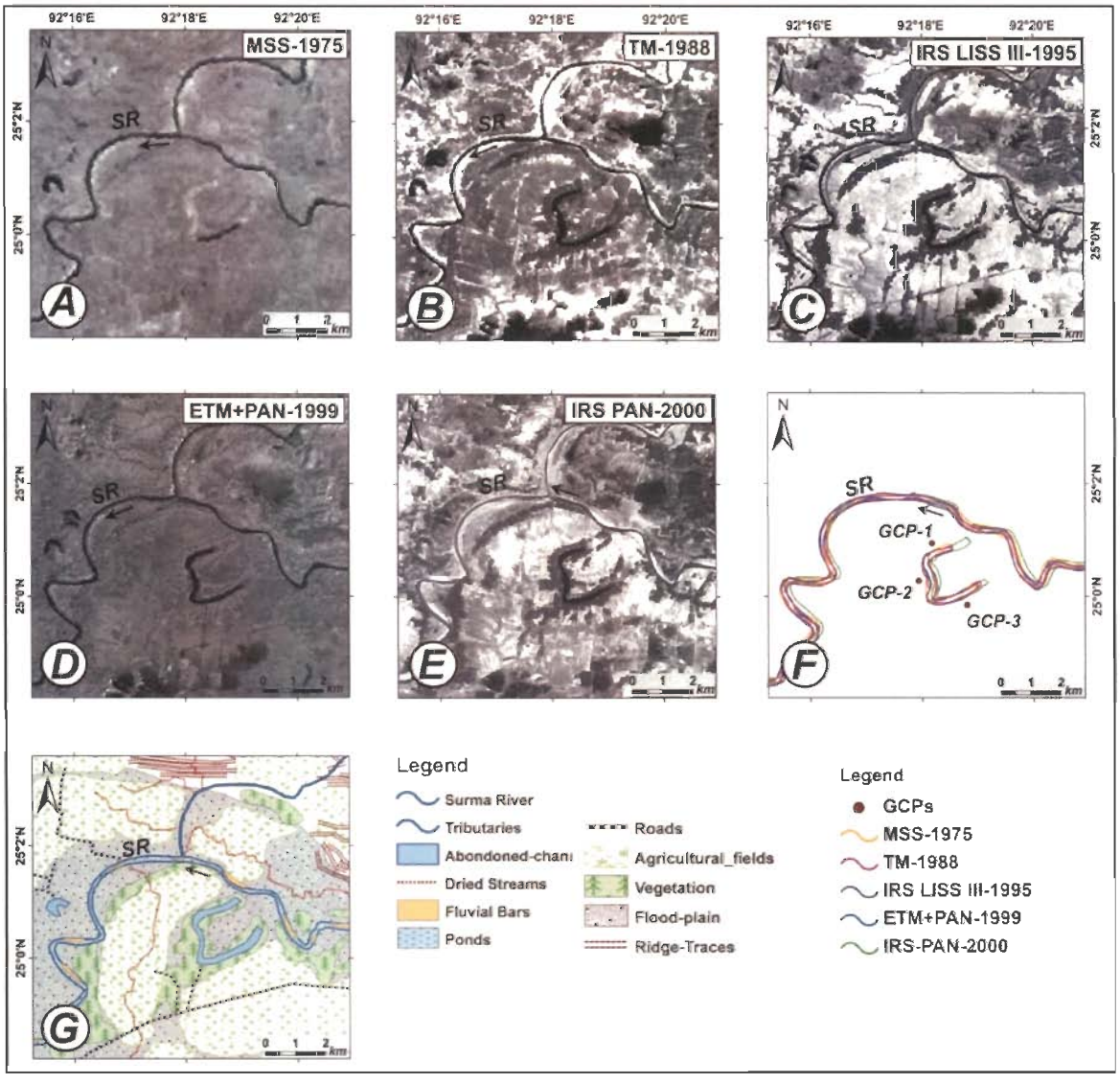

Figure 4.35 Block-8 showing Surma river through different years, geomorhology and vectorised river morphology from different datasets along with GCPs.

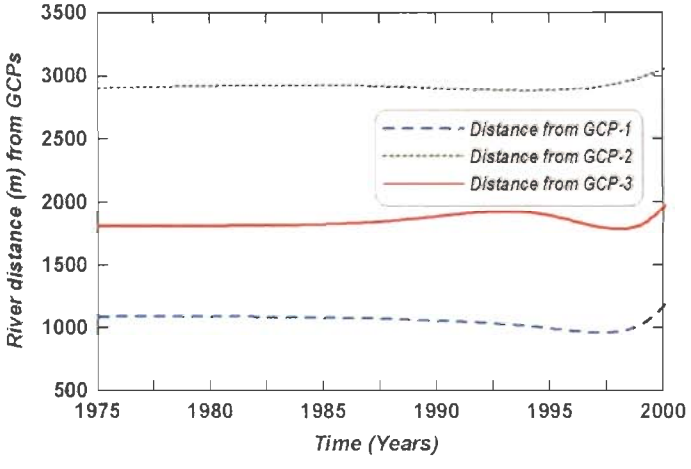

Figure 4.36 River channel positions from GCPs in different years for Block-8.

4.8.2 Madhura River

Madhura is the major northern bank tributary of the Barak river and joins near Udarbond area. Madhura river show highly meandering course especially when it enters into lower region. It shows a large southward curvature in its course. A small meandering loop has also been observed just near the junction of Barak-Madhura rivers (Figure 4.37A). Geomorphologically the area is dominated by the cultivation land and vegetation cover (Figure 4.37B).

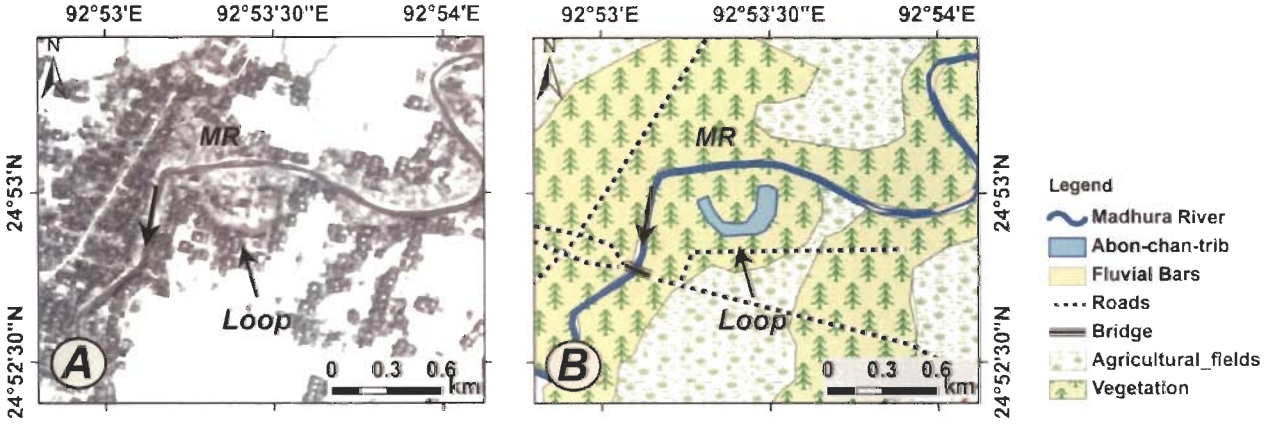

Figure 4.37 Madhura river channel course (A) and geomorphological characteristics (B).

4.8.3 Jiri River

Jiri river is originated from the Manipur hills joining the Barak River near Jiribam area is an important northern bank tributary. River is flowing sothward showing intense meandering at various places. Two blocks of meandering cut-offs have been identified and discussed (Figure 4.38).

The block-1 lies southward a little off from the Jiribam city. Two meandering loops are present in the western side of the river. Here a narrow notch also can be seen, which is likely to suffer neck cut-off in the near future (Figure 4.38A). In this area river has also

changed its course and flow in the NE direction instead of normal NS trend. Most of the flood plain is covered by vegetation and agricultural fields. River is actively incising the valley as various fluvial bars have developed at the deposition sides. In Block-2 river has changed its course and starts flowing in the NW-SE direction. River is also showing intense meandering and exhibited three abandoned channels or loop in the northern side (Figure 4.38C). An anticlinal ridge is located just beside the river and at this location river has entered wider valley

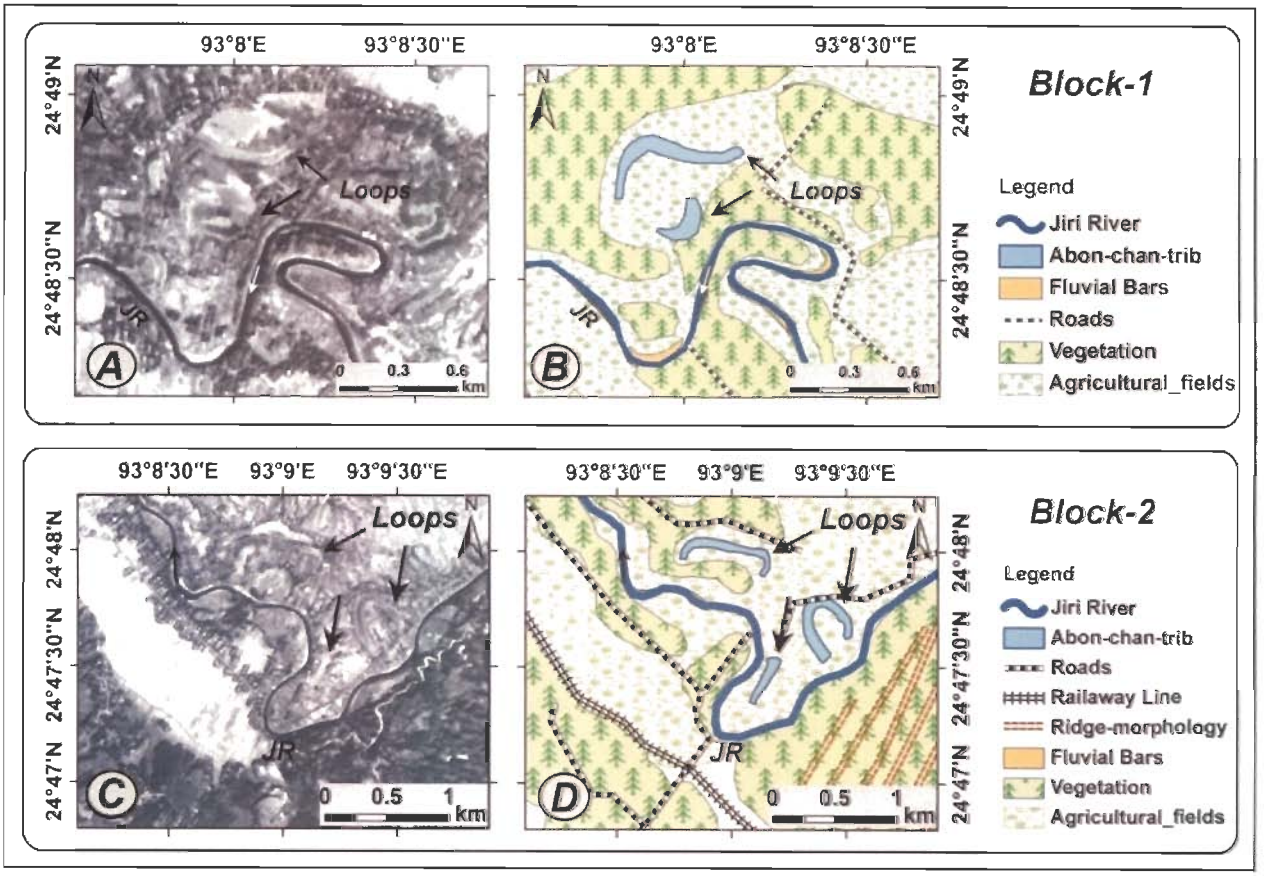

Figure 4.38 Block 1 and 2 of Jiri river (JR). River channel and loops are shown in (A,C) with geomorphological characteristics in (B,D).

4.8.4 Dhaleshwari and Katakhal Rivers

Dhaleshwari is originated from northern part of Mizoram (known as Thang in Mizoram) and is flowing towards north through the middle of the Hailakandi district of Assam. Originally it is used to flow along the western side of the district and fall into the river Barak near Panchgram. Dhaleshwari is a major and one of the longest tributary of the Barak river. Mean sinuosity of the river is 1.9, ranges between maximum 3.8 to minimum 1.2.

This river crosses the Bhairabhi anticline through a faulted zone and changes its course northward (Figures 4.39 A & A'). Again at other location it crosses two fold limbs (Figures 4.39 B & B'). In this region 'stream capturing' has been observed. This river is actually diverted from its actual course due to faulting of anticlines. Katakhal river is an artificially branched out river which later joins the Barak river. Dhaleshwari river exhibits highly meandering course leaving a number of meandering loops. Eight locations of meandering cut offs have been identified and stream pattern and various gomorphological characteristics are shown in figures 4.40 and 4.41.

4.8.4.1 Blocks 1 to 8

Block 1 is the southernmost block and falls near Kukichara region, where river valley is narrow and the surrounded by the anticlinal ridges. In this block an abandoned large partially dried up loop is present at the western side of the river (Figure 4.40a). Vegetation shows a linear trend following the river banks (Figure 4.40b). The river in block-2 exhibits intense meandering and abandoned loop can be seen on the northern side (Figure 4.40c). Further shifting of channel might also occur at this location. Vegetation has grown over the older meandering path and arranged in the linear pattern. Cultivated lands cover the flood plain (Figure 4.40d). Block-3 is located just adjacent to the block-2. This is marked by an abandoned meandering loop towards western side (Figure 4.40e). At this location the Dhaleshwari river branches out and a river known as Katakhal river forms. Both the rivers start flowing parallel to each other from this point. In block-4 Dhaleshwari river shows intense old meandering pattern. An abandoned

meandering channel is present towards the eastern side (Figure 4.40g). Here river valley gets wider therefore, agricultural fields and cultivated lands covers large area of flood plain. Various man made ponds also can be observed all over the valley (Figure 4.40h).

In block-5 a small rounded loop has been identified in the region towards eastern bank of the river (Figure 4.41a). Channel shows westward shifting. The block-6 lies near the Hailakandi city wherein the river has abandoned a loop near the western bank and shifted its course towards the east (Figure 4.41c). Western bank of the river is mainly occupied by the vegetation and agricultural fields. On the eastern bank urbanized area of Hailakandi city is located (Figure 4.41d). A large and a small abandoned loop at the eastern side can be seen in block-7. River exhibits westward curvature and seems to have shifted towards west (Figure 4.41e). Sinuosity of the channel is very high in this block. The block-8 is the northernmost block of Dhaleshwari river where a large loop has been identified on the western side (Figure 4.41g). Whole region is highly cultivated and several naturally occurring depressions are developed (Figure 4.41h).

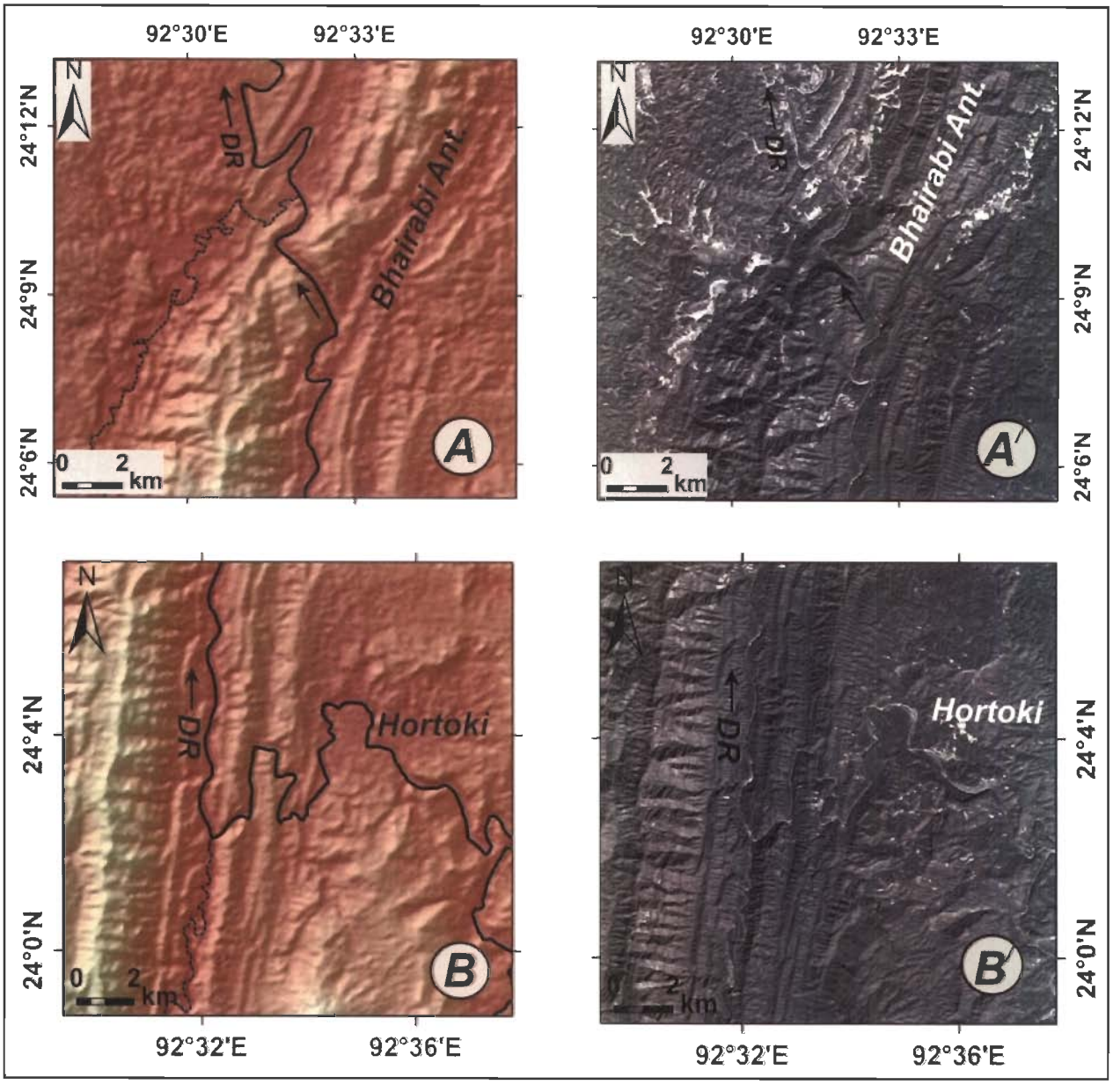

Figure 4.39 Dhaleshwari river crossing Bhairabhi anticline (A and A') and two fold limbs (B and B') shown on color coded ASTER-DEM (A, B) and IRS PAN-D image (A', B').

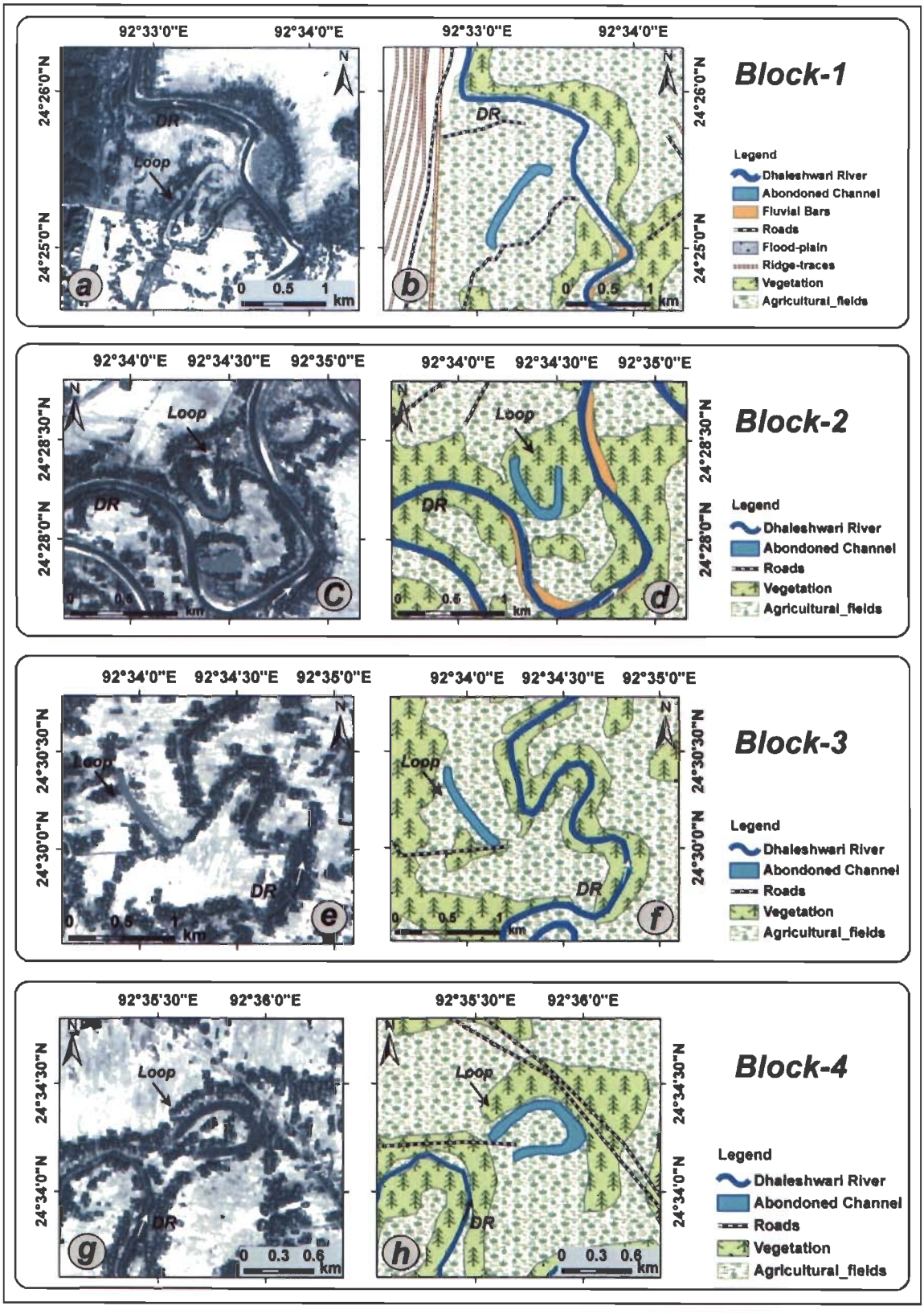

Figure 4.40 Block 1 to 4 of Dhaleshwari river (DR). River channel and loops are shown in (a, c, e, g) with geomorphological characteristics in (b, d, f, h).

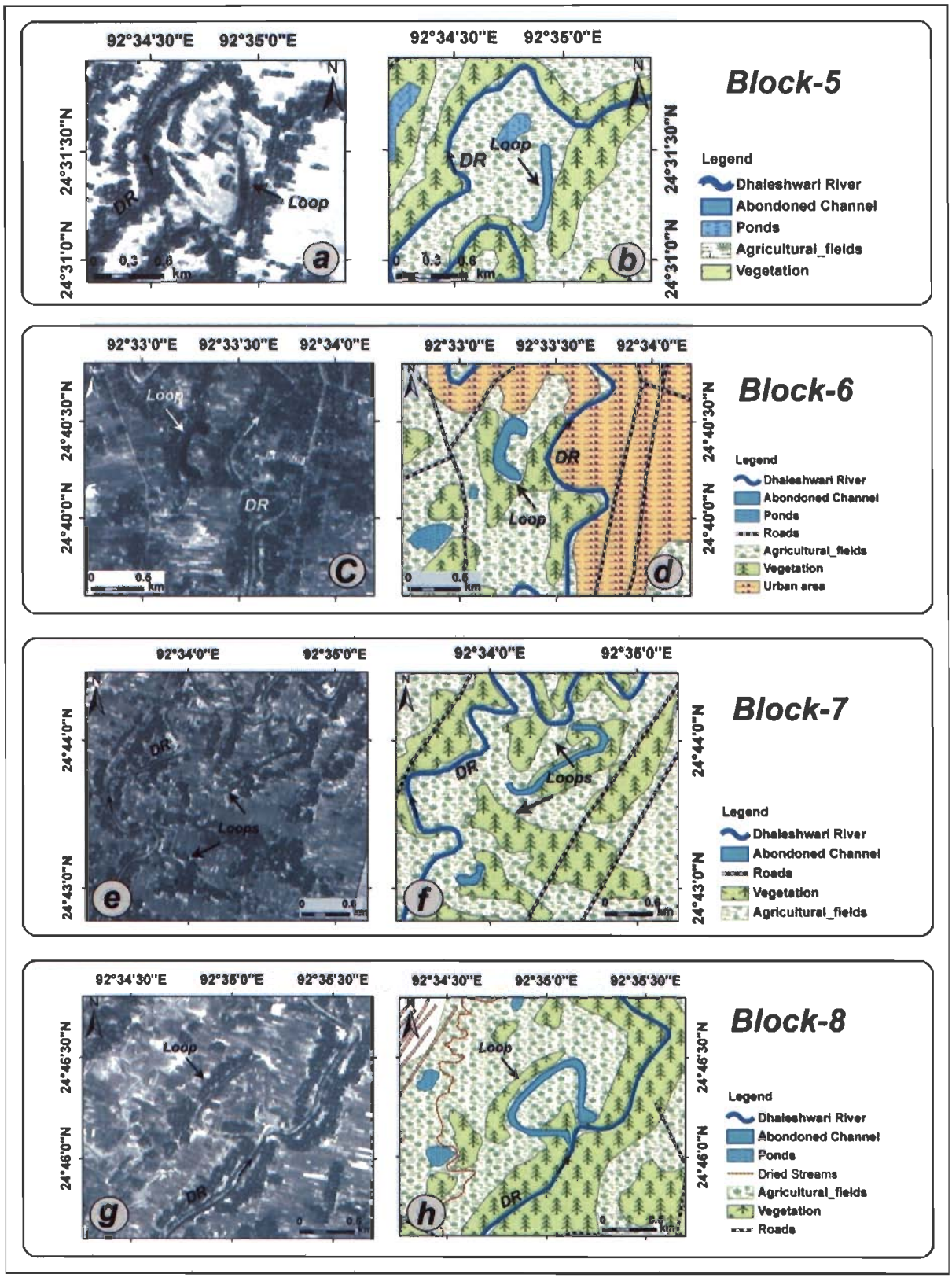

Figure 4.41 Block 4 to 8 of Dhaleshwari river (DR), River channel and loops are shown in (a, c, e, g) with geomorphological characteristics in (b, d, f, h).

4.8.5 Sonai River

Sonai river is also an important southern bank tributary of the Barak river joined near Lakhipur area. It is flowing from the south to the north. Sonai river shows intense meandering specially in the lower reaches. It also shows various meandering cut-off and changes its course several times. Total 5 cases of meandering cut offs have been studied from block 1 to 5 and are shown in figures 4.42 and 4.43.

Block-1 is the northern most block showing three meandering loops of Sonai river (Figure 4.42a). All the loops are dried up and have been converted into the agricultural field (Figure 4.42b). Block-2 also lies at the southern end showing a large meandering loop in the western side. River exhibits shifting towards east (Figure 4.42c). In block-3 a smaller loop has been identified on the eastern side. River has shifted towards the west after abandoning loop (Figure 4.42e). In this block vegetation is scattered and agricultural fields are developed in the flood plain of the river (Figure 4.42f). At this location Sonai river enters onto the Barak basin and bends towards west and change its course almost in west-east bearing. Block-4 shows a large meandering loop towards west and here Sonai river again start turning toward the normal N-S course (Figure 4.43a). In this block whole flood plain is transformed into cultivated land. Vegetation is linear following the river banks (Figure 4.43b). The block-5 is the northern most one showing two smaller loops one toward east and the other toward west (Figure 4.43c). At this location river shows intense meandering and joins the Barak river. Flood plain of both Barak and Sonai rivers are merged at this location and agricultural fields and manmade canals and ponds are developed in the region (Figure 4.43d).

4.9 Results

On the basis of satellite image and DEM studies a few cases of fault propagation folding could be identified from the study area. Several instances of river crossing the faulted part of fold ridge indicate that the fold belt has also suffered later deformation forming the transverse faults. The fold pattern, in general, although appear to be simple but detailed analysis of fold morphology with the help of satellite images and 90m-SRTM-DEM of the study area several types of fold geometry could be identified and delineated.

This effort also provided insight into the image characteristics of the fold patterns. Plunging fold noses have been identified and delineated which are otherwise not apparent. Overlapping nature of anticlinal ridges could be studied well using DEM and satellite images. Remarkable western anticlinal limb bulging is found to be attributed to normal faulting and the geomorphological features of faulted anticlinal limbs are well expressed on satellite image. Further, interesting features formed in the region are elliptical and cusp shaped synclines bounded by fault affected ridges and an anticline within the earlier wide anticline.

Rivers response to the tectonic deformation is very prompt and the study of Barak river through temporal data set specify the same. In the initial part (eastern side) of the study area the Barak river show distinct northward shift. Northward shift is occurring actively as indicated by recent abandoning of a loop by the neck cut-off process. GIS technique used for quantifying the amount of shift of the channels selecting some ground control points. Here, the river has shifted northward for considerable distance and even the tributary stream on the north also show northward shift. In this area shift is occurring northward even though there exist an area of depression towards south. Occurrence of linearly arranged vegetation marks the position of where the river existed earlier. Intensity of meandering has considerably been reduced in the initial part and the river show tendency to straighten up. These changes appear to be attributed to northward tilting of the alluvium possibly caused by tectonic movement in the river basin as corroborated by the occurrence of earthquake (5.5 Mb) of 1984 and seismic activities in the Indo-Burman fold belt. Tributaries of Barak river exhibit active meandering and interesting variations. Dhaleshwari and Sonai river course are affected by the faults and fold ridges.

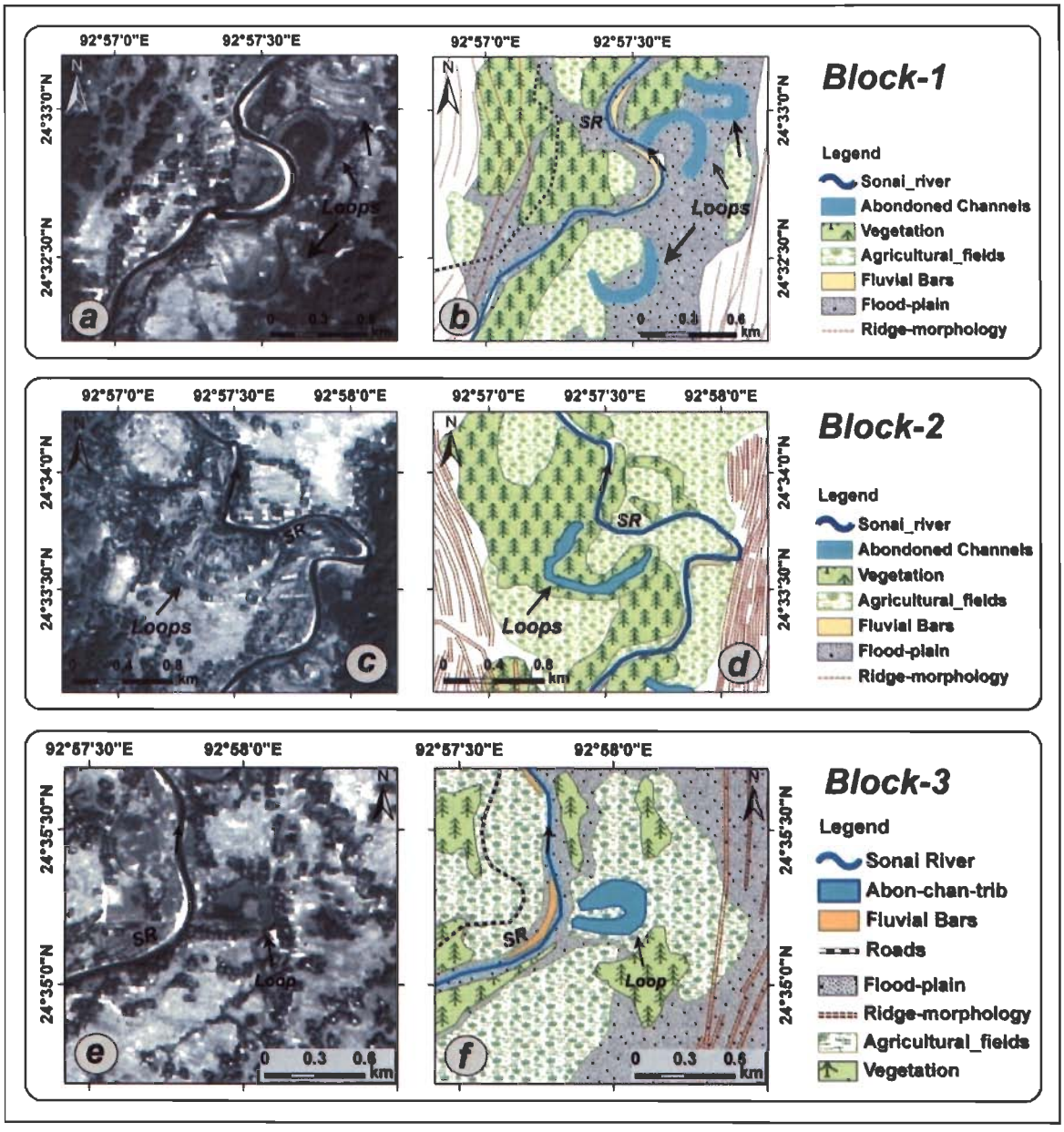

Figure 4.42 Block 1 to 3 of Sonai river (SR). River channel and loops are shown in (a,c,e) with geomorphological characteristics in (b,d,f).

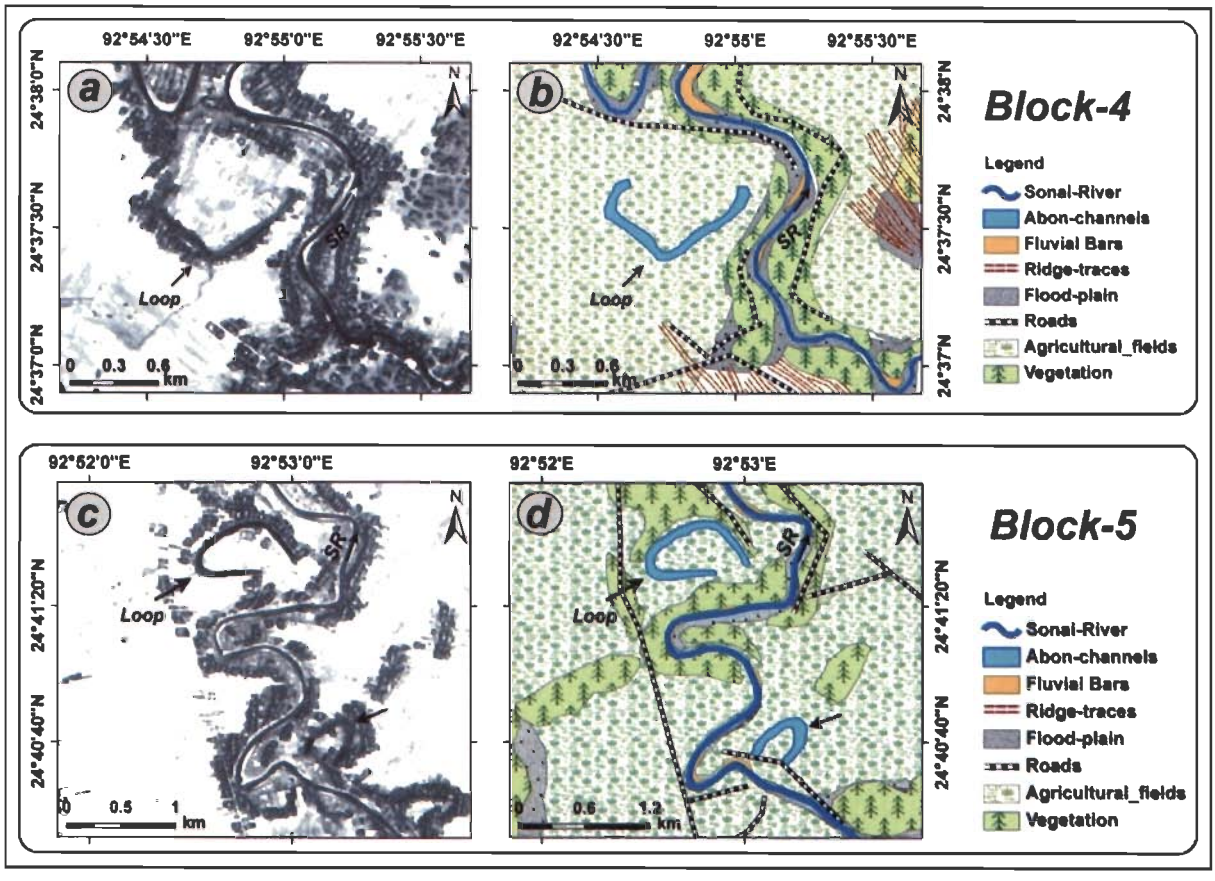

Figure 4.43 Block 4 and 5 of Sonai river (S R). River channel and loops are shown in (a, c) with geomorphological characteristics in (b,d).

CHAPTER -V

Morphometrics of synclinal basins, western Tripura and Lengpui regions

5.1 Introduction

A few selected geomorphological features viz. synclinal basins, frontal slope and Lengpui valley occurring in the Surma Basin with morphotectonic significance warrant detailed morphometric analysis. The Lengpui valley displays a unique topography as the valley is formed by several larger gently sloping surfaces. These select areas have been studied in details by extracting and analyzing drainage parameters and presented in this chapter. Drainage networks were extracted from DEM and satellite images using GIS tools. However, automatically derived stream network need to be verified on the satellite images as the DEM extracted stream network might miss the meandering pattern of the rivers especially in wide valleys where slope variation is considerably low. Various stream anomalies like sudden change in flow direction, increase in meandering intensity, straightened courses, stream flow against the local gradient of the area, channel incision, can be easily delineated from the satellite image and DEM. Drainage divide area, drainage asymmetry, basin elongation ratio, river sinuosity and other drainage parameters are widely used for morphotectonic studies.

5.2 Major synclinal basins

In this work various drainage indices have been calculated for all the major synclines of the Surma Basin to understand prevailing tectonic scenario. Figures 5.1a and b are representing the drainage divides and drainage networks derived from SRTM-DEM for the major synclinal valleys.

5.3 Analysis of drainage parameters

5.3.1 Channel sinuosity (S), proposed by Muller (1968) is used to understand the active tectonism (Susan, 1993). This is defined as S=SL/VL, SL=Stream Length, VL-Valley Length. Sinuosity values indicate nature of river course such as S is 1.0 for straight course; S = 1.0 – 1.5 for sinuous course and S > 1.5 for meandering course. Many causative factors force it to deviate from its straight course. Channel sinuosity is very useful to understand the response of streams to the operating tectonic activity.

Highest river sinuosity resulted from the Manu river of the Manu syncline. An interesting channel pattern could be identified from the Khowai river of Khowai syncline. This river shows meandering course in northern valley while sinuous in the southern valley region as evident by the sinuosity values (Table 5.1). In fact this synclinal valley has suffered from the 'uparching' due to which a drainage divide is created and both the southern and northern drainages are following the opposite trend.

5.3.2 Drainage basin asymmetry analysis helps in identifying neotectonic in areas underlain by weakly consolidated surficial material particularly in poorly exposed quaternary alluvial areas (Cox et al., 1994).

5.3.2.1 ***Asymmetry Factor (AF)****:* Asymmetry factor is a qualitative index which helps in evaluating basin asymmetry. AF = 100(Ar/At) Ar - the area of the basin to the right (facing downstream) of the trunk stream; At - total area of drainage basin. AF has considerable importance in identification of tectonic deformation. AF is sensitive to tilting perpendicular to the main channel in a basin. In a stable basin AF is equal to 50. AF value more or less than 50 indicates a tilt. The computed asymmetry factors for all the drainage basins of study area are either more or less than 50 which ranges from 46 to 66. Minimum value was found from the Hailakandi and highest from the Khowai north. All the other synclines also show the values greater than 50.

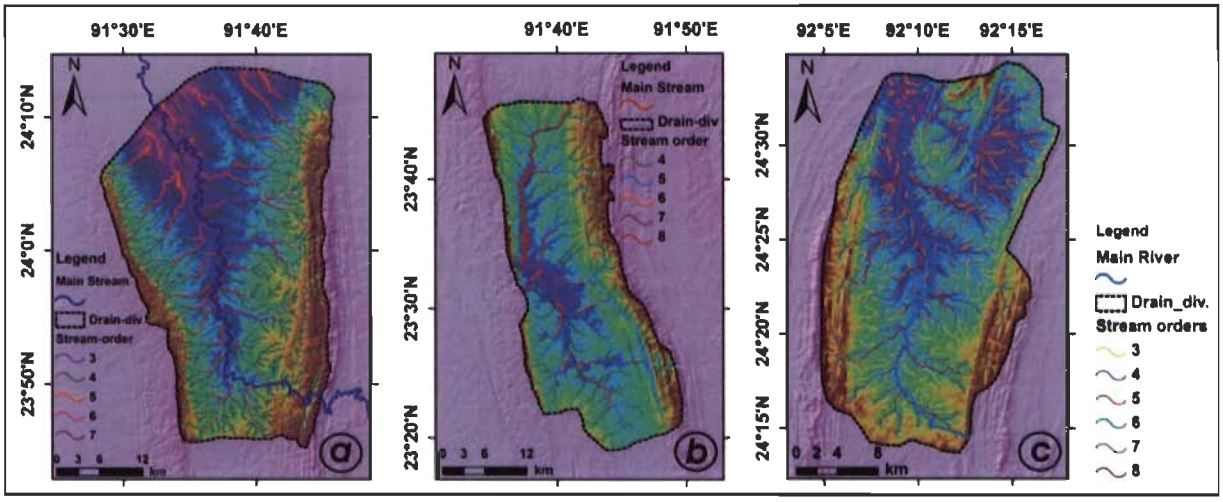

Figure 5.1a Drainage networks of Khowai-N (a), Khowai-S (b), and Dharmanagar Synclines (c) shown on color coded SRTM-DEM and shaded relief models.

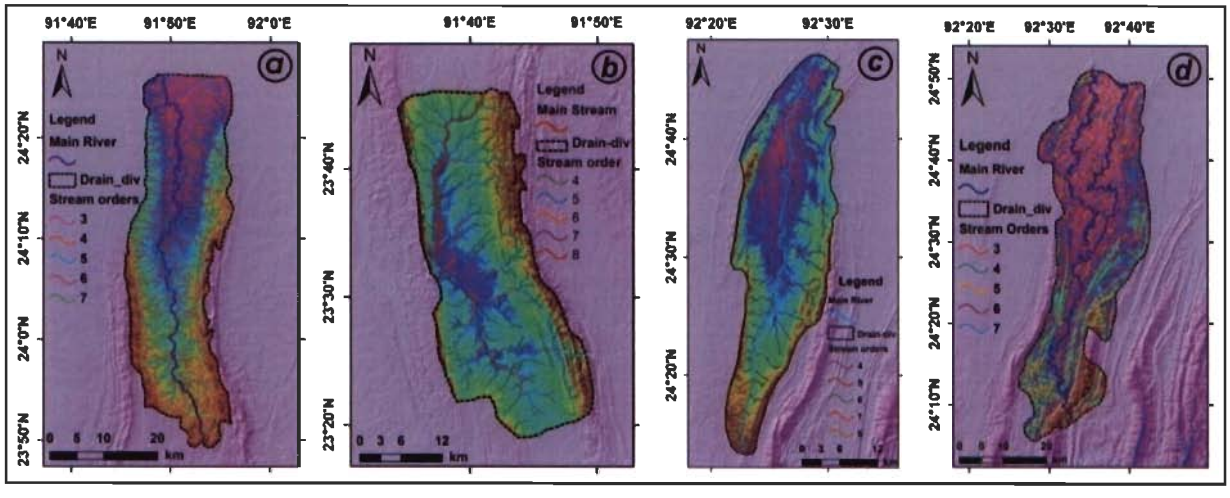

Figure 5.1b Drainage networks of Manu (a), Dolai (b), Sonbil-N (c) and Hailakandi (d) Synclines, shown on color coded SRTM-DEM and shaded relief models.

5.3.2.2 ***Transverse Topographic Symmetry:*** T = Da/Dd , where Da is the distance from the mid-line of the drainage basin to midline of the active channel or meander belt, and Dd is the distance from the basin midline to the basin divide (Figure 5.2). Topographic symmetry is useful for quantification of basin morphology. Perfectly symmetrical basin has value of topographic symmetry as zero, as the asymmetry increases T increases and reach the value of one. All the synclines show the value greater than zero which indicates that all are asymmetric. Lowest value was obtained from the Sonbil and Hailakandi basins. Both the valleys are narrower and are located towards the southern end. Highest value of about 0.79 resulted from the Dharmanagar syncline represented by wider valley lying in the central part of Surma Basin.

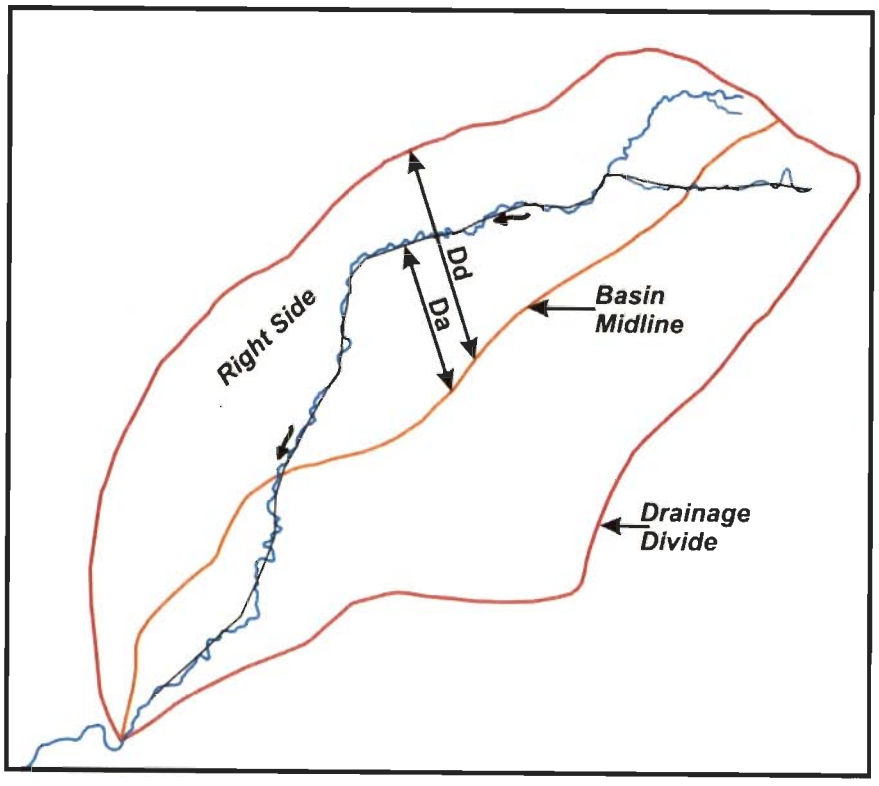

Figure 5.2 Drainage basin showing drainage divide, basin mid line and transverse distances Dd and Da.

5.3.3 Basin Elongation Ratio (Re) is proposed by Bull and Mc Fadden (1997) is one of the proxy indicators of recent tectonic activity (Cuong and Zuchiwicz, 2001). The basin elongation ratio, Re = ($2\sqrt{A}$: $\sqrt{\lambda}$)/L, A = Basin area, L = Basin Length. Drainage basin in arid and semi-arid climates shows Re values of less than 0.50, between 0.50-0.75 and more than 0.75 for tectonically active, slightly active and inactive settings. All the synclinal valleys exhibits extremely high values of Re, ranges between 10 (Sonbil) to 24 (Khowai north) indicating activeness of the region.

All the estimated morphometric parameters for various synclines are given in Table 5.1.

Table 5.1 Morphometric properties for various synclines of Surma Basin.

Synclines	Drainage Symmetry	Transverse Symmetry	Stream Sinuosity	Basin Elongation Ratio
Khowai-N-Syncline	66.43	0.74	1.57	24.21
Khowai-S-Syncline	64.19	0.80	1.30	13.22
Dolai-Syncline	56.16	0.70	1.61	14.19
Manu Syncline	53.81	0.62	1.66	16.86
Dharmanagar Syncline	58.78	0.89	1.53	15.21
Sonbil Syncline	56.02	0.53	1.30	10.37
Hailakandi Syncline	46.06	0.55	1.50	15.66

5.4 Western Tripura region

Morphometric characteristics of Tripura region are presented through the study of river channel characteristics and derivation of morphometrical indices. The rivers and different stream network developed in the western Tripura region remained sensitive to the present topography which is the manifestation of tectonic and erosional activities operated in the region.

The area represents a gentle westerly sloping area named Agartala slope originating from the Baramura anticlinal ridge lying west of another anticline, the Atharamura Anticline and intervening Khowai and Ampi-Bazar synclinal valleys falling in the westernmost part of Tripura, Northeast India adjoining the Bangladesh (Figure 5.3). The area occupied is approximately 9800 km^2 comprising of Agartala slope (around 2826 km^2), Baramura anticline (around 850km^2) and Atharamura anticline (around 1786km^2).

The fold belt also forms a topographically high zone from where the terrain slopes down to northward as well as southward. This topographical characteristic is well displayed by the nature of drainage network of the region with a drainage divide. The region appears to have suffered uparching and beneath the Agartala region a dome structure has been recognized based on seismic survey (Ganguly, 1993). Following the natural topographical slope, several drainage networks can be seen developed in the area along with two large active rivers which cut crosses the anticlinal ridges before entering onto the Bangladesh plains. The drainage networks on the Agartala slope have their origin at the Baramura anticline having mainly the ephemeral characteristic. These drainage networks (DN) on the Agartala slope have been labeled, from north to south, as DN1- DN8 (Figure 5.3).

5.5 Approach

Drainage network has been automatically extracted from the DEM and then cross checked with the corresponding satellite images. In some parts of the stream the DEM extracted drainage line does not follow the meandering path resulting in an offset of streams from the ground condition. This offset was subsequently corrected with the help of stream path digitally drawn from satellite image displaying the ground condition. Considering the area covered by the Agartala slope, anticline and syncline (approximately 9800 km^2) 90m spatial resolution of DEM found to be workable for a reasonable description and interpretation of the drainage network and morphology. However, at this resolution the shallow river valley i.e. wherever the elevation difference between the river bed and its bank topography is pretty low the extracted drainage line became off from the actual channel line on ground as the DEM extracted stream followed the lowest elevation cells having 90 meters dimension. In such a case special care was taken by correcting the DEM extracted drainage network comparing with the stream information derived from the satellite image.

5.6 Geomorphology

Geomorphologically the area is represented by elongated hill ridges, basin, ephemeral and dried streams (Figure 5.4). Stream network development in the synclinal basin is governed by both region of up-arching and the bounding anticlinal ridges on eastern and western sides whereas; the stream network on the Agartala slope is controlled by the arched nature of the slope. Characteristics of main geomorphological units from the region as seen on the satellite images (PAN and FCC) are described in Table 5.2.

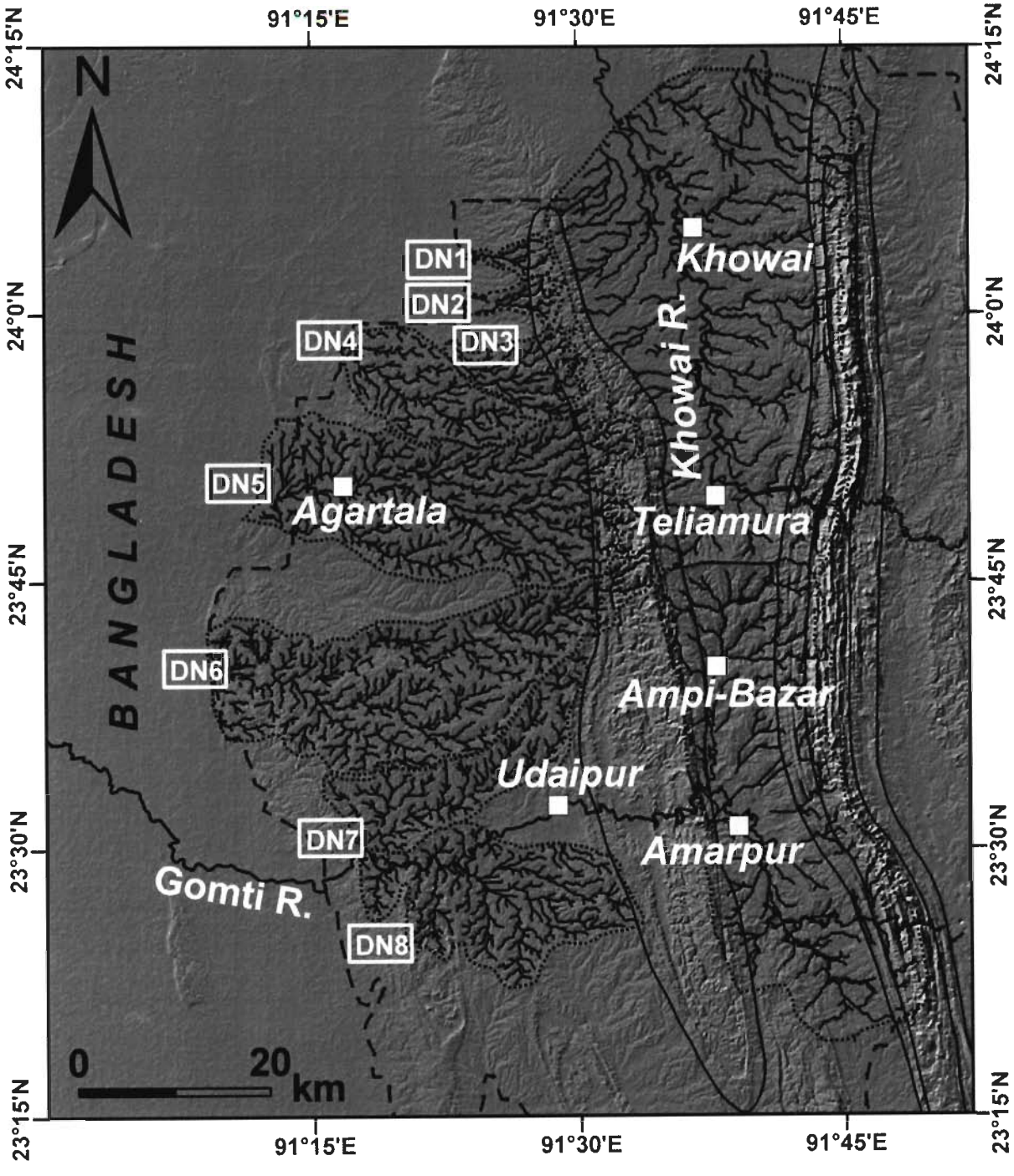

Figure 5.3 Agartala slope, anticlinal ridges and synclinal valleys (Khowai and Ampi-Bazar) are shown by shaded relief model of SRTM-DEM. Drainage networks (DN1 - DN8) of the Agartala slope are shown.

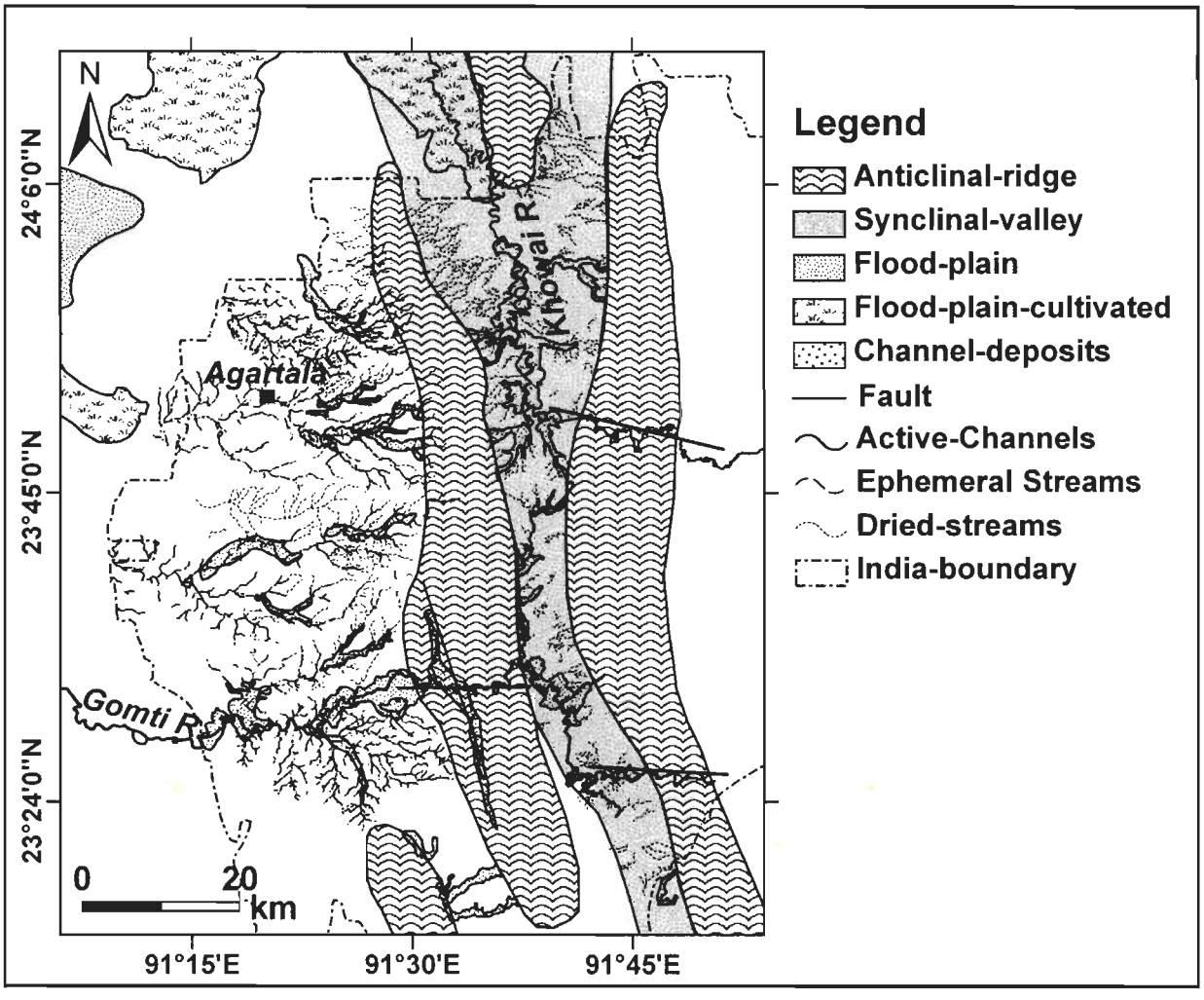

Figure 5.4 Geomorphological map of the western Tripura region depicting different geomorphological units.

Table 5.2 Characteristics of the main geomorphological units present in the western Tripura region as revealed by satellite images.

S. No.	Geomorphic Unit	Image Properties		Geomorphological Characteristics
		PAN image	FCC image	
1.	Anticlinal Ridge (denuda-tional)	Dark tone and linear texture	Reddish tone and linear texture	The elongated hill ridges constitute of sandstone, shale and siltstone mainly. Two sides of the anticlinal ridge with top surface eroded out exhibit linear beds dipping in opposite direction away from the ridge crest. Dark and reddish tone due to vegetation cover and linear texture formed by linearly arranged fold limbs.
2.	Synclinal valley	Dark and bright tones and planar rough texture	Mixture of Reddish (vegetation), bright (soil) and bluish (water and moist soil)	Synclinal basin is filled up by sediments forming a planar area with depression. Due to intense weathering activity and development of drainage network the area is giving rugged appearance.
3.	Flood plain	Darker tone and smooth texture.	Bluish yellow with speckled texture.	Area formed due to flooding and depositing of fine sediments. High moisture content and composed of silt, sand and clays brought down by the Gomti river system and others.
4.	Channel deposits	Bright tone with semi-smooth texture	Bright tone with slightly Coarse texture	Occurring in the rivers and along the river banks. These are the fresh deposits by the river action which is more on the concave side of the river.

5.7 Linear features / faults

Geomorphologically significant linear features occurring across the anticlinal ridges paved way for the rivers to cross otherwise the higher topographical regions (Figures 5.3 and 5.4). The Gomti and Khowai rivers cross anticlinal ridges at two and one places respectively. In fact, the part of the Baramura anticlinal ridge through which the Gomti river crosses has been affected by longitudinal as well as transverse faults. The transverse faults have created low land across the anticlinal ridges allowing advancing of the Gomti river channel whereas, the longitudinal fault caused widening of the western limbs of the anticline. E-W oriented faults strongly control the channel course of Gomti and Khowai rivers in the anticlinal ridges as well as in the intervening syncline.

5.8 Drainage pattern

Satellite image of the western Tripura region exhibits intense development of drainage network on the Agartala slope. The entire drainage network originates from the Baramura anticline and flow westward (Figure 5.3). At the contact zone of western limb of the anticline and slope all the stream forms wider valley as they enters on to lower regions. In general the drainage networks are relatively smaller in extent except the network that developed in the central part of the slope. The upstream part of the drainage network (DN5, Figure 5.3) developed at the central part is considerably wide as several tributaries have formed and joined with the Haora river. This nature is due to the fact that this drainage network got developed over the highest part of the Agartala slope forming an almost planar area. All the tributaries to this river are of ephemeral nature and are rain fed. Main stream only has some water flow. All the river channels form very wide river erosional plain and especially the main river even in the up-stream side adjacent to the Baramura ridge. Another drainage network, the DN3 (in Figure 5.3), also forms very wide river erosional plain. However, unlike other drainage system this one takes a north-eastward swing at latitude $23^{\circ}56'$ and longitude $91^{\circ}24.75'$.

The whole Agartala slope exhibits development of extensive drainage network as indicated by a network of minor gullies giving rise to dissected appearance of the area. Many stream networks have gone dry and agricultural fields have been developed along the dried up channels at several places.

Westward flowing meandered Haora river through the central part of the Agartala slope exhibits northward curvature between the Dudhpatil and Agartala regions (Figures 5.5a and b). It is important to notice that most of the tributaries of the Haora river developed on the southern side have become dry now. Whereas on the northern side one large tributary was in existence has also gone dry. On the northern side of Haora river wide flood plain (dark tone area on satellite image, figure 5.5a) has formed by a river which used to flow parallel to the Haora river compared to the southern side. The Haora river appears to have shifted its course northward (as shown by the arrows in figure 5.5b) between Dudhpatil and Agartala and at present flows through an urban area located at the central part of the area. Further, nature of present elongated flood plain on the southern side of the Haora river along with the impression of meeting zone of southerly tributaries indicates that the Haora river once flowed through that region (Figure 5.5b).

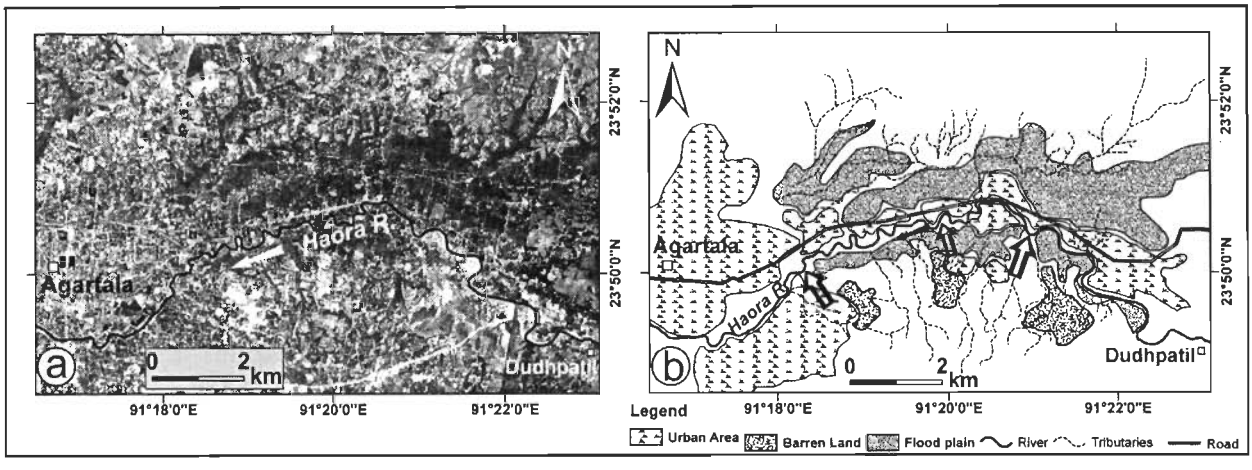

Figure 5.5 Northward convexity of Haora river as displayed by IRS-1D PAN satellite image (a) and the interpretation map along with various geomorphological units (b). Arrows indicate shift direction of the Haora river.

The Gomti and Khowai rivers are the main two long rivers of the western Tripura region. Both these rivers follow extremely zig-zag path especially in the synclinal basin area. On the southern side of the Agartala slope, the Gomti river flows westward making intense meandering loops and dissects both the Atharamura and Baramura anticlines (Figures 5.6a, b & c). The total meandering length is 356km and the valley length is only 116km. High meandering intensity can be observed in the region of Ampi-Bazar syncline. Also, the river had to follow very zigzag path while crossing the several fold limbs of the Baramura anticlinal ridge. This river first crosses Atharamura anticline flowing westward and then flows northward before taking westward turn near Amarpur for crossing the Baramura anticline. The Baramura anticline at this place has been affected by the transverse faulting and longitudinal limb parallel faulting on the western side just east of Udaipur (Das et al., 2010). The western limbs show westward bulging (east of Udaipur) and in the inter-limb region streams have developed on both sides of the Gomti river. The Gomti river channel also exhibit loop abandoning in the western inter-limb area of Baramura anticline where a loop has been shifted northward for about 900 meters (Figures 5.6b & c).

Similarly, the Khowai river also follows a very intense meandering path in the Khowai syncline as well as within the Atharamura anticlinal ridge. The total meandering length is 171 km and the valley length is only 81 km. The Khowai river originating from a region lying east of the Atharamura anticline flows westward and crosses the anticline and then flows southward through the Khowai syncline after taking a turn at Teliamura (Figure 5.6b). Within the Atharamura anticline the Khowai river follows an extremely zig-zag path and at western limb side a large river loop has been abandoned (Figures 5.7a, b & c). Abandoning of a Khowai river loop as seen on satellite image (Figure 5.7b) and the interpretation map of the same is shown in figure 5.7c. The Khowai river loop within the anticlinal ridge shifted northward for about 1 km.

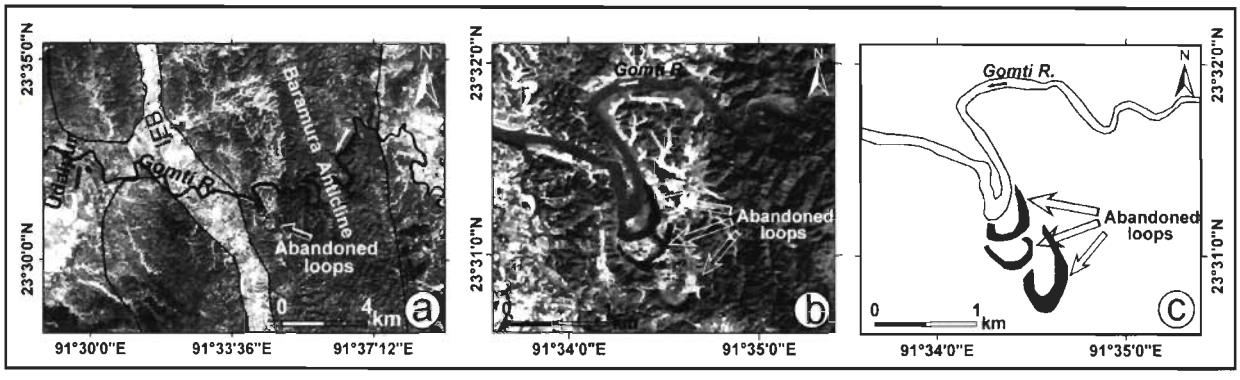

Figure 5.6 Meandering shape of Gomti river within the Baramura anticlinal ridge and the abandoned loop. PAN image showing meandering trend and faulted western limb creating interlimb elongated basin (IEB) (a). Abandoned meandered loop as displayed by IRS-1D PAN image (b) and digitally traced part of the Gomti river and abandoned loop (c).

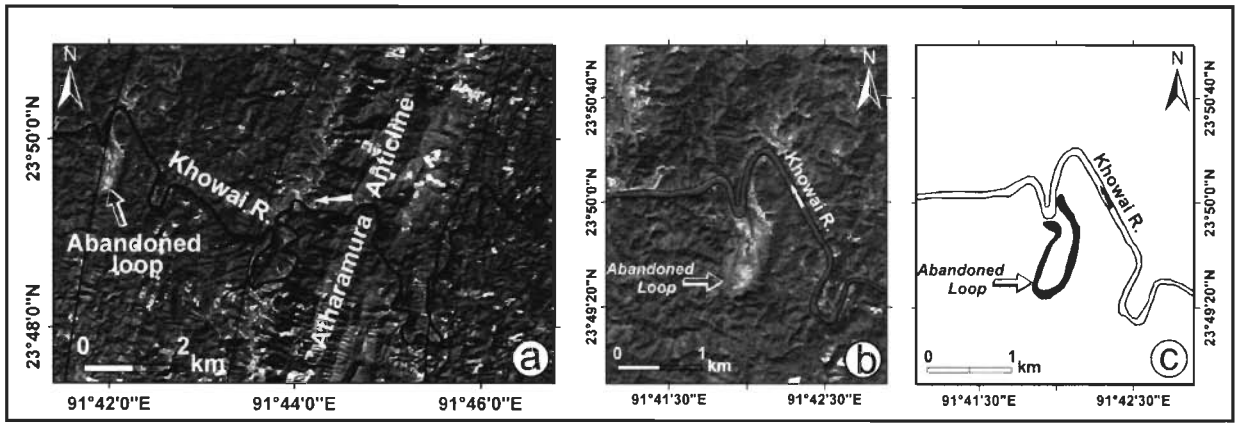

Figure 5.7 Meandering shape of Khowai river within the Atharamura anticlinal ridge and the abandoned loop. IRS-1D PAN image showing meandering trend (a). Abandoned meandered loop as displayed on image (b) and digitally traced part of the Khowai river and abandoned loop (c).

It is important to note that both the Gomti and Khowai rivers exhibit abandoning of southerly occurring loops and shifted northward within the anticlinal ridges. The Gomti river indicated three stages of loop abandoning by the presence of three paleo-loops (Figures 5.6b & c) whereas, the Khowai river exhibits only one stage of loop abandoning (Figures 5.7b & c). It appears that both rivers loops have shifted towards the fault probably due to later activity along the fault.

A significant topographical effect on the drainage network is observed for a particular zone falling along the latitude 23°45′N. Tributaries of the Khowai and Gomti rivers flow in opposite direction lying in between the Baramura and Atharamura anticlines from the above mentioned high zone. Further, the entire easterly lying stream network is also marked by opposite flow directions (Figure 5.8a). This higher topographical zone forms a water divide. This also coincides with the highest part of the Agartala slope.

In order to verify the effect of uparching (doming) of the folded belt drainage network has been extracted from the SRTM-DEM considering larger area mainly east of Agartala slope (Figure 5.8a). The drainage network setup of the region reflects clearly the flow direction and trend from the drainage divide (DD) from where all the streams flow in opposite directions. However, drainage network developed on the Agartala slope flows westward following the natural slope. Topographic profiles are also taken from the SRTM-DEM at some places over the Agartala slope and easterly occurring fold belt (Figure 5.8a). Topographic profiles have been smoothed considering the maximum elevation points as the extracted profiles came out to be extremely zig-zag following the undulating landform. The profiles are: two longitudinal profiles (TPL-1 and 2) and one transverse profile (TPT-1) over the Agartala slope and two longitudinal profiles along the synclinal basins (TPLS-1 and 2) of the fold belt (Figures 5.8a - f). The entire longitudinal profiles trend show higher elevation across the zone of drainage divide indicating uparching effect of the region. Whereas, the transverse profile (TPT-1) show eastward increase in height of the Agartala slope. This profile also show occurrence of two anticlinal ridges (Baramura and Atharamura) towards right or eastern side.

5.9 Morphometric properties

Various morphometric indices have been estimated for all the drainage basins on the Agartala slope, Khowai and Ampi-Bazar synclines. Average channel sinuosity for the entire studied streams falls in the range from 1.21 - 1.67. The computed asymmetry factors for all the drainage basins of area are either more or less than 50 which ranges from 30.90 - 79.80. Transverse topographic symmetry calculated for all the drainage basins at different locations and the average value ranges from 0.63 - 0.89. In case of Agartala slope consistently high values of basin elongation ratio has been found. This value ranges from 2.05 - 24.21 for this area. Table 5.3 lists computed morphometric indices for the above.

Table 5.3 Morphometric indices for different streams and drainage networks.

Streams / Drainage Network		Sinuosity (S)	Drainage Asymmetry (AF)	Transverse Symmetry (T)	Basin Elongation Ratio (Re)
Agartala Slope and its Drainage Networks	DN1	1.49	37.85	0.66	02.05
	DN2	1.21	35.27	0.67	02.69
	DN3	1.67	64.60	0.82	04.78
	DN4	1.51	57.98	0.71	06.16
	DN5	1.36	55.11	0.63	12.55
	DN6	1.44	30.90	0.71	10.10
	DN7	1.50	79.80	0.89	06.61
	DN8	1.35	36.58	0.72	09.48
Khowai Syncline	Basin	1.57	66.43	0.74	24.21
Ampi-Bazar Syncline	Basin	1.65	64.19	0.80	13.22

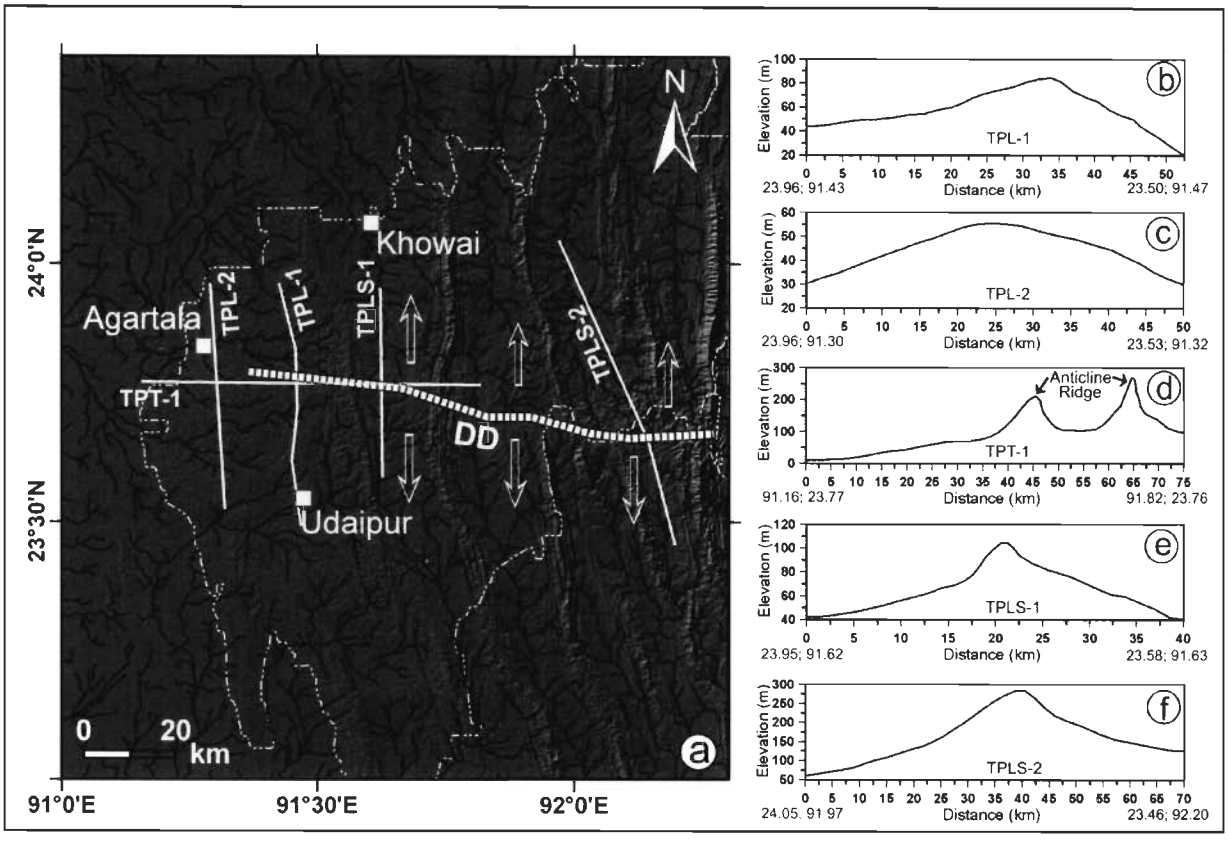

Figure 5.8 Drainage network and topographic profiles. Drainage network derived from SRTM-DEM and overlaid on shaded relief model (a). Arrows show flow directions of the stream network from the DD. Arrows indicate direction of the stream networks flow and topographic slope. Topographic profiles are (b - f): Topographic Profile Longitudinal (TPL-1, 2) over the Agartala slope, Topographic Profile Transverse (TPT-1) over the Agartala slope (Baramura and Atharamura anticline ridges area shown as Anticline Ridge in d), Topographic Profile Longitudinal along synclinal basins (TPLS-1,2), Drainage Divide (DD).

5.10 Lengpui region

Lengpui region is located in the central part of the Surma Basin and west of the Aizwal. This area is an intermountain valley and demonstrates a different topographical appearance from the surrounding regions. The whole region shows anomalous and interesting slope variations as revealed by the morphometric study of this region. DEM of the area displays relatively smooth topography and large gently sloping surfaces deviating from normal synclinal topography. Streams also show divergence from normal concave profiles. Dhaleshwari River, a major tributary of the Barak is the main river of this region and many small streams join it from various drainages basins. This river is highly active and show intense meandering nature. River also involve in active downcutting of the valley resulting into deep steep sided V-shaped valley. Figure 5.9 is showing the Lengpui region along with Dhaleshwari river and adjoining area.

5.11 Topographic variations

Topographic profiles were derived for better understanding of the variation in topography from place to place. Total 8 transverse profiles were extracted from the ASTER-DEM of the region from north to south (Figure 5.10).

All the profiles are exhibiting a narrow deeper V-shaped river valley. It was observed that the valley becomes narrower toward the south. Profile TP-1 is the northern most profile of the river is showing that valley is more nearer to a U-shaped valley (Figure 5.10-TP1). But toward south the depth of the valley as well as steepness of walls increases. The Dhaleshwari river actively incising the valley floor in this region, and shows a valley depth of more than 400m at some places (Figures 5.10, TP3 - TP6). Other than this it is also evident from the profiles that the surrounding region is also showing upliftment as well as tilting.

5.12 Morphometric analysis

In Lengpui and surrounding region very anomalous and interesting slope variations have been observed. This whole region is comprises of large lower gradient flat surfaces as can be seen on DEM. Morphometric study of the region has been carried out to understand the behavior of the topographic slope and variations in the valley. Stream length gradient index (SL index), slope index (S-Index) and hypsometric integral (I_{hyp}) has been calculated for the region using ASTER-DEM. Total 21 basins were selected for analysis of all the morphometric indices. Figure 5.11 is representing all the basins along with their respective streams.

5.12.1 Stream length gradient index (SL-Index)

The SL Index correlates to stream power and rock resistance. The total stream power available at a particular channel reach is an important hydraulic variable as it relates to the capability of a stream to transport sediments and to erode its bed. The SL index is very sensitive to channel slope, and is a practical tool for measuring perturbations along stream longitudinal profiles. It also allows one to evaluate possible relationships between tectonic activity, rock resistance and topography (Burbank and Anderson, 2001). Furthermore, SL Index may be used to detect recent tectonic activity by identifying anomalously high index values on a specific rock type (Merritts and Vincent, 1989; Keller and Pinter, 1996; Brookfield, 1998; Chen et al., 2003).

This index is defined as

$$SL = (dh/dl) * L$$

SL is the index, h is the height of segment investigated, in this study, a contour interval (h) of 50m is used and l is the horizontal distance of the same 50m contour interval segment, **dh/dL** is the stream gradient at a specific site in the channel and **L** is the total channel length from the site upstream to the highest point on the channel.

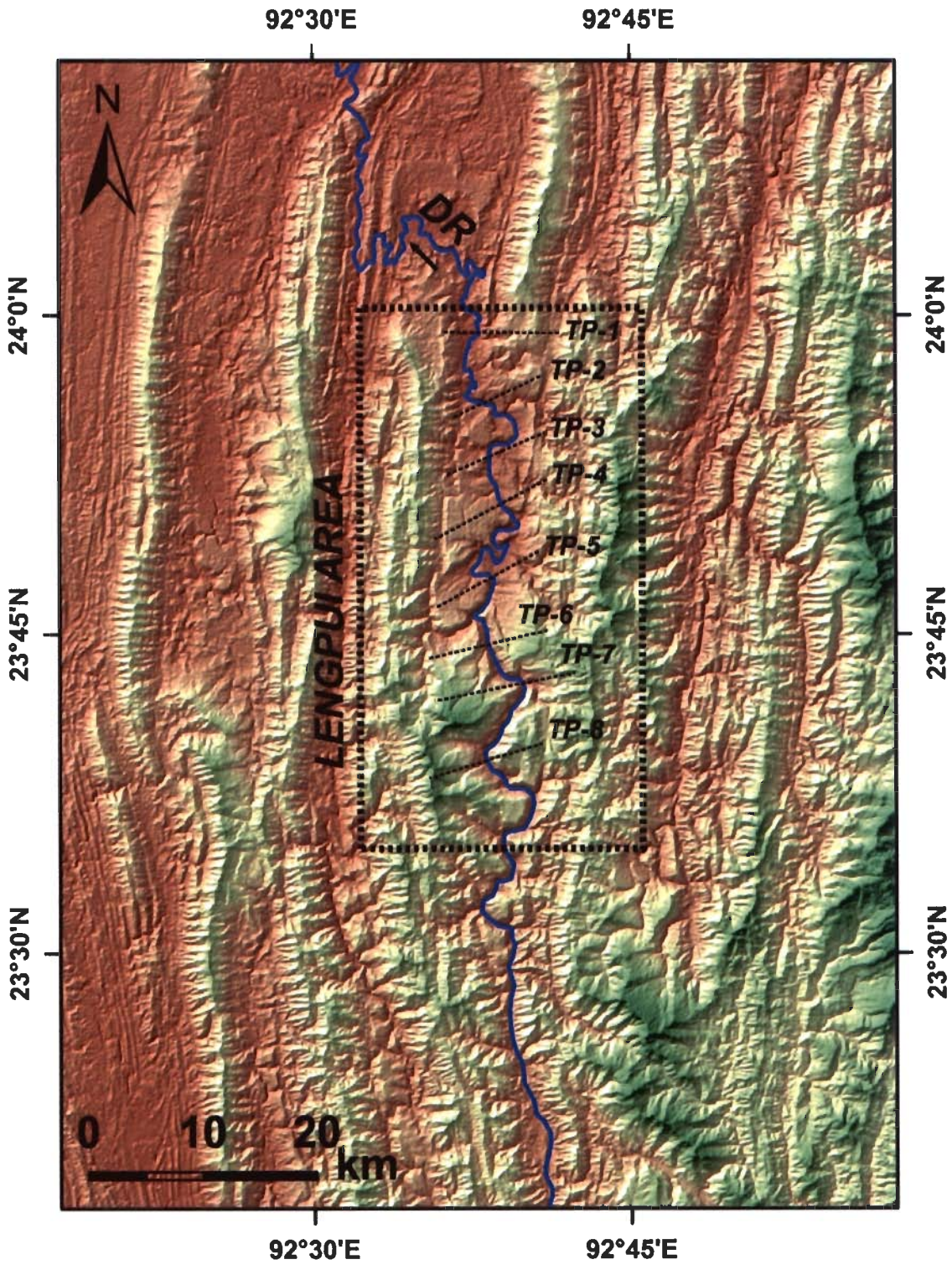

Figure 5.9 Lengpui area with adjoining region shown by color coded shaded relief model of ASTER-DEM. Location of transverse topographic profiles TP1-TP8 is marked here along with Dhaleshwari river (DR).

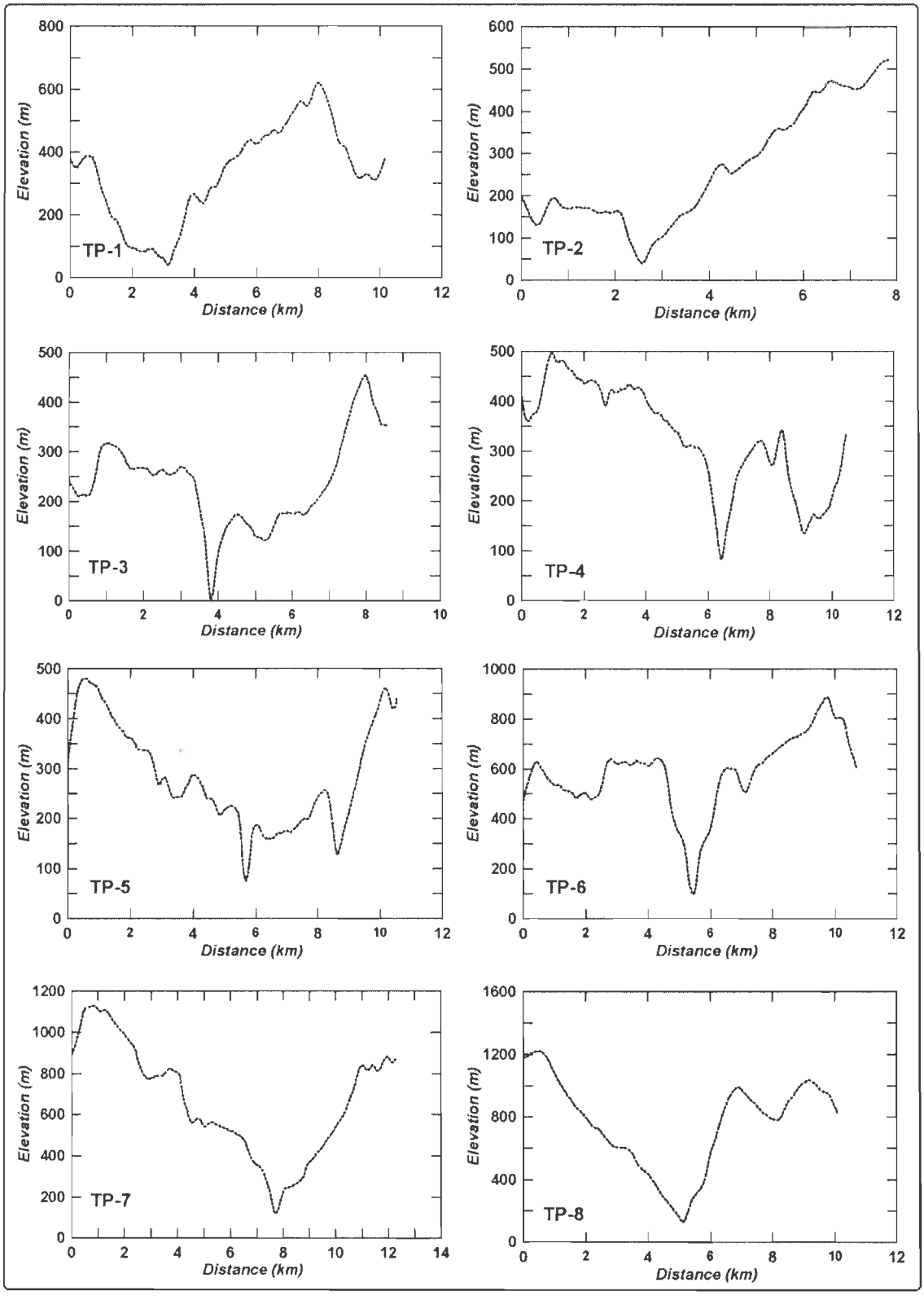

Figure 5.10 Transverse topographic profiles of Lengpui area. Location of the profiles is shown in figure 5.9.

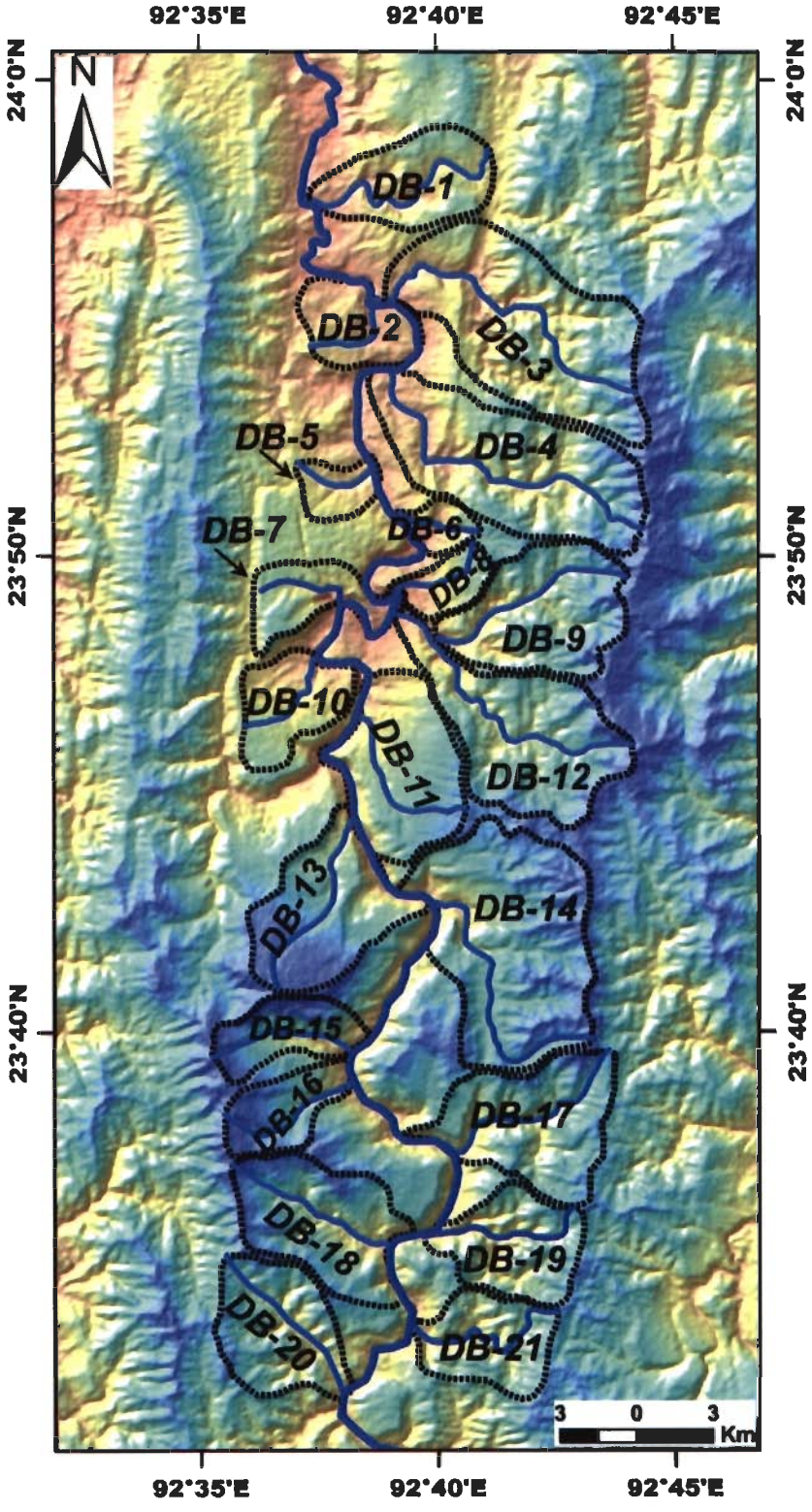

Figure 5.11 Location of various drainage basins (DB1 - DB21) of Lengpui area shown on color coded shaded relief model of ASTER-DEM.

For calculation of the SL index all the values have been extracted from the 30m ASTER-DEM. Boundaries of all the basins were digitized manually to avoid the chance of errors during the basin boundary delineation. Small subset for each basin has been created to get the greater accuracy and contours were dynamically generated with 50m interval for each basin. It was found that sometimes contours have not been generated at few places if the larger area is used. All the processing steps were carried out using ArcGIS 9.3 tools.

The SL index is roughly related to the stream power which is particularly sensitive to changes in slope and lithology and this sensitivity allows the evaluation of the relationship between possible tectonic activity and rock resistance. This means that values of the index are high in areas where the rocks are significantly resistant or where active tectonics is present. Therefore, anomalously high SL values or fluctuation of the SL values in rock of uniform resistance is a possible indicator of active tectonics (Keller 1986). Theoretically, the low S value (close to 1) and the high SL value (over 200) indicate active tectonic region (Keller and Pinter, 1996).

In Lengpui region, except few, all the basins show a mean SL index values >200. SL index for all the studied basins are given in Table 5.4. In this region exceptionally low (26) and higher (2347) SL values have been obtained. Therefore, the region might have suffered tectonic deformation along with resistant lithology which contributes to high SL values in the region. Figure 5.12 is showing the SL values at each stream segments. An interesting fact has been revealed from the SL and S index values is that the main river Dhaleshwari is a young river which is actively incising the valley floor. A closer view of the figure 5.12 illustrates that majority of the higher values are concentrated near the valley, which indicate that the exceptionally higher values are actually the result of the very high and steep gradient of the valley walls.

5.12.2 Slope gradient Index (S-Index)

Slope gradient index (S) illustrates the change in SL index between segments and gives an idea about the highest rates of SL variations. S is defined as

$$S = \Delta slope/\Delta L \times L$$

Where, Δ-slope is the difference in slope between two adjacent segments. ΔL is the mid-point between the lengths of the two segments. L is the total channel length from the point of interest where the slope gradient index is being calculated to the source of the channel. S Index was also calculated for all the basins using the same contour interval of 50m. S index values for all the studied basins are given in Table 5.4. The dimensionless values of S can be positive or negative. For a constant gradient, S=0, positive values means gradient is changing from steep to gentle and negative values indicate the slope is changing from the gentle to steep.

SL and S index anomaly maps have been generated for the region to achieve detailed picture of negative and positive anomalies (Figure 5.13). These maps have been prepared by the interpolation of SL and S index values. These maps also show that the central and southern region has more anomalous SL and S index values. Steep sided wall of this narrow V-shaped valley are the main reason behind the concentration of the high SL values near the stream ends (Figure 5.13A). Similar results were found from the S-index anomaly map. Although, from the analysis of absolute mean values for all the streams it is very much clear that most of the streams show gentle to moderate S-index values ranges from 12-78. Only few basins show the mean values greater than the 100 and 200 respectively (Figure 5.13B).

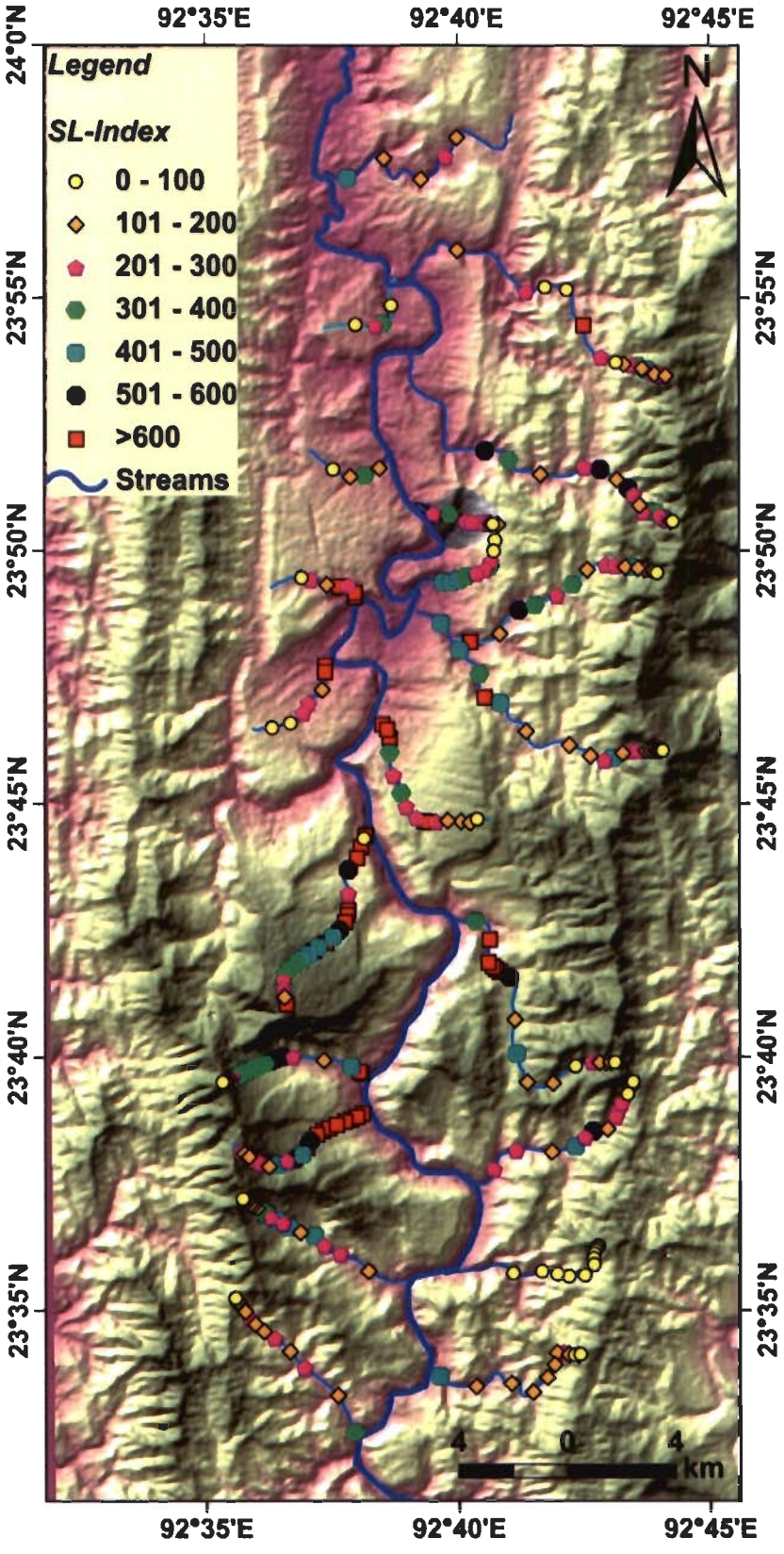

Figure 5.12 SL index variation for each stream segment.

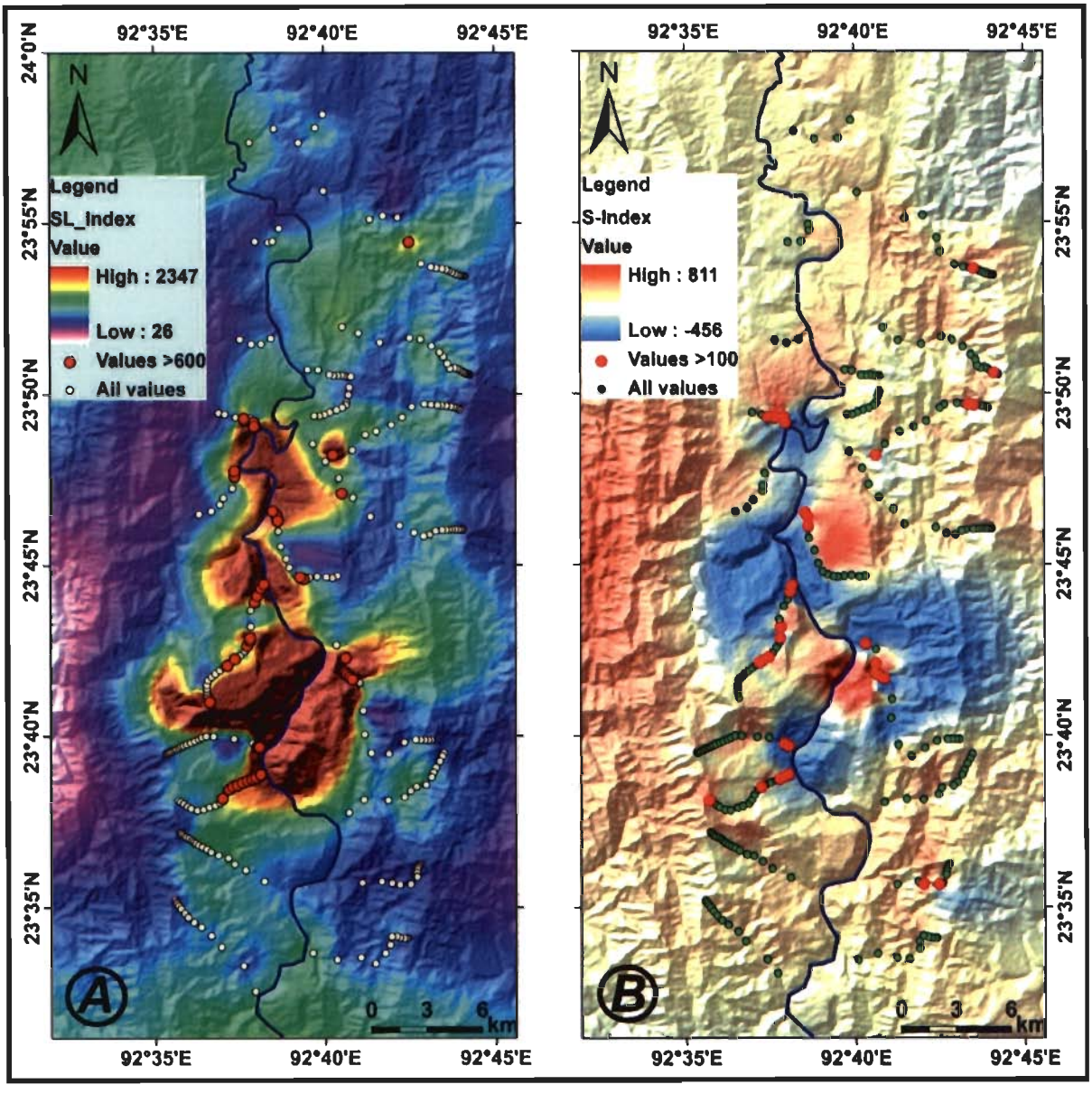

Figure 5.13 SL (A) and S-Index (B) anomaly maps for the Lengpui area.

5.12.3 Hypsometry

Hypsometry is the relative portion of areas at different elevations within a region lying below a given height (Strahler, 1952). For a selected basin, the range of elevations is divided into equal elevation intervals. For each interval the proportion of basin area is calculated. Elevations are normalized by the relief of the catchment so that they range from 0 to 1.0. The hypsometric integral (I_{hyp}) is an index for characterizing the shape of the hypsometric curve by calculating the area under the curve.

$$I_{hyp} = (h_{mean} - h_{min})/(h_{max} - h_{min})$$

Where, h_{mean} is the average height, h_{min} and h_{max} are the minimum and maximum height of the catchment. I_{hyp} falls between 0 and 1 and is independent of the basin size and absolute elevation (Figure 5.14).

Hypsometric integral is used to infer the stages of geomorphic development (1) a convex shaped hypsometric curve characterizes basins in the stage of youth, (2) an S shaped hypsometric curve (concave upwards at high elevations and convex downwards at low elevations) characterizes basins in the stage of maturity, and (3) a concave hypsometric curve characterizes basins in the peneplain stage (Figure 5.14). Strikingly high or low values may be indicative of neotectonic deformation (Keller and Pinter, 2002) as subsidence has a smoothing effect while uplift leads to dissection. However, marked regional differences in erosional processes may also generate considerable variations of I_{hyp} values. Therefore, I_{hyp} help us to understand the simultaneous impact of tectonic as well as erosional processes. Figures 5.15a and b are showing the hypsometric curves for all the 21 basins falling in this region.

For this area values of I_{hyp} have ranges between 0.309-0.666. Lowest I_{hyp} values are indicated by the basins DB-3 and 4. Both the basins show normal trend and the streams also follow a smooth gradient through a lower and highly eroded portion towards east. Highest values come from the DB-5, 14 and 16 (Figures 5.15a and b). All these basins show convex upward curves which indicate that the rate of erosion is slower and the area also show a little upliftment. In DB-7 the curve is highly deformed and shows a knick point which indicates that basin is uplifted. Majority of the basins show high value of hypsometric integral between 0.45-0.5. Hypsometric integral values for 21 basins are given in Table 5.4. All the streams seem to follow a smoother pattern and hypsometric curves are either straight or slightly S-shaped. But they are not perfect S-shaped which indicate that neotectonic processes are operating in the region. Most of the streams are in their youthful stage and are actively incising the valleys.

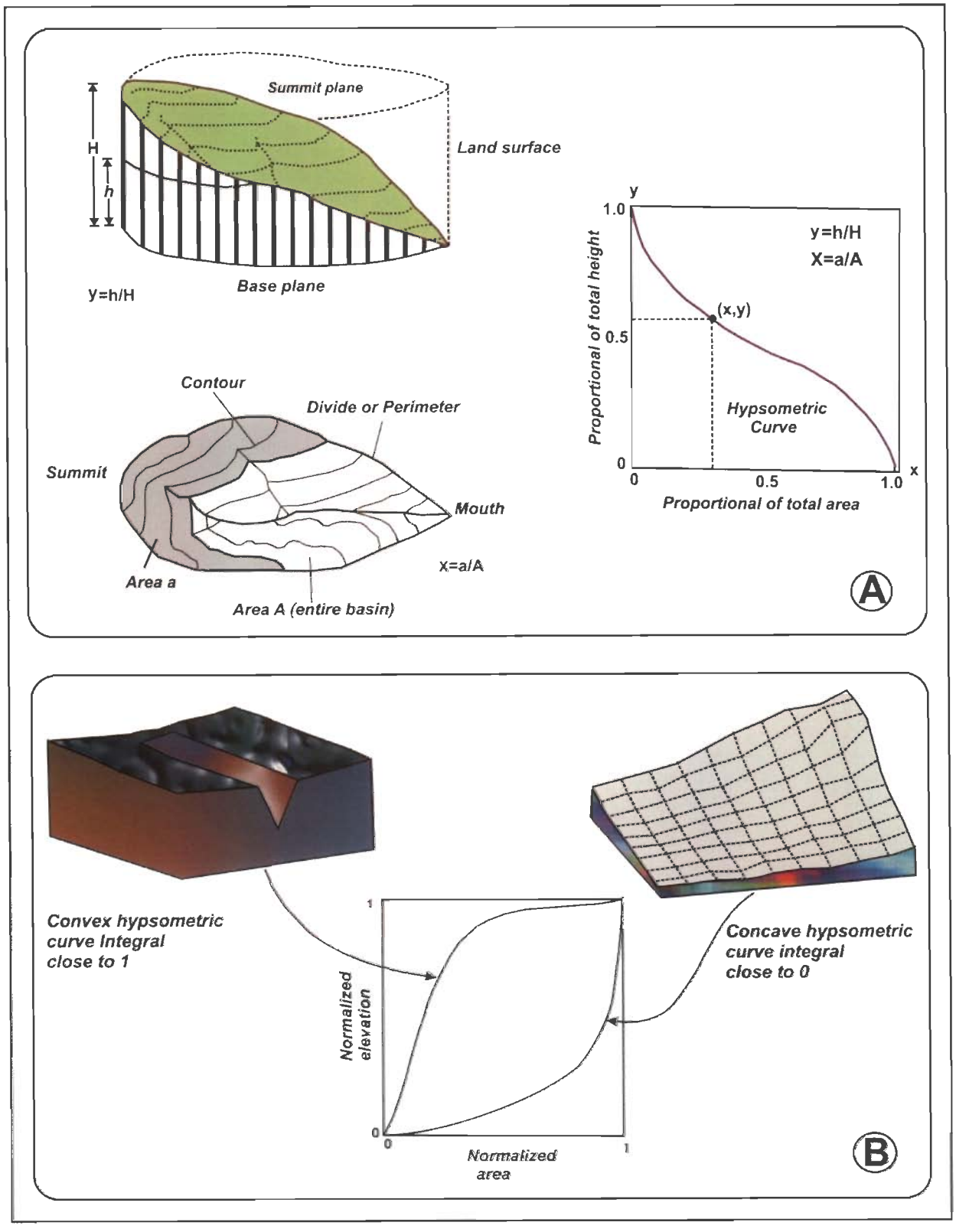

Figure 5.14 Drainage basin along with contours and hypsometry parameters (A), Hypsometric curves of youthful and mature stage (B). (Source: http://rst.gsfc.nasa.gov/Sect17/Sect17_9.html)

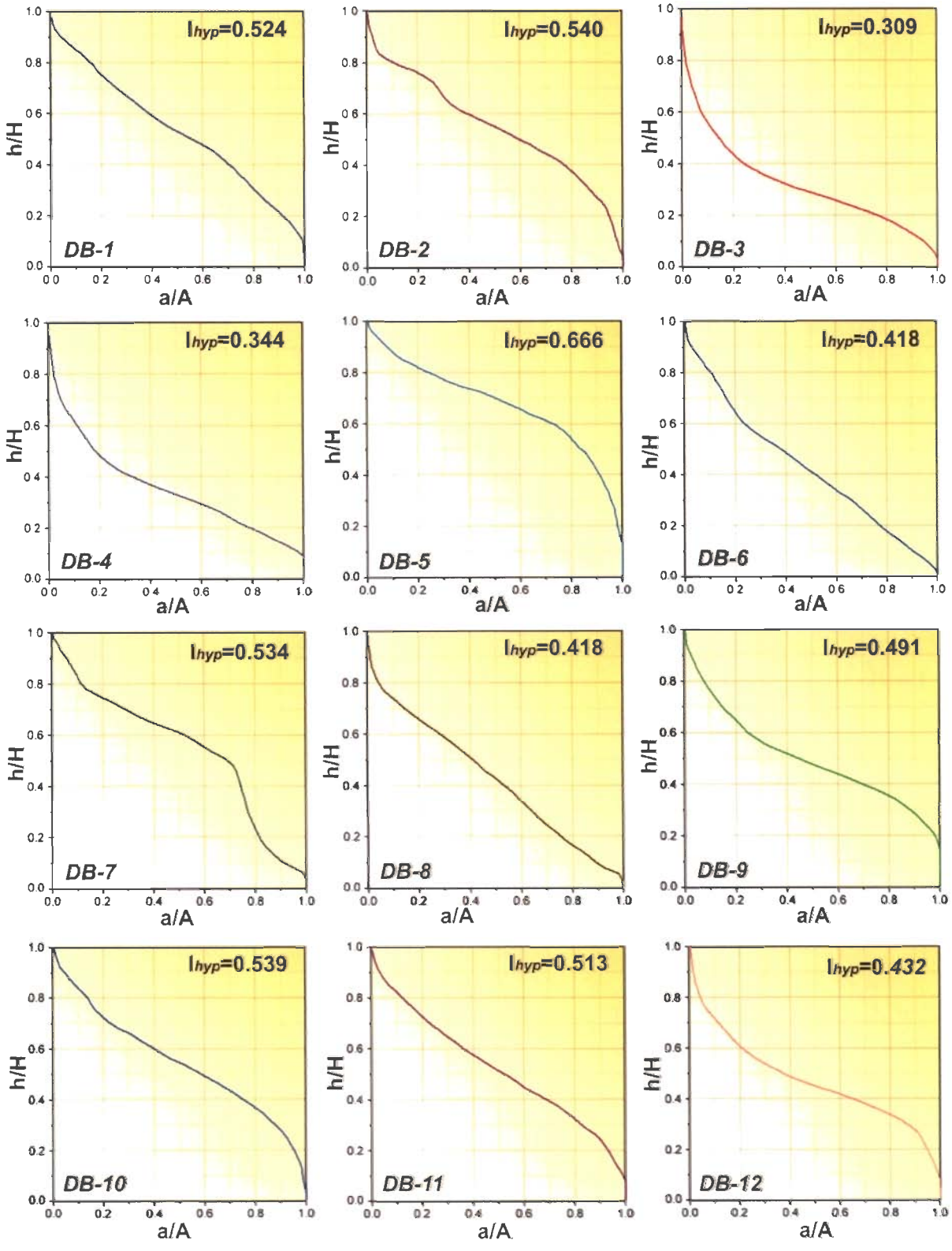

Figure 5.15a Hypsometric curves for drainage basins 1 to 12.

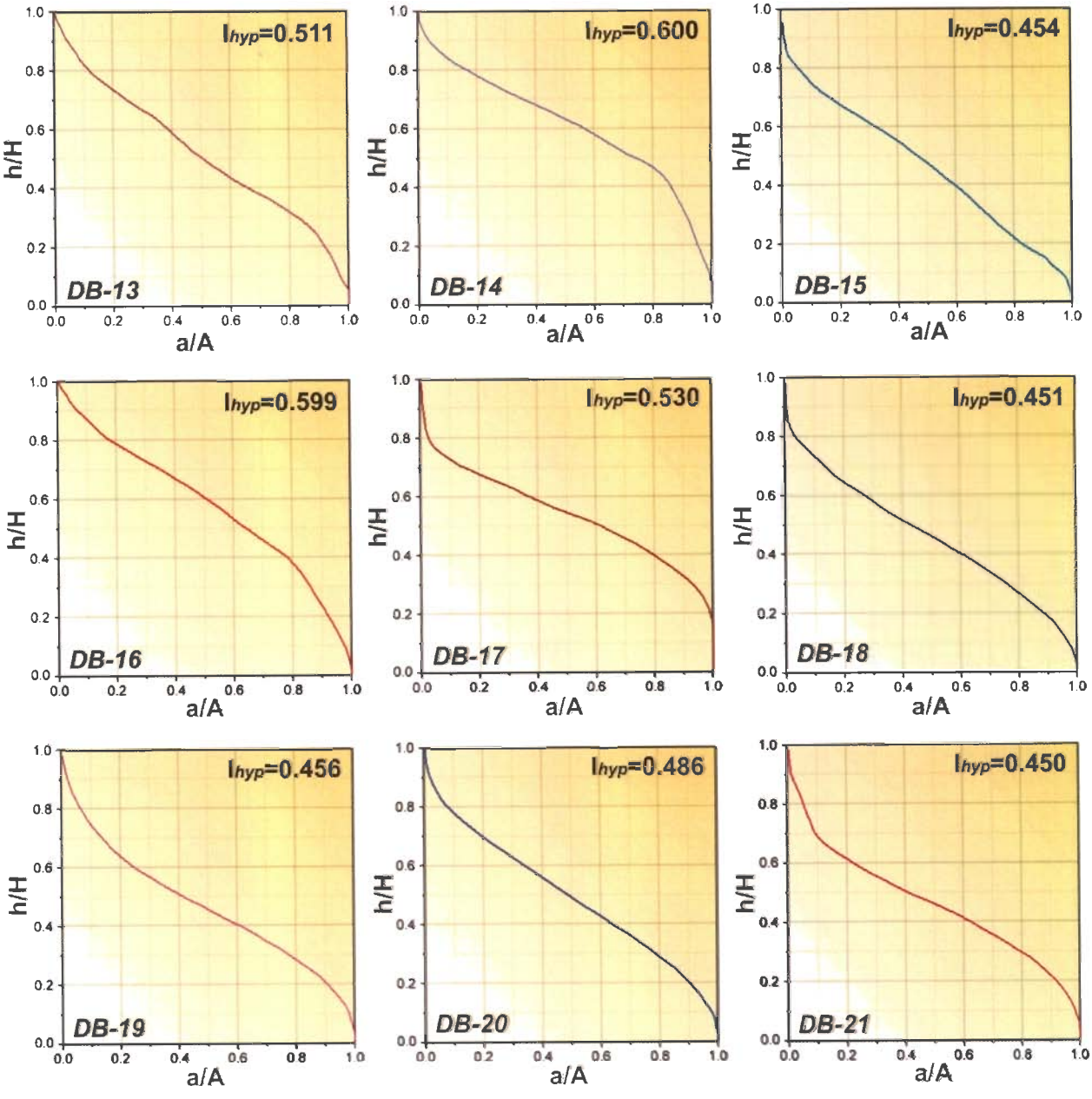

Figure 5.15b Hypsometric curves for drainage basins 13 to 21.

Table 5.4 Morphometric parameters of different drainage basins, Lengpui region.

Drainage Basins (DB)	SL Index (mean)	S index (absolute mean x100)	I_{hyp}
1	230.27	8.93	0.52
2	232.99	39.31	0.54
3	249.46	43.85	0.31
4	281.13	50.29	0.34
5	168.22	23.82	0.67
6	211.88	40.27	0.42
7	575.51	183.59	0.53
8	286.29	21.27	0.42
9	323.81	47.94	0.49
10	378.40	27.54	0.54
11	488.54	83.68	0.51
12	309.79	30.64	0.46
13	1186.89	338.66	0.51
14	1092.16	204.56	0.60
15	548.63	78.90	0.45
16	589.71	72.72	0.60
17	232.14	24.61	0.53
18	255.81	38.39	0.45
19	43.12	71.36	0.46
20	172.99	18.89	0.49
21	163.56	16.56	0.45

5.13 Results

A few well developed selected synclinal basins are found to have dense drainage networks. Computed morphometric indices indicate that the drainage basins are highly asymmetrical and stream networks are tectonically influenced. Most of the stream follow either meandering or sinuous channel pattern.

The present topography of the Agartala slope can be seen as a surface dissected with intensively developed drainage network. Several streams have gone dry through space and time and now the agricultural fields have been developed along these streams. Faulting of the anticlinal ridges influence greatly the river course and creates passage paths, although very zig-zag, through the ridge parts. Some abandoned river loops, northward convexing of Haora river just upstream of Agartala and drying up of several streams points towards a possible change in tectonic scenario as well as in environment. Computed morphometric parameters indicate certain changes in the topographic setting most likely attributed to the tectonic activity. That the Agartala slope and easterly lying fold belt has been uparched is well reflected through the nature of developed stream network, a zone of drainage divide and topographic profiles.

Interestingly, the Lengpui synclinal valley represented by larger gently sloping surfaces and shows very contrasting morphometric indices. A consistent very high gradient has been obtained from the streams falling in the southern part of the valley and decreases northward. The Dhaleshwari river valley is steep sided (V-shape) and is very much evident from the high SL values in the lower reaches of the streams. Slope index values and hypsometric integral indicate that most of the drainages are deviated from normal concave profiles. Similarly topographic profiles also seem to support the facts revealed by the SL index and hypsometric curves of the region. The topographic profiles exhibit plateau like slope appearance on both the sides of the river valley which results into the smooth topographic appearance of the region and also at some places tilting has been observed. Therefore it was found that region is undergone neotectonic processes. All the streams including the major river Dhaleshwari are in their youthful stage and are actively incising the valleys.

CHAPTER-VI

DEM generation and comparison

6.1 Introduction

Digital Elevation Model (DEM) has many potential real life applications. Various methods and data sources are available for generation of DEMs. DEMs have been generated for the Bhuban anticlinal hills falling in the northeastern part of Surma Basin from topographic contours and Cartosat-1 stereo data. Spatial resolution for both the DEMs has been fixed to 20m. DEM generation from contours involve tedious contour digitization whereas Cartosat-DEM generation requires careful processing, accurate Ground Control Points (GCPs) and tie point locations in order to achieve reliable accuracy in DEMs. Therefore it is required that proper care is taken in selection of GCPs locations especially the elevation values.

The potential of DEMs for solving the geohydrological problems related to hilly terrain has long been known. Therefore, their accuracy is always remains a matter of concern for researchers. Accuracy of DEM determines its reliability for various morphometric parameters. DEM quality selection is mostly application dependant. For example, high spatial resolution and topographic quality DEM are not essential for regional, small scale analyses and for calculating average altitudes. However, topographic accuracy is more sensitive for analyses that use algorithms based derivates like slope, aspect, drainage, path simulation, etc. In distributed hydrological modeling, output is affected by model input to a large extent and researchers have found that DEM quality and resolution significantly affect the accuracy of extracted hydrological features (Kenward et al., 2000). Therefore, both the contour and Cartosat-DEM have been compared from already available SRTM and ASTER-DEMs on the basis of topographic

derivatives. Cartosat-DEM found to have high accuracy and quality and has been used for the detailed morphotectonic and morphometric analysis of Bhuban Hills.

6.2 Digital Elevation Model (DEM)

DEM is a digital and numerical representation of topography made up of equal-sized grid cells, each with a value of elevation representation of ground surface topography or terrain. A DEM can be represented as a raster (a grid of squares) or as a triangular irregular network. Now-a-days DEMs are commonly built using remote sensing techniques however, they may also be built from land surveying. DEMs are used often in GIS, and are the most common basis for digitally-produced relief maps (Maune, 2001). Its simple data structure and widespread availability have made it a popular tool for land characterization. Because topography is a key parameter controlling the function of natural ecosystems, DEMs are highly useful to deal with ever-increasing environmental issues.

6.3 Methodology

6.3.1 DEM generation from contour lines

DEM from contour lines used extensively earlier to get grid DEM because of its low cost and the convenience to get contour maps. Contour lines and DEM are both a representation of the same real topography. They just correspond to different ground surface sampling strategies as topographic profiles or grid sampling facilitates to build a relation between them (Rognant et al., 2001). In this study contour line of Bhuban Hills area having 20m elevation difference have been digitized from topographical maps of 1:50000 scale. The elevations of contour lines were mapped into the cell matrix using GIS. Input consists of contour lines in vector format, which are dynamically rasterized with a resolution that is independent of the spacing of the resulting grid DEM, but a function of both the input map scale and the distance between the neighboring contour pair (Wood, 1994; Clarke, 1982).

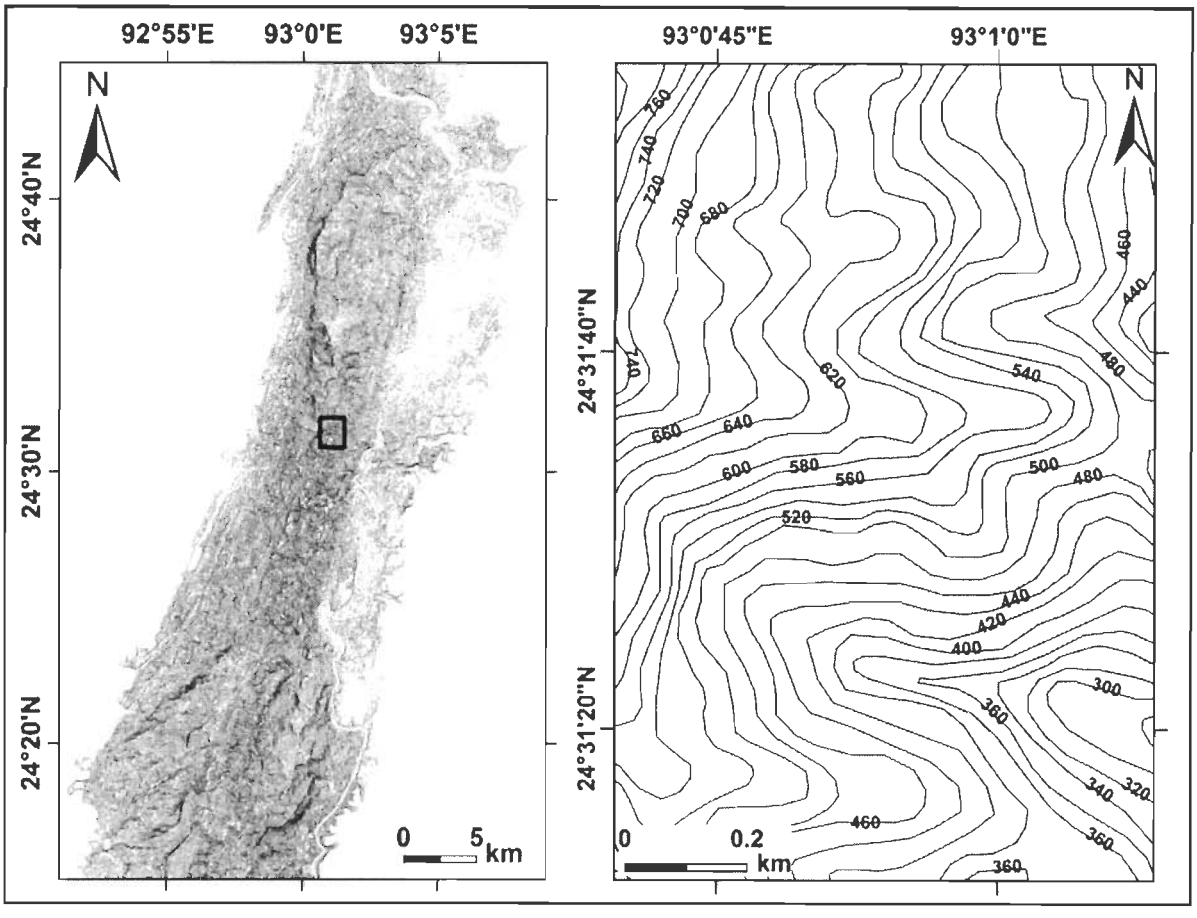

Figure 6.1 Contour map of the Bhuban Hills along with enlarged view of contours for a small area (shown in a box).

Accuracy of DEM relies on the accuracy of digital contour map and implemented interpolation techniques (Wise, 1998). Therefore, contour data and elevation values should be checked prior to use. Minor refinement can be made for contour lines during vectorisation in steep slope areas (Kunqing, et al., 2003). The contour map of the Bhuban Hills is shown in the figure 6.1. Delaunay Triangulation is the mostly used method for interpolation and conversion of contours into TIN (Triangulated Irregular Network).

6.3.1.1 Triangulated Irregular Network (TIN) Model

TIN models are sets of adjacent, non-overlapping triangles computed from contours with x/y coordinates and z-values. TIN models are used to provide better control over terrain slope, aspect, surface areas, volumetric and cut-fill analysis and generating contours (Lee, 1991). The TIN models vector data structure is based on irregularly-spaced point, line and polygon data interpreted as mass points and break-lines and stores the topological relationship between triangles and their adjacent neighbors. The process of TIN generation is based upon the Delaunay triangulation method. It is a proximal method that satisfies the requirement that a circle drawn through the three nodes of a triangle will contain no other node (Figure 6.2). The triangles are as equi-angular as possible, and every point on the surface is as close as possible to a node. All the vertices of the contour lines are used as mass points for triangulation. Delaunay triangulation is independent of the order the points are processed.

The TIN model of Bhuban Hills generated from contours of 20m intervals is shown in figure 6.2. In case of flat areas where contours are sparse the model fits triangles having zero slopes and without defined aspect. These might cause problems when the flat surface is used for modeling and can be avoided by adding more mass points, more break-lines within the flat area manually. This TIN model then converted into DEM by creating a raster surface using '3D Analyst' tool in ArcGIS 9.3 (Fig. 6.3).

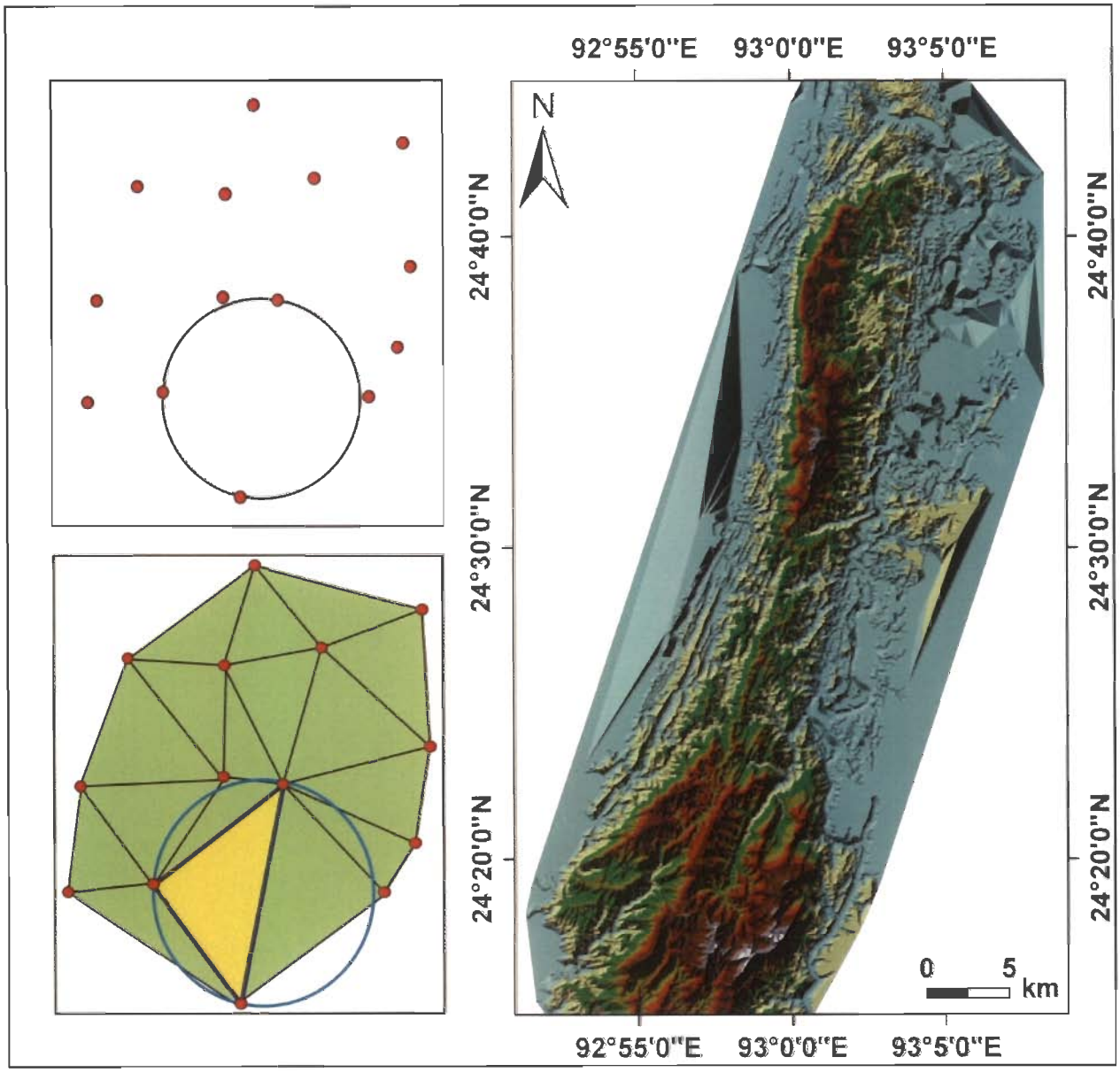

Figure 6.2 Delaunay Triangulation and generated TIN Model of Bhuban Hills.

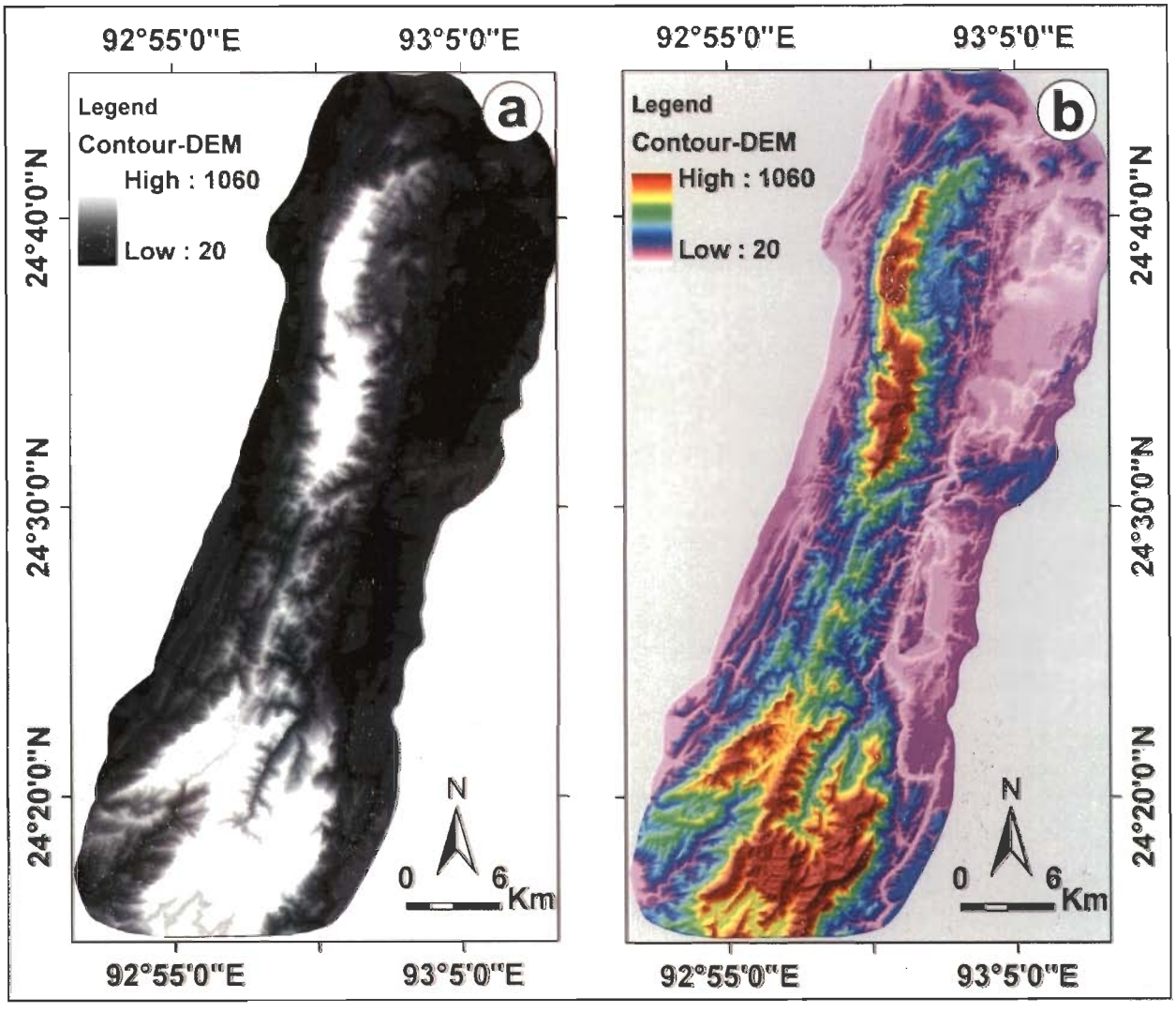

Figure 6.3 DEM generated for Bhuban Hills from contours (a), and color coded shaded relief model (b).

6.3.2 Generation of DEM from satellite imagery

DEM can be generated from stereo image scenes acquired by the satellite stereo digital aerial photographs at various spatial resolutions. Cartosat-1 stereo orthokit data have been used for generation of DEM for Bhuban Hills.

Launch of Cartosat-1 has provided with high spatial resolution data opening a new era in the field of cartographic applications. The Cartosat-1 stereo pair data along with the Rational Polynomial Coefficients (RPCs) can be used to generate DEM. RPC model in general is used to represent the imaging geometry of Cartosat-1 which is expressed as a ratio of two cubic polynomials which are functions of ground coordinates (Kalyanaraman, et al,. 2006). Stereo orthokit is one of the important products recognized for Cartosat-1. Cartosat-1 orthokit products are already in demand among global users as the data can be subjected to the required geometric processing beside DEM generation and ortho-rectification with the help of any standard commercial-off-the-shelf software package (Jacobson et al., 2004).

Orthokit product basically consists of radiometrically corrected image in GeoTIFF format, corresponding RPCs in a file and a metadata file, which gives the description of the data. In stereo orthokit product, image data from both cameras i.e. FORE and AFT is provided along with their corresponding RPCs, whereas in the other product Geo Orthokit which is under consideration for Cartosat-1 geometrically corrected image is planned to be supplied along with associated RPCs (Kumar and Giribabu, 2006). One of the advantages of this product is that the users can directly utilize the product for their applications since the image supplied is already corrected for mean height. The other advantage is that it will ease the DEM generation process by properly utilizing the reconstruction of epi-polar geometry.

The procedure adopted for DEM generation from the above images using Leica Photogrammetry Suite (LPS) of ERDAS-Imagine is described below. A block file is created first which includes image location, interior orientation and exterior orientation information, GCPs, auto tie points, and ortho images. During the creation of a block, if the block coordinate system is set by importing a coordinate system from a raster, the

horizontal units will not be set correctly. The appropriate horizontal unit (WGS-84) should be set by selecting one from the dropdown list for the 'Horizontal Units' in the 'Reference Coordinate System' dialog box. The minimum and maximum elevation should also be set according to terrain topography in block set up dialogue box. Here minimum elevation was set as 20m while the maximum elevations as 900m, 1000m and 1200m respectively for successive three images based on the altitude data of the Bhuban Hills.

In general, the procedure for DEM generation from stereoscopic views can be summarized as follows (Shin et al., 2003):

- Feature selection in one of the scenes of a stereo-pair: Selected features should correspond to an interesting phenomenon in the scene and/or the object space.

- Identification of the conjugate feature in the other scene: This problem is known as the matching/correspondence problem within the photogrammetric and computer vision communities.

- Intersection procedure: Matched points in the stereo-scenes undergo an intersection procedure to produce the ground coordinates of corresponding object points. The intersection process involves the mathematical model relating the scene and ground coordinates.

- Point densification: High density elevation data is generated within the area under consideration through an interpolation in-between the derived points in the previous step.

Three different 'Fore' and 'Aft' images of 612-283, 612-284 and 612-285 data products were used for this work as shown in the figure 6.4. Where 612 denotes path and 283, 284 & 285 are rows of the images respectively.

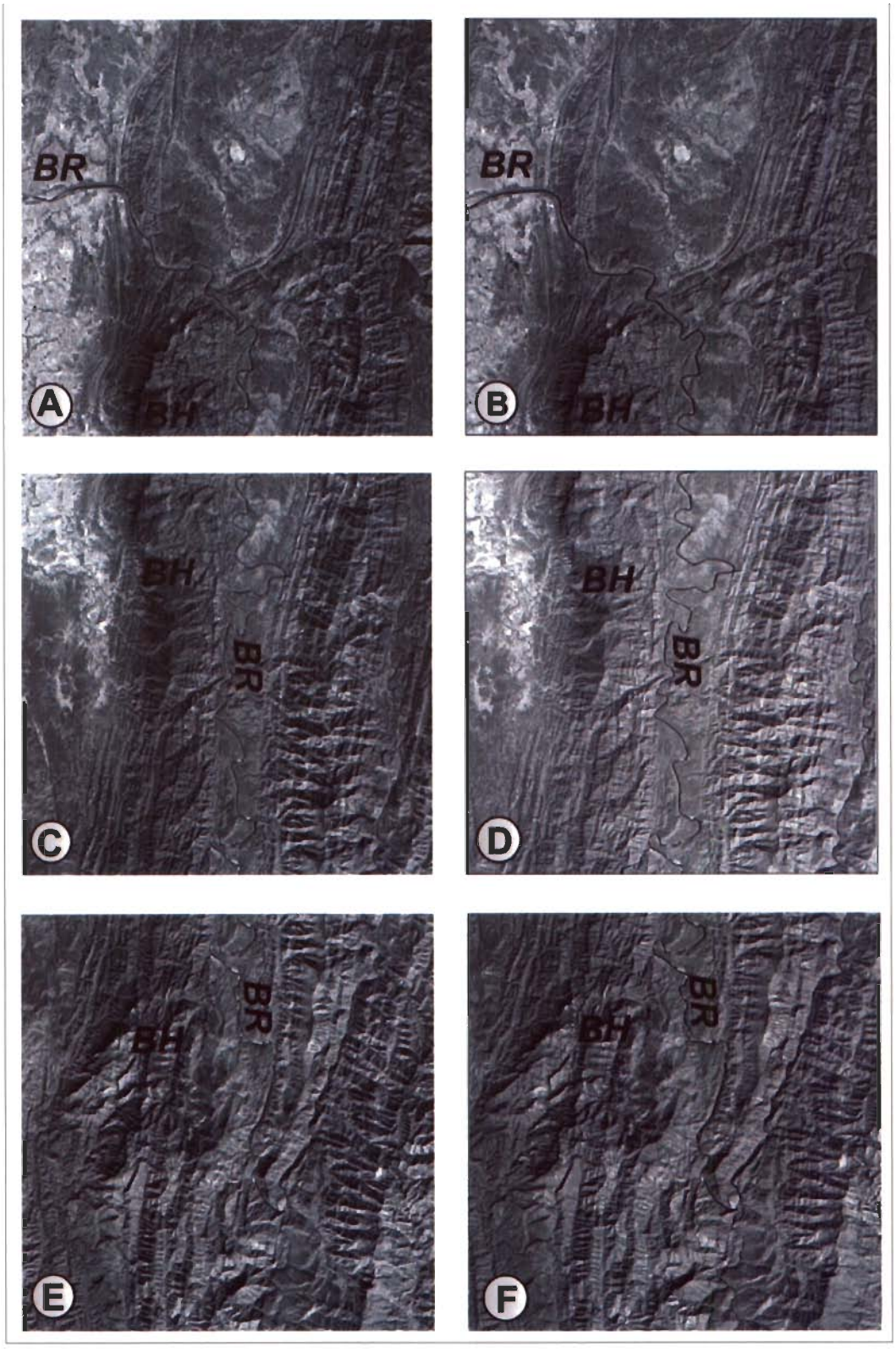

Figure 6.4 Cartosat-1 stereo images (A) Fore scene of P612-R283 image, (B) Aft scene of P612- R283 image, (C) Fore scene of P612-R284, (D) Aft scene of P612- R284 image, (E) Fore scene of P612-R285 image, (F) Aft scene of P612- R285 image. (BH-Bhuban Hills, BR-Barak River)

6.3.2.1 Sensor model definition

A sensor model describes the properties and characteristics associated with the camera or sensor used to capture an image. Internal sensor model information describes the internal geometry, including focal length and lens distortion. Interior orientation is primarily used to transform the image pixel coordinate system to the image space coordinate system. Image position of the fiducial marks are measured on the image and then compared to the calibrated coordinate of each fiducial mark. The measured image coordinates of the fiducial marks are referenced to a pixel or file coordinate system. The pixel coordinate system has an *x* coordinate (column) and a *y* coordinate (row). The origin of the pixel coordinate system is the upper left corner of the image having a row and column value of 0 and 0, respectively. The relationship between the pixel coordinate system and the image space coordinate system defined using the 2D affine transformation equations (Internet: http://gi.leica-geosystems.com/documents/pdf/LPSNASAArticle.pdf). The affine transformation also defines the translation between the origin of the pixel coordinate system and the image coordinate system (*xo-file* and *yo-file*). Additionally, the affine transformation takes into consideration rotation of the image coordinate system by considering angle Θ. Figure 6.5a shows transformation of image pixel coordinate system to image space coordinate system.

External sensor model information describes the position and angular orientation of each image as it existed when the imagery was collected. The variables defining the position and orientation of an image are referred to as the elements of exterior orientation. The positional elements of exterior orientation include Xo, Yo, and Zo, which define the position of the perspective center O with respect to the ground space coordinate system X, Y, Z. Zo is referred as the height of the sensor above sea level (Figure 6.5b), which is commonly defined by a datum (Rao, et al., 2007). The angular or rotational elements of exterior orientation describe the relationship between the ground space coordinate system (*X*, *Y*, and *Z*) and the image space coordinate system (*x*, *y*, and *z*). Three rotation angles to define angular orientation are Omega (ω), Phi (ϕ), and Kappa (κ). Omega is a rotation about the photographic x-axis, Phi is a rotation about the photographic y-axis, and Kappa is a rotation about the photographic z-axis.

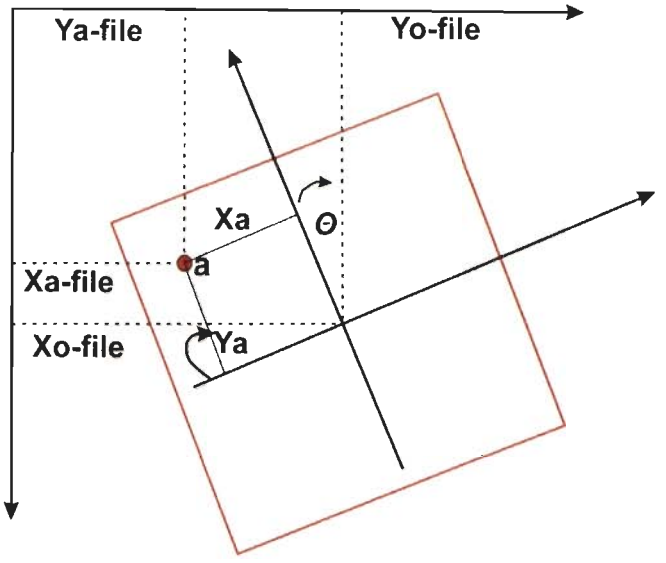

Figure 6.5a Transformation of image pixel coordinate system to image space coordinate system (Internal sensor model). a–fiducial mark, Xa,Xo,Ya,Yo-file are coordinate system (Source: Rao et al., 2007).

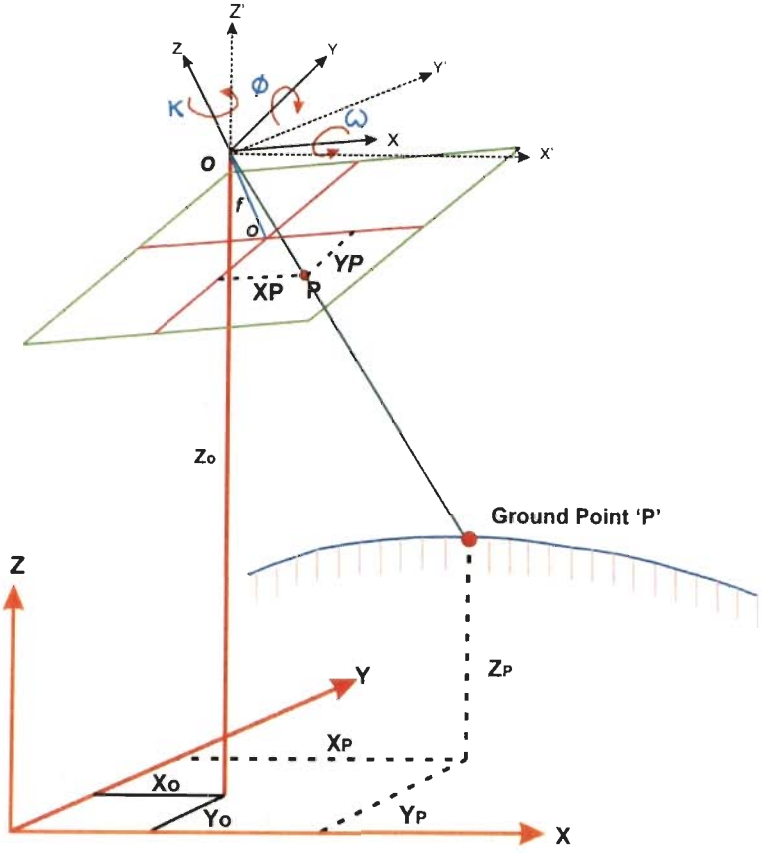

Figure 6.5b Relation between the ground space coordinate system (X, Y, Z) and image space coordinate system x, y, z. f-focal lengh, ω, ϕ and κ are three rotation angles to define angular orientation (Source: Rao et al., 2007).

Orthokit dataset is ingested along with the corresponding RPC files and interior and exterior orientation was carried out considering required parameters from the RPC file. Without this information, value added data layers such as oriented images, 3D feature datasets, DEMs and orthorectified images cannot be derived from imagery.

6.3.2.2 Creation of Ground Control Points (GCPs)

Ground Control Points (GCPs) are used to establish a geometric relationship among the images in a project, the sensor model and the ground so that fairly accurate data can be collected from the imagery. The GCP has three coordinates: x, y and z, which are measured across multiple images. GCPs can be collected from existing vector files, orthorectified images, DEMs, topographic maps and from the GPS surveys. For the Bhuban Hills area, about 10 GCPs for the first image (612-283) and 7 and 8 GCPs for the second and third image (612-284, 612-285) were selected. The elevation values are taken from topographic map of the area. Co-ordinate and elevation values and other details of GCPs are given in the Annexure I.

6.3.2.3 Tie-point generation

Tie points are the points whose ground coordinates are not known. But they can be identified in the overlap area between the images. Ground coordinates for these tie points are calculated during triangulation. Tie points should be evenly well distributed throughout the overlap area. LPS software can automatically generate the tie points between the images in their overlap region. Manually some more tie points are added for even distribution throughout the image overlap region.

These tie points are visually checked for their location accuracy. Both optical window matching and feature matching is necessary for tie point generation. Cartosat-1 stereo image are generated using only Rational Polynomial Coefficients (RPCs) with positional accuracies in the order of 100 to 250 meters, since these RPCs suffer from positional bias. In case of stereo images, tie point evaluation error cause DEM error

(Lopez, 1997). Various kinds of error sources which have an effect on DEM accuracy are enumerated below.

- Tie Point Evaluation Error:
  Absolute error= (tie point displacement value)/ (B/H)
  where, B/H=base to height ratio
- Pitch Motion:
  no direct effect on DEM value
- Yaw Motion:
  no direct effect on DEM value
- Satellite Altitude Error:
  Relative Error=altitude difference/Designed Altitude

Careful examination of all these errors is important in order to have greater accuracy in DEM. In addition to these altitude data quality is also very important because it has a greater impact on DEM accuracy. For greater accuracy elevation values from toposheet have been used.

6.3.2.4 Triangulation

Triangulation is the process of establishing a mathematical relationship between the images, sensor model and ground. The raw accuracy of the stereo models using only RPC values may have systematic offsets and errors in the scenes locations. Therefore, accuracy can be improved by using accurate GCPs. The information resulting from triangulation is required as input for the orthorectification process. A block adjustment or triangulation can obtain internal and external sensor model information, 3D coordinates of tie points, and additional parameters that characterize the sensor model (Kalyanaraman etal., 2006; Rao etal., 2007; Habib and Beshah, 1998). The LPS software generates automatically the x, y, and z values of tie points after the triangulation process. Triangulation is also performed to check the model accuracies at all the tie points. Tie points having high residual error (wild points) has been eliminated. Manual adjustments of GCPs also been made for refinement of errors and offsets. RMSE of about 1 or less pixel

shows that performed triangulation is good. If the error is more than one pixel manual adjustment of tie point as well as GCPs can be made. Total RMSE of 1.973, 1.487, and 1.33 pixels were obtained in three successive scenes after triangulation. These errors resolved to less than one pixel by refining the location of tie-points. Results and summary of the points, their respective co-ordinate values and errors are shown in the Annexure I.

6.3.2.5 DEM generation

DEM is generated after the satisfactory model accuracy is achieved. Cell values have been fixed as 20m as that of contours DEM. Automatic generation of terrain models from overlapped images is currently the most important way to generate a DEM. The DEM extraction module in LPS concentrates on improving the reliability, speed and productivity of the DEM extraction process. In order to improve reliability and speed, an integrated image matching strategy is developed. LPS software creates TIN model first and then convert it into DEM. Accurate sensor model information from block adjustment is used to transform the image positions of the ground points into 3D coordinate information (Davis, and Wang, 2003). After the automated DEM extraction process is completed, a series of evenly distributed, 3D mass points are located within the area and can be used to create a Triangular Irregular Network or a Raster DEM. Terrain corrections can also be made into this DEM.

Ortho-rectification is the process of correcting the imagery into a planar map and the errors occurred during various steps was reduced. Using sensor model information generated by block adjustment and a DEM, errors associated with sensor orientation, topographic relief displacement, earth curvature and other sources can be removed (Wang and Ellis, 2005). Ortho-images have also been generated for comparing the accuracy and overlap of both the scenes. DEM generated for the Bhuban Hills from the Cartosat-1 stereo images is shown in figure 6.6.

6.4 Accuracy assessment and comparison of DEMs

Both contour and Cartosat-DEMs have been studied and compared on the basis of their relative accuracy, drainage and topographic derivatives. Accuracy and quality of the different DEMs have been assessed using a quantitative approach. Drainage networks, streams, catchment, relief and watershed divides are important properties in the landscape, which significantly contribute to material flow (Burrough and McDonnell, 1998). Quality of a DEM is a measure how accurately it predict the elevation values at each pixel and its ability to represent the morphology. Therefore, the vertical and horizontal accuracies of all the four DEMs have been calculated. Both Contour and Cartosat-DEMs (generated for this work) then compared with the SRTM and ASTER DEMs (available) on the basis of drainage parameters and topographic derivatives.

Figure 6.7 depicts all four DEMs of the Bhuban Hills. These are the shaded relief models of DEMs generated with sun azimuth 315, sun altitude 45 and z factor of 0.00000956. Also enlarged view of a small selected portion of all the DEMs is shown for the purpose of visualizing the topographical differences.

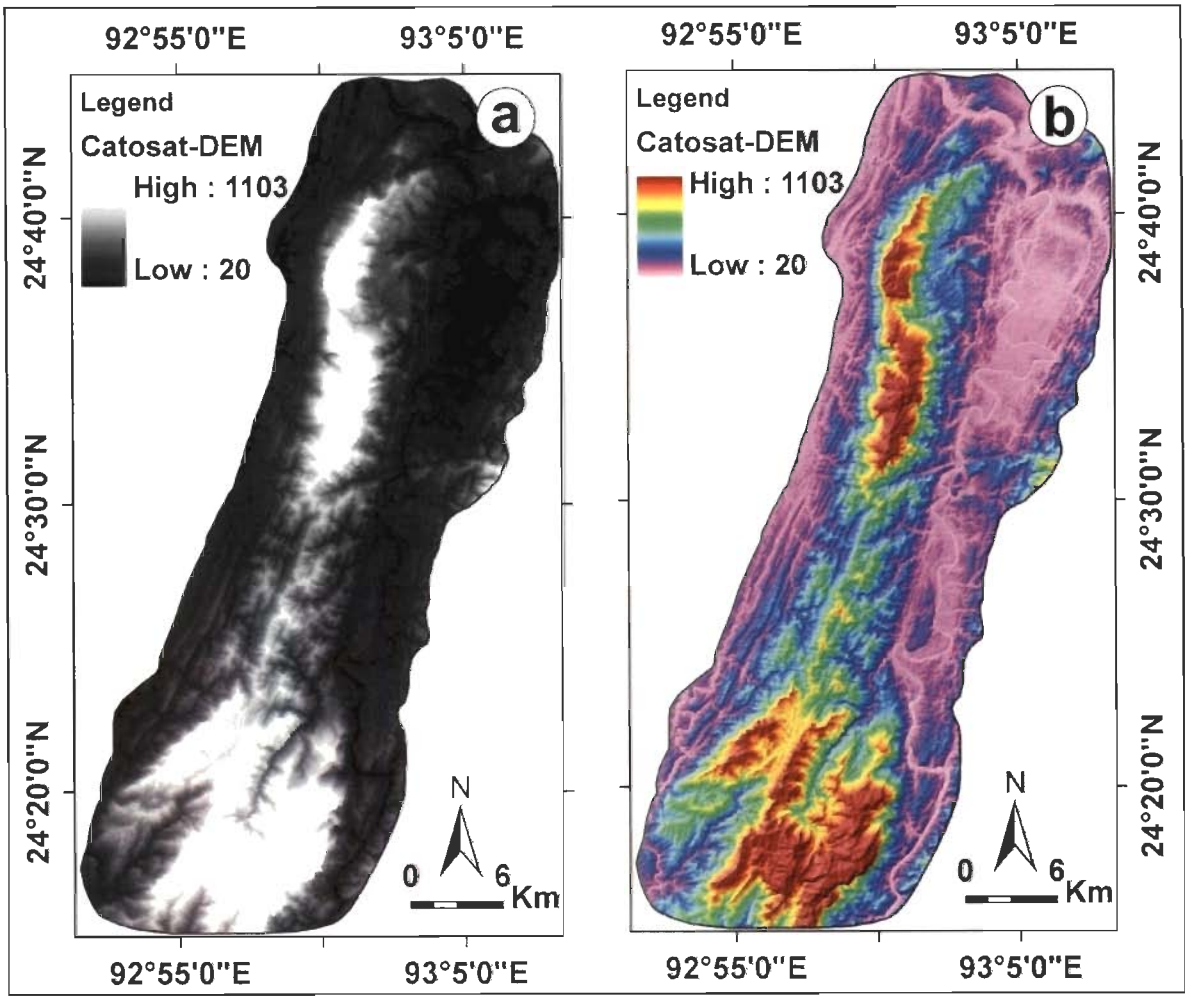

Figure 6.6 DEM of Bhuban Hills generated from Cartosat-1 stereo data (a) and color coded shaded relief model (b).

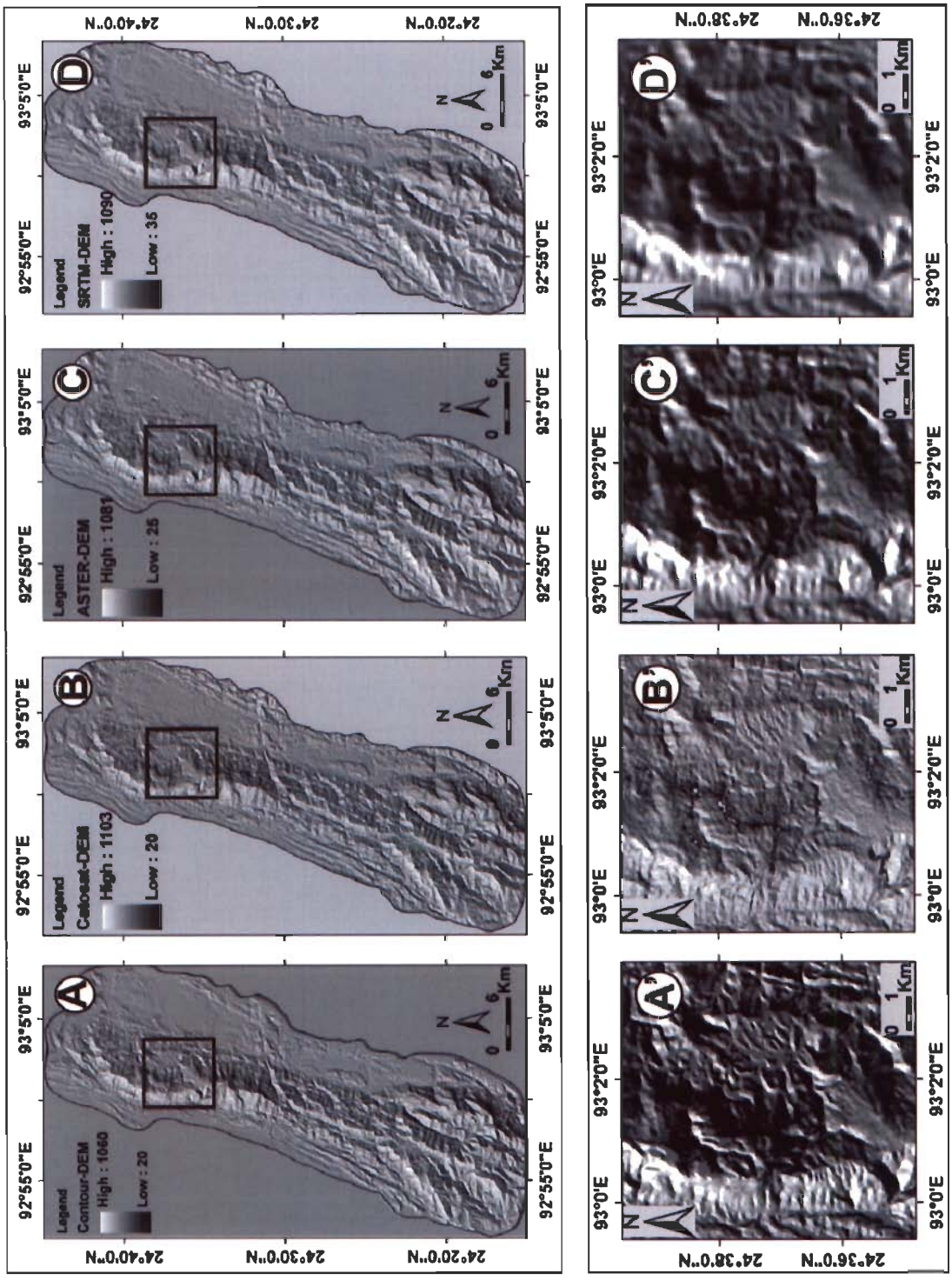

Figure 6.7 Shaded relief models of Contour (A), Cartosat (B), Aster (C), SRTM (D) DEMs for the Bhuban Hills and enlarged views of small part (shown by box) of respective DEMs (A', B', C', D').

Maximum, minimum, mean, and standard deviation for each DEM elevations have been extracted. Each DEM predicted different higher elevation values. Cartosat-DEM produces maximum elevation (1103m) while Contour-DEM produces least (1060m). Attributes of all the DEMs are summarized in the Table 6.1.

Table 6.1 Attributes of elevation values for all DEMs.

DEMs / Elevation (in meter)	Contour	Cartosat	ASTER	SRTM
Maximum	1060	1103	1081	1090
Minimum	20	20	25	35

6.5 Accuracy Assessment

6.5.1 Vertical accuracy

Vertical accuracy is the measure of the ability of a DEM to predict the accurate Z-values. About 71 spot heights (Figure 6.8) from topographic maps of the Bhuban Hills region were used as reference points for calculation of vertical accuracy of all the four DEMs. Discrepancy found in elevation values are presented in the form of Mean Error (ME), Absolute Mean Error (AME) and Root Mean Square Error (RMSE). The vertical RMSE statistics is used to describe the vertical accuracy of a DEM, encompassing both random and systematic errors introduced during production of the data. The RMSE is defined as:

$$RMSE = \sqrt{\frac{\sum (Zi - Zt)^2}{n}}$$

Where *Zi* = DEM elevation of a test point, Zt = true elevation of a test point (spot heights), *n* = number of test points. The highest vertical error has been found in the ASTER-DEM showing a large deviation from spot height elevations especially at the topographic highs and lows. SRTM and Contour-DEMs elevation discrepancy values do not differ much and they match with each other. While Cartosat-DEM shows least vertical error and it gives very good results even in area of complex topography. Calculated error parameters are shown in the Table 6.2.

Table 6.2 Calculated error parameters from all DEMs.

DEMs / Error Parameters (in meters)	Cartosat	Contour	ASTER	SRTM
ME	7.408	14.154	23.070	14.309
AME	8.394	14.661	23.887	15.267
RMSE	13.298	18.654	27.959	19.052

Besides, 128 elevation test points distributed all over the area of Bhuban Hills were also selected for further vertical error analysis. Figure 6.8 shows location of elevation test points and spot heights used for analysis. The maximum discrepancies and variation were found in ASTER-DEM. The reason might be the presence of more pits and no-data values (as determined by the 'Sink' tool of ArcGIS) in ASTER data. All these no data values results into underestimation of sample points during the processing. The errors in contour-DEM are mainly found in the flat regions because in flat regions contours are far apart and density of sample point decreases resulting in to an averaged surface. Cartosat-DEM is able to generate maximum higher elevation values in comparison to others with least errors.

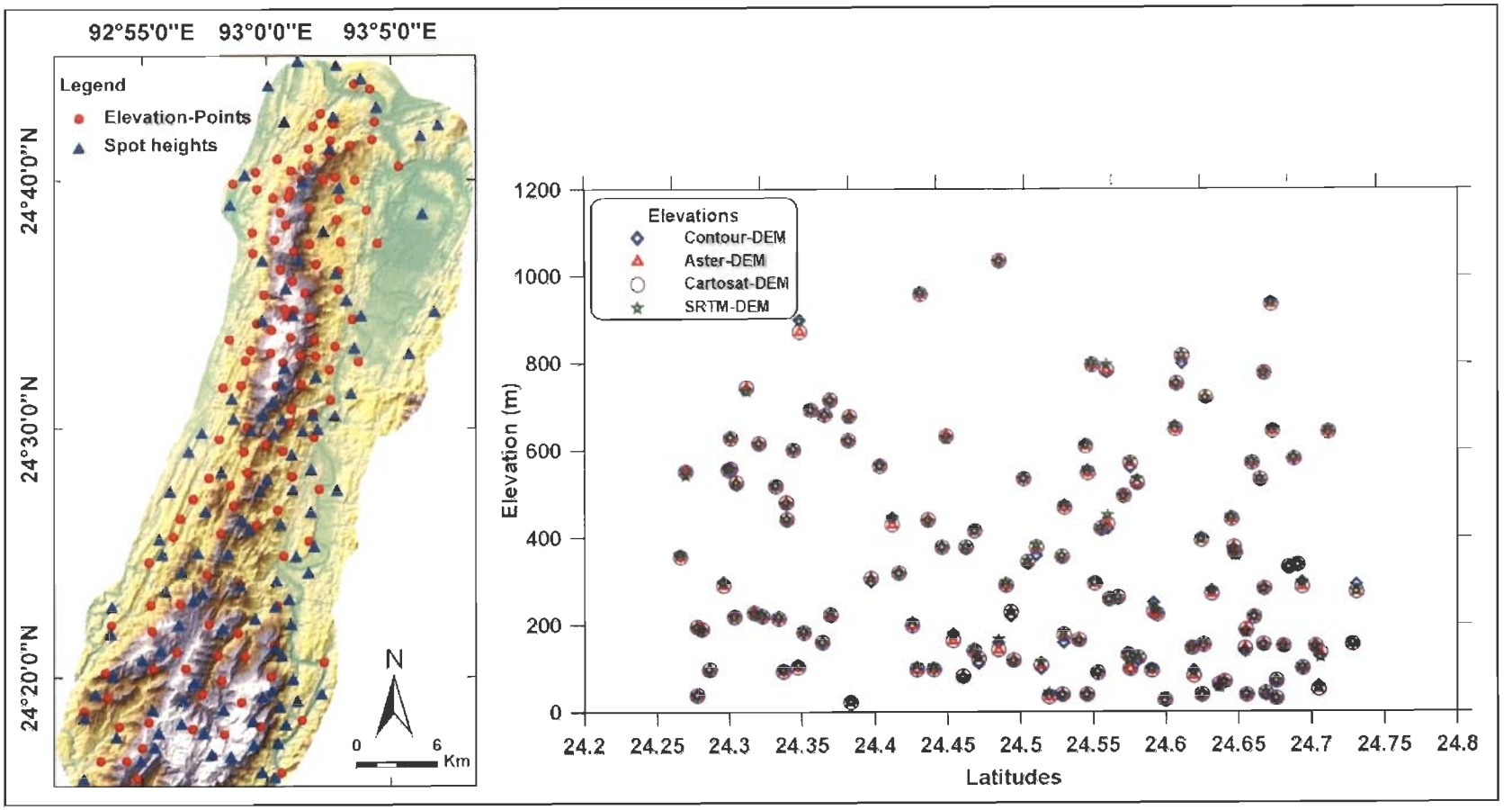

Figure 6.8 Geographical distribution of spot heights and elevation test points over the Bhuban Hills shown on color coded Cartosat-DEM.

6.5.2 Horizontal accuracy

For hydrological analysis, it is necessary to report the horizontal accuracy along with elevation parameters. Calculation of horizontal accuracy is much more complicated task in comparison to vertical accuracy. Referenced data selection is always a matter of concern, as it requires highly accurate georeferenced data. For this, stream network from georectified IRS-PAN images (5.8m spatial resolution) were extracted and use it as reference for comparing the synthetic stream network generated from various DEMs. A small watershed was selected (shown in box 'a' of figure 6.11) for measuring the stream mismatch. Mean values were computed for each individual stream (S-1 to S-14) displacements in order to have quantitative assessment for horizontal accuracy. For extraction of synthetic stream networks from DEMs ArcHydro tools have been used. Here, mainly the higher order streams were considered, because they were easily predictable even for coarser resolution as SRTM. Mean stream displacement for each stream is represented in the Fig. 6.9.

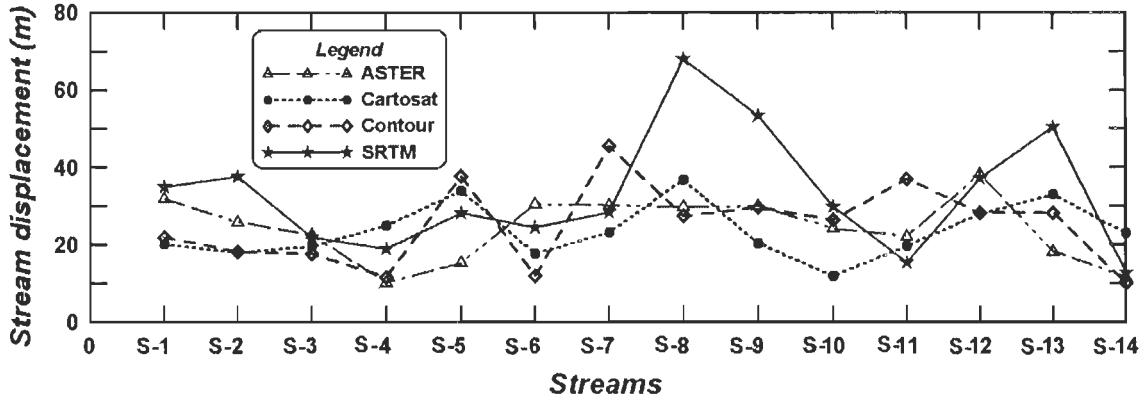

Fig. 6.9 Horizontal stream displacement (mean values for each stream) of all DEMs.

The major displacement of streams found in SRTM-DEM in case of streams S1, S2, S8, S9 and S13. The reason of least horizontal accuracy in case of SRTM-DEM is coarse resolution due to which it could not predict the meandering course of the streams properly. ASTER-DEM shows poor flow direction prediction specifically where topography is complex. Similarly, in case of contour the reason might be the time of survey which was done long back in 1977, due to which it lacks some information regarding stream

variations over time. Largely, all DEM derived stream except SRTM, are in good agreement with the referenced streams.

6.6 Quality assessment

6.6.1 Analysis of drainage parameters

Delineation accuracy of different topographic parameters greatly depends on how accurately the DEM depict the terrain shape. It is a well known fact that the geomorphic features viz., stream network on earth surface and outline of basin boundary are closely tied to the shape of its topography. It is very much depend upon the accurate prediction of flow direction and elevation values. Beside above, drainage density is also another important measure of DEM quality.

6.6.2 Basin boundary delineation

Basin boundary delineation has been carried out using ArcGIS hydrology tools for each DEM. Flow direction grids were generated from the filled DEMs. Basin tool was applied for creation of basin grids. These grids were transformed to shapes using 'Raster to feature' tool and then reclassified. Figure 6.10 is showing the boundaries and interconnection of different basins extracted from four DEMs. Visual inspection of basin boundaries indicated that Cartosat-DEM could generate greater details and fine information regarding basin boundaries. ASTER-DEM missed some information and is not able to predict the whole basin boundary. Similarly, in case of SRTM, the basin boundary shows straightening effect especially in the area of complex topography. Contour-DEM gives much better representation but still it does not offer as much detail about basin shape as the Cartosat-DEM provides. Red circles in the figure are showing the areas of major mismatch and discrepancies. In case of SRTM-DEM at some places it shows two basins as single unit which might be due to poor resolution of SRTM. Therefore least number of basins were delineated from the SRTM-DEM. While in ASTER-DEM problems are with steeper and flat areas, mainly due to poor prediction of flow direction in these regions.

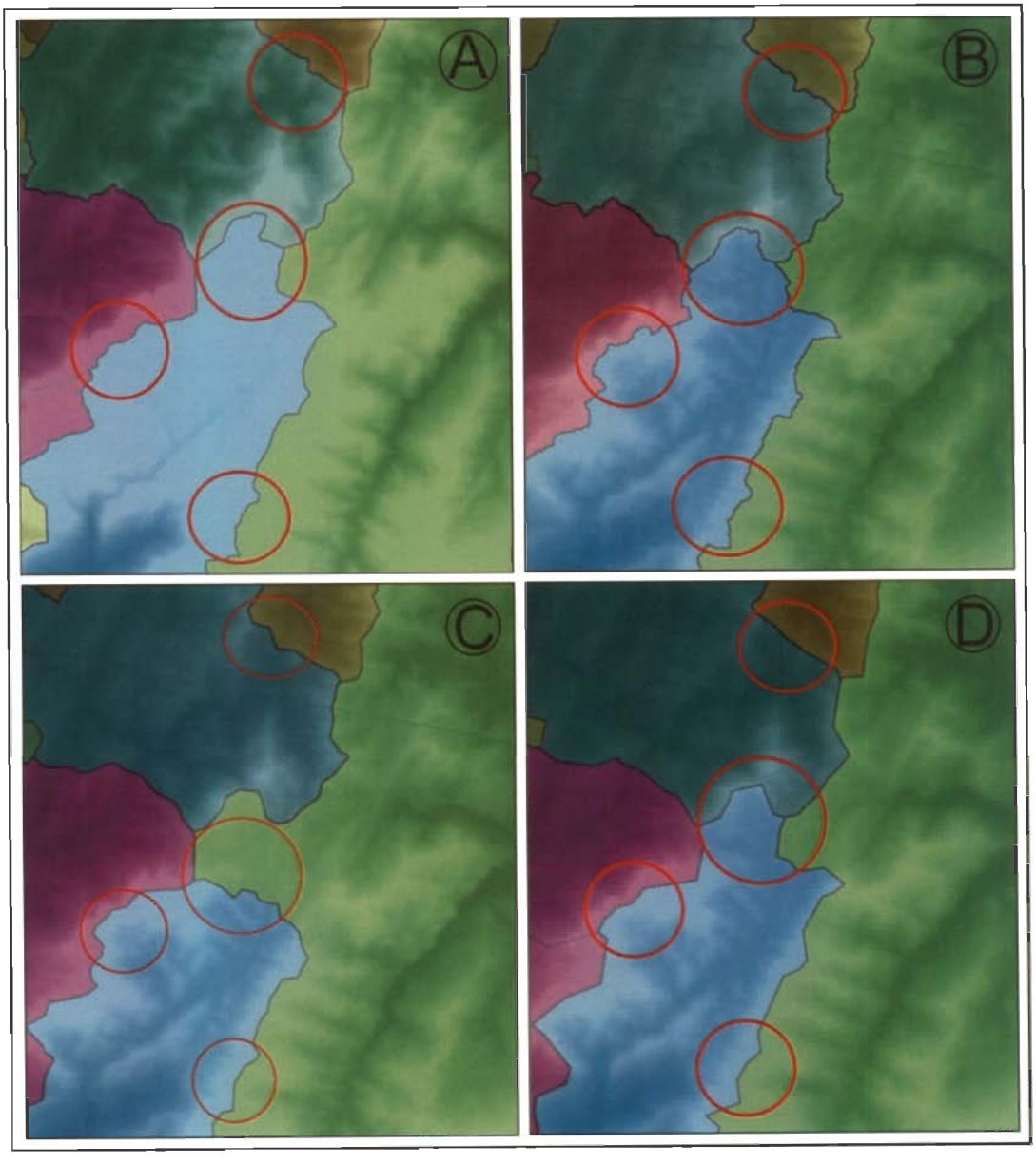

Figure 6.10 Basin boundaries of Contour- Cartosat-ASTER-SRTM DEMs. Circled area shows the differences and deviation in basin boundaries.

6.6.3 Stream network delineation

Stream networks from each DEM were derived automatically using Arc Hydro tools. In grid DEMs sinks and pits comprising grid cells surrounded by higher-elevation neighbors occur due to deficiencies in DEM generation processes (Jenson and Domingue, 1988; Jenson, 1991). Just few sinks in DEM may have disastrous effect on results. Therefore, prior to use all the sinks should be filled. Flow direction and flow accumulation grids have been generated. Then stream networks were derived from each DEM by assigning a same threshold value of 0.200 km^2.

6.6.3.1 Hill area: Most of the drainage networks in the higher elevation regions are well matched (enlarged view, figure 6.11). Major deviation and errors are found in the flat regions. In Contour and ASTER-DEM streams lost their meandering pattern and show straightening in their paths. But the trend of all the stream networks is almost same and they are in well agreement with each other. In addition to this, visual analysis of all the stream networks indicated better representation of higher order streams in all the four DEMs, while lower order streams are well defined by the higher resolution DEMs only. Stream feathering effect (parallel alignment of streams) is found in contour and ASTER-DEM mostly in near valley regions (Figure 6.11).

6.6.3.2 Valley region: Channel pattern of a wider valley river (Barak River) from all the DEMs also have been analyzed especially for interpreting the behavior of DEM derived streams in lower elevation and valley areas. Valley river morphometry is best described by Cartosat-DEM. Interestingly, despite the coarse resolution SRTM gives very good results. ASTER and Contour DEMs are not able to show the bends and meandering curves properly. At few places they show broken paths. In figure 6.12, circles are showing the bends where ASTER and Contour extracted streams are deviated from their paths.

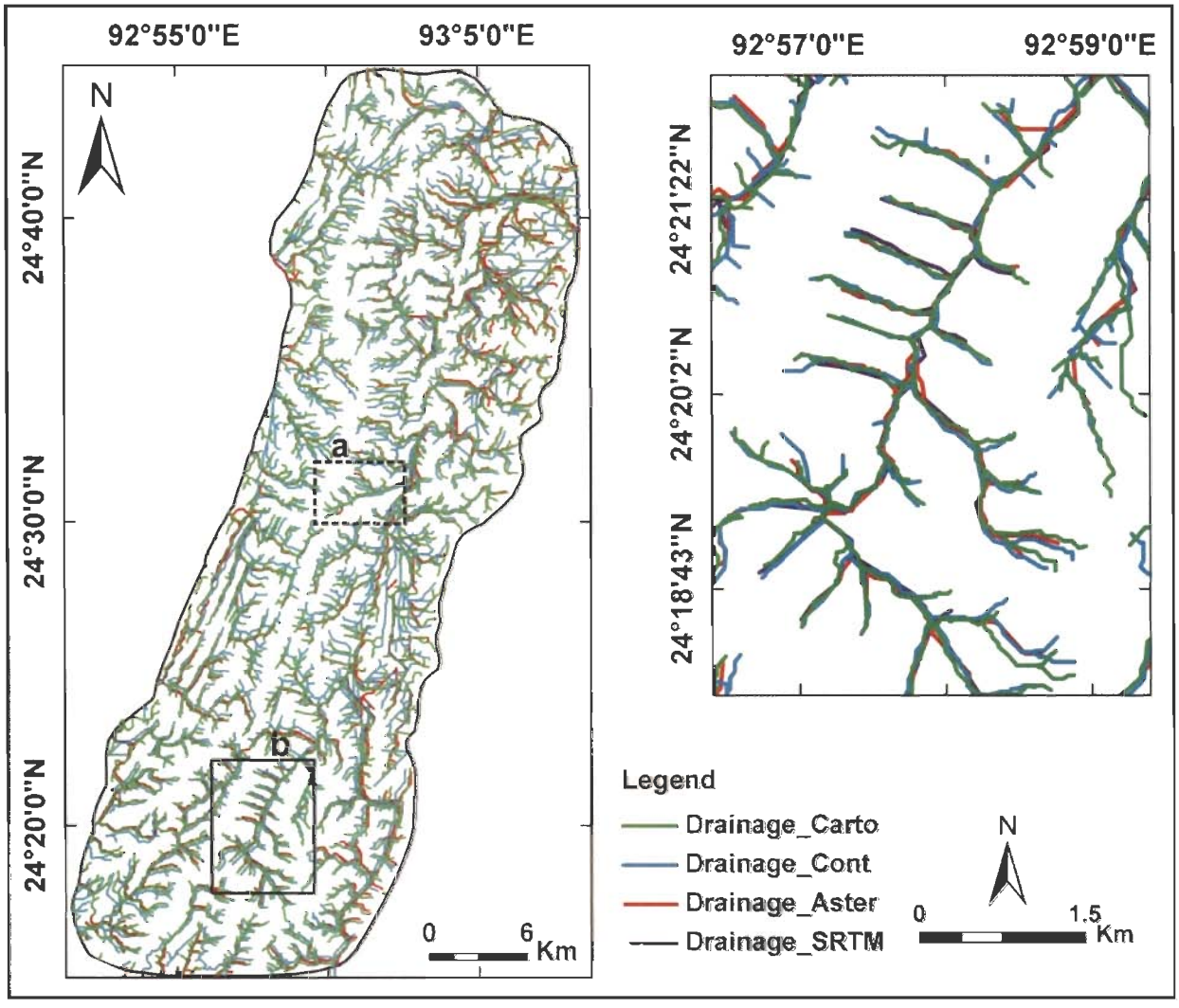

Figure 6.11 Stream networks of Bhuban Hills derived from all DEMs, and enlarged view of small area (shown in box b). (Box 'a' represents stream network of a drainage basin used for calculation of horizontal stream displacement as discussed in section 6.5.2)

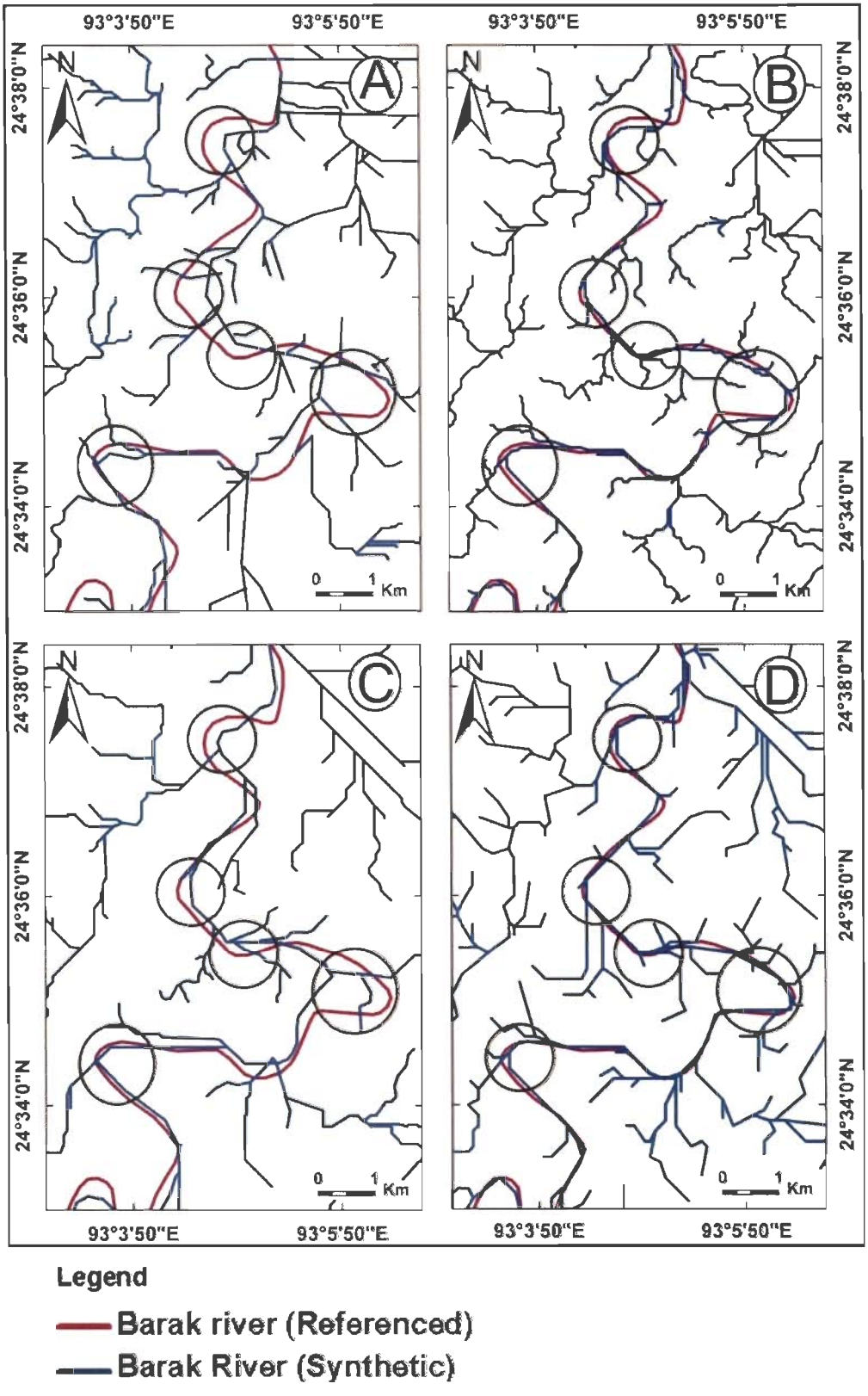

Figure 6.12 Barak River pattern extracted from Contour (A), Cartosat (B), ASTER (C), SRTM (D) DEMs.

6.6.4 Drainage density calculation

The term drainage density was first introduced by Horton (1932) and is determined by dividing the total length of streams within a drainage basin by the drainage area. DEM resolution has strong impact on the drainage density. For comparison of drainage densities calculated from all DEMs, same threshold value of 0.200 km^2 were assigned so that coarser resolution SRTM-DEM can also be able to predict the sufficient streams. Here it is important to note that relative densities haven compared instead of absolute values. Varying threshold values causes variation in drainage density, a lower threshold value results into dense drainage and vice versa. For drainage density calculation drainage length and catchments area has been calculated using Arc Hydro, terrain analysis tools. Drainage densities (DD) of all DEMs with total catchment's area and total stream length are shown in the Table 6.3.

Table 6.3 Drainage density (DD) evaluation of all DEMs.

DEMs / Parameters	Contour	Cartosat	ASTER	SRTM
Stream length (in km)	1259	1342	1269	1265
Catchment area (in km^2)	800	816	811	829
Drainage density (per km)	1.573	1.645	1.565	1.526

Cartosat-DEM shows highest stream density of about 1.64 per km, while SRTM-DEM gives lowest drainage density of about 1.525 per km. At complex terrain SRTM-DEM could not predict all the streams as it has coarse resolution of 90m. As it was discussed earlier that ASTER and Contour-DEMs show poor performance at peaks and valleys respectively, which results into relatively poor drainage density also. Similarly, it

was also found that stream length of an individual stream also vary in each DEM which results into variation in total length.

6.7 Analysis of topographic derivatives

Digital elevation models are base datasets used in topographic analysis from which various topographic parameters can be digitally generated. DEM resolution significantly affects the reliability and accuracy of results for topographic variables (Vaze and Teng, 2007).

6.7.1 Topographic profiles

Topographic profiles of the Bhuban Hills have been extracted using 3D Analyst of ArcGIS. One longitudinal (LP-1) and 10 transverse profiles (TP-1, to TP-10) were derived digitally from all the DEMs for the purpose of comparison. The locations and extent of these profiles are shown in figure 6.13.

These topographic profiles are actually representative of all the undulation present on the hills and no smoothing has been carried out. As a result slight mismatch has occurred although all the profiles are in good agreement (figure 6.14). On the basis of visual inspection of profiles it was analyzed that SRTM-DEM shows less variation, because it gives least details about the ruggedness of topography. Cartosat-DEM shows high variation profiles followed by Contour and ASTER-DEMs as they provide finer details about the terrain shape.

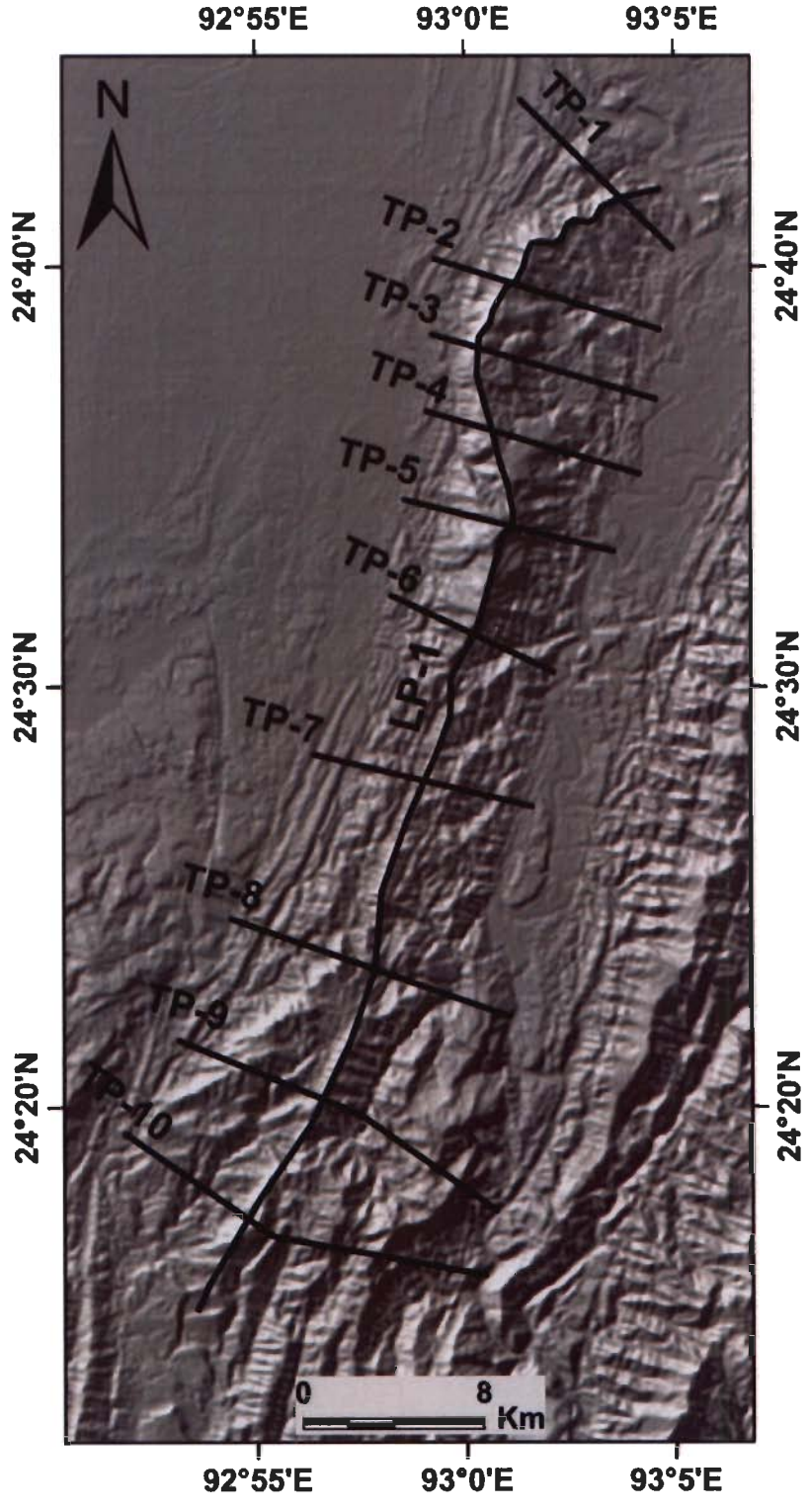

Figure 6.13 Location of topographic profiles on shaded relief model of SRTM-DEM. LP-1: Longitudinal profile. TP-1 to 10: Transverse profiles.

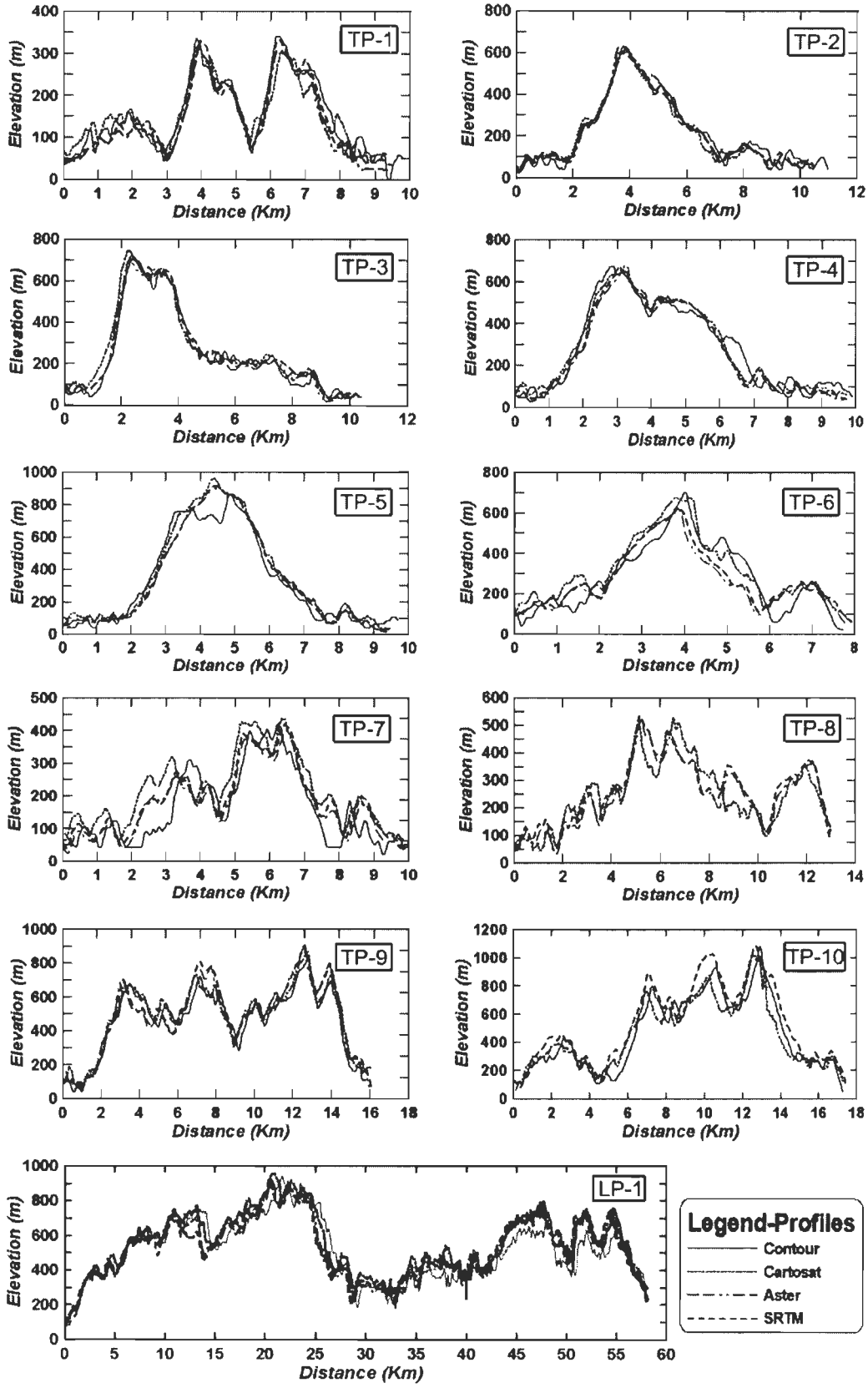

Figure 6.14 Topographic profiles (one longitudinal and ten transverse) derived from Contour, Cartosat, ASTER and SRTM DEMs.

6.7.2 Slope and Aspect analysis

It is the terrain slope which controls the movement of water through channel initiation. Slope and aspect both have been calculated for the whole Bhuban Hills using surface analysis tool of ArcGIS 9.3. Z value used as 0.00000956 for each DEM and cell size was dynamically fixed according to spatial resolution. Maximum, minimum and mean values of slopes are calculated (Table 6.4) and slope variation is shown in a small watershed comprises steepest slopes (figure 6.15). Here, it is noticed that DEM resolution has a large impact on topographic derivatives in comparison to other parameters. Cartosat-DEM predicts the steepest slopes with maximum value of about 87°. Contour and ASTER DEMs give slightly less values around 85°. SRTM-DEM gives very low maximum slope of 55° only which is attributed to very coarse resolution resulting into more averaging during the processing. SRTM may also exhibit radar artifacts including scattered voids due to shadowing effect and poor signal return. These phenomena are more common in mountainous regions and steeper slopes.

Table 6.4 Slope parameters of Contour, Cartosat, ASTER and SRTM DEMs.

DEMs / Slope (in degrees)	CONTOUR	CARTOSAT	ASTER	SRTM
Minimum	0	0	0	0
Maximum	85.45	87.30	84.44	55.27
Mean	8.14	17.45	7.51	12.63
Std. Dev	12.05	11.11	10.03	8.52

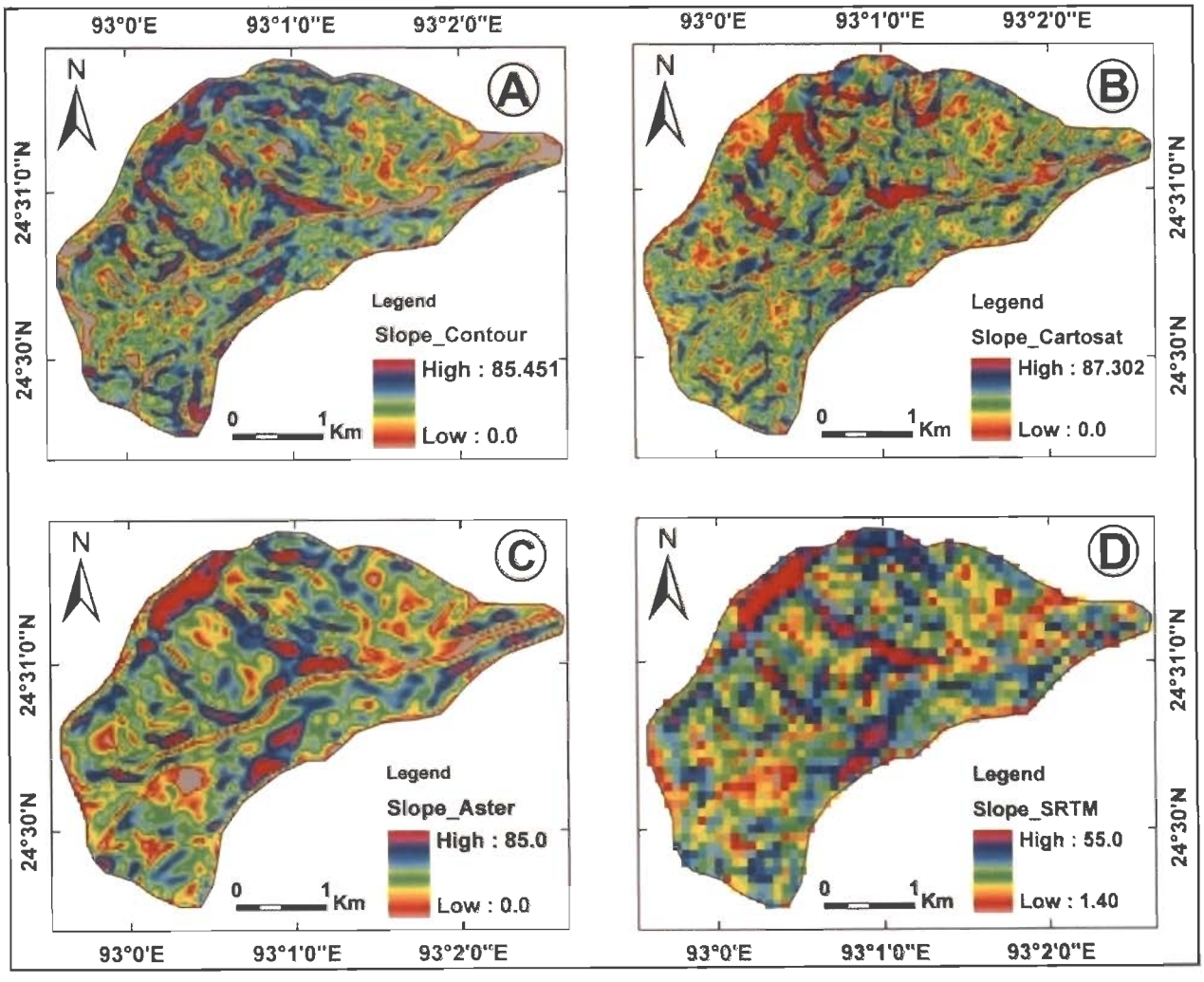

Figure 6.15 Slopes (in degrees) from Contour (A), Cartosat (B), ASTER (C) and SRTM (D) DEMs.

Aspect is calculated in degrees from north direction using surface analysis tools of ArcGIS 9.3. Figure 6.16 is showing aspects computed for a selected drainage basin from Contour, Cartosat, ASTER and SRTM-DEMs. In aspect grids zero slope surface are more clearly visible than the slope grid. From the visual inspection it was found that ASTER-DEM gives maximum flat areas (grey color areas with zero slopes). Similarly, Contour-DEM also shows some flat regions, which also supports our earlier observations regarding accuracy and drainage parameters. Cartosat-DEM gives maximum details about slope directions, even very steep slope directions can be seen prominently. In case of SRTM-DEM not any significant information can be drawn. It shows a general trend of topographic slope and aspect but finer and small scale details are missing.

6.7.3 Topographic Index

The topographic index (TI) was first introduced by Beven and Kirkby (1979) as part of the runoff model TOPMODEL. Beven (1985) has developed TOPMODEL to simulate runoff production from a watershed. Topographic Index maps are grids derived from digital elevation models (DEMs). These grids include only topographical information. It makes use of an index of hydrological similarity based on topographic data. TOPMODEL was one of the first attempts to model distributed hydrological responses based on variable contributing area concepts. It is represented by the following formula.

$$\lambda = \ln\left(\frac{\alpha}{\tan\beta}\right)$$

Where, λ is the topographic index, α is the upslope contributing area per unit length of contour, and β is the topographic slope of the cell.

Topographic index varies with the DEM quality and resolution. TI was calculated by using ILVIS slope, and flow accumulation algorithm. In this method all the zero values slope has been replaced with the very small positive values (0.0001), so that the index can be defined throughout the catchments. Same watershed used for the TI calculation

which was used for the calculation of other topographic derivatives. Slope is calculated in degrees, using surface analysis tools. Tangent of the slope has been calculated by using the formula script in Raster calculator and all zero values were removed. Finally TI was calculated by applying the formula (Ln((([FlowAcc_BH]+1)* 20) / [BH_Rads_No0])). Here, 20 is cell size, which can be changed accordingly for each DEM. Maximum, minimum, mean and standard deviation values have been calculated and compared with each other (Table 6.5).

Table 6.5 Derived topographic index parameters for all DEMs.

DEM / TI	CONTOUR	CARTOSAT	ASTER	SRTM
Minimum	0.914	0.291	1.714	3.098
Maximum	22.236	27.763	20.180	14.992
Mean	5.656	5.490	6.137	6.542
Std. Dev	2.045	2.073	1.849	1.928

Spatial heterogeneity of the topography depends upon the DEM quality and resolutions. From the calculated results highest value 27.76 of topographic index is shown by the Cartosat-DEM. Visual analysis shows that Cartosat-DEM defined the higher accumulation areas in greater detail. In all DEMs, the red color areas indicate well drained (figure 6.17). Contour-DEM has the higher value of 22.23 and also gives informative results, followed by ASTER which is 20.18. But ASTER-DEM shows some breaching effect at the steeper slope regions due to poor reflection or some other unwrapped errors. SRTM-DEM shows very low index value of 14.99 only, which is very much influenced from the poor prediction of slope values and scattered pixels at small scale. Range of index distribution is also affected by the resolution. High resolution Cartosat-DEM shows wider distribution range in comparison to low resolution SRTM-DEM. Not only higher and lower values are clear, intermediate values are also very well distributed in Cartosat, followed by Contour and ASTER DEMs.

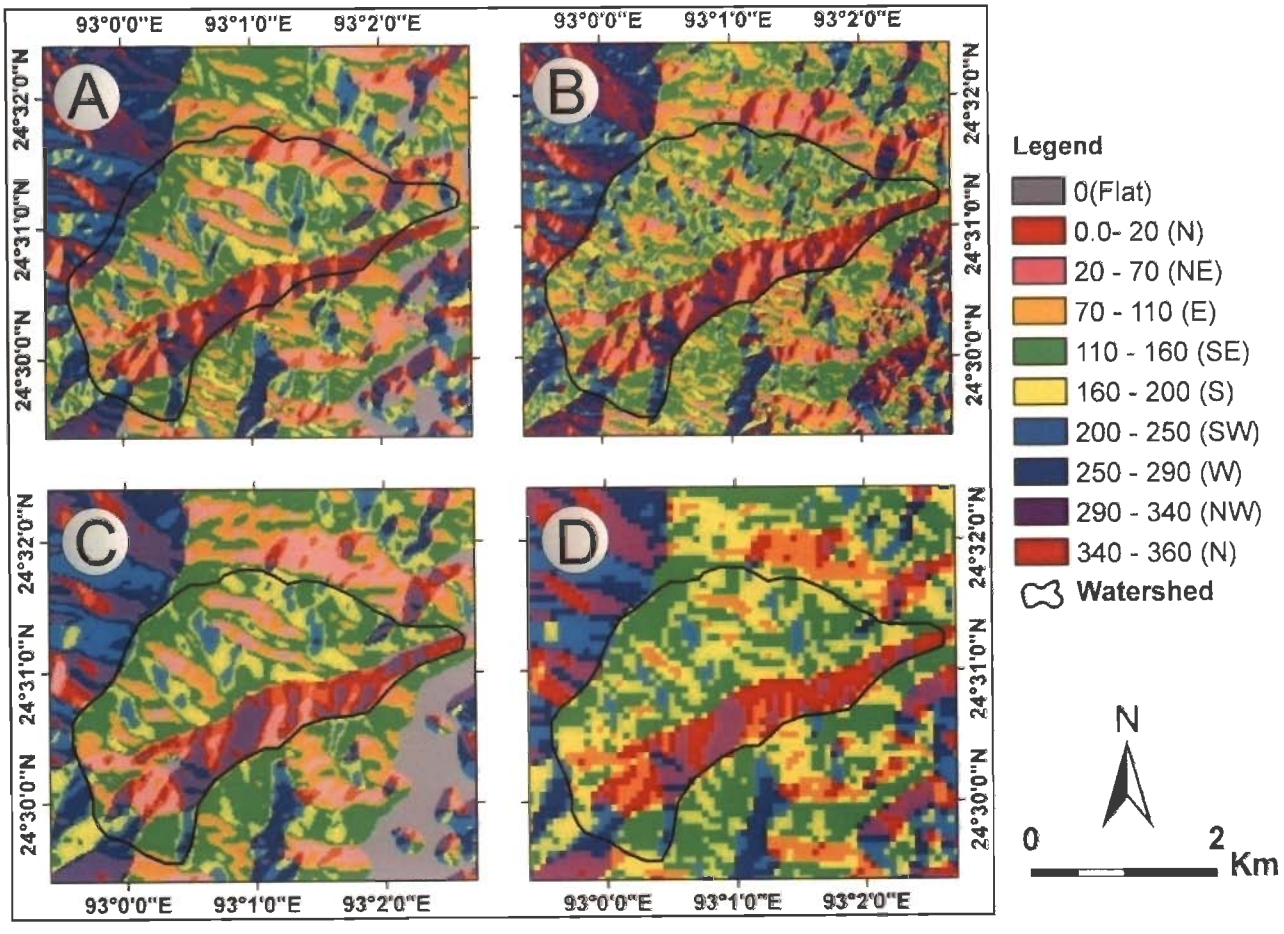

Figure 6.16 Aspects from Contour (A), Cartosat (B), ASTER (C) and SRTM (D) DEMs

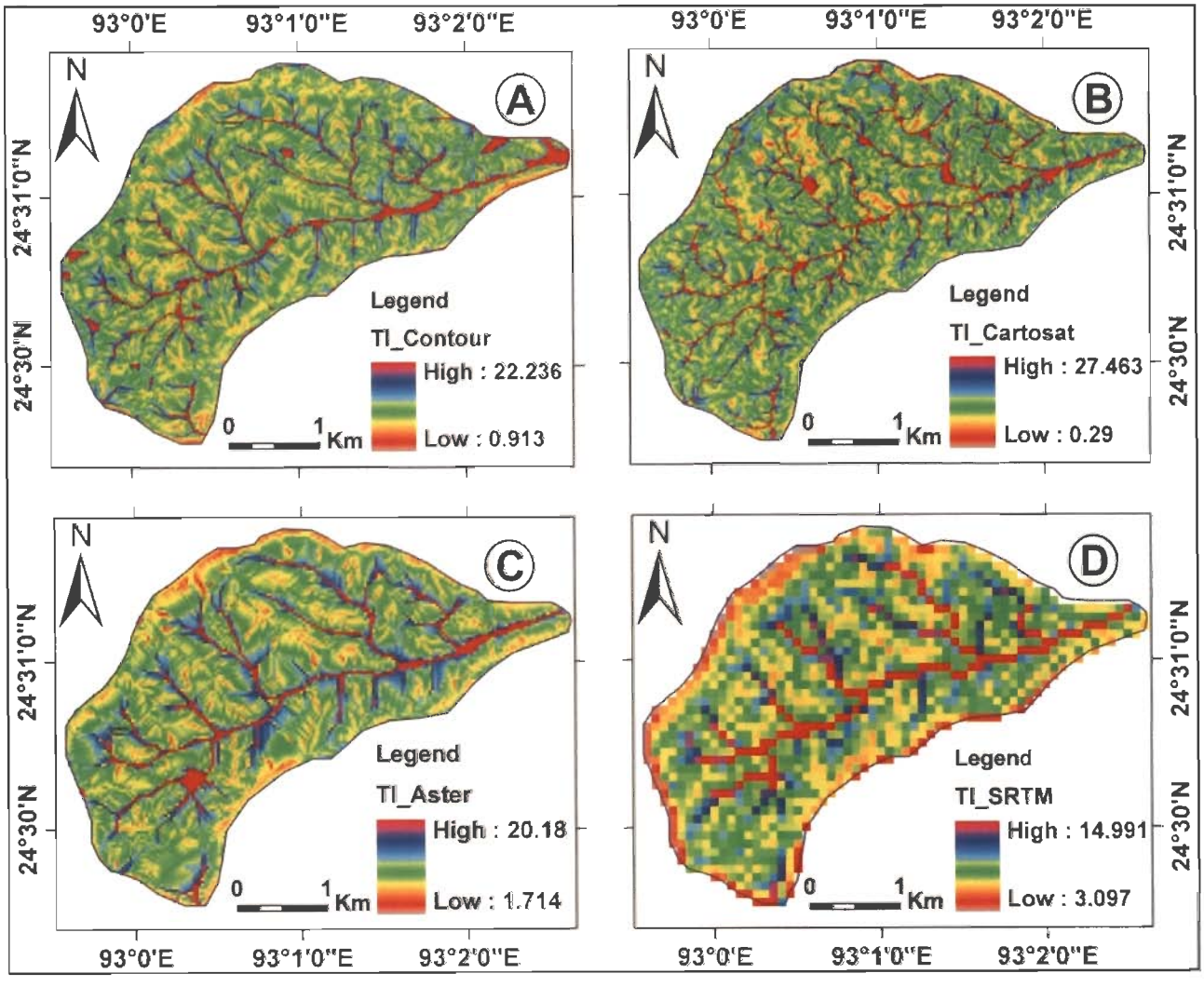

Figure 6.17 Topographic Index calculated from all DEMs

6.8 Results

DEMs generated for the Bhuban anticlinal hills from Contour and Cartosat-1 stereo data remained extremely useful for carrying out several studies related to accuracy, comparison and extraction of terrain information. In case of Contour-DEM standard methodology viz., contour digitization, generation of TIN model and raster creation were adopted in GIS environment. Elevation surface generation for Contour-DEM was mainly governed by the contour intervals and digitization accuracy. Therefore, in relatively flat areas having less contour density the errors in elevation estimation found to be more. Cartosat-DEM was generated using three stereo pairs of Cartosat-1 images using various steps of Leica Photogrammetric Suite of ERDAS-Imagine 9.3. Tie-point matching is an important step. In case of Cartosat-DEM elevation surface is generated through continuous gridding and therefore minimizes the errors in elevation estimation compared to Contour-DEM.

The generated Contour and Cartosat-DEMs were compared with the available SRTM and ASTER-DEM. On the basis of accuracy assessment it was found that Cartosat-DEM shows highest vertical accuracy, whereas in case of horizontal accuracy all the DEMs except SRTM-DEM show near similar variations. DEM derived drainage parameters and hydrological features such as basin boundary and stream network delineation are sensitive to both accuracy and resolution. Therefore, Cartosat-DEM is the best options for hydrological studies. Despite coarse resolution SRTM-DEM provides good results for regional analysis but for detailed analysis high resolution DEM should be preferred. Slope and aspect analysis information from Contour and ASTER-DEMs underestimated very gently sloping river valley as flat slopes. Here it is important to note that in case of drainage analysis and topographic derivatives, D8 flow direction algorithm have been employed which considers the equal flow in all the direction. Accuracy of topographic derivatives is governed by both the quality and resolution of the DEMs. Cartosat-DEM shows highest vertical and horizontal accuracy and gives consistently good results in all estimations.

CHAPTER-VII

Morphotectonics and morphometrics of Bhuban Anticlinal Hills

7.1 Introduction

Tectonic movement in any region generally gets manifested through the morphological modifications. These changes can, many a times, be recognized and delineated using satellite images and Digital Elevation Models (DEMs). An anticlinal ridge (known as Bhuban Hills) located in the Surma Basin displays significant morphological changes as can be seen on satellite images and DEM. This hill has been considered for carrying out detailed morphotectonic and morphometric analysis in order to understand how a ridge can undergo different styles of deformations. It is obvious that high resolution spatial data would be more helpful in understanding and generating more meaningful relevant information. Proper blending of appropriate information from various sources like Survey of India topographic maps (1:50000), satellite image and DEMs has been introduced for extracting the morphotectonic parameters of the Bhuban Hills. Morphometric indices viz., stream-length gradient index, slope gradient index and hypsometric integral have been computed towards detailed morphotectonic analysis of Bhuban Hills. High resolution Cartosat-DEM (generated for this study) has been used to perform the task as these parameters are more resolution dependent.

Morphotectonic analysis using geomorphic indices has been developed as a basic reconnaissance tool in order to recognize areas experiencing both rapid and slow tectonic deformation. Geomorphic evaluation of active tectonics depends on the use of geomorphic indices, which relate the sensitivity to rock resistance, climatic change and tectonic processes with the production of a certain landscape. Several present-day

tectonic land forms have been used to indicate the activeness of crustal structures (Keller and Pinter, 1996). Erosion is controlled by climate, relief of the landscape, and tectonic processes which have a major effect on topographic variations. Where tectonic processes, uplift and deformation predominate over erosion, relief increases and topography becomes more complex.

7.2 Bhuban Hills

Bhuban anticlinal hills lies in a tectonically active frontal part of the Indo-Burman fold belt. This hill trends north-northeastwardly following the trends of all other anticlinal ridges present in the region. Geologically, the Bhuban Hills is made up of sandstone, shales, soft clays and mudstone of Miocene age (Das Gupta and Biswas, 2000). Present topography of Bhuban Hills, is an aberration from a normal anticlinal morphology and exhibits several transverse and longitudinal fault affected segments resulting into distinct morphotectonic units. Alike Bhuban Hills there are several anticlinal ridges present in the region however, the Bhuban Hills is unique in view of its strong variation in topography along its N-S extension.

7.3 Morphotectonic features

In the Bhuban Hills region several longitudinal and transverse faults could be demarcated and due to faulting six distinct morphotectonic units or segments (MU1 to MU6) have developed displaying unique topography (Figure 7.1). North-northeasterly running linear ridges especially along western side of the northern part of Bhuban Hills is placed at very lower relief compared to the elevated ridge. Different morphotectonic units are displayed by satellite image (Landsat ETM$^+$, band-5) as well as by shaded relief model of 90m resolution SRTM-DEM (Figures 7.1a and b).

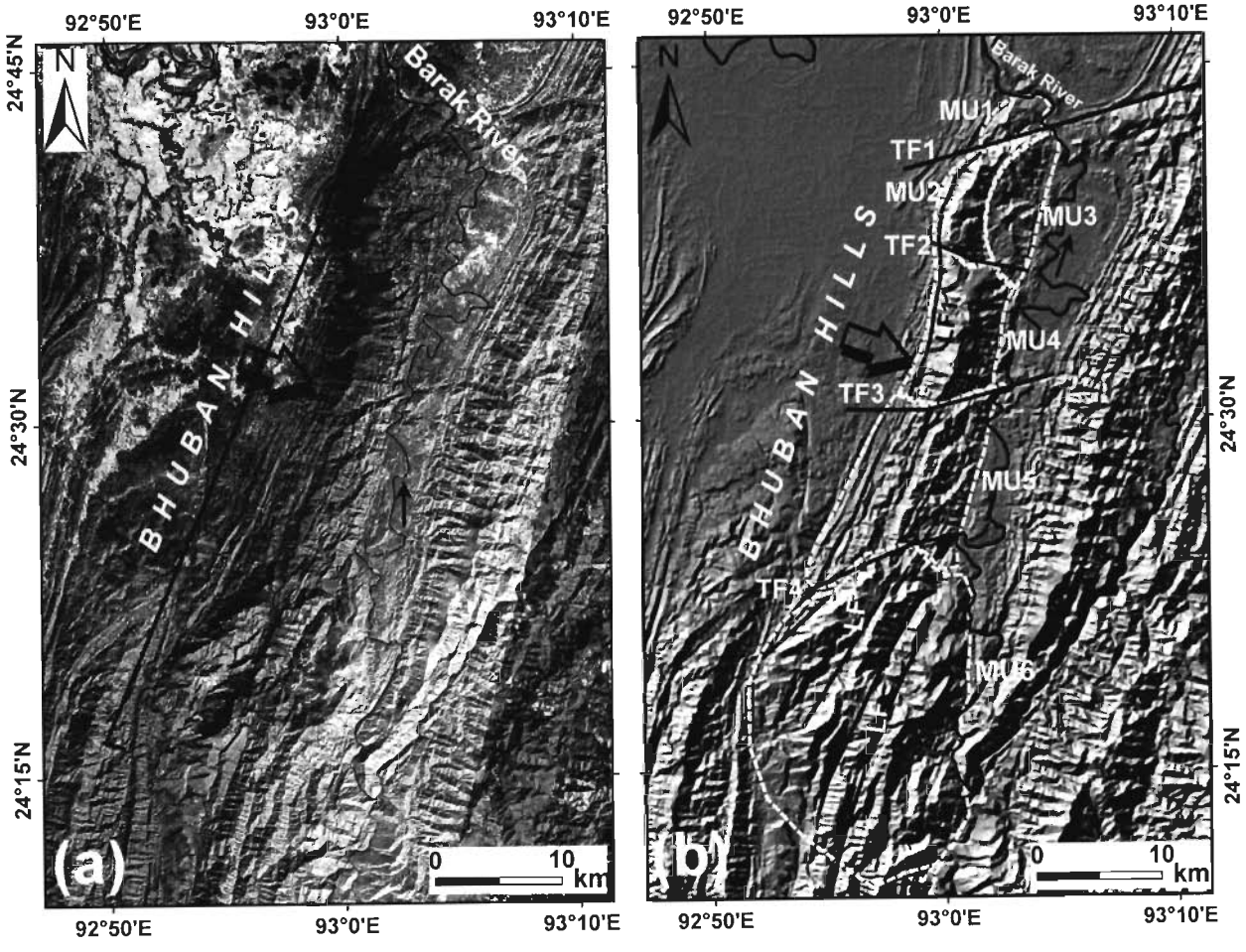

Figure 7.1 Satellite image-Landsat ETM (a) and shaded relief model of SRTM-DEM of Bhuban Hills (b). Different morphotectonic units (MU1 to MU6), longitudinal (LF) and transverse (TF1 to TF4) faults of the Bhuban Hills are shown.

First unit (MU1) is the northernmost part represented by a small hill appears to have detached from the main hill due to transverse faulting (TF1) across the ridge. Morphotectonic units MU2 and MU3 are the adjacent western and eastern blocks of hills respectively. MU2 forms high linear ridge with the formation of extremely steep escarpment on the western side with westward convex topography (Figures 7.2 a - c). Whereas, MU3 forms the eastern slope of the hill ridge but with a sudden drop in the topography as this unit suffered less upthrusting than the MU2.

Bhuban Hills show very interesting slope properties and are characterized by very steep more than 80° slope mainly on the western side of MU2. The eastern side (MU3) is marked by gradually decreasing slope of about 10°- 30° (Figures 7.2a and 7.4). Western steep slope displayed by the northern part of Bhuban Hills is a direct effect of longitudinal reverse faulting. Due to which part of ridge has been uplifted in the form of a wall as can be seen in field photographs (Figures 7.2a-c). MU3 topography is considerably rugged and eastward dipping beds are exposed. Topographical features in MU2 and MU3 have developed in response to intense deformational process in this part.

One portion of higher ridge in MU2 formed into an easterly sloping table land with development of streams which falls suddenly on to a lower relief area on the east. To the south of table land a deep erosional valley and considerably large northward slope has formed across the ridge (Figure 7.2a). Figure 7.3 is showing these two areas in closer view on high resolution Cartosat-DEM. It was clearly analyzed that ridge crest shows the deviation from normal anticlinal topography. For these two parts slope and contours have also been derived from the Cartosat-DEM with 20m interval. Contours of any hilly region are an important expression of slope gradient, facilitated interpretation of the slope direction and gradient. The ridge area marked as 1 is considerably wide with very gentle inward slope even at the ridge tops culminating to eastward slope (Figures 7.3a, b and c). This specific topography is well revealed through DEM, slope map and contours. Development of this type of slope is supposed to be caused by differential upliftment and deformation of the ridge. In another case the hill top exhibit northward slope marked as 2 in figure 7.3. In this case the topography of the ridge top breaks up from the main fold

ridge which becomes narrow and drops down towards north. The eastern slope of the ridge also forms a downthrown zone (Figures 7.3a', b' and c').

Prominent stream network of the eastern slope (MU3) as depicted by DEM is shown in figure 7.4(b). All the streams are ephemeral in nature but their deep cut into the topography indicate tectonic upliftment and subsequent heavy erosion.

MU2 exhibits gradual increase in altitude from north to south up to the transverse fault TF2. Also, around the fault TF2 the part of ridge has been severely dissected forming a transverse wind gap. The fourth unit (MU4) extends from 24.6° to 24.5°N showing high ridge with steeper western slope. From the nature of topographic feature it appears that this part also suffered upthrusting along a longitudinal fault on western side of the hill. Altitude of this part is higher than the first part and bounded by TF2 and TF3. Fifth unit (MU5) in bounded by two transverse faults (TF3 and TF4) and extends from 24.5°N southward with low altitude ridges formed by anticlinal limbs and appear to have suffered subsidence. MU6 has altogether different topographic expression as this part is represented by bulged out four ridges affected by low magnitude fault-propagation folding. Westernmost ridge of this unit show remarkable westward rotation. All the transverse faults as discussed above are shown in figure 7.1.

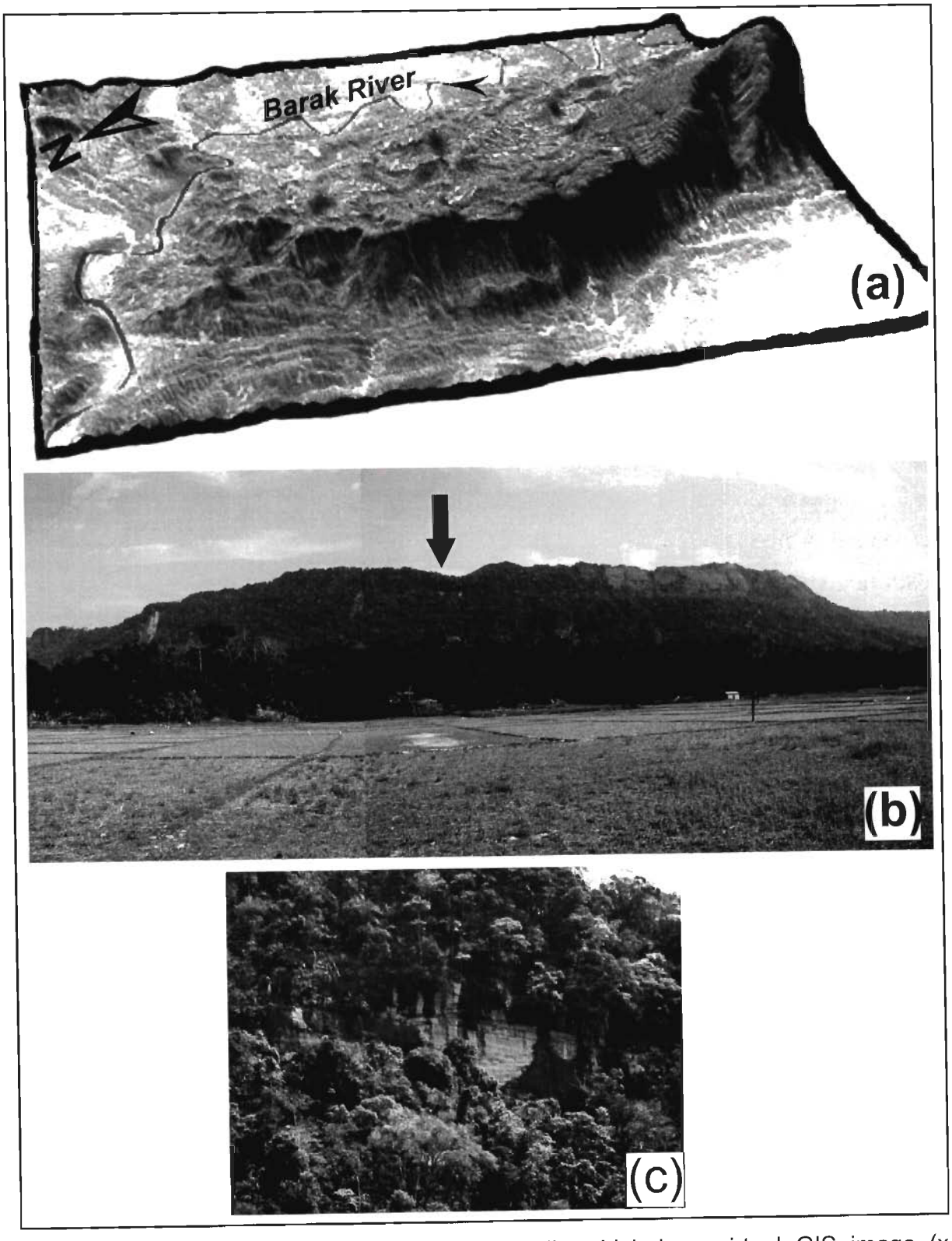

Figure 7.2 Western steep slope of Bhuban Hills which is a virtual GIS image (x4 exaggeration) generated using satellite image draped on digital elevation model (a), Field photograph of western view of the northern Bhuban Hills (b), Field photograph showing exposed steep escarpment of the Bhuban Hills at a location shown by a pointer in figure 7.2b (c).

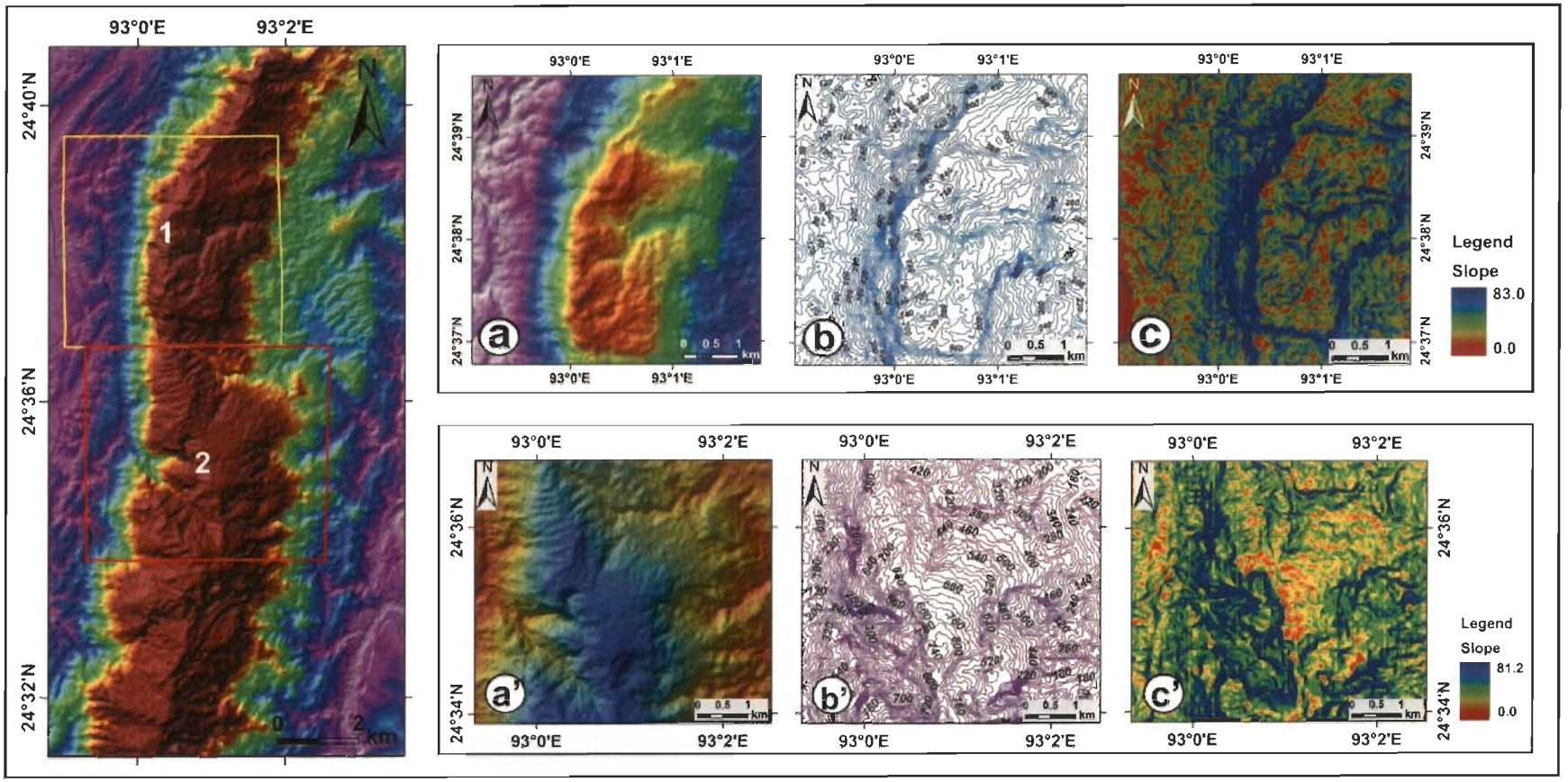

Figure 7.3 Hills top showing slope variation in color coded shaded relief model of Cartosat-DEM at locations 1 and 2. Inward Slope on the Hill-top shown in (a) Shaded relief model of Cartosat-DEM, (b) Contours and (c) Slope of the region. Downward decrease in Slope along Fault, (a') Shaded relief model of Cartosat-DEM, (b') Contours and (c') Slope of the region.

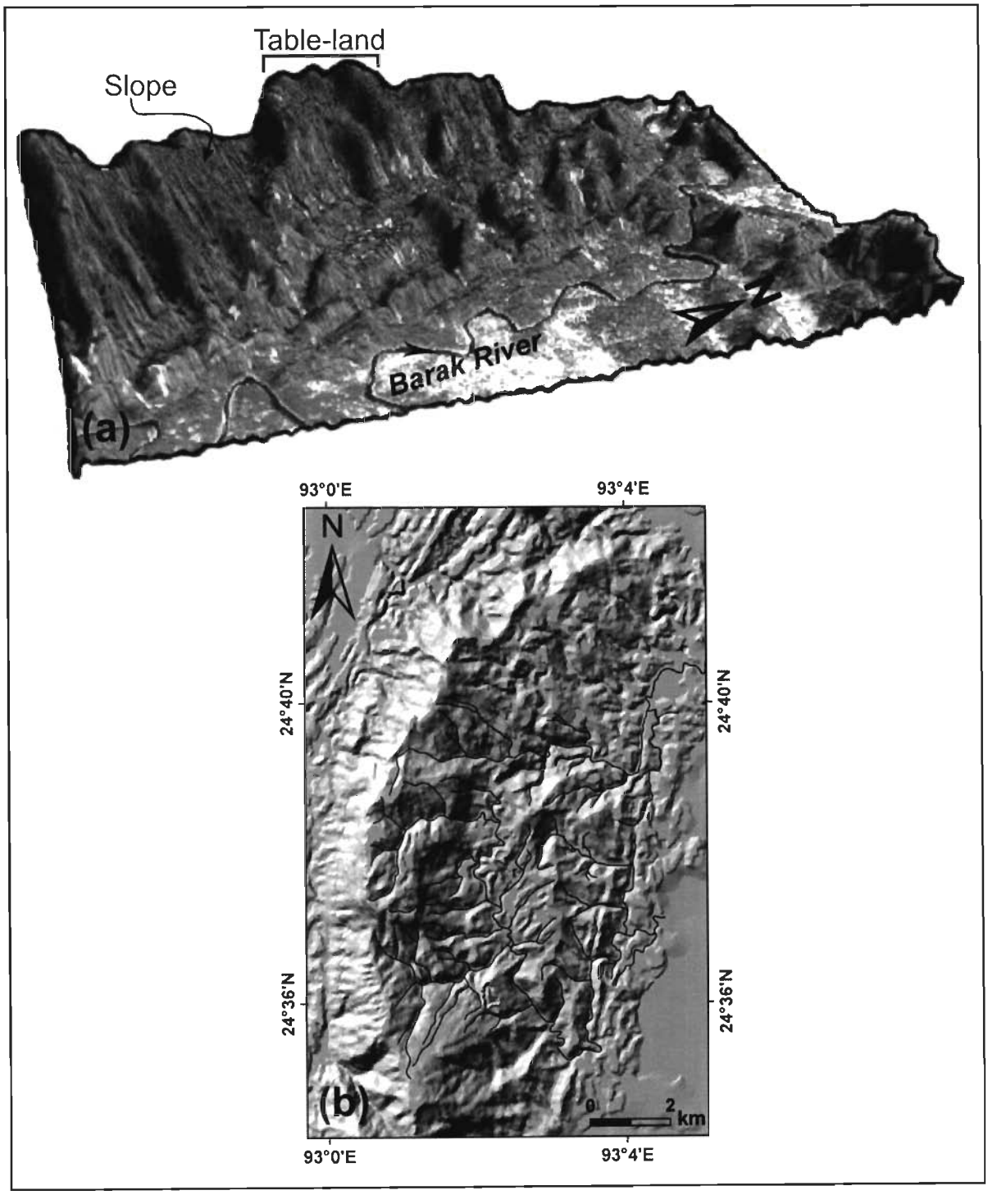

Figure 7.4 Eastern view of northern Bhuban Hills showing high and low topography-a virtual GIS image (x5 exaggeration) generated using satellite image draped on digital elevation model (a). Main stream network in MU2-MU3 region of the eastern side of hills (b).

7.4 Topographic variations

Topographic variation in the Bhuban Hills region can be assessed on the basis of topographic profiles showing elevation variation along and across the ridge. Locations and extent of the topographic profiles for which information on topographic variations have been extracted are shown in figure 7.5. All the profiles have been extracted from the Cartosat-DEM.

7.4.1 Longitudinal Profile (LP)

This profile is following the ridge top of the Bhuban Hills. Figure 7.6 is showing the longitudinal elevation profile along with three transverse faults. Upliftment and subsidence can be easily assessed from this profile. This profile also showing four distinct segments which are upthrust convex part (MU2), upthrust part (MU4), subsided part (MU5) and bulged out ridges part (MU6) as discussed earlier. Faulted parts of the ridge exhibit sharp drop in elevation and most prominent drop in elevation may be observed in subsidence zone.

7.4.2 Transverse Profiles (TP-1 to TP-8)

These transverse profiles are taken at some intervals across the Bhuban Hills covering significant topographical features and the elevation information is digitally derived from Cartosat-DEM. First transverse profile taken across the northernmost part of ridge shows two peaks having altitude more than 300 meters (Figure 7.7). These ridges have been dissected due to faulting. The second transverse profile shows one peak of about 600 meters with very steep western slope and gentle eastern slope which is due to the very steep topography of the Bhuban Hills in that part (Figure 7.7). This topography is the result of reverse longitudinal faulting as discussed earlier. Topography along the profile TP2 exhibit sharp peak with slightly inwardly curved western slope and moderate eastward slope whereas, the ridge is wider along the profile TP3 with steep eastern and western slopes. High topographical difference on the east side along the profile TP2 indicates differential upliftment or subsidence of that part. The third transverse profile

(TP3) shows a wider ridge part having altitude more than 600m with steep western side. Whereas, on the eastern side the topography initially show steep slope followed by a very gentle slope. Wider ridge part forms table type topography than the narrow ridge topography as the normal anticlinal ridge would have been. Both the transverse topographic profiles exhibit sudden drop in topography on the eastern side followed by gentle rugged slope. The fourth transverse profile (TP4) is showing peak of about 600m altitude. This profile passes through northward slope formed on the ridge just south of transverse fault (TF2) which must have remained responsible for this type of slope.

Fifth transverse profile (TP5) passes across the highest region of Bhuban Hills forming wide rounded ridge top with steeper eastern and western slopes and represented by a peak of about 1000 meters (Figure 7.7). The transverse profile number six (TP6) is showing a sharp peak with elevation more than 600m and a small peak on east side as the profile crosses a transverse fault and deep stream valley. Topographic profile (TP7) traverses through the subsided ridge part showing rugged topography with two peaks and the profile representing fold limbs by several peaks both on the eastern and western slopes. Whereas, the topographic profile (TP8) exhibit three distinct peaks which have suffered bulging due to faulting.

7.5 Morphometric study of Bhuban Hills

In order to understand the effect of tectonics and faulting on the morphology of Bhuban Hills, stream length gradient index, slope gradient index and hypsometric integral have been evaluated. A total of 39 small drainage basins and streams were investigated (Figure 7.8) for each parameter. Among these geomorphometric parameters, the stream length gradient index (SL) has been used to characterize fluvial systems in relation to tectonic movements. Several steps which were also involved in this process have already been discussed in section 5.12.1 of Chapter 5.

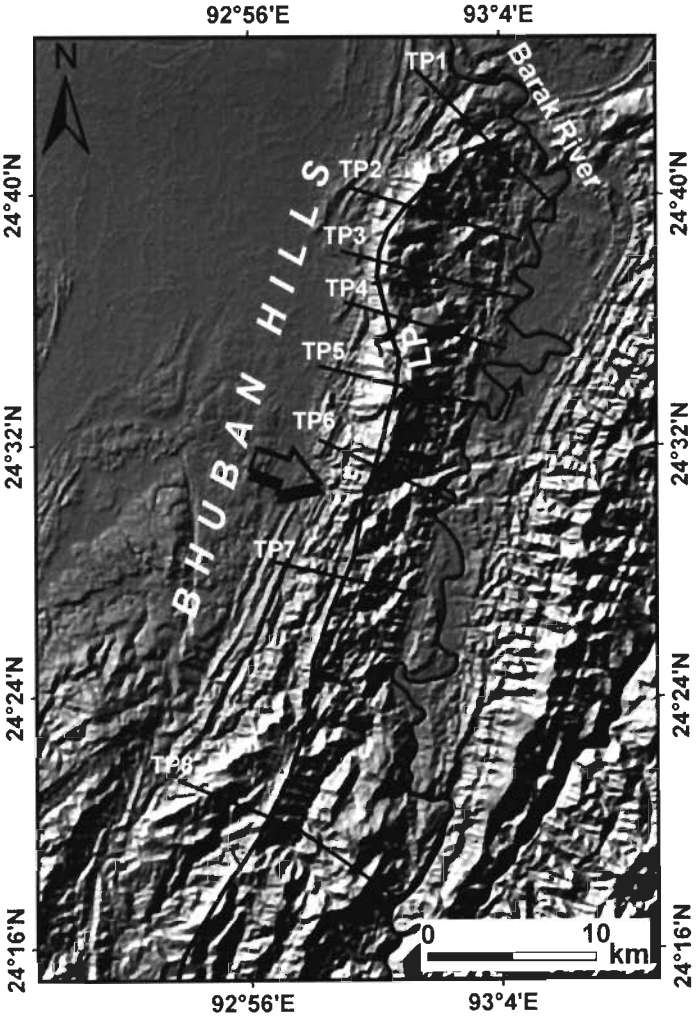

Figure 7.5 Topographic profile lines of the Bhuban Hills showing a Longitudinal Profile LP and Transverse Profiles TP-1 to TP-8.

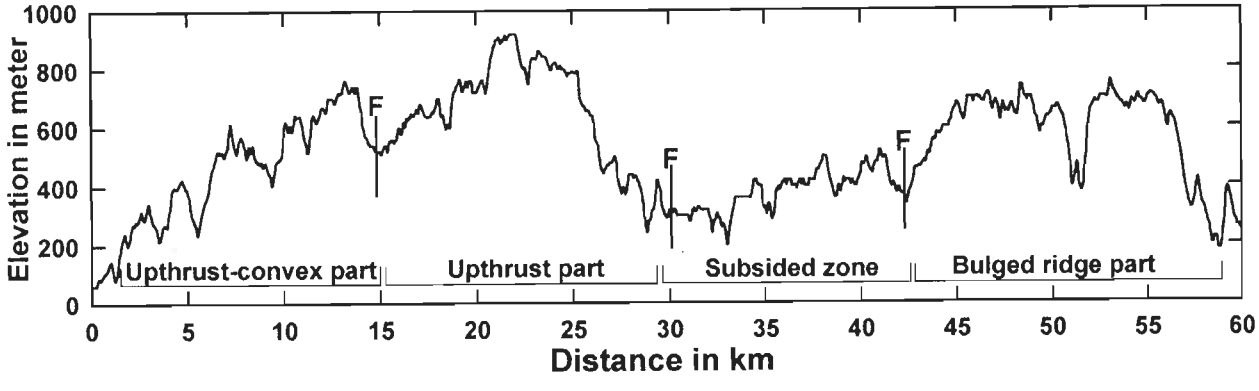

Figure 7.6 Longitudinal profile of the Bhuban Hills showing different zones and fault (F) locations. Longitudinal profile location is shown in figure 7.5.

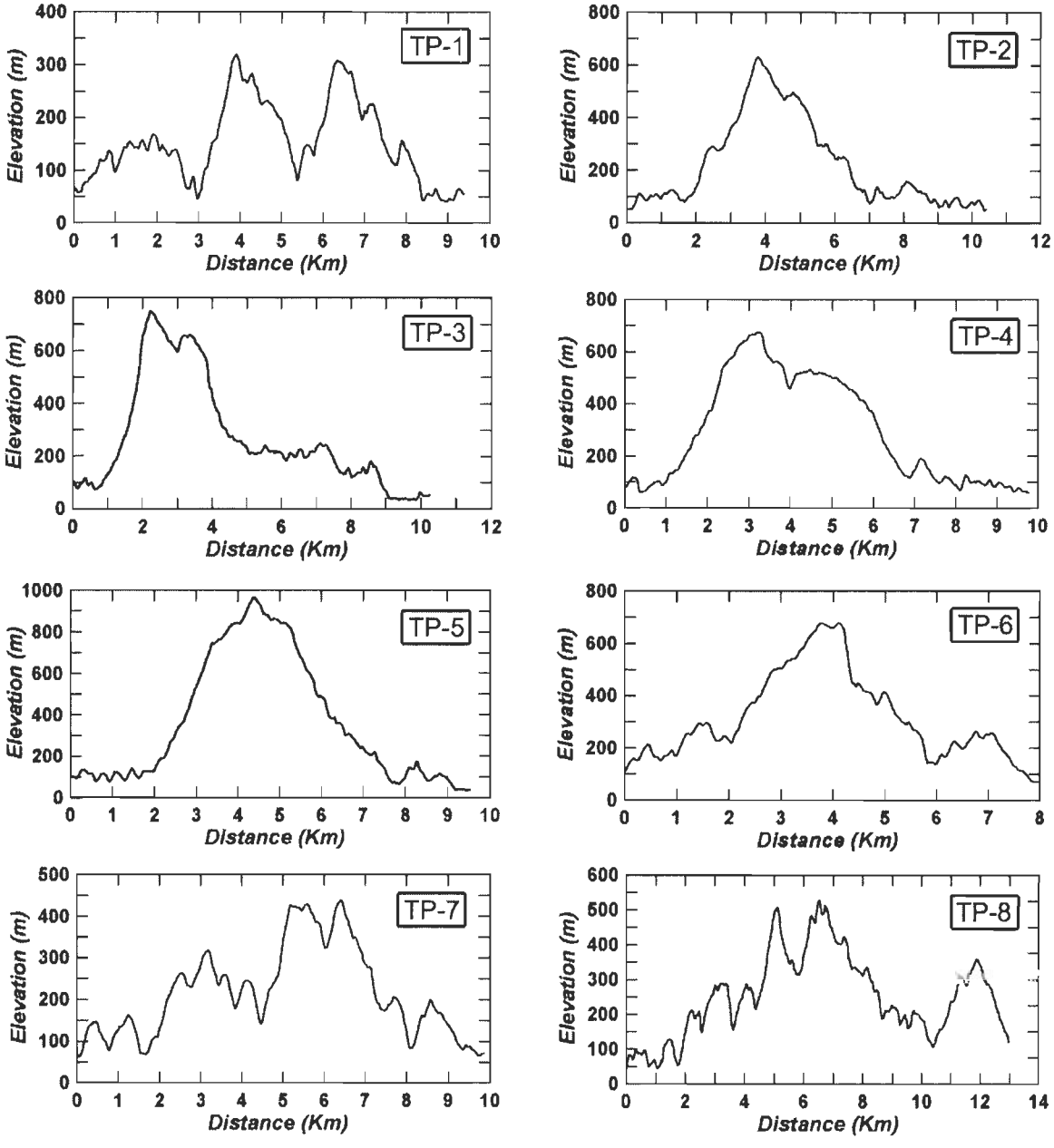

Figure 7.7 Transverse profiles across Bhuban Hills. Location of these profiles is shown in figure 7.5.

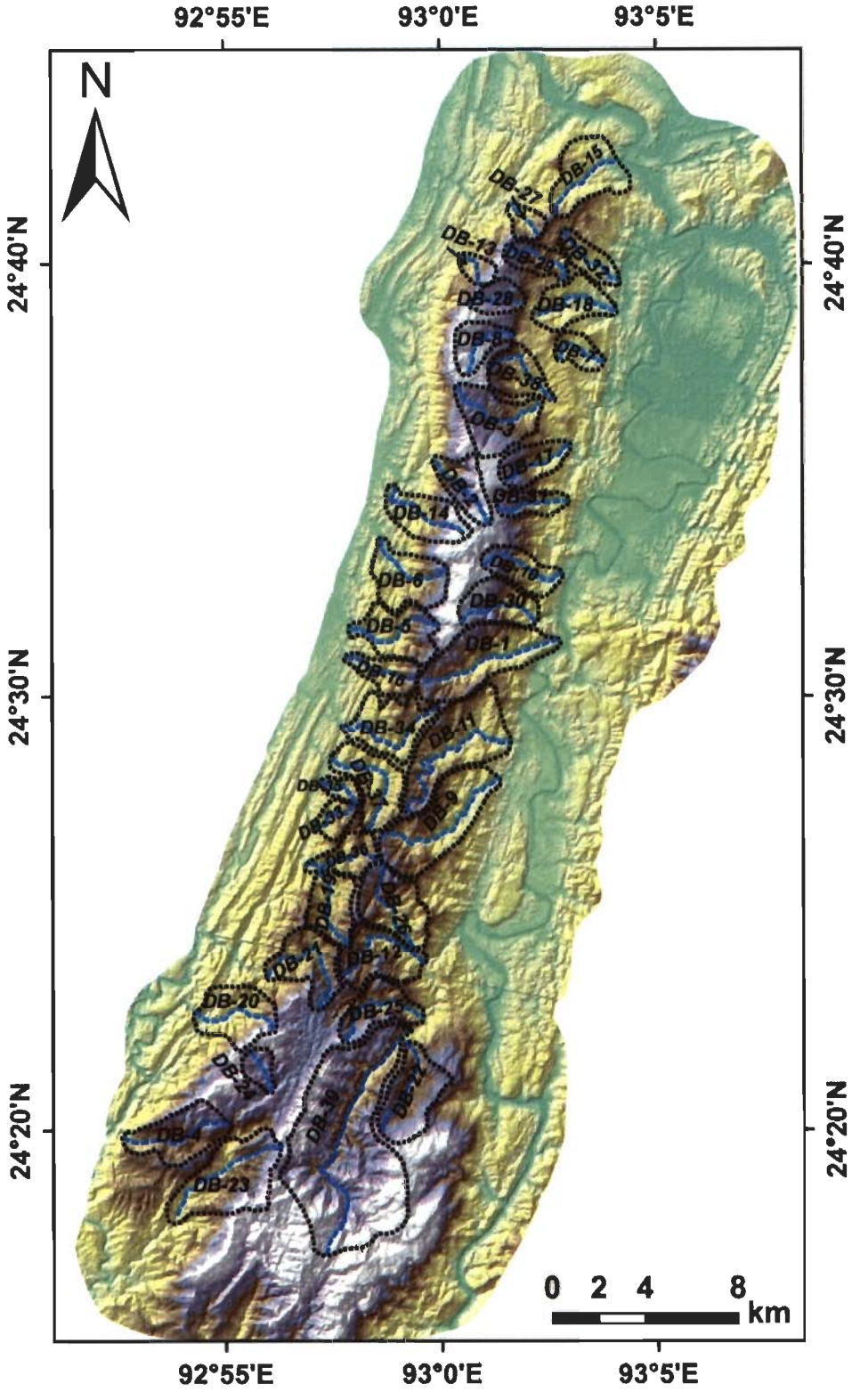

Figure 7.8 Location of various drainage basins (DB) and their respective streams selected for the morphometric analysis of Bhuban Hills shown on color coded Cartosat-DEM.

7.5.1 Stream length gradient index (SL-Index)

Tectonic deformation is usually manifested by a change in drainage system which adjusts to the change in topographic slope gradient by changing its course. SL index has been calculated here to understand the topographic variation and effect of faulting on the morphology of Bhuban Hills. SL index for a stream has been calculated from gradient of the reach and total channel length. Contours with 50m contour interval were dynamically derived from Cartosat-DEM using ArcGIS 3D Analyst tool. Then distance between two contours *(dl)* and the total distance *L* from the DEM for each segment have been calculated keeping the fixed value of *dh* as contour interval (50m). SL values were calculated at the middle point of the two segments. As discussed above all the drainage basins were digitized from the Cartosat-DEM. In order to have better control all the basins were selected manually, as it is known that even high quality DEM has some limitation in delineating basin boundary automatically and utmost care is required for marking boundaries of the drainage basins properly. In automatic extraction chances of error propagations are very high although it is fast and easier.

Figure 7.9 is showing the variation of SL values for each stream. SL values for different stream segments ranges between very low 28 to extremely high 2608. Theoretically, the low SL value (close to 1) and the high SL value (over 200) indicate that the region is influenced by active tectonics (Keller and Pinter, 1996). It has been found that mean SL value for 13 streams among 39 drainage basins is greater than 200. A closer examination of figure 7.9 indicates that the anomalous high SL values are falling either at the fault offsets or near the faults. These fault immensely modified the topography which resulted in radical gradient change. Some streams follow the normal gradient but suddenly they suffered from very high or low SL values. For example, in case of drainage basin 2, 4, and 5 very high SL values were obtained (> 2000) only at one or two stream segments, while all other segments show moderate values.

Similarly, from the slope gradient Index (S-index) same results have been obtained. Slope gradient is actually a derivative of SL index. It describes the change in SL between segments and shows where the highest rates of SL changes are located. For slope index calculation all the parameters viz., L denoting total length, dl the difference in slope between two stream segments for fixed dh (50m) were extracted from the Cartosat-DEM. All step and methodology for S index calculation has already been discussed in section 5.12.2 of Chapter 5. Slope gradient Index provides more detailed view of slope gradient variation and stream behaviour as it can predict the mild variations in each stream segment. For Bhuban Hills the absolute mean values (X100) of S index ranges between -886 to 1403 which indicates highly anomalous slope variation. Both negative and positive values are high which also shows that slope is changing from steeper to gentler and vice versa unpredictably due to faulting.

Figures 7.10 (a) and (b) are showing the interpolated maps of SL-Index variation and S-Index variation. The obtained spatial distributions of all SL values points to anomalous zones with high and low SL values. The very high SL values (>600) are lying adjacent to mapped fault scarps and characterized by changes in flow direction. It is also evident from the figure 7.10 that both SL and S anomalies are closely overlaps with each other. In case of slope values significant information has been extracted. Both positive and negative anomalies were obtained which indicate that slope is very rapidly changing from steep to gentle and vice versa with the each stream segment. Various colored fringes in the figure outside data points are due to the interpolation errors. Mean values of the SL-Index and absolute mean of the S-Index of all the basins of Bhuban Hills are shown in Table 7.1.

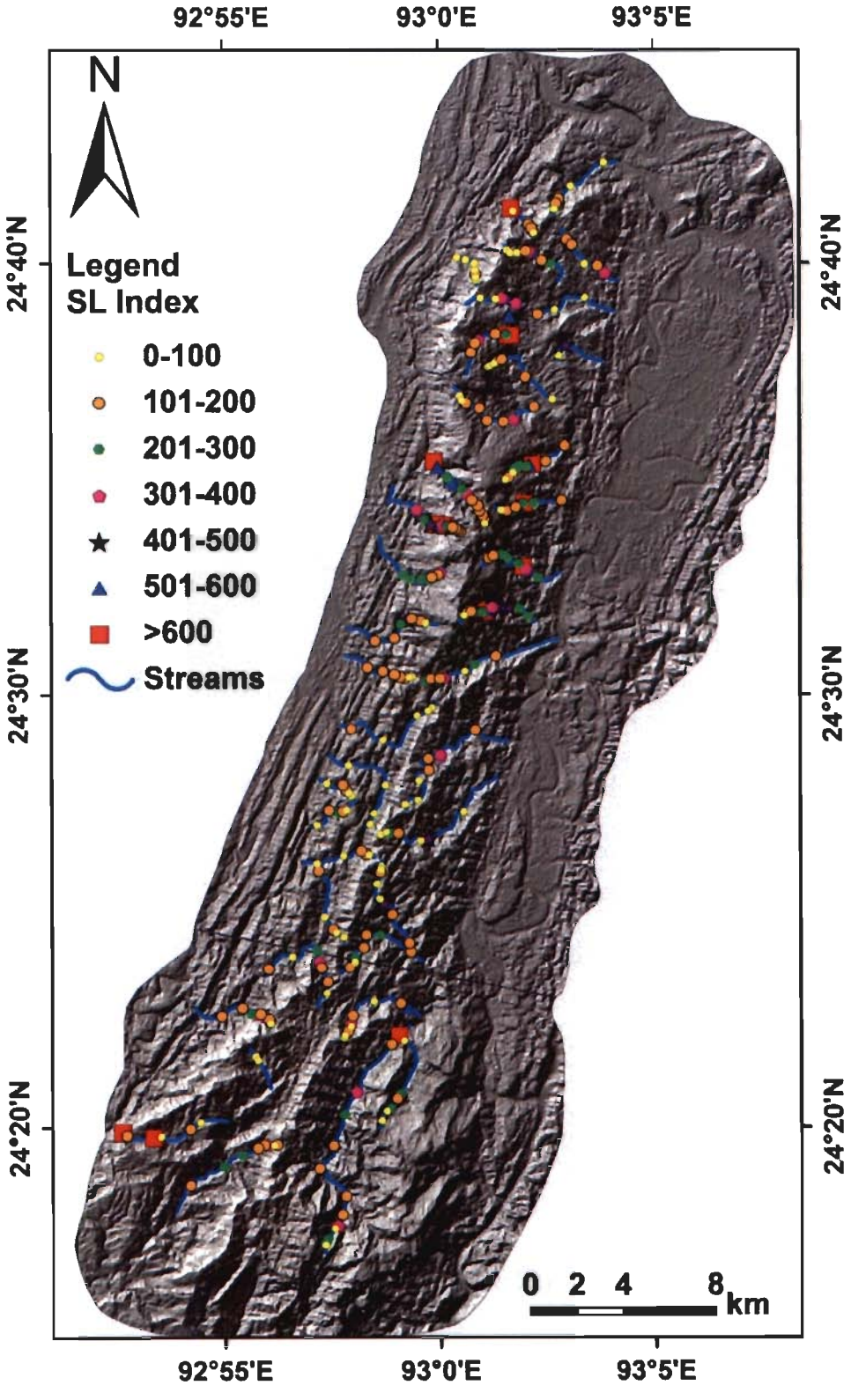

Figure 7.9 Spatial location of streams of Bhuban Hills (as shown by shaded relief model of Cartosat-DEM) used for SL index estimation and the variation for each segments as shown by symbols and corresponding values for each stream.

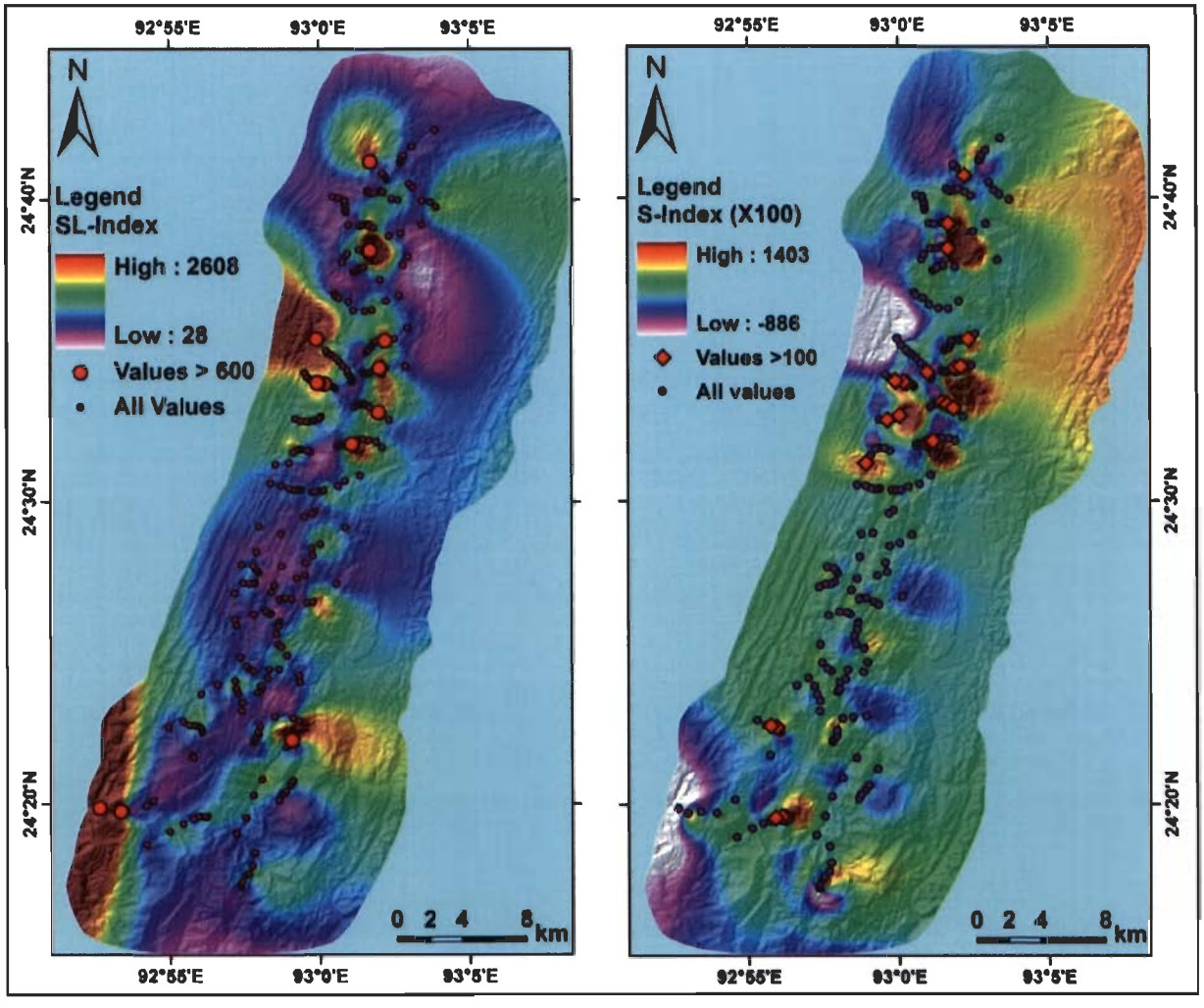

Figure 7.10 Stream length gradient Index (SL-Index) and slope gradient index (S-Index) anomaly maps.

7.5.2 Hypsometric Integral (I_{hyp})

As discussed earlier that 'Hypsometric Integral' is an index for characterizing the shape of the hypsometric curve by calculating the area under the curve. This index has considerable importance in identifying the tectonically affected topography. The hypsometric curves have been derived for all the drainage basins as shown in figure 7.8 using ArcGIS 'CalHypso' tools by defining the drainage basin boundary shape and extraction of required height and area ratios from Cartosat-DEM.

In case of Bhuban Hills I_{hyp} varies from 0.25 to 0.61, which itself an indicative of complexity in topography of Bhuban Hills. Hypsometric curves for all the basins of the Bhuban Hills are shown in the figures 7.11, 7.12, 7.13 and 7.14. It was found that the majority of the basins of the Bhuban Hills represents high value of I_{hyp} nearly 0.5. Most of them show that the stream curves are deviated from the normal S-shaped profile which is indicative of equilibrium state. Drainage basins 2, 8, 12, 21, 28, and 34 show convex upward curves mainly in the lower portion which are indicative of upliftment in that region. Similarly, drainage basins 6, 7, 14, 15, 20 and 38 shows strikingly low values representing subsidence in the region. Relatively straight curves are mainly associated with the streams having moderate hypsometric integral values.

Table 7.1 Calculated morphometric indices for Bhuban Hills.

Drainage Basins (DB)	SL-Index (Mean)	S-Index (x100) (Absolute Mean)	Hypsometric Integral (I_{hyp})
DB-1	191.86	42.38	0.39
DB-2	365.07	85.52	0.53
DB-3	163.02	16.87	0.47
DB-4	608.45	103.29	0.49
DB-5	235.46	55.96	0.43
DB-6	243.75	95.53	0.34
DB-7	31.83	10.33	0.35
DB-8	657.06	374.87	0.68
DB-9	149.44	44.36	0.40
DB-10	306.54	129.74	0.34
DB-11	126.95	8.66	0.47
DB-12	152.58	19.96	0.59
DB-13	70.42	24.06	0.43
DB-14	382.99	146.36	0.33
DB-15	115.72	46.50	0.35
DB-16	111.38	14.31	0.39
DB-17	244.04	63.91	0.44
DB-18	78.33	16.59	0.41
DB-19	98.99	22.62	0.37
DB-20	199.43	64.94	0.29
DB-21	161.26	27.80	0.50
DB-22	141.92	29.86	0.46
DB-23	187.04	68.12	0.35
DB-24	48.44	22.91	0.43
DB-25	161.16	44.08	0.48
DB-26	142.74	26.79	0.45
DB-27	207.72	66.43	0.39
DB-28	307.45	58.04	0.56
DB-29	156.87	33.63	0.39
DB-30	344.55	109.60	0.45
DB-31	343.02	236.28	0.41
DB-32	172.11	25.38	0.45
DB-33	123.12	23.26	0.52
DB-34	72.20	8.85	0.41
DB-35	102.55	27.02	0.42
DB-36	81.66	17.71	0.43
DB-37	40.17	10.12	0.41
DB-38	103.18	22.08	0.25
DB-39	249.09	52.61	0.52

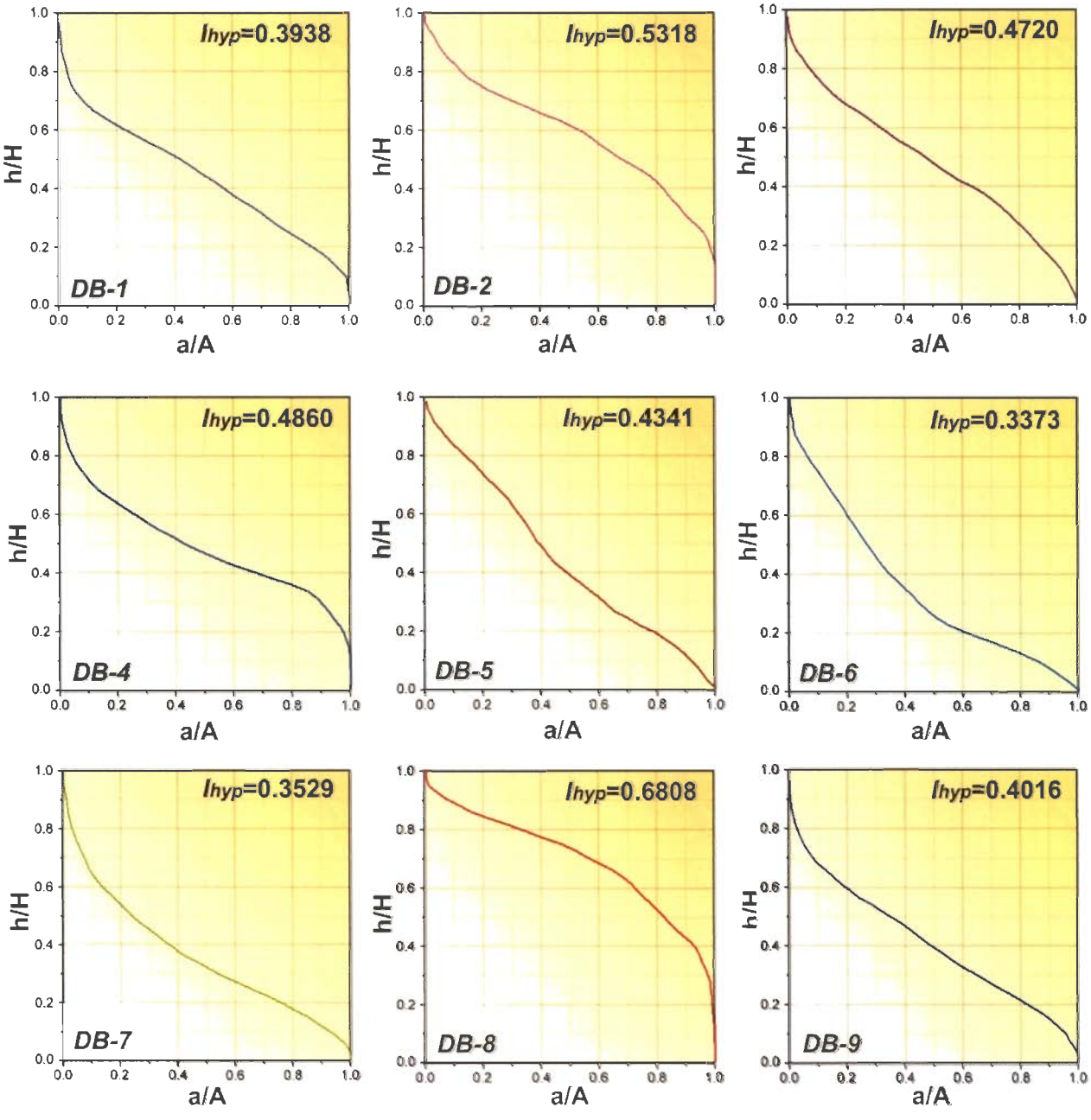

Figure 7.11 Hypsometric curves for the drainage basins (DB) 1 to 9.

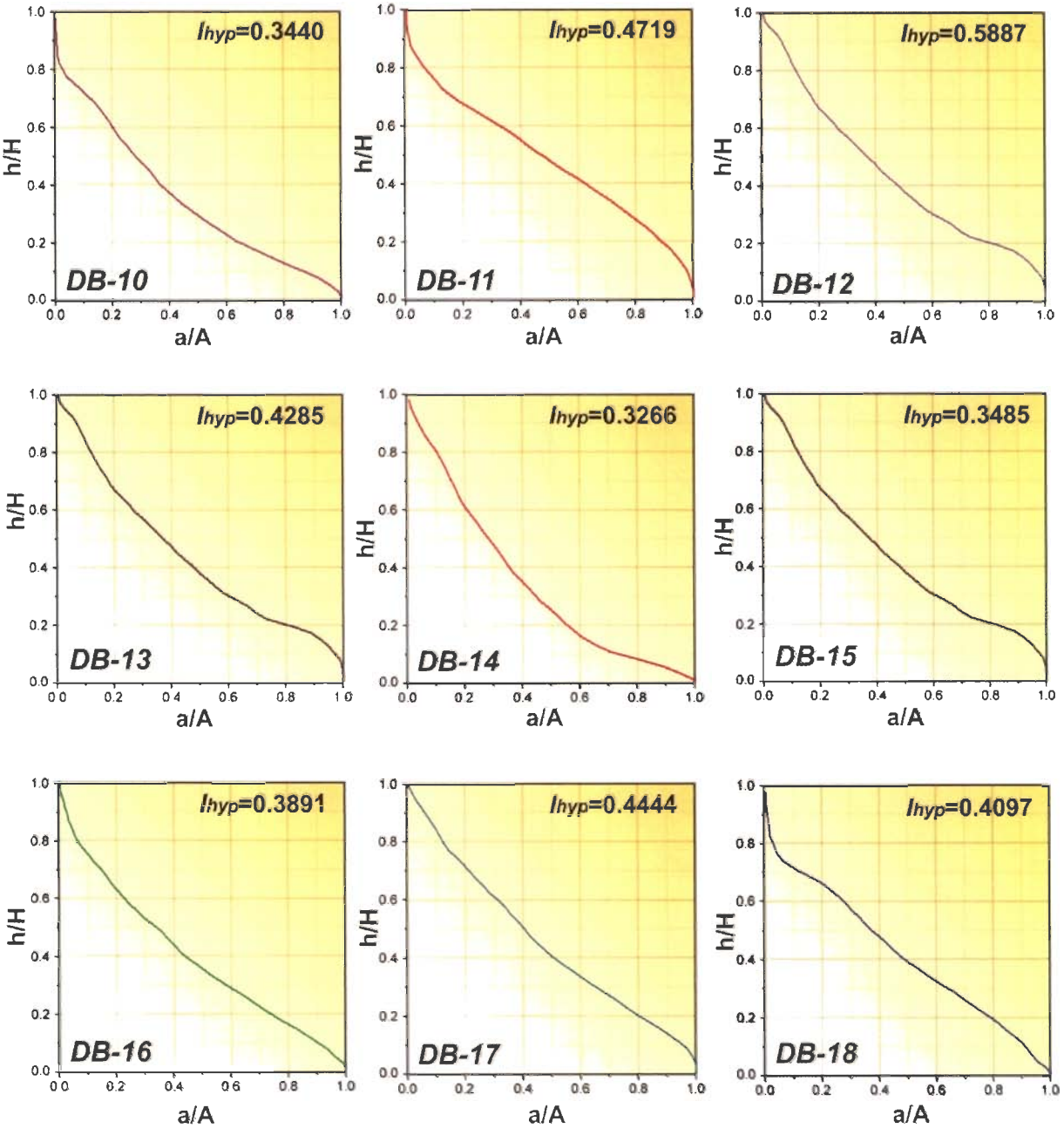

Figure 7.12 Hypsometric curves for the drainage basins (DB) 10 to 18.

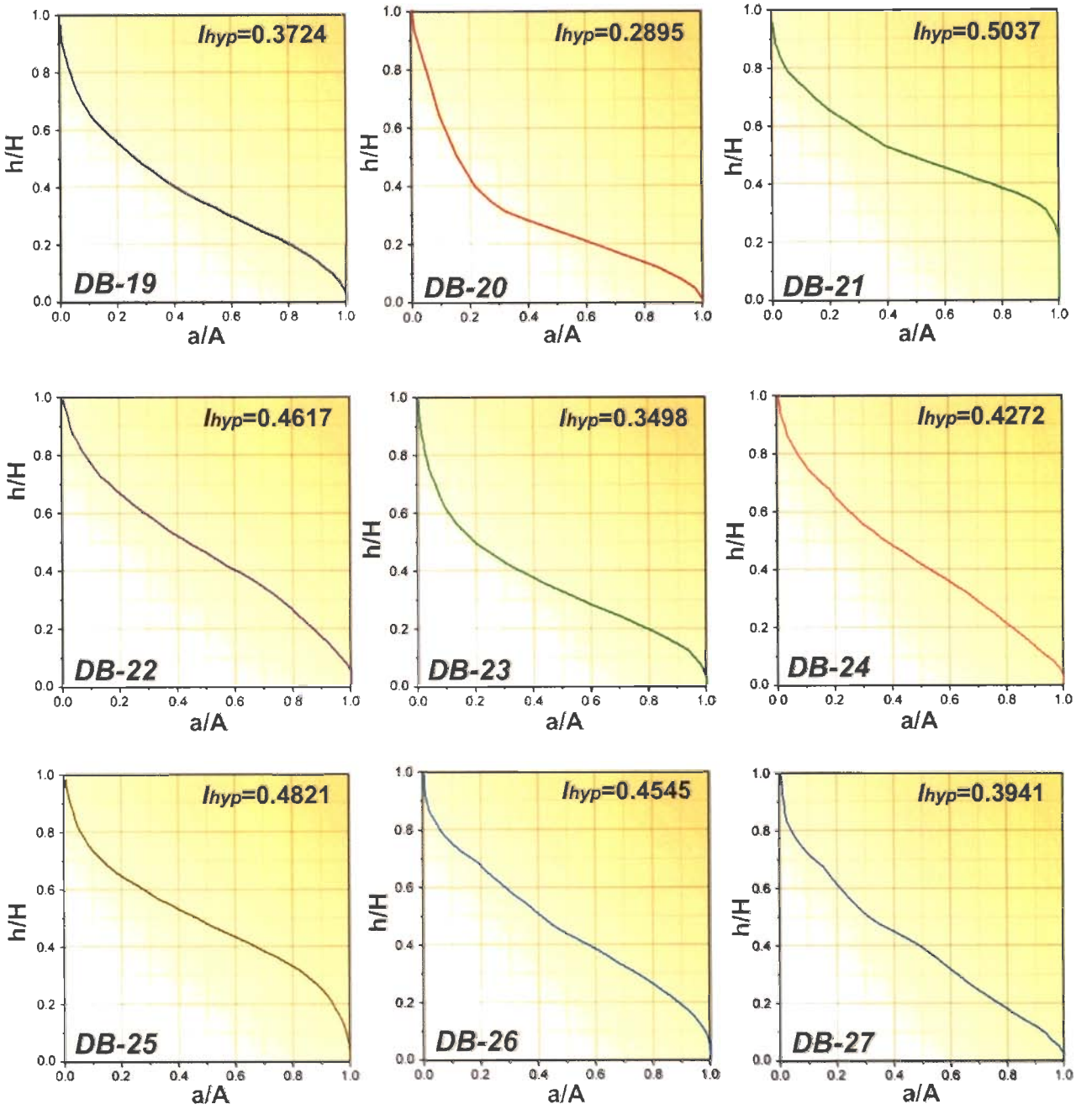

Figure 7.13 Hypsometric curves for the drainage basins (DB) 19 to 27.

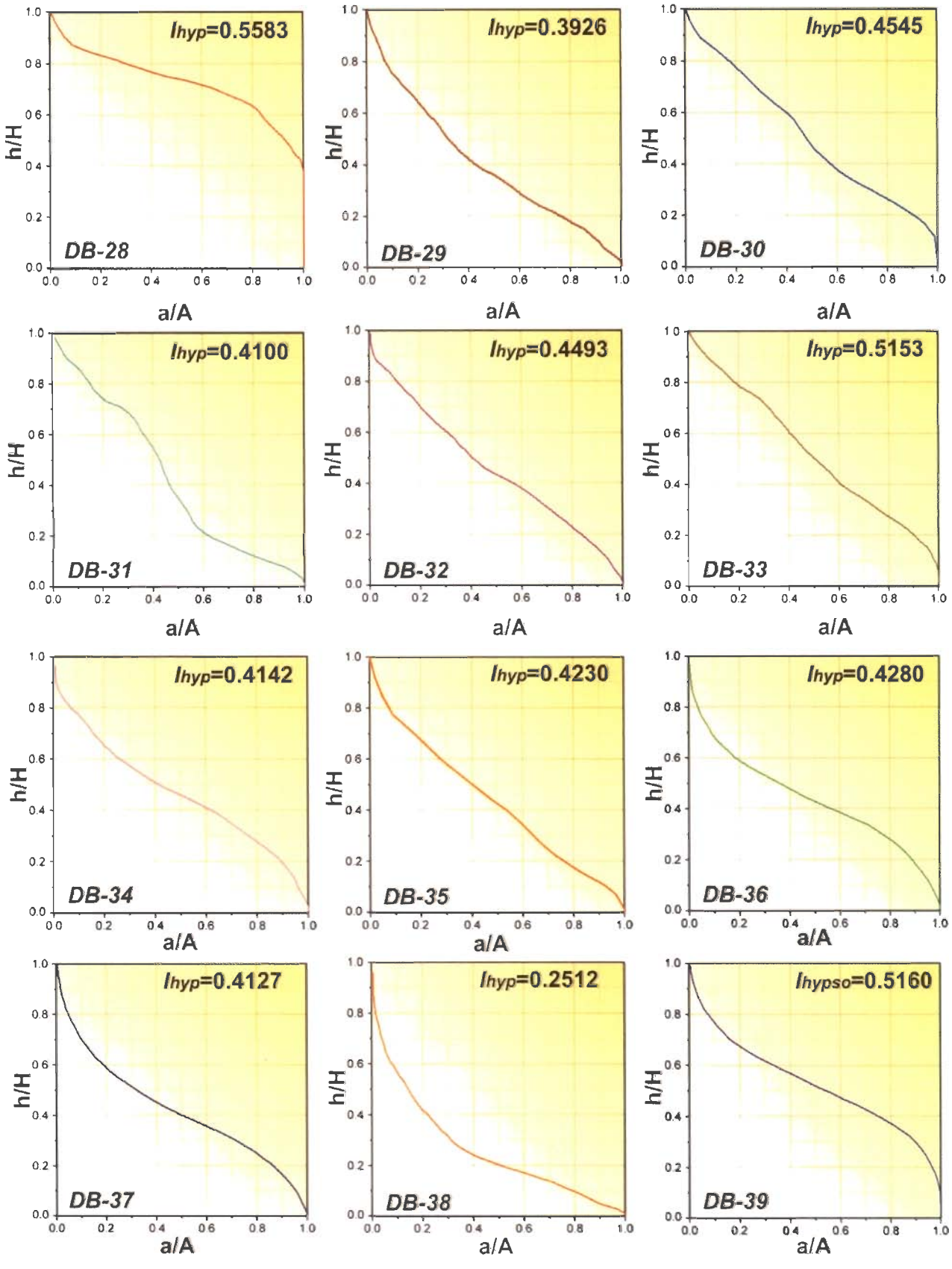

Figure 7.14 Hypsometric curves for the drainage basins (DB) 28 to 39.

The most important, but still moderate, difference arises from the comparison of hypsometric curves calculated from DEMs of different origins and differing resolutions. In order to verify this factor hypsometric curve of basin 39 drawn from four different DEMs viz., Cartosat, contour, ASTER, and SRTM of differing resolution (Figure 7.15). It has been found that varying resolution does not have significant impact on I_{hyp} values. Slight variation in I_{hyp} values could be observed when hypsometric curves derived from all the DEMs. Highest value of 0.516 obtained from Cartosat-DEM whereas the value is nearly similar and slightly less for ASTER (0.509), Contour (0.502), and SRTM (0.501) DEMs. Overall analysis of the calculated results (Figure 7.15) shows that the hypsometry of a basin is a geomorphic parameter which is robust against varying DEM resolution. This quality makes I_{hyp} more applicable and reliable than the other morphometric indices. Table 7.1 gives I_{hyp} of all the basins of Bhuban Hills.

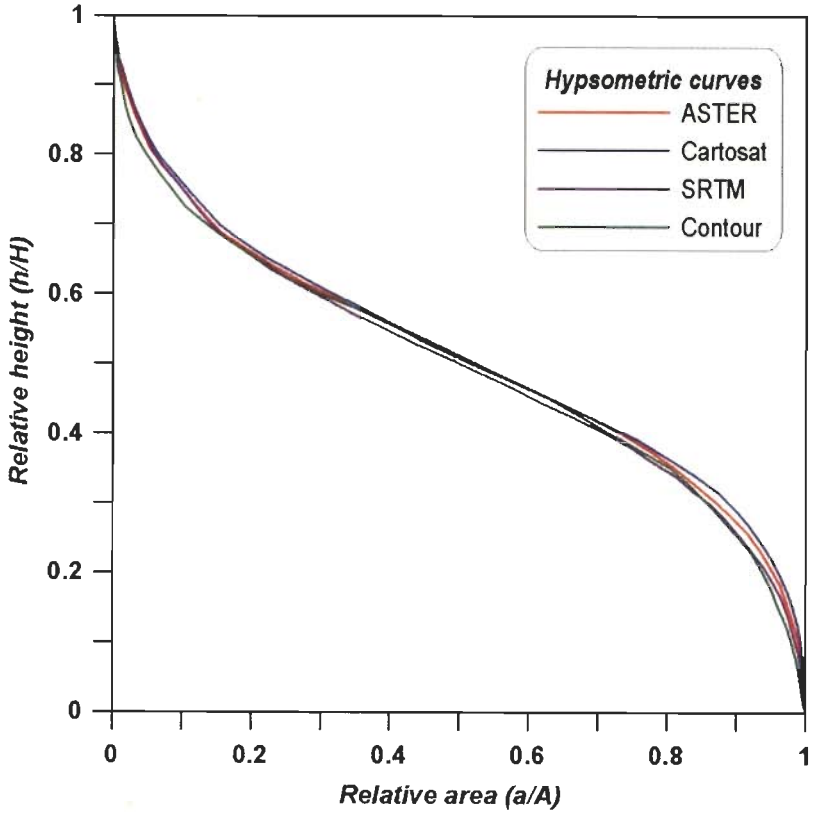

Figure 7.15 Hypsometric curves drawn from different DEMs for a basin 39.

Stream profiles have been extracted from Cartosat-DEM for understanding stream behavior and to figure out the upliftment and subsidence respectively. Only streams with anomalous values viz. hypsometric integral higher than 0.5 and SL index more than 200 has been considered for deriving the profiles. Stream profiles can provide the direct clue about the areas of slope breaks, upliftment, subsidence and erosion.

7.6 Synthesis of morphotectonic and morphometric evidences

All the evidences from regional morphotectonic study and morphometric analysis seem to support highly deformed morphology of Bhuban anticlinal hills. Present topography of Bhuban Hills, lying in the Indo-Burman frontal fold belt of northeastern part of India, is a deviation from a normal anticlinal morphology and exhibits several transverse and longitudinal fault affected segments resulting into distinct morphotectonic units. Six different morphotectonic units (MU1 to MU6) could be delineated along N-S stretch of the hill ridge. The western side of the northern most part of the hill ridge forms steep escarpment as this portion has been affected by the longitudinal faulting representing a case of fault propagation folding. The northernmost segment comprising three morphotectonic units (MU1 to MU3) is unique in the sense that this part exhibits effect of both the longitudinal and transverse faulting, uplifted narrow ridge with downthrown eastern side (MU2). Northern part of the Bhuban Hills has become curved westward due to the right lateral movement along the transverse fault TF1. The fifth morphotectonic unit (MU5) has undergone subsidence whereas, the sixth unit (MU6) exhibit bulging effect as this part experienced differential fault movements. Stream profiles, longitudinal and transverse topographic profiles extracted from various DEMs corroborated with morphometric and the topographical anomalies developed over the Bhuban Hills.

Hypsometric curve is a useful parameter for characterizing the topographic relief and variations within a drainage basin and, hence, establishing comparisons between different basins (Perez-Pena et al., 2009). The shape of the hypsometric curve is related with the stage of geomorphic development of the basin. 'CalHypso' extension has been used to generate the curves for each morphotectonic unit of Bhuban Hills. The main

advantage of this extension is that the user can extract multiple hypsometric curves directly within the ArcGIS software and calculate the main statistics related to these hypsometric curves. For detailed comparative study, all the hypsometric curves for each unit were derived. MU1 region has only one drainage basin numbered 15 with moderate I_{hyp} and SL values 0.35 and 115 respectively (Figure 7.12 and Table 7.1). It lies toward northernmost part of the Bhuban Hills and form a gentle sloping surface near LF1 (Figure 7.1).

Figure 7.16 is showing the hypsometric curves of the all delineated basins falling in the morphotectonic unit MU2. MU2 is highly deformed unit as discussed earlier. It is subjected to upliftment as well as convexing towards west due to simultaneous impact of transverse and longitudinal reverse faults. Mixed response of hypsometric curves as resulted from this unit indicate tectonically controlled drainage. Maximum value of I_{hyp} is shown by the DB-8 (0.6808) and DB-28 (0.5583) both lies in the convex western steep slope part. Stream 8 developed over the table land clearly exhibit a vertical drop of about 175 meter at place with latitude 24.6°N and longitude 93.03°E. Other streams profiles indicate undulated gentle gradient as these streams now have cut deeper into the topography otherwise having steeper slopes. Deformed morphometry of these tectonically affected streams and highly undulating topography in MU2 is very much evident from the streams profile extracted from DEM as shown in figure 7.17. DB-27 show higher value of SL index but moderate I_{hyp} value as it lies near the longitudinal fault LF-1 adjacent to MU1 toward north. Small basin DB-13 shows very low SL index because it initiated at the lower altitudes but suffered from the upliftment supported by the slight convexing in the lower part of hypsometric curve. In MU2 region most anomalous and interesting slope variations are present. Here, in most cases, both I_{hyp} and slope values are directly proportional to each other i.e. drainage basins with high hypsometric integral also show high stream length gradient indices.

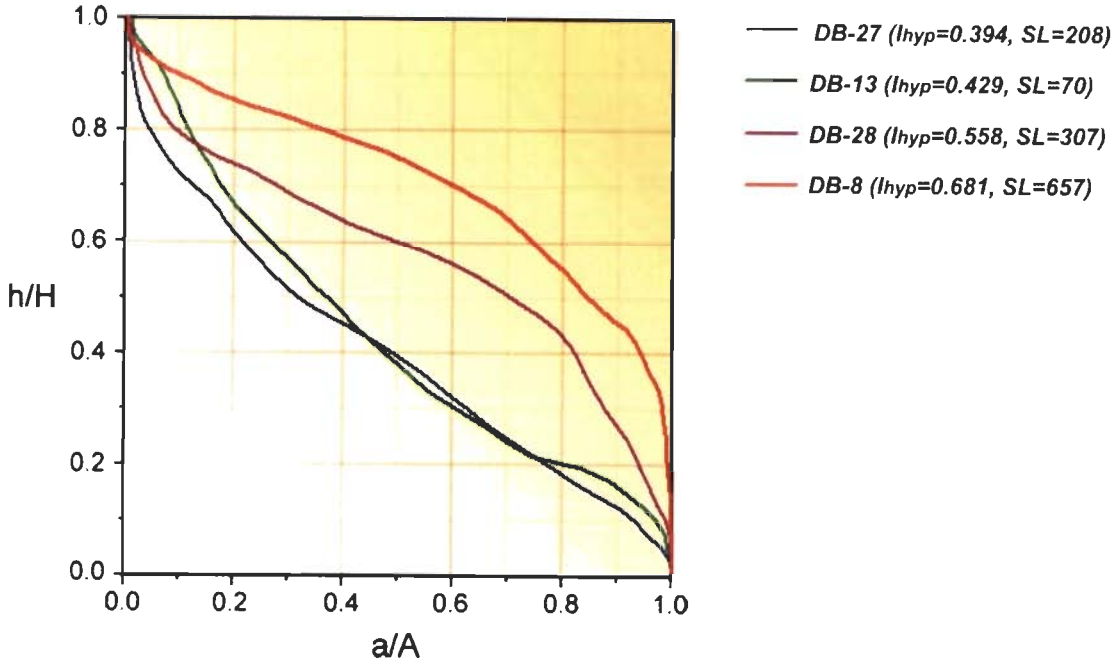

Figure 7.16 Hypsometric curves for all drainage basins falling in MU2.

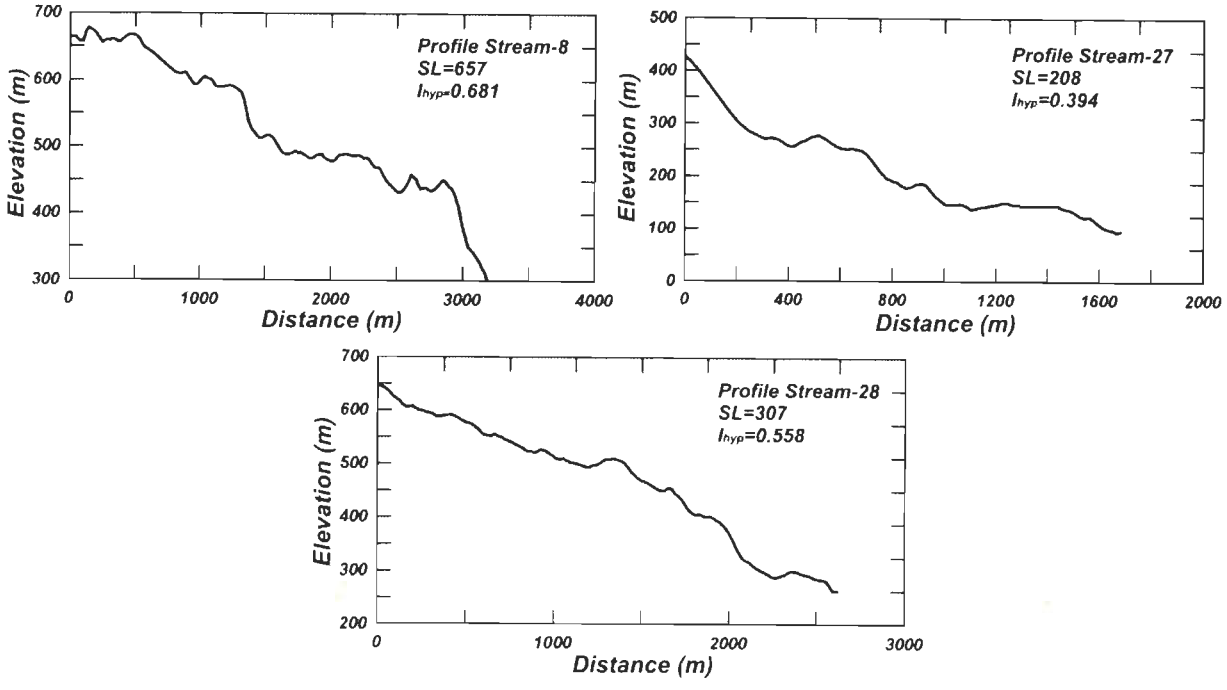

Figure 7.17 Profiles of stream with anomalous behavior in MU2.

The differences between the western and eastern Bhuban Hills slope hypsometric curves corroborates with the main tectonic setting that is exhibited by the anticlinal ridge. These observations support that western and eastern slopes of the Bhuban Hills i.e. MU2 and MU3 are both geomorphologically and tectonically very different from each other. Convex upward nature of hypsometric curves on the western slope indicates upliftment stage due to the tectonic activity along the longitudinal reverse fault LF1. The eastern slope reveals concave patterns in most of the hypsometric curves due to basin degradation induced by erosional processes coupled with tectonic subsidence (Figure 7.18). All the basins show low to moderate values of both I_{hyp} and SL index. Relatively higher value of I_{hyp} is reported from DB-3 and 32 which exhibits very low curvature and lies near the transverse fault TF-2 at the transition zone from MU3 to MU4.

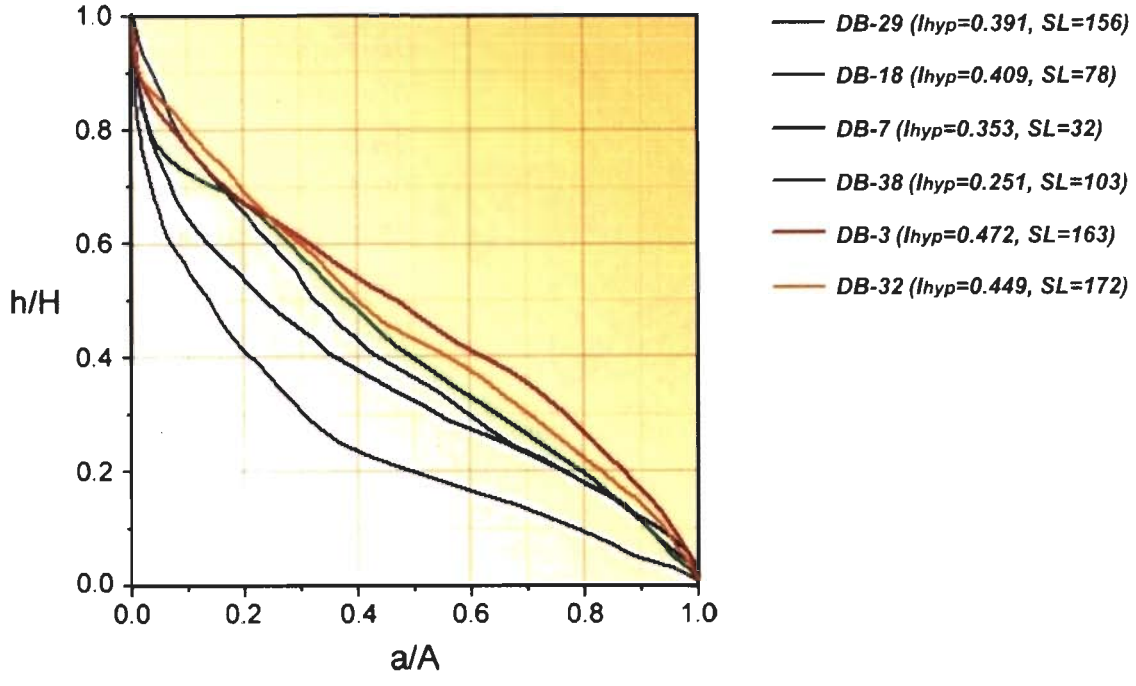

Figure 7.18 Hypsometric curves for all drainage basins falling in MU3.

Morphotectonic unit MU4 is bounded by the transverse faults from both the ends and is recognized as uplifted block. Unlike MU2 and MU3, it exhibits normal anticlinal topography which is also revealed by the transverse profiles as well as from calculated

morphometric indices. Maximum hypsometric integral (0.53) is reported in DB-2 which falls at the transition zone between MU3 and MU4 and upliftment is evident from the hypsometric curve (Figure 7.19). A few stream profiles shows concave nature (Figure 7.20) corroborating high rate of degradation with anomalous drop in stream gradient which lies near the transverse fault TF-2. All other drainage basins represent moderate I_{hyp} values. Interestingly in this unit despite of moderate I_{hyp} values very high SL values has been reported. Except DB-1 (SL=191), all the drainage basins shows the SL values greater than 200, which represents that tectonic forces remained dominant and drainages are tectonically controlled as all the streams have very high gradient. Consistent higher SL values again seem to support the tectonic upliftment in this unit.

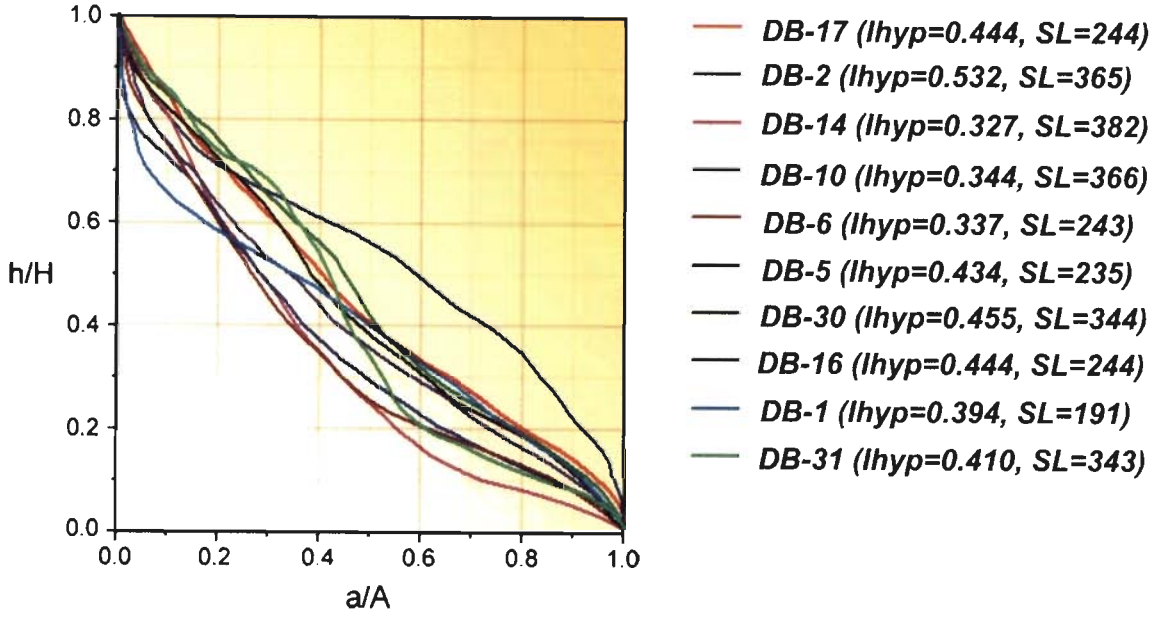

Figure 7.19 Hypsometric curves of the drainage basins falling in the MU4.

Stream profiles are showing the topographic variation in detail (Figure 7.20). Most of the streams show the normal profile of anticlinal topography. Stream-5 shows interesting break in slope and drop of about 200m in upper reaches and then follow the normal downward decreasing trend. This break is actually the indicative of faulting as S-5 falls near the TF-3 at the transition zone between MU4 and MU5. Streams profiles in this

unit are also less varying which are indicative of stream gradient adjustment in response to tectonic activity.

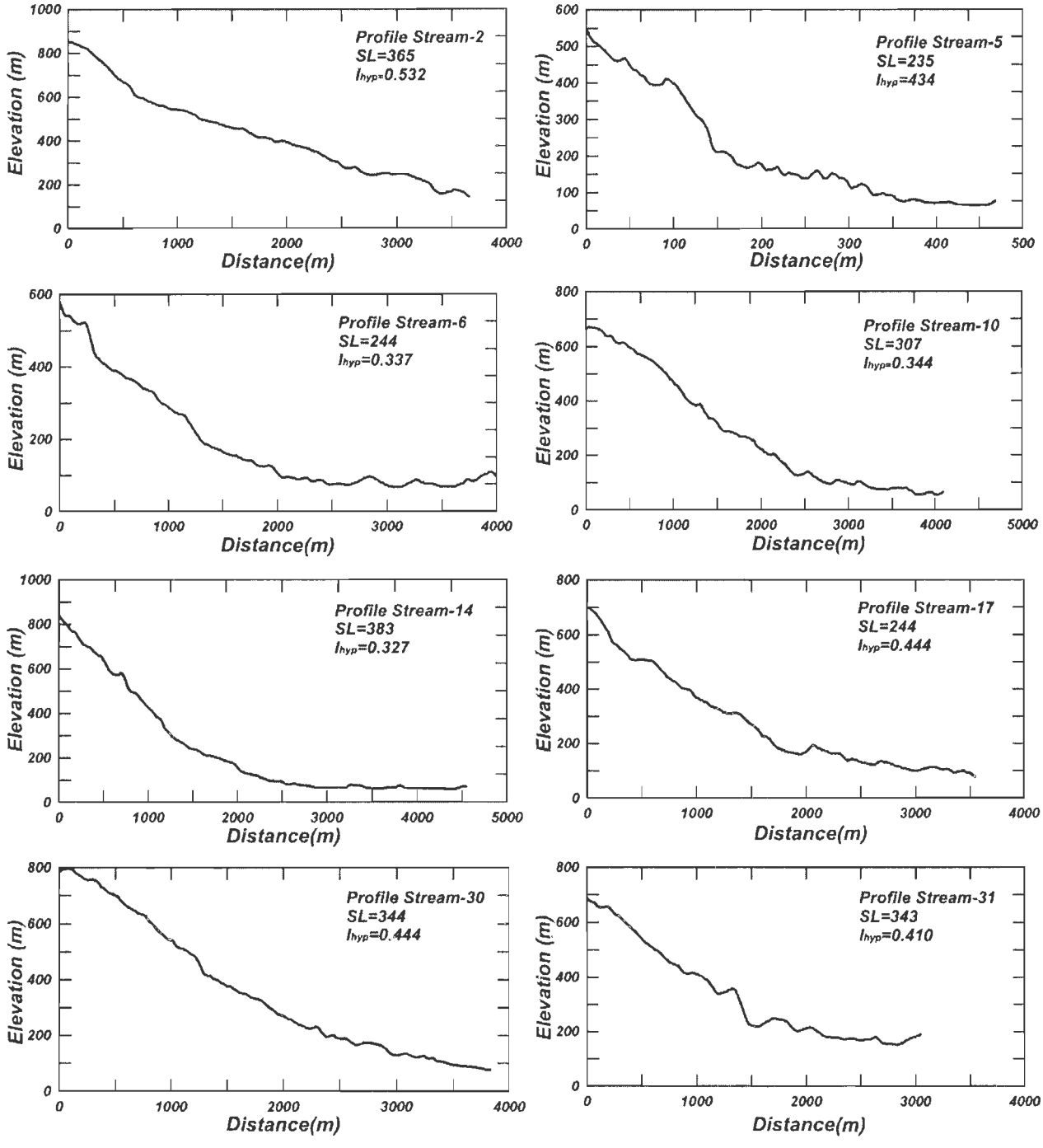

Figure 7.20 Profiles of stream in MU4 with anomalous behavior.

As discussed in section 7.3, the morphotectonic unit MU5 is characterized by subsidence and exhibit relatively lower altitudes. This is also very much evident from the lower values of SL index. Hypsometric integral values are moderate, although curves are deviated from the normal shape and indicate deformation. Drainage basins 12 and 21 give relatively high hypsometric integral because both of these basins actually form part of the smaller and higher ridges of MU6 resulting in higher I_{hyp} value. Incidentally these two basins also falls at the transition zones between MU5 and MU6 near TF-4 leading to topographical variation as also evident from hypsometric curves. Higher I_{hyp} value in DB-33 is the results of active erosion in this region as the curves show convexing in the upper part. All other stream curves are slightly concave in this unit exhibiting dynamic erosion in this region (Figure 7.21). Highly variable and zig-zag stream profiles also support the evidences of active erosion in this unit (Figure 7.22).

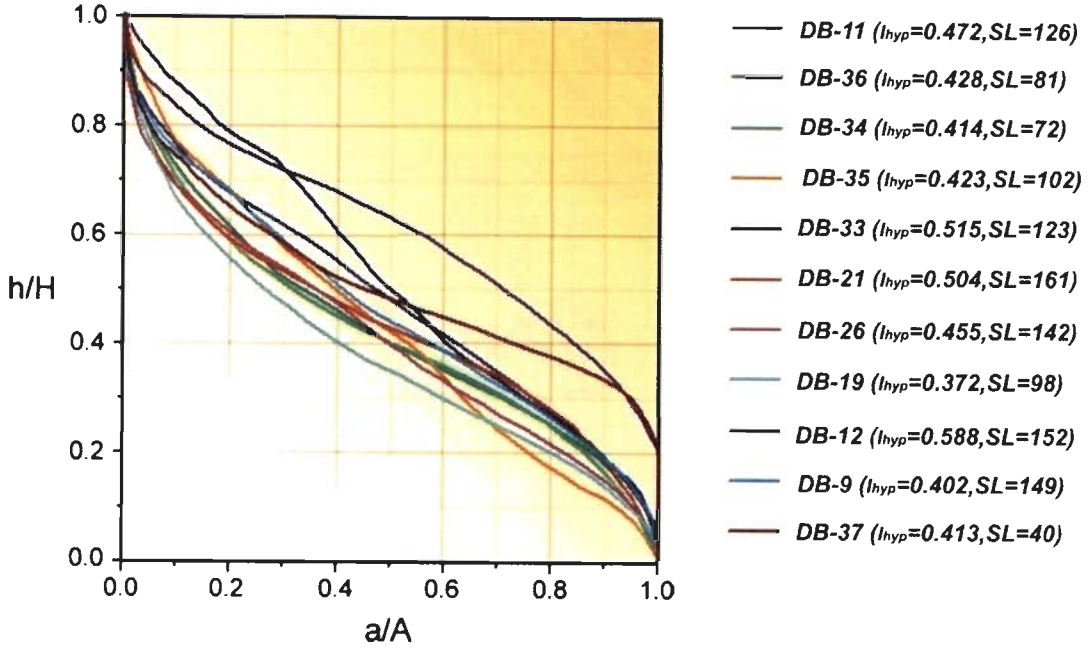

Figure 7.21 Hypsometric curves of the drainage basins lying in the MU5.

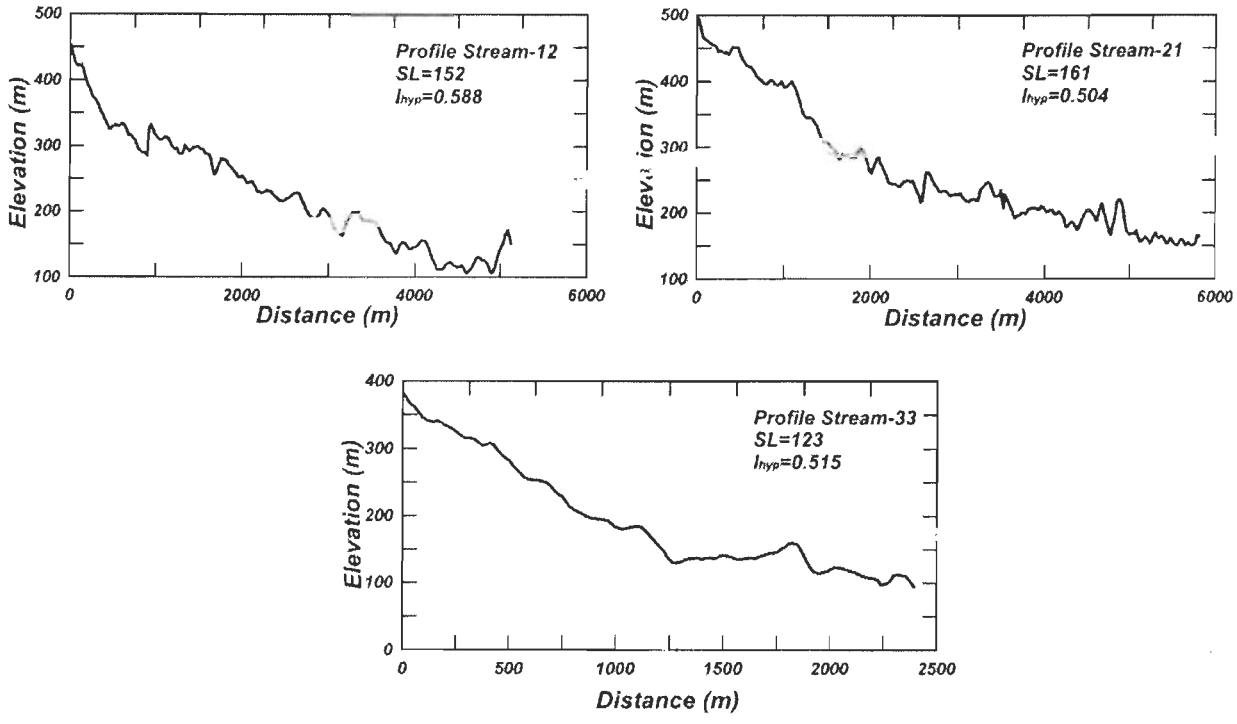

Figure 7.22 Profiles of stream in MU5 with anomalous behavior.

MU6 is the wider part of the Bhuban Hills and bulging topography is exhibited by this unit. It is affected by a number of low magnitude longitudinal faults results into smaller ridge and valley topography as discussed above in section 7.3. In this unit highly variable SL and I_{hyp} values have been reported (Figure 7.23). Lowest SL index is reported from DB-24 lying near one of the longitudinal faults while highest value is shown by DB-4. The drainage basin DB-4 is initiated from one of the uplifted small ridge and slightly convexed upward lower part I_{hyp} curve support tectonic uplift. It can be seen clearly in the stream profile of DB-4 (Figure 7.24). Similarly from I_{hyp} values it is also very much evident that tectonically influenced erosional processes are dominating in MU6. Highest I_{hyp} value (0.52) is reported from the DB-39, a near perfect S-shaped curve of this basin represent the valley erosion while the lowest value (0.29) comes from the DB-20 which shows a concave curve indicating heavy erosion. Relatively lower and moderate values of I_{hyp} and SL index are reported from all other drainage basins of this unit (Figure 7.23). Profiles of streams also shown that in this unit higher I_{hyp} values are results of the high rate of erosion while higher SL index value is mainly the result of intense longitudinal faulting.

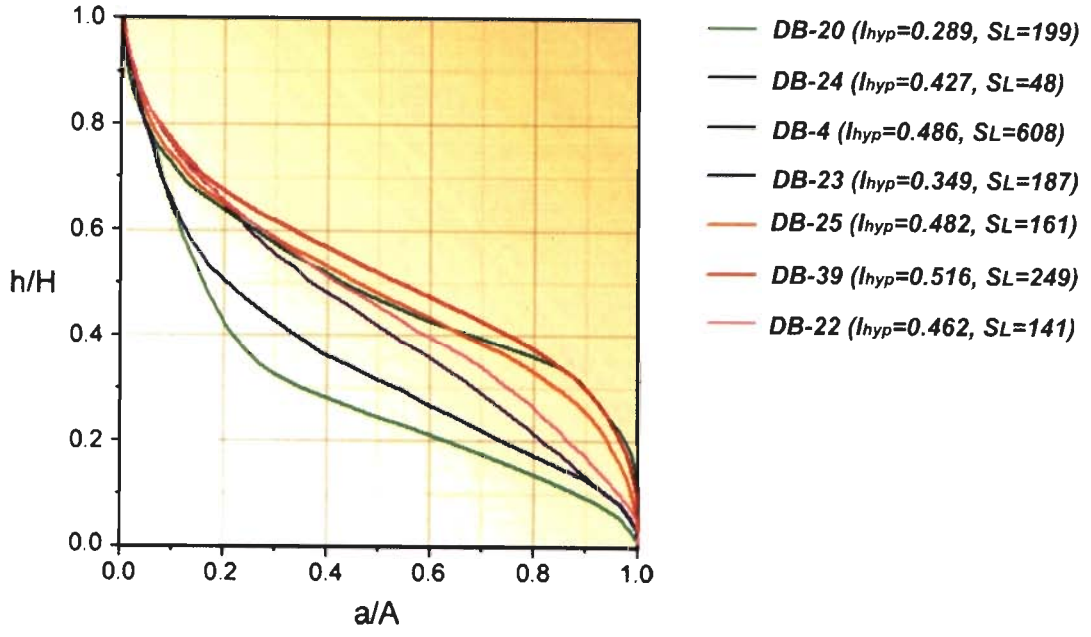

Figure 7.23 Hypsometric curves of the drainage basins falling in MU6.

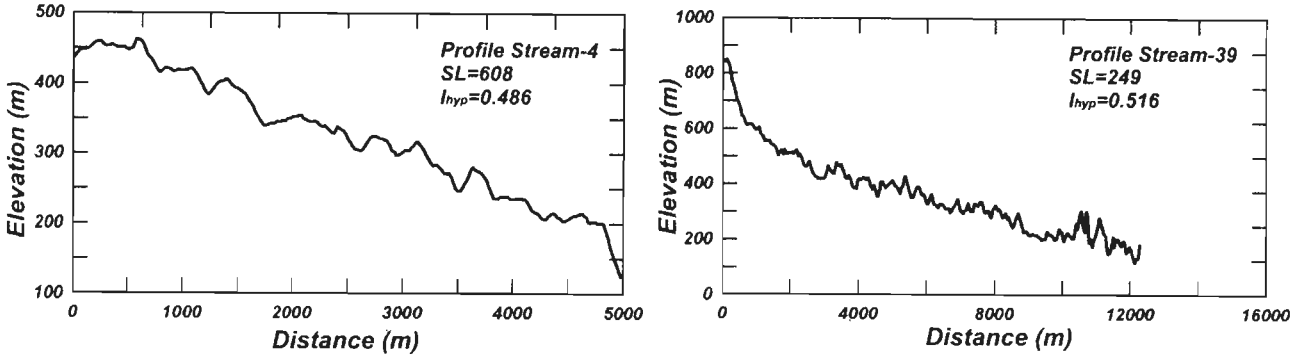

Figure 7.24 Profiles of streams in MU6 with anomalous behavior.

7.7 Results

From the morphotectonic evidences and investigation of geomorphic indices it may be concluded that Bhuban Hills are tectonically deformed. Six different morphotectonic units (MU1, MU2....MU6) could be identified in the region. All the calculated geomorphic indices seem to support upliftment, subsidence and fault propagation folding in the Bhuban Hills. The SL index is roughly related to the stream power and is particularly sensitive to changes in slope and lithology and this sensitivity allows the evaluation of the relationship between possible tectonic activity and rock resistance. This means that values of the index are high in areas where the rocks are significantly resistant or where active tectonics is present. Since constituent rocks of the Bhuban Hills have less strength the outcome of morphometric analysis may be attributed to tectonic activity. Estimated SL values found to be strikingly high or low and may be indicative of neotectonic deformation. Therefore, anomalously high or fluctuated SL values for a terrain made up of rocks of uniform resistance are a possible indicator of active tectonics. The SL variations can be related mainly to a differential uplift or subsidence and are independent of differential erosion. Hypsometry has been shown to be sensitive to different forcing factors in landscape building. Hypsometric curves are deviated from normal s-shaped morphology indicating mixed response in Bhuban Hills. It is also one of the robust morphometric parameters against varying DEM resolution. The scale dependence of hypsometry supports the results that this geomorphic parameter is very sensitive to the processes involved in landscaping, forcing factors that control elevations within a basin (such as tectonics), erosional processes (such as climate and drainage area) and topographic variations.

CHAPTER-VIII

Summary and Conclusions

Morphotectonics of any region can be defined as the impact of tectonic activities on the landforms evolution. Landform developments in tectonically affected areas are attributed to the complex integration of endogenetic (tectonic) and exogenetic (surface) processes. Regional scale tectonic plate motions results in both vertical and horizontal subsurface crustal deformation due to folding, faulting and thrusting and subsequent erosion and deposition on the surface. The relationship between geological structure and landscape, which has always remained important in geomorphology attracted increased interest during recent decades.

Morphotectonic evolution of a region can be investigated with substantial accuracy employing advanced geoinformatic approach as well as the latest morphotectonic and morphometric methodologies. Satellite image provides a synoptic view and therefore is very useful in understanding regional tectonics of a region as well as minor structural features using higher resolution satellite data. Digital Elevation Models (DEMs) are widely used product for characterizing the terrain parameters. Availability of high resolution DEMs enabled detailed information of topographic derivatives with greater efficiency. In the present work topographic maps (1955 and 1972), satellite data (Landsat-MSS, TM & ETM+, IRS LISS-III & PAN and Cartosat-1 spanning from 1975 to 2006) and DEMs (Contour, Cartosat, SRTM and ASTER) were brought into use for the extraction of various morphotectonic and morphometric parameters. This extensive data set and its handling, processing, analysis, important morphological parameter extraction and presentation by employing ArcGIS and ERDAS-Imagine software shaped up a realm of geoinformatics.

This research work focuses on study of various structural features, detailed morphotectonic and morphometric characteristics for select locales in the frontal part of Indo-Burman fold belt comprising Surma Basin. Indo-Burman frontal fold belt which is one of the most tectonically active regions of the world lies in the northeastern part of India. Whole fold belt is deformed into a series of north-south trending fold ridges formed due to east-west oriented tectonic forces owing to the eastward subduction of the Indian Plate beneath the Burmese Plate. The complexity and intensity of folded strata increases eastward towards the leading edge of subducting plate. The Surma Basin consists of a repetitive succession of mainly Neogene arenaceous and argillaceous sediments, known as rhythmites, with thinning upward sequence. The rhythmites of marine origin were followed later by continental type fluvial deposits of Dupitila and Quaternary-Recent river deposits in the topographic and structural lows. In general, the sediments in the Surma Basin are mainly of Miocene-Pleistocene age.

The major objective of this work is to investigate the effect of neotectonic deformation of geological structures as well as the recent tectonic scenario on the basis of fold pattern, river/drainage anomalies, topographic and morphometric indices employing geoinformatics. A large scale morphotectonic analysis of the study area could be most useful approach for producing the required basic neotectonic information extracted using satellite data and DEMs. All morphological features such as unique fold geometries, faulting in anticlines, river channel anomalies, fault propagation folding etc. that could be considered as surface manifestations of tectonics are identified and mapped. Cases of fault propagation folding have been identified in the Bhuban, Rengte, Chatachara and Serkhan anticlines.

Fold ridges of the Indo-Burman frontal belt although appear to be simple, but actually they exhibit interesting morphology. For the purpose of enhancing the morphological characteristics, image processing techniques such as image fusion and principal component analysis have been applied. The doubly plunging fold ridges not only show varied sizes and shapes but also exhibit numerous kinds of folding patterns. Occurrence of anticlinal plunging co-noses can be seen at the southernmost tip of the Atharamura anticline near Bandarban area. Bulging along the western limb of the Baramura and

Langtarat anticline occurred due to growth faulting. Intricately overlapped folds pattern are seen to have formed at a few places and a fork like structure developed due to diagonal displacement along the faulted western limb of the Jampai and nearly placed Bakhan anticlines. Other interesting features are cuspate and elliptical valleys that developed due to anticlinal bifurcation and reunion exhibited by the Jampai anticline.

In an active region rivers response to prevailing tectonic activities remain recorded as the rivers and streams adjust their course with topographic slope and tilting due to tectonic deformation. In the study area several cases of river crossing the anticlinal ridges through the faulted part have been observed. Barak, a major river of the Surma Basin takes a hair pin bend near Tipaimukh by changing its southward flow into northward flow and also crosses two anticlinal ridges at two locations. Also, the other rivers viz., Tlabung, Deo, Gomti and Dhaleshwari also cross several anticlinal ridges at various places.

The Barak which flows from east to west is highly meandering and changed its course several times. The Barak river along with its major tributaries were investigated for their responses to the neotectonic activities prevailing in the area. A change detection analysis of the Barak river including branched out Surma and Kushiara rivers has been carried out using the topographic maps and satellite data of different years from 1955 to 2000. Remarkable shift in the river channel including loop cut-off and neck cut-off could be identified in seven blocks. In the easternmost part, the Barak river has shifted northward for about 3.7km as indicated by the presence of abandoned channel. Similarly, in the downstream part, in block-3 the river has shifted northward for about 2.4km. Barak river exhibits a prominent neck cut-off reported to have occurred on 16-10-1992 in block-2 resulting in abandoning of river channel on the south.

Barak river has numerous large and small tributaries on its northern and southern bank and the major tributaries viz., Madhura, Dhaleshwari, Jiri, Sonai, Longai are highly active and show intense meandering while flowing through the synclinal valleys. Dhaleshwari and Sonai rivers are greatly affected by the tectonic features like faults and fold ridges. The Dhaleshwari river cut crosses two anticlinal ridges and Sonai river exhibits considerable shift.

All the major synclines were also investigated for revealing the impact of tectonics. Using DEMs, drainage divides and drainage networks were extracted for each synclinal valley. Drainage indices like, asymmetry factor, basin elongation ratio, river sinuosity and bifurcation ratios were calculated for all the synclines of the Indo-Burman frontal fold belt region. It was found that all the rivers are showing either sinuous or meandering paths. Values of asymmetric factor are either lower or higher than 50 and ranges from 46 to 66, indicating that the drainage basins are highly asymmetrical in shape. Similarly high values of basin elongation ratio (10-24) indicate that drainage is also tectonically influenced.

A detailed morphotectonic investigation of the western Tripura region has been carried out using topographic and drainage parameters as the proxy indicator of the tectonics. Intense drainage network has developed on the Agartala slope. The area comprises a gentle westerly sloping area named Agartala slope originating from the Baramura anticlinal ridge. Another anticline located beside the Baramura anticline towards east called as Atharamura anticline along with Khowai and Ampi bazaar synclines were also studied for their associated deformation. The Indo-Burman frontal fold belt forms a topographically high zone from where the terrain slopes down to northward as well as southward. The region appears to have suffered uparching, and this domal high zone creates a drainage divide in the area resulting into southward and northward diversion of stream networks. Major geomorphological features of the area are characterized by the elongated ridges, valleys, flood plains and intense drainage network. Gomti and Khowai are the major rivers and crosses anticlinal ridges at various locations through faulted ridge. Both the rivers are tectonically controlled and also show intense meandering course and left various meandering loops. Similarly, Haora river shows a northward convexing in its course between the Dudhpatil and Agartala regions and has shifted its course northward.

Topographic profiles extracted from SRTM-DEM shows topographic variation along and across the western Tripura region. All the longitudinal profiles demonstrate uparching in the region while transverse profiles show the eastward increase in the elevation of the Agartala region. Values of asymmetric factor (30.9 to 79.8) and transverse topographic symmetry (63-89) indicate that basins are highly asymmetric and therefore tectonically

deformed. Further, consistently high values of basin elongation ratio (2.1 to 24.2) are also indicative of neotectonic activities.

In this study, DEMs have been used extensively and is considered as an important product. Therefore, a detailed analysis of the applicability of the DEMs has also been investigated. For that purpose two DEMs (one from topographic contours and the other from the Cartosat stereo orthokit data) have been generated for the Bhuban Hills with spatial resolution of 20m. Generation of DEM from topographic contours pose problem in the areas having widely spaced contours and of course dependant on contour intervals. On the other hand DEM generated from satellite data has the capability to resolve slight elevation differences. Both accuracy and quality comparison were made using various topographic and drainage derivatives. Vertical accuracy and horizontal discrepancies have been calculated using spot heights, elevation test points and stream displacement as proxy indicators. A detailed comparative analysis has been carried out by extracting the stream networks and basin boundaries deviations. Topographic parameters like slope, aspect, and topographic index were also derived.

Contour and Cartosat-DEMs were also compared with the available (in public domain) SRTM and ASTER DEMs for the Bhuban Hills area. DEM extracted parameters demonstrated that Cartosat-DEM generates highest vertical accuracy followed by contour, SRTM and ASTER DEMs. In case of horizontal accuracy, except SRTM all the DEMs show near similar results. Topographic derivatives exhibit considerable variation with spatial resolution of DEM. Although for drainage parameters estimation DEM accuracy is relatively more important, except for drainage density which is more resolution dependant. Despite coarse resolution SRTM provided good results for regional analysis but for detailed analysis high resolution DEM may be preferred.

Morphotectonic study of the Bhuban anticlinal hills has also been carried out using DEMs and satellite data. Bhuban Hills is located in northeastern part of the study area and is intensely faulted and shows various tectonic segments. On the basis of deformational pattern six morphotectonic units could be identified in the Bhuban anticlinal hills on the satellite images and DEMs. Towards the north, three units have been

demarcated. All the units are bounded by various transverse faults. MU1 is a detached part and located at the northern most side. MU2 and MU3 are the western and eastern sides of the Bhuban Hills. MU2 is characterized by the sharp and steep scarp, while MU3 exhibits a gently sloping surface. MU4 is bounded by the transverse faults from both the ends and is the uplifted unit. Whereas, MU5 is the subsided block and exhibits intense erosional activity. MU6 shows bulging topography resulted due to the presence of various longitudinal fault zones in this area. Most prominent case of fault propagation folding could be recognized from the Bhuban Hills. All the morphometric indices viz., stream length gradient index (SL-Index), slope gradient index (S-index) and hypsometric integral also seems to support the above morphotectonic evidences.

Lengpui area (near Aizwal) shows deviation from the normal synclinal valley topography. The region is marked by relatively large gentle slopes as exhibited by the continuous smooth feature on the satellite data and DEM. Dhaleshwari river (a major tributary of the Barak) is the main river of this region which is in its youthful stage and actively incising the valley floor resulting into the formation of the steep sided V-shaped valley as it is also corroborated by topographic profiles. The area show anomalous slope variation and drainage is also showing deviated patterns. Morphometric indices support the evidences of tectonic constraints on the drainage of the area and valley erosion processes.

Conclusions

This research work is the first report of spatial technology based detailed morphotectonic and morphometric investigations of the Indo-Burman frontal fold belt encompassing Surma Basin. Significant outcomes which could be achieved from this endeavor are:

- Various fold patterns have been identified on the satellite images and more representative view of the deformed anticlines were generated employing enhancement techniques like image fusion and principal component analysis. Instances of enechelon folding observed in a few places. Baramura and Langtarat anticlines show bulging topography due to the effect of faulting in the fold limbs. Cases

of fold bifurcation, cuspate and elliptical valley formation are recorded from the Jampai anticline near Tuibangadam area. Cuspate and elliptical structures could have developed due to fault propagation folding and associated deformation.

- The Barak river exhibits various instances of channel shifts, abandoned loops and neck cutoff. Most prominent northward shift occurred in eastern most side wherein very recent shift also could be noticed. This and general northward shift of the river in eastern part seems to be attributed to the seismic activity. All the tributaries of the Barak river follow highly meandering courses and shifting of channels including a tributary crossing anticlinal ridges at two places.

- Morphometric analysis of all the major synclines demonstrates that the drainage of the Surma Basin is tectonically controlled. Drainage basins are highly asymmetrical and very intense drainage has developed. Trunk streams of various synclinal valleys show very high sinuosity and meandering course, which is indicative of youthful and active river channels. Various stream anomalies like sudden change in flow direction, increase in meandering intensity, straightened courses, channel incision, were delineated from the satellite data.

- Morphotectonic study of the western Tripura region comprising Agartala slope anticlines and synclinal valleys indicate that the area has suffered from the uparching and the drainage is tectonically influenced. Both Gomti and Khowai rivers are highly meandering exhibiting loop abandoning and cross the anticlines (Baramura and Atharamura) at different locations through faulted ridges. Similarly Haora river also shifted its course northward on the Agartala slope.

- Lengpui region located close to Aizwal shows an anomalous topographic expression on the satellite images and DEMs from the surrounding area. This area is marked by very large and nearly flat slope surfaces generating a unique appearance. The Dhaleshwari river of this area is actively incising forming a steep sided V-shaped valley. SL and S-Index values show abrupt increase at the points near the valley

where the slope is very steep. Higher values of the I_{hyp} are perhaps the effect of the intense valley erosion and tilting.

- Generation of DEMs formed an important component of this work. It provided a detailed knowledge about the advantages and shortcomings of the various DEMs. Comparative analysis of Contour, Cartosat, SRTM and ASTER-DEMs, indicated that the Cartosat-DEM is best among all. It provided greater accuracy and quality followed by Contour, SRTM and ASTER-DEMs. Cartosat-DEM facilitated extraction of topographic and drainage indices in greater details with least errors and discrepancies and therefore is more reliable in drainage and hydrological related studies.

- In case of Bhuban anticlinal hills six different morphotectonic units could be demarcated. Three most distinct units are the northernmost (MU2) exhibiting steep western slope; in the middle portion (MU5) undergone subsidence and the southern part (MU6) suffered bulging. Both the northern and southern parts exhibit fault propagation folding with high prominence in the northern part. Morphometric properties also support all the findings. SL-Index values > 200 in several cases indicate that neotectonic activities are prevailing in the region. Further, consistently high S-Index and I_{hyp} values also suggest that Bhuban anticlinal hills are highly deformed and upliftment, subsidence, and active erosion occurred in the various units.

Future scope of the work

The present research provides a detailed description about the applications of integrated remote sensing and GIS techniques for the morphotectonic studies. The morphotectonic and morphometric study of this area has been implemented for the first time and therefore, it provides the sound base for the future research in other tectonically active areas. The results of this research can also be used as a preliminary data for the geotectonic hazard assessments in the Indo-Burman fold region. The enumerated procedure of the morphotectonic investigation can become useful guidelines for the areas which are still unexplored.

BIBLIOGRAPHY

1. Ahnert, F., 1973, COSLOPE 2- A comprehensive model program for simulating slope profile development. Geocommunication Programs, 8, 99-119, London.

2. Alavi, M., 2004, Regional stratigraphy of the zagros fold-thrust belt of iran and its proforeland evolution. American Journal of Science, 304, 1–20.

3. Anbazhagan, S., and Archana, M. Nair, 2004, Geographic Information System and groundwater quality mapping in Panvel basin, Maharashtra, India. Environmental Geology, International Journal of Geosciences. Online publication DOI.10.1007/s00254-003-0932-9.

4. Anbazhagan, S., Ramasamy, S.M. and Dasgupta, S., 2004, Remote sensing and GIS artificial recharge study, runoff estimation and planning in Ayyar basin, Tamil Nadu, India. Environmental Geology, 48(2), 158-170, DOI: 10.1007/s00254-005-1284-4.

5. Anderson, R. C. and Beratan K. K., 1994, Identify characteristics of geomorphologic surfaces, Whipple Mountains, Southeastern California. Geological Society of America Abstracts with Programs, 26, 34-35.

6. Anderson, R. C. and Beratan K. K., 1993, Identification of geomorphic surfaces from Landsat data, Whipple Mountains, Southeastern California. Geological Society of America Abstracts with Programs, 25, A-106.

7. Anhert, F., 1984, Local relief and height limit of mountain ranges. American Journal of Science, 284, 1035-1055.

8. Aronoff, S., 1989, Geographic Information Systems: A Management Perspective (Ottawa: WDL Publications), p294.

9. ASTER-GDEM, 2009, available online at: http://www.gdem.aster. ersdac.or.jp /search.jsp (accessed on 10 March 2009).

10. Avena, G.C., Giuliano G. and Lupia Palmieri, E., 1967, On the quantitative assessment of hierarchy and evolution of river networks. Bulletin of the Italian Geological Society, 86, 781-796.

11. Avouac, J. P. and Peltzer, G., 1993, Active tectonics and southern Xinjiang, China: analysis of terrace riser and normal fault scarp degradation along the Hotan-Qira fault system. Journal of Geophysical Research, 98, 21773-21807.

12. Bammler, R., 1999, The SRTM Mission: A World-Wide 30m-Resolution DEM from SAR Interferometry in 11 days. Photogrammetric Week 1999, Stuttgart.

13. Batten, P., 1999, Landscape mapping: the development of a new methodology. BSc. (Hons.) Research Thesis, Department of Physical Geography, Macquarie University, Australia.

14. Beanland, S., and Clark, M.M., 1994, The Owens Valley fault zone, eastern California, and surface faulting associated with the1872 earthquake. U.S. Geological Survey Bulletin, 1982, 29.

15. Belisario, F., Del Monte, M., Fredi, P., Funiciello, R., Lupia Palmieri, E. and Salvini F., 1999, Azimuthal analysis of stream orientations to define regional tectonic lines. Zeitschrift fur Geomorphologie N.F ., Suppl.Bd. 118, 41-63

16. Beratan, K. K. and Anderson, R., 1998, The use of Landsat Thematic Mapper data for mapping and correlation of Quaternary geomorphic surfaces in the Southern Whipple Mountains, California. International Journal of Remote sensing, 19 (12), 2345-2359.

17. Beven, K. J., 1985, Distributed Models, Hydrological Forecasting, John Wiley & Sons Ltd.

18. Beven, K. and Kirkby, M.J., 1979, A physically based variable contributing area model of basin hydrology. Hydrol. Sci. Bull. 24, 43–69.

19. Bhatt, C.M., Chopra, R. and Sharma, P.K., 2007, Morphotectonic analysis in Anandpur Sahib area, Punjab (India) using remote sensing and GIS approach. J. Indian Society of Remote Sensing, 35 (2), 129-139.

20. Bhatt, A. and Bisht, M. P. S., 2010, Landslide hazard spatial analysis and prediction using GIS in the Balkhila watershed (Garhwal Himalaya), Mountain Resources Management (Application of Remote Sensing and GIS), (Eds) M. P. S. Bisht and D. Pal, Transmedia Publication, Srinagar (Garhwal), 160–166.

21. Bisht, M. P. S., Mehta, M., Nautiyal, S. K., Rana, V., 2010, Application of RS and GIS in the Natural Resources Management – a case study of Nanda Devi Biosphere Reserve, Central Himalaya. Published in Mountain Resource Management (Application of Remote Sensing and GIS), (Eds) M. P. S. Bisht and D. Pal Transmedia Publication, Srinagar (Garhwal), 98 – 101.

22. Bisht, M. P. S., Bhatt A., Champatiray, P. K., 2009, Landslide Hazard Zonation using information value method in Balkhila watershed (Garhwal Himalaya), GEOMATICS 2009, National Conference on Geomatics and Impact of climate change with specific reference to Mountain Ecosystem 4 – 6 February 2009, Dehradun.

23. Biswas, S. and Dasgupta, A., 1986, Some observations on the mechanism of earthquakes in the Himalaya and the Burmese arc. Tectonophysics, 122, 325-343.

24. Bitelli, G., Carrara, A. and Vittuari, L., 1996, Comparison of DTMs derived from contour lines and digital photogrammetry. In Reports on Surveying and Geodesy, edited by M. Unguendoli, (Nautilus, Bologna: DISTART), 159-179.

25. Bitelli, G., Carrara, A., de Torres Curth, M. S. and Folloni, G., 1993, Topographical database for EFEDA GIS, Echival Field Experiment in a Desertification-Threatened Area (EFEDA). Annex to Final Report, FU Berlin, Berlin.

26. Brookes, A., 1987, River channel adjustments downstream from channelization works in England and Wales. Earth Surface Processes and Landforms, 12, 337–351.

27. Brookfield, M.E., 1998, The evolution of the great river systems of southern Asia during the Cenozoic India–Asia Collision Rivers draining southwards, Geomorphology, 22, 285–312.

28. Brunnschweiler, R. O., 1966, On the geology of the Indo-Burman ranges. J. Geol. Soc. Aust., 13, 137-194.

29. Budai, T., Csaszar, G., Csillag, G., Dudko, A., Koloszar, L., and Majoros, G., 1999, Geology of the Balaton Highland, Geological Institute of Hungary, Budapest (in Hungarian with English summary).

30. Bull, W. B., 1977, Tectonic geomorphology of the Mojave Desert. U.S. Geol. Surv. Contract Rep. 14-08-001-G-394, Office of Earthquakes, Volcanoes and Engineering, Menlo Park, Calif., 188.

31. Bull, W. B., 1978, Geomorphic tectonic activity classes of the south front of the San Gabriel Mountains, California. U.S. Geol. Surv. Contract Rep. 14-08-001-G-394, Office of Earthquakes, Volcanoes and Engineering, Menlo Park, Calif., 59.

32. Bull, W. B. and McFadden, L. D., 1977, Tectonic geomorphology north and south of the Garlock fault, California. Geomorphology in Arid Regions, Proc. 8th Ann. Geomorph. Symp., (Ed) Doehring, D. O., State Univ. of New York at Binghamton, 115–138.

33. Bull, W. B., 1964, Geomorphology of segmented alluvial fans in western Fresno County, California. U. S. Geological Survey Professional Paper 352-E, 89-129.

34. Bull, W.B. and Mc Fadden, L. M., 1997, Tectonic geomorphology north and south of the Garlock Fault, California. Journal of Geomorphology, 1, 15-32.

35. Bull, W.B., 1979, Threshold of critical power in streams. Geological Society of America Bulletin 90, 453–464.

36. Bull, W.B., 1991, Geomorphic Responses to Climate Change. Oxford Univ. Press, Oxford, UK.

37. Buonasorte, G., Ciccacci S., De Rita, D., Fredi P. and Lupia Palmieri, E., 1991, Some relations between morphological characteristics and geological structure in the Vulsini Volcanic Complex (Northern Latium, Italy). Zeitschrift fur Géomorphologie N.F, Suppl. Bd. 82, 59-71.

38. Burbank, D. W. and Pinter, N., 1999, Landscape evolution: the interactions of tectonics and surface processes. *Basin Research*, 11(1), 1 – 6.

39. Burbank, D. W., and Anderson, R. S., 2001, Tectonic Geomorphology. Blackwell Science, Cambridge, p274.

40. Burbank, D. W., Meigs, A., and Brozovic, N., 1996, Interactions of growing folds and coeval depositional systems. Basin Research 8, 199–223.

41. Burbank, D.W., 1992, Causes of recent Himalayan uplift deduced from deposited partterns in the Ganges basin. Nature, 357, 680-682.

42. Burbank, D.W., Leland, J., Fielding, E., Anderson, R. S., Brozovic, N., Reid, M. R. and Duncan, C., 1996, Bedrock incision, rock uplift and threshold hillslopes in the north-western Himalayas. Nature, 379, 505-510.

43. Burnett, A. W., and Schumm, S. A., 1983, Alluvial-river response to neotectonic deformation in Louisiana and Mississippi. Science, 22 (4169), 49–50.

44. Burrough, P. A., 1986, Principles of Geographical Information Systems for Land Resources Assessment (Oxford: Clarendon Press).

45. Burrough, P.A., McDonnell, R.A., 1998, Principles of Geographical Information Systems. Oxford University Press, New York. 333 pp.

46. Büyüksalih, G. and Jacobson, K., 2008, Digital heights model in Mountainous regions based on Space Information. EARSel Workshop, Remote Sensing- New Challenges of High Resolution, Bochum 2008.

47. Büyüksalih, G., Kocak, M.G., Oruc, M., Akcin, H. and Jacobsen, K, 2003, Handling of IKONOS-images from Orientation up to DEM Generation, Joint Workshop "High Resolution Mapping from Space 2003". Hannover 03– see alsohttp://www.ipi.uni-hannover.

48. Byrd, J.O.D., Smith, R.B. and Geissman, J.W., 1994, The Teton fault, Wyoming: neotectonics, and mechanisms of deformation, Journal of Geophysical Research, 99 (B10), 20095–20122.

49. Chediya, O. K., 1986, Morphostructures and neo-tectonics of the Tien Shan, Frunze. Academia Nauk Kyrgyz CCP, 313.

50. Carla, R., Carrara, A. and Federici, G., 1987, Generation of digital terrain models with high precision, Dept. of Civil Engineering Notebooks 0/87, Florence, Evaluating the quality of DTMs, 473.

51. Carrara, A., 1988, Drainage and divide networks derived from high fidelity digital terrain models. In Quantitative Analysis of Mineral and Energy Resources, edited by C.F. Chung, A.G. Fabbri and P. Larsen (Dordrecht: NATO-ASI Series, D. Reidel Pub. Co.), 581-597.

52. Carrara, A., 1994, Comparative analysis of methods for generating digital terrain models, Spa-Insiel Province of Trento, Technical Report, Udine.

53. Carrara, A., Bitelli, G. and Carla, R., 1997, "Comparison of techniques for generating digital terrain models from contour lines". International Journal of Geographical Information Science, 11 (5), 451-473.

54. Carrara, A., Cardinali, M., Guzzetti, F. and Reichenback, P., 1995, GIS technology in mapping landside hazard. Geographical Information Systems in Assessing Natural Hazards, edited by A. Carrara and F. Guzzetti (Dordrecht: Kluwer Publishing Co.), 135-176.

55. Carrara, A., Carla', R., De Fent, I. and Giovannini, F., 1996, Comparative analysis of techniques for generating digital terrain models. Italian Journal of Remote Sensing, 6, 19-30.

56. Cartier, K., Alt, D., 1982, The bewildering Bitterroot, the river that won't behave. Montana Magazine, 12, 52-53.

57. Centamore, E., Ciccacci, S., Del Monte, M., Fredi P., and Lupia Palmieri E., 1996, Morphological and morphometric approach to the study of the structural arrangement of the North-Eastern Abruzzo (Central Italy). Geomorphology, 16, 127-137.

58. CGIAR-CSI (Consultative Group on International Agricultural Research and Consortium for Spatial Information), 2009, available online at: http://srtm.csi.cgiar.org/ (accessed on 15 March 2009).

59. Champel, B., Vander Beek, P., Mugnier, J. L., and Leturmy, P., 2002, Growth and lateral propagation of fault related folds in the Siwaliks of western Nepal: rates, mechanism, and geomorphic signature. Journal of Geophysical Research, 107 (B6), doi: 10.1029/2001JB000578.

60. Chandra, U., 1975, Seismicity, earthquake mechanisms and tectonics of Burma, 20°N-28° N. Geophys. J.R. Astron. Soc., 40, 367-381.

61. Chang, H.H., 1979, Minimum stream power and river channel patterns. Journal of Hydrology, 41, 303– 327.

62. Chang, H.H., 1980, Geometry of gravel streams. Journal of Hydraulic Division, ASCE 106, 1443– 1456.

63. Chappell, J., 1974, Geology of coral terraces, Huon Peninsula, New Guinea: A study of Quaternary tectonic movements and sea-level changes. Geological Society of America, 85, 553-570.

64. Chavez, P.S., Sides, S.C. and Anderson, J.A., 1991, Comparison of three different methods to merge multi resolution and multi spectral data: Landsat TM and SPOT panchromatic. Photogrammetric Engineering and Remote Sensing, 57, 295-303.

65. Chen, W. P. and Molnar, P., 1990, Source parameters of earthquakes and intraplate deformation beneath the Shillong plateau and the northern Indo-burman ranges. J. Geophys. Res., 95, 12527-12552.

66. Chen, Y.C., Sung, Q.C. and Cheng, K.Y., 2003, Along-strike variations of morphotectonic features in the western foothills of Taiwan: tectonic implications based on stream gradient and hypsometric analysis. Geomorphology, 56, 109–137.

67. Chiang, C. S., and Yu, H. S., 2006, Morphotectonics and incision of the Kaoping submarine canyon, SW Taiwan orogenic wedge. Geomorphology, 80,199–213.

68. Chorowicz, J., Collet, B., Bonavia, F. F., Mohr, P., Parrot, J. F., and Korme, T., 1998, The Tana Basin, Ethiopia: intra-plateau uplift, rifting and subsidence. Tectonophysics, 295, 351-367.

69. Chorowicz, J., Dhonte, D. and Gundogdu, N., 1999, Neotectonics in the eastern North Anatolian Fault region (Turkey) advocates crustal extension: mapping from SAR ERS imagery and Digital Elevation Model. Journal of Structural Geology, 21, 511-532.

70. Chorowicz, J., Kim, J., Manoussis, S., Rudant, J., Foin, P. and Veillet, I., 1989, A new technique for recognition of geological and geomorphological patterns in Digital terrain models. Remote Sensing Environ. 29, 229–239.

71. Chorowicz, J., Parrot, J. and Taud, H., 1995, Automated pattern recognition of geomorphic features from DEMs and satellite images. Journal of Geomorphology, Supplementary Band, 101, 69-84.

72. Chrowicz, J, Breard, J., Guillande, R., Moraase, C., Prudon, D. and Rudant, J., 1991, Dip and strike measured systematically on digitized three dimensional geological map. Photogrammetric Engineering and Remote Sensing, 57, 431-436.

73. Ciccacci, S., Fredi, P., Lupia Palmieri. E. and Salvini, F., 1986, An approach to the quantitative analysis of the relations between drainage pattern and fracture trend. International Geomorphology, 2, 49-68.

74. Clark, C.D., and Wilson, C., 1994, Spatial analysis of lineaments. Comput. Geosci. 20, 1237–1258.

75. Clarke, A. L., Gruen, A. and Loon, J. C., 1982, The application of contour data for generating high fidelity grid digital elevation models. In Proceedings of AutoCarto, (Falls Church: American Congress on Surveying and Mapping), 381- 400

76. Clich, G., Bonn, F., and Teillet, P., 1985, Integration of the SPOT Pan channel into its multispectral mode for image sharpness enhancement. Photogrammetric Engineering and Remote Sensing, 51, 311-316.

77. Collen, J. D. and Vella, P., 1984, Hautotara, Te Muna and Ahiaruhe Formations, middle to late Pleistocene, Wairarapa, New Zealand. Journal of the Royal Society of New Zealand, 14, 296–317.

78. Collet, B., Taud, H., Parrot, J.F., Bonavia, F. and Chorowicz, J., 2000, A new kinematic approach for the Danakil block using a Digital Elevation Model representation. Tectonophysics, 316, 343–357.

79. Colman-Sadd, S.P., 1978, Fold development in Zagros simply folded belt, Southwest Iran. American Association of Petroleum Geologists Bulletin, 62, 984–1003.

80. Cong, D. Ch. and Feigl, K. L., 1999, Geodetic measurement of horizontal strain across the Red River fault near Thac Ba, Vietnam 1963–1994. J. Geod., 73, 298–310.

81. Cotilla, M. O., Córdoba D. and Calzadilla M., 2007, Morphotectonic Study of Hispaniola. Geotectonics, 2007, 41 (5) 368–391.

82. Cotilla, M. O. and Cordoba, D., 2004, Morphotectonics of the Iberian Peninsula. Pure and Applied Geophysics, 161, 755–815.

83. Cowie, J. D., 1964, Loess in the Manawatu district, New Zealand. New Zealand Journal of Geology and Geophysics. 7, 389–396.

84. Cowie, J. D., Milne, D. G., 1973, Maps and sections showing the distribution and stratigraphy of North Island Loess and associate deposits. New Zealand Soil Survey Report, 6. DSIR Soil Bureau, Lower Hutt, New Zealand.

85. Cox, R. T., 1994, Analysis of Drainage basin asymmetry as a rapid technique to identify areas of possible Quaternary tilt – block tectonics: an example from the Mississippi embayment. Geological Society of American bulletin, 106, 571-585.

86. Cracknell, A. P., 1998, Synergy in remote sensing – what's in a pixel? International Journal of Remote Sensing, 19, 11, 2025 – 2047.

87. Cracknell, A. P., 1997, Advanced Very High Resolution Radiometer AVHRR, Taylor & Francis Books Ltd., London, p968.

88. Cracknell, A. P. and Hayes, L., 1991, Introduction to Remote Sensing, Taylor & Francis, London, p304.

89. Csillag, G., 1989, Lineament map of the Balaton Highland. Research Report, Orszagos Foldtani es Geofizikai Adattar, Hungary.

90. Csillag, G., 2004, Geomorphological levels of the Kali Basin and vicinity. Foldtani Intezet Evi Jel. 2002. Evrol., Budapest, 95–110 (in Hungarian).

91. Cuong, N. Q. and Zuchiewicz, W. A., 2001, Morphotectonic properties of the Lo river fault near Tam Dao in North Vietnam. Journal of Natural Hazards and Earth System Sciences, 1, 15-22.

92. Cuong, N. Q., Zuchiewicz, W., and Tokarski, A. K., 1999, Morphotectonic evidence for right-lateral normal slip in the Red River Fault Zone: insights from the study on Tam Dao fault scarp (Vietnam). J. Geol., Ser. B, 13–14, 57–59.

93. Currado, C. and Fredi, P., 2000, Morphometric parameters of drainage basins and morphotectonic setting of eastern Abruzzo. Memorie della Societa Geologica Italiana, 55, 411-419.

94. Curran, P.J., 1988, The semivariogram in remote sensing: an introduction. Remote Sens. Environ. 24, 493–507.

95. Dai, F. C., Lee, C. F., Wang, S. J., 2003, Characterization of rainfall-induced landslides. International Journal of Remote Sensing, 24 (23), 4817 – 4834.

96. Dai, F. C. and Lee, C. F., 2002, Landslide characteristics and slope instability modelling using GIS, Lantau Island, Hong Kong. Geomorphology, 42, 212 – 228.

97. Dalati, M. 1994, Applications of Remote Sensing for Tectonic Purposes in El-Rouge Depression, North West of The Syrian Arab Republic. Proceedings of the International Symposium on Spectral Sensing Research, ISSSR, II, 859-867, San Diego, California, USA.

98. Das Gupta, A. B., 1977, Geology of Assam Arakan region. Quat. Jour. Geol. Min. Met. Soc. India, 49 (122), 1-53.

99. Das Gupta A. B. and Biswas, A.K., 2000, Geology of Assam. Geological Society of India Publication, Bangalore, India, p169.

100. Das Gupta, S. and Nandy, D. R., 1982, Seismicity and tectonics of Meghalaya Plateau, Northeastern India. VII Symposium on Earthquake engineering, University of Roorkee, 1, 19-24.

101. Das Gupta, S. and Nandy, D. R., 1995, Geological framework of the Indo-Burmese convergence margin with special reference to ophiolite emplacement. Indian Journal of Geology, 67, 120-125.

102. Das, J. D., Dutta, T, and Saraf, A.K., 2007, Remote sensing and GIS application in change detection of the Barak river channel, N.E. India. Journal Indian Society of Remote Sensing, 35, 309-320.

103. Das, J. D., Yazdana Shujat, Saraf, A.K., Rawat, V., Sharma, K., 2011, Morphotectonic features and fault propagation folding of Bhuban Hills, NE India using Satellite image and DEM. Indian Society of Remote Sensing. DOI 10.1007/s12524-011-0066-6.

104. Das, J. D., Yazdana Shujat and Saraf, A.K., 2011, Spatial technologies in deriving the morphotectonic characteristics of tectonically active western Tripura region, Northeast India. Indian Society of Remote Sensing. DOI 10.1007/s12524-011-0090-6.

105. Das, J.D., Saraf, A. K. and Yazdana, S., 2010, Remote sensing technique in identifying geometry and geomorphic features of Indo-Burman frontal fold belt. International Journal of Remote Sensing, 31 (16), 4481-4503.

106. Dasgupta, S., Mukhopadhyay, M., Bhattacharya, A. and Jana, S.K., 2003, The Geometry of the Burmese-Andaman subduction lithosphere. Journal of Seismology, 7, 155-174.

107. Davis, G.H. and Reynolds, S.J., 1984, Structural geology of rocks and regions. John Wiley and Sons Inc., New York, p776.

108. Devi, R. K. M., and Singh, T., 2006, Morphotectonic setting of the Ganga Lake, Itanagar capital complex, Arunachal Himalaya, Geomorphology, 76, 1-11.

109. De Mets, C., Gordon, G.G., Argus, D.F., and Stein, S., 1994, Effect of recent revisions to the geomagnetic reversal time scale on estimates of current plate motions. Geophysical Research Letters, 21(20), 2192–2194.

110. De Roo, A. P.J., Wesseling, C. G., Cremers, N. H. D. T., and Offermans, R.J.E., 1994, A New Physically-based Hydrological and Soil Erosion Model in a GIS-environment, Theory and Implementation. IAHS Publication, 224, 439-448.

111. Deffontaines, B., and Chorowicz, J., 1991, Principles of drainage basin analysis from multi-source data: application to the structural analysis of the Zaire Basin. Tectonophysics, 194, 237–263.

112. Delcaillau, B., 2004, Reliefs et Tectonique recente, In: Veubert (Ed.), p262.

113. Delcaillau, B., Carozza, J. and Laville E., 2006, Recent fold growth and drainage development: The Janauri and Chandigarh anticlines in the Siwalik foothills, northwest India. Geomorphology, 76, 241-256.

114. Delcaillau, B., Deffontaines, B., Angelier, J., Deramond, J., Floissac, L., Souquet, P. and Chu, H. T., 1998, Morphotectonic evidence from lateral propagation of an active frontal fold; the Pakuashan anticline, foothills of Taiwan. Geomorphology, 24, 263-290.

115. Desikachar, S. V., 1974, A review of the tectonic and geological history of eastern India in terms of plate tectonic theory. J. Geological Society of India, 15: 137-149.

116. Detti, R. and Pasqui, V., 1995, Vector and raster structures in generating drainage-divide networks from digital terrain models. In Geographical Information Systems in Assessing Natural Hazards, edited by A. Carrara and F. Guzzetti (Dordrecht: Kluwer Publishing Co.), 35-56.

117. Dohrenwend, J. C., Mcfadden, L. D., Turrin, B. D., and Wells, S. G., 1984, K-Ar dating of the Cima volcanic field, eastern Mojave Desert, California: Late Cenozoic volcanic history and landscape evolution. Geology, 12, 163-167.

118. Doornkamp, J.C., 1972, Trend-surface analysis of planation surfaces, with an East-African case study. In: Chorley, R.J. (Ed.), Spatial Analysis in Geomorphology, Methuen, London, 247–281.

119. Drury, S. A., 2001, Image interpretation in Geology. Nelson Thornes Ltd., UK, 304.

120. Dumont, J. F., Santana, E., Vilema, W., Pedoja, K., Ordonez, M., Cruz, M., Jimenez, N., and Zambrano, I., 2005, Morphological and microtectonic analysis of Quaternary deformation from Puna and Santa Clara Islands, Gulf of Guayaquil, Ecuador (South America). Tectonophysics, 399, 331-350.

121. Ehlschlaeger, C., and Shortridge, A., 1996, Modeling Elevation Uncertainty in Geographical Analyses. Proceedings of the International Symposium on Spatial Data Handling, Delft, Netherlands, 9B.15 - 9B.25.

122. Elliot, G., 1976, The energy balance and deformation mechanism of thrust sheets. Philosophical transaction of the Royal Society of London, 238, 289-312.

123. Evans, I. S., 1972, General geomorphometry, derivatives of altitude and descriptive statistics. In Spatial Analysis in Geomorphology, edited by R.J. Chorley (London: Methuen), 17-90.

124. Evans, I.S., 1980, An integrated system for terrain analysis for slope mapping. J. Geomorphol. 36, 274–295.

125. Evans, P., 1932, Tertiary succession in Assam. Trans. Min. Geol. Inst. India, 27 (3), 80-96.

126. Fairbanks, R.G., 1989, A 17,000 year glai-eustatic-sea-level record: Influence of glacial melting rates on the Younger Dryas events and deep ocean circulation. Nature, 342, 637-642.

127. Fairfield, J. and Leymarie, P., 1991, Drainage networks from grid digital elevation models. Water Resources Research, 27, 709-717,

128. Falcidieno, B. and Spagnuolo, M., 1991, A new method for characterization of topographic surfaces. International Journal of Geographical Information Systems, 5, 397-412.

129. Fergusson, R.J., and Brierley, G.J., 1999, Downstream changes in valley confinement as a control on floodplain morphology, Lower Tuross River, New South Wales, Australia: a constructivist approach to floodplain analysis. In: Miller, A.J., Gupta, A. (Eds.), Varieties of fluvial form. Wiley, Chichester, New York, 377–407.

130. Fisher, P., 1991, First Experiments in View-shed Uncertainty: The Accuracy of the View-shed Area. Photogrammetric Engineering and Remote Sensing, 57 (10), 1321-1327

131. Fitch, T. J., 1972, Plate convergence, transcurrent faults, and internal deformation adjacent to southeast Asia and the Western Pacific. J. Geophysical Research, 77, 4432-4460.

132. Flam, L., 1993, Fluvial geomorphology of the lower Indus basin (Sindh, Pakistan) and the Indus Civilization. In Shroder, J. F., Jr (ed.), Himalaya to the sea, Routledge, London, 265-287.

133. Florinsky, I. V., 1998, Combined analysis of digital terrain models and remotely sensed data in landscape investigations. Progress in Physical Geography, 22 (1), 33–60.

134. Florinsky, I. V., 2000, Relationship between topographically expressed zone of flow accumulation and sites of fault intersection: analysis by means of digital terrain modeling. Environmental Modeling Software, 15, 87-100.

135. Ford, M., Williams, E.A., Artoni, A., Verges, J., and Hardy, S., 1997, Progressive evolution of a fault-related fold pair from growth strata geometries, Sant Lorenc de Morunys, SE Pyrenees. Journal of Structural Geology, 19, 413- 441.

136. Formento-Trigilio, M. L., Burbank, D. W., Nicol, A., Shulmeister, J., and Rieser, U., 2003, River response to an active fold and thrust belt in a convergent margin setting, North Island, New Zealand. Geomorphology, 49, 125-152.

137. Fraser, A.J., Huggins, P., Cleverley, P., and Rees, J. L., 1995, A satellite remote-sensing technique for geological horizon structure mapping. SEG Annual Meeting, Expanded Technical Program Abstracts with Biographies. Society of Exploration Geophysicists, Tulsa, OK, United States, 65, 134–137.

138. Fraser, C., and Hanley, H., 2003, Bias Compensation in rational functions for IKONOS satellite imagery. Photogrammetric Engg. & Remote Sensing, 69, 53-58.

139. Frisch, W., 1997, Tectonic Geomorphology. In Proceeding of the Fourth International Conf. on Geomorphology, Z. Geomorphol. N. F., Supplementary Band, 118.

140. Gallant, J.C. and Hutchinson, M.F.,1996, Towards an understanding of landscape scale and structure. Proceedings, Third International Conference /Workshop on Integrating GIS and Environmental Modeling, Santa Fe, NM, January 21-26, 1996. Santa Barbara, CA: National Center for Geographic Information and Analysis: http://www.ncgia.ucsb.edu/conf/SANTA_FE_CD-ROM/main.html.

141. Ganguly , S., 1993, Stratigraphy, sedimentation and hydrocarbon prospects of the Tertiary succession of Tripura and Cachar (Assam). Indian Journal of Geology, 65 (3), 145-180.

142. Ganguly, S., 1984, Tectonic evolution of the orogenic belt of Tripura. Quat. Jour. Geol. Min. Met. Soc. India, 56 (3), 128-137.

143. Ganesser, A., 1983, Geology of the Bhutan Himalaya. Birkhauser Verlag, Switzerland, p181.

144. Garcia-Melendez, E., Goy, J. L. and Zazo, C., 2003, Neotectonic and Plio-Quaternary landscape development within the eastern Huercal-Overa Basin (Betic Cordilleras, Southeast Spain). Geomorphology, 50, 111-133.

145. Ghani, M.A., 1978, Late Cenozoic vertical crustal movements in the central part of New Zealand, New Zealand. Journal of Geology and Geophysics, 21, 117– 125.

146. Gianinetto, M., 2008, Automatic digital terrain model generation using Cartosat-1 stereo images. Sensor Review, 28 (4), 299–310

147. Gilbert, G. K., 1890, Lake Bonneville: United States Geological survey Monograph, 1, 438.

148. Gillespie, A. R., Kahle, A. B., and Polluconi, F. D., 1984, Mapping Alluvial fans in Death Valley, California using multi-channel thermal infra-red image. Geophysical Research Letters, 11, 1153-1156.

149. GLCF, 2004, Global Land Coverage Facility, http://www.glcf.umiacs.umd.edu (accessed on March 2009).

150. Gloaguen R., Marpu. P., and Niemeyer, I., 2007, Automatic Extraction of Faults and Fractal Analysis from Remote Sensing Data. Nonlin. Processes Geophys., 14, 131–138.

151. Goldsworthy, M. and Jackson, J., 2000, Active normal fault evolution in Greece revealed by geomorphology and drainage patterns. Journal of the Geological Society, London, 157, 967-981.

152. Gonzalez, R.C., and Woods, R.E., 1993, Digital Image Processing. Addison-Wesley Publishing Company, New York.

153. Graf, W.L., 1983, Downstream changes in stream power in the Henry Mountains, Utah. Annals of the Association of American Geographers, 73, 373– 387.

154. Grant, G. and Swanson, F.J., 1990, Wolman, M.G., Pattern and origin of stepped-bed morphology in high gradient streams, Western Cascades, Oregon. Geological Society of America Bulletin, 102, 340–352.

155. Grapes, R.H., 1991, Aggradation surfaces and implications for displacement rates along the Wairarapa Fault, southern North Island, New Zealand. Catena, 18, 453–469.

156. Gupta, S., 1997, Himalayan drainage patterns and the origin of fluvial mega-fans in the Ganges foreland basin, Geology, 25, 11-14.

157. Gupta, S., and Ellis, M., 2004, Does the topography of actively ground folds mimic folds structures? The case of the Mohand Anticline, Frontal Himalaya. Geophysical Union, Annual meeting, April 2004.

158. Guth, P. L., 1997, Tectonic Geomorphology of the White Mountains, Eastern California. Geological Society of America, 1997, Annual Meeting, Abstracts with Programs, 29, 235. Geological Society of America (GSA). Boulder CO, United States.

159. Habib, A., and Beshah, B., 1998, Multi Sensor Aerial Triangulation. ISPRS Commission III Symposium, Columbus, Ohio, July 6 to 10.

160. Habib, A., Kim, E., Morgan, M. and Couloigner, I., 2004, DEM Generation from High Resolution Satellite Imagery Using Parallel Projection Model, Proceeding of the

XXth ISPRS Congress, Commission 1, TS: HRS DEM Generation from SPOT-5 HRS Data, 12-23 July 2004, Istanbul, Turkey, 393-398.

161. Hack, J.T., 1960, Interpretation of erosional topography in Humid temperate regions. American Journal of Science, 258-A, 80-97.

162. Hack, J.T., 1973, Stream-profile analysis and stream-gradient index. U.S. Geological Survey Journal of Research, 1, 421– 429.

163. Hancock, P. and Skinner J. B., 2000, "Morphotectonics", The Oxford Companion to the Earth, Encyclopedia.com. (April 28, 2010). http://www.encyclopedia.com/doc/1O112-morphotectonics.html

164. Hantke R. and Scheidegger A.E., 1998, Morphotectonics of the Massacre Island, Annali di Geofisica, 41 (2), 165-181.

165. Harbor, D.J., Schumm S.A., and Harvey, M.D., 1994, Tectonic control of Indus River in Sindh, Pakistan, In Schumm S. A. and Winkley, B. R. (eds.) The variability of large alluvial rivers. American Society of Civil Engineers Press, New York, 161-175.

166. Hardy, S., and Poblet, J., 1994, Geometric and numerical model of progressive limb rotation in detachment folds. Geology, 22, 371– 374.

167. Hare, P.W. and Gardner, T.W., 1985, Geomorphic indicators of vertical neo-tectonism along converging plate margins, Nicoya Peninsula, Costa Rica. Tectonic Geomorphology, Proceedings of the 15th Annual Binghamton Geomorphology Symposium, (Eds) Morisawa, M. and Hack, J. T., September 1984, Allen and Unwin, Boston, 90–104.

168. Harrison, J.M., and Lo, C., 1996, PC-based two-dimensional discrete spectral transform programs for terrain analysis. Comput. Geoscience, 22, 419–424.

169. Hessel, R., Jetten, V., Liu, B., Zhang, Y., and Stolte, J., 2003, Calibration of the LISEM model for a small loess plateau catchment. Catena, 54, 235-254.

170. Hessel, R. and van Asch, T., 2003, Modeling gully erosion for a small catchment on the Chinese loess plateau, Catena, 54, 131-146.

171. Hobbs, B.E., 1976, An outline of structural geology. John Wiley & Sons, New York, p577.

172. Hobbs, W.H., 1912. Earth Features and their Meaning. McMillian Co., New York, p506.

173. Holmes, K., Chadwick, O. and Kyriakidis, P., 2000, Error in a USGS 30-Meter Digital Elevation Model and Its Impact on Terrain Modeling. Journal of Hydrology, 233, 54-174.

174. Holtrop, J. F., and Kaizer, J., 1970, Some aspects of the stratigraphy and correlation of the Surma basin wells, East Pakistan. ESCAFE Miner. Resour. Dev. Ser. 36, 143–154

175. Hooke, J.M., 1995, River channel adjustment to meander cut-offs on the River Bollin and River Dane, NW England. Geomorphology, 14, 235-253.

176. Horton, R.E., 1932, Drainage Basin Characteristics. Transactions; American Geophysical Union, 13, 350-361.http://herkules.oulu.fi/isbn9514267117/ html/x504.html, http://www.ifp.unistuttgart.de/publications/phowo99/bamler.pdf, http://www.ipi.uni-hannover (publication)

177. Huchon, P., Le Pichon, X., and Rangin, C., 1994, Indo-china Peninsula and the collision of India and Eurasia. Geology, 22, 27–30.

178. Humphrey, N.F., and Heller, P.L., 1995, Natural Oscillations in coupled geomorphic systems: An alternative origin for cyclic sedimentation. Geology, 23, 499-502.

179. Hunter, G. and Goodchild M., 1997, Modeling the Uncertainty of Slope and Aspect Estimates Derived from Spatial Databases. Geographical Analysis, 29(1), 35-49.

180. Hurtrez, J.E., Sol, C. and Lucazeau, F., 1999, Effect of Drainage Area on Hypsometry from Analysis of Small-scale Drainage Basins in the Siwalik Hills (Central Nepal). Earth Surface Processes and Landforms, 24, 799-808.

181. Husson, L., and Mugnier, J. L., 2003, Three Dimensional horizon reconstruction from outcrop structural data, restoration and strain field of the Baisahi anticline, western Nepal. Journal of structural Geology, 25 (1), 79-90.

182. Hutchinson, M. F., 1989, A new procedure for gridding elevation and stream-line data with automatic removal of spurious pits. Journal of Hydrology, 106, 211- 232.

183. ILWIS, 1997, The Integrated Land and Water Information System. Reference Guide, ILWIS Department, ITC, Enschede.

184. Jackson, J. and Leeder, M., 1994, Drainage systems and the development of normal faults - An example from Pleasant valley, Nevada. J. Structural Geology, 16 (8), 1041-1059.

185. Jackson, J., Van Dissen, R., and Berryman, K., 1998, Tilting of active folds and faults in the Manawatu region, New Zealand: evidence from surface drainage patterns, New Zealand. Journal of Geology and Geophysics, 41, 377-385.

186. Jacobsen, K., 2003, Orthoimages and DEMs by QuickBird and IKONOS, EARSeL Ghent. Remote Sensing in Transition, Millpress, ISBN 90-77017-71-2, 513-525.

187. Jacobsen, K., 2004, DEM Generation from Satellite Data. Remote Sensing in Transition, Millpress Rotterdam, ISBN 90 5966 007 2, 513 –525.

188. Jain, S. and Verma, P.K., 2006, Mapping of active tectonics intensity zones using remote sensing and GIS. J. Indian Society of Remote Sensing, 34, 131-142.

189. Jain, M., Woodcock, N.H., Tandon, S.K., 1998, Neotectonics of western India: evidence from deformed Quaternary fluvial sequences, Mahi River, Gujarat. Journal of the Geological Society, 155, 897-901.

190. Jasrotia, A.S., and Singh, R., 2006, Modeling Runoff and Soil Erosion in a Catchments Using GIS, in Himalayan region. Environmental Geology, International Journal of Geosciences, 51 (1) 143-150.

191. Jasrotia, A.S., Kumar, R. and Saraf, A.K., 2007, Delineation of groundwater recharge sites using integrated remote sensing and GIS in Jammu district, India. International Journal of Remote Sensing, 28 (22), 5019–5036.

192. Jenson, S.K. and Domingue, J.O., 1988, Extracting Topographic Structure from Digital Elevation Data for Geographic Information System Analysis. Photogrammetric Engineering and Remote Sensing, 54(11), 1593-1600.

193. Jenson, S. K., 1991, Applications of Hydrologic Information Automatically Extracted From Digital Elevation Models. Hydrological Processes, (1), 31-44.

194. Jones, R., 2002, Algorithms for using a DEM for mapping catchment areas of stream sediment samples. Computers & Geosciences, 28, 1051-1060.

195. Jordan, G. , Meijninger, B.M.L., van Hinsbergen, D.J.J., Meulenkamp, J.E. and Van Dijk, P.M, 2005, Extraction of morphotectonic features from DEMs: Development and applications for study areas in Hungary and NW Greece. International Journal of Applied Earth Observation and Geoinformation, 7, 163–182.

196. Jordan, G., 2003, Morphometric analysis and tectonic interpretation of digital terrain data: a case study. Earth Surface Processes and Landforms, 28, 807–822.

197. Kalyanaraman, K., Mohan, M. and Roy, P.S., 2006, Photogrammetric applications of Cartosat-1 data. NNRMS Bulletin (B)-31, 11-18, December 2006.

198. Kaessner A. and Gloaguen R., Recent Tectonics in the Eger Rift? Neotectonic Information from River Analysis. International Journal of Earth Sciences (accepted).

199. Kaewyana, W., 1980, Late Quaternary alluvial terraces and their cover bed stratigraphy, Eketahuna and Pahiatua districts, New Zealand. MS Thesis, Victoria University of Wellington, New Zealand.

200. Kahle, A.B., Shumate, M.S., and Nash, D.B., 1984, Active airborne infrared laser system for identification of surface rocks and minerals. Geophysical Research Letters, 11, 1149-1152.

201. Kayal J.R. and Zhao. D., 1998, Three-dimensional seismic structure beneath Shillong Plateau and Assam Valley, Northeast India, Bulletin of the Seismological Society of America, 88 (3), 667-676.

202. Keller, E., 1986, Investigation of active tectonics: use of surfacial earth processes. In: Wallace, R.E. (eds). Active tectonics studies in geophysics. National Academy Press, Washington, D.C. 136-147.

203. Keller, E.A., and N. Pinter, 2002, Active Tectonics: Earthquake, Uplift, and Landscape, second edition, Prentice Hall, New Jersey, p362.

204. Keller, E.A. and Pinter, N., 1996, Active Tectonics: Earthquakes, Uplift and Landscapes. Prentice Hall, Upper Saddle River, New Jersey, p337.

205. Keller, E.A., Rockwell, T.K., Clark, M.N., Dembroff, G.R. and Johnson, D.L., 1982, Tectonic geomorphology of Ventura, Ojai and Santa Paula areas, western Transverse Ranges, California. In: Cooper, J.D. (Ed.), Neotectonics in Southern California: Geologic Society of America Cordilleran Section Field Guidebook, 25–42.

206. Kennedy, N.M., Pullar, W.A., and Pain, C.F., 1978, Late Quaternary land surfaces and geomorphic changes in the Rotorua Basin. New Zealand Journal of Science, 21, 249– 264.

207. Kenward, T., Lettenmaier, D.P., Wood, E.F. and Fielding, E., 2000, Effects of Digital Elevation Model Accuracy on Hydrologic Predictions. Remote Sensing of Environment, 74 (3), 432-444.

208. Khan Maroof, M.A., 1980, A brief account of hydrocarbon and exploration in Bangladesh. Proc. 3rd Offshore S. E. Asia Conf. SEAPAX, Singapore.

209. Kimura, K., 2004, Comparative morphotectonics in the Himalayan foreland and the forearc of Southwest Japan. Himalayan Journal of Sciences, 2, 4 (special issue).

210. Knighton, A.D., 1996, Fluvial Forms and Processes. Arnold Publishers, London, p383.

211. Knighton, A.D., 1999, Downstream variation in stream power. Geomorphology, 29, 293–306.

212. Kobor, J.S. and Roering, J.J., 2004, Systematic variation of bedrock channels gradients in the central Oregon Coast Range: implications for rock uplift and shallow landsliding. Geomorphology, 62, 239–256.

213. Kocak, G., Buyuksalih G. and Oruc M., 2005, Accuracy assessment of interferometric digital elevation models derived from the Shuttle Radar Topography Mission X- band and C-band data in a test area with rolling topography and moderate forest cover. Optical Engineering, 44(3).

214. Koch, A., Heipke, C., and Lohmann, P., 2002, Analysis of SRTM DTM - Methodology and practical results, IntArchPhRS, Com.IV, Ottawa, XXXIV Part 4, 470-475.

215. Koike, K., Nagano, S., and Kawaba, K., 1998, Construction and analysis of interpreted fracture plane through combination of satellite image derived lineaments and digital elevation model data. Computer Geosciences, 24, 573-583.

216. Kolbl, O., 1996, Application of digital photogrammetric workstations. Proceeds. OEEPE Workshop, Lausanne 4-6, March 1996.

217. Krzystek, P. and Ackermann, F., 1995, New investigations into the practical performance of automatic DEM generation. In Proceedings of the ACSM/ASPRS Annual Conference, (Bethesda: American Society for Photogrammetry and Remote Sensing and the American Congress on Surveying and Mapping), 372- 390.

218. Kumar, S. and Giribabu, D., 2006, Improving the accuracy of Cartosat-1 stereo data using DGPS GCPS. NNRMS Bulletin (B)-31, 19-25.

219. Kunqing Xie, Yongqiu Wu, Xiujun Ma, Yu Liu, Baoyuan Liu, and Hessel, R., 2003, Using contour lines to generate digital elevation models for steep slope areas: a case study of the Loess Plateau in North China. Catena, 54, 161-171.

220. Lave, J., Avouac, J. P., 2000, Active folding of fluvial terraces across the Siwaliks Hills, Himalayas of central Nepal. Journal of Geophysical Research 105 (B3), 5735–5770.

221. Lawler, D.M., Grove, J.R., Couperthwaite, J.S. and Leeks, G.J.L., 1999, Downstream change in river bank erosion rates in the Swale–Ouse system, northern England. Hydrological Processes, 13, 922–977.

222. Le Dain, A. Y., Tapponnier, P., Molnar, P., 1984, Active faulting and tectonics of Burma and surrounding regions. J. Geophysical Research, 89, 453-472.

223. Le Turdu, C., Coussement, C., Tiercelin, J. J., Renaut, R. W., Rolet, J., Richert, J. P., Xavier, J. P., and Coquelet, D., 1995, Rift basin structure and depositional patterns interpreted using 3D remote sensing approach: the Barongo and Bogoria basins, Central Kenya Rift, East Africa. Bulletin Centres Re'cherches, 19, 1-37.

224. Leamy, M. L., Milne, J. D. G., Pullar, W. A. and Bruce, J. G., 1973, Paleopedology and soil stratigraphy in the New Zealand Quaternary Succession. New Zealand Journal of Geology and Geophysics, 16, 723– 744.

225. Lee, J., 1996, Digital Elevation Models: Issues of Data Accuracy and Applications. ESRI User Conference Proceedings. http://gis.esri.com/library/userconf/proc96/ TO150/PAP145/ P145.HTM, (accessed on May 26, 2010).

226. Lee, J., 1991, Comparison of existing methods for building triangular irregular network models of terrain from grid digital elevation models. International Journal of Geographical Information Systems, 5, 267-285.

227. Lee, J., Snyder P., and Fisher, P., 1992, Modeling the Effect of Data Errors on Feature Extraction from Digital Elevation Models. Photogrammetric Engineering and Remote Sensing, 58 (10) 1461-1467.

228. Li, Z., 1994, A comparative study of the accuracy of digital terrain models (DTMs) based on various data models, Journal of Photogrammetry and Remote Sensing, 49, 2-11.

229. Lifton, N.A. and Chase, C.G., 1992, Tectonic, climatic and lithologic influences on landscape fractal dimension and hypsometry: implication for landscape evolution in the San Gabriel Mountains, California. Geomorphology, 5, 77–114.

230. Lillesand, T. M. and Kiefer, R. W., 2000, Remote sensing and image interpretation. John Wiley and Sons, New York, p736.

231. Liu, R., 1994, The Effects of Spatial Data Errors on the Grid-Based Forest Management Decisions. Ph.D. Dissertation, State University of New York College of Environmental Science and Forestry, Syracuse, NY, 209.

232. Liu, X., Ji, Sh., Zhang, L., and Zhong, J., 1990, The Ailao Shan/Red River metamorphic belt: Tertiary left-lateral shear between Indo-china and South China. Nature, 343, 431–437.

233. Lupia Palmieri E., Centamore, E., Ciccacci, S., D 'Alessandro L., Del Monte M., Fredi P., Pugliese, F., 1998, Quantitative geomorphology and morphodynamics of Abruzzo.II. Il Tordino River catchment. Physical Geography and Quaternary mica Dina, 21, 113-129.

234. Lupia Palmieri, E., Biasini, A., Caputo, C., Centamore, E., Ciccacci S., Del Monte M., Fredi P., Pugliese, F., 2001, Quantitative geomorphology and morphodynamics of Abruzzo. III. Il catchment area of the Saline River. Physical Geography and Quaternary Dynamics, 24, 157-176.

235. Lupia Palmieri, E., Ciccacci, S., Civitelli, G., Corda, L., D' Alessandro, L., Del Monte, M., Fredi, P., Pugliese, F., 1995, Quantitative geomorphology and morphodynamics

of Abruzzo. I. II River Basin Sinello, Physical Geography and Quaternary Dynamics, 18, 31-46.

236. Maiti, S., and Bhattacharya, A. K., 2011, Application of Satellite Remote Sensing in Coastal Change Studies through a Three-unit Based Approach, International Journal of Remote Sensing, 32 (1), 209-229.

237. Maiti, S., and Bhattacharya, A. K., 2009, Shoreline Change Analysis and its Application to Prediction – A Remote Sensing and Statistics Based Approach, Marine Geology, 257, 11 – 23.

238. Mallet, F. R., 1876, On the coalfields of Naga Hills bordering Lakhipur and Sibsagar districts, Assam. Mem. Geological Survey of India, 12, (pt. 2), 269-363.

239. Marden, M., and Neall, V. E., 1990, Dated Ohakean terraces offset by the Wellington Fault, near Woodville, New Zealand. New Zealand Journal of Geology and Geophysics, 33, 449–453.

240. Mark, D.M., 1975, Geomorphometric parameters - a review and evaluation. Geografiska Annaler, 57A, 165-77

241. Marple, R.T. and Talwani, P., 1993, Evidence of possible tectonic upwarping along the South Carolina coastal plain from an examination of river morphology and elevation data. Geology, 21, 651– 654.

242. Marshall, J.S., and Anderson, R.S., 1995, Quaternary uplift and seismic cycle deformation, Peninsula de Nicoya, Costa Rica. Geological Society of America, 107, 463-473.

243. Martin, Y. and Church, M., 2000, Re-examination of Bagnold's empirical bedload formulae. Earth Surface Processes and Landforms, 25, 1011 –1024.

244. Masek, J. G., Isacks, B. L., Gubbels, T. L. and Fielding, E. J., 1994, Erosion and tectonics at the margins of continental plateaus. Journal Geophysical Research, 99 (B7), 13,941-13,956.

245. Mathur, L. P., and Evans, P., 1964, Oil in India. Proceedings International congress of India, 22nd Session, 1-85.

246. Maune, D., 2001, Digital Elevation Model technologies and applications. The DEM Users Manual (Maryland: ASPRS).

247. Mayer, L., 1990, Introduction to Quantitative Geomorphology. Prentice Hall, Englewood Cliffs, New Jersey, p380.

248. McFadden, L. D., Ritter, J. B., and Wells, S. G., 1989, Use of multiparameter relative age method for age estimation and correlation of alluvial fans surfaces on the desert piedmont, eastern Mojave Desert, California. Quaternary Research, 32, 276-290.

249. McFadden, L.D., Tinsley, J. C., and Bull., W. B., 1982, Late Quaternary pedogenesis and alluvial chronologies of the Los Angeles basin and St. Gabriel mountain areas, southern California in Tinsley, J.C., Matti, J. C., and Mcfadden, L. D., eds., Late Quaternary pedogenesis and alluvial chronologies of the Los Angeles basin and St. Gabriel mountain areas, southern California, and Holocene faulting and and alluvial stratigraphy within the Cucamonga fault zone; Field Trip 12, Cordilleron Section of the Geological Society of America, 1-13.

250. McQuarrie, N., 2004, Crustal scale geometry of the Zagros fold–thrust belt, Iran. Journal of Structural Geology, 26, 519–535.

251. Medwedeff, D. A., 1992, Geometry and Kinematics of an Active, Laterally Propagating Wedge Thrust, Wheeler Ridge, California. In: Mitra, S., Fisher, G. W., (Eds), Structural Geology of Fold and Thrust Belts, John Hopkins Studies in Earth and Space Sciences, 5, 1-28.

252. Merritts, D. J., Vincent, K. R. and Wohl, E. E., 1994, Long River profiles, tectonism, and eustasy: a guide to interpreting fluvial terraces. Journal of Geophysical Research, 99 (B7), 14031– 14050.

253. Merritts, D. and Vincent, K.R., 1989, Geomorphic response of coastal streams to low, intermediate, and high rates of uplift, Mendocino Triple Junction region, Northern California. Geological Society of America, 110, 1373–1388.

254. Miliaresis, G. C., Paraschou, C. V. E., 2005, Vertical accuracy of the SRTM DTED level 1 of Crete. International Journal of Applied Earth Observation and Geoinformation, 7(1), 49-59.

255. Milne, J. D. G., and Smalley, I. J., 1979, Loess deposits in the southern part of the North Island of New Zealand: an outline stratigraphy. Acta Geologica Academiae Scientiarum Hungaricae, 22, 197–204.

256. Mitra, S., 1990, Fault-propagation folds: geometry, kinematic evolution and hydrocarbon traps. American Association of Petroleum Geologists Bull. 74, 921–945.

257. Molnar, P., and England, P., 1990, Late Cenozoic uplift of mountain ranges and global climate change: Chicken or egg? Nature, 106, 595-606.

258. Molnar, P., Brown, E. T., Burchfiel, B. C., Deng, Q., Feng, X., Li, J., Raisbeck, G. M., Shi, J., Wu, Z., Yiou, F., and You, H., 1994, Quaternary climate change and the formation of river terraces across growing anticlines on the north flank of the Tien Shan China. J. Geology, 102, 583–602.

259. Molnar, P., Fitch, T. J. and Wu, F. T., 1973, Fault plane solutions of shallow earthquakes and contemporary tectonics in Asia. Earth Planet. Sc. Lett., 19, 101-112.

260. Montgomery, D.R. and Buffington, J.M., 1997, Channel-reach morphology in mountain drainage basins. Geological Society of America Bulletin, 109, 596–611.

261. Morgan, J. P. and McIntire W. G., 1959, Quaternary geology of the Bengal Basin, East Pakistan and India. Geol. Society of America Bull., 70, 319-42.

262. Mueller, K. and Talling, P., 1997, Geomorphic evidence for tear faults accommodating lateral propagation of an active fault bend fold, Wheeler Ridge, California. Journal of Structural Geology, 19 (3-4), 397-411.

263. Mukherji, A. D., and Iyer, S. D., 1999, Synthesis of morphotectonics and volcanics of the central Indian Ocean Basin. Indian Journal of Marine Sciences, 19, 13-16.

264. Mukhopadhyay, M., 1984, Seismotectonics of transverse lineaments in the eastern Himalaya and its foredeep. Tectonophysics, 109, 227-240.

265. Mukhopadhyay, M. and Das Gupta, S., 1988, Deep structures and tectonics of Burmese Arc: constraints from Earthquake and gravity data. Tectonophysics, 149, 299-322.

266. Mulller, J. E., 1968, An introduction to the hydraulic and topographic sinuosity indexes. Annals Association of American Geographers, 58, 371- 385.

267. Nandy, D. R., 2001, Geodynamics of northeastern India and the adjoining region. ACB Publications, Kolkata, p209.

268. Nandy, D. R., 1980, Tectonic pattern in NE India. Indian Journal of Earth Sciences, 7 (1), 103-107.

269. Nandy, D. R., 1981, Tectonic pattern in NE India: A discussion. Indian Journal of Earth Sciences, 8 (1), 82-86.

270. Nandy, D. R., Das Gupta, S., Sarkar, K., Ganguly, A., 1983, Tectonic evolution of Tripura Mizoram fold belt, Surma basin, NE India. Quat. Jour. Geol. Min. Met. Soc. India, 55 (4), 186-194.

271. Novak, I.D., and Soulakellis, N., 2000, Identifying geomorphic features using LANDSAT-5/TM data processing techniques on Lesvos, Greece. Geomorphology, 34,101–109.

272. Ollier, C. D., 1981, Tectonics and landforms, Longman Group Limited, Harlow, England, p324.

273. Onorati, G., Poscolieri, M., Ventura, R., Chiarini, V., and Crucilla, A., 1992, A digital elevation model of Italy for geomorphology and structural geology. Catena, 19, 147-178.

274. Osterkamp, W.R. and Hedman, E.R., 1982, Perennial stream flow related to channel geometry and sediment in Missouri River Basin. United States Geological Survey Professional Paper, 1242, 1– 37.

275. Ouchi, S., 1985, Response of alluvial rivers to slow active tectonic movement. Geological Society of America, 96, 504-515.

276. Pascoe, E. H., 1973, A manual of the geology of India and Burma, Vol III (3rd Ed.), published by Govt. of India, Geol. Surv. India, 1345-2136.

277. Passini, R., Betzner, D., and Jacobsen, K. 2002, Filtering of Digital Elevation Models. American Society of Photogrammetry and Remote Sensing annual convention, Washington 2002.

278. Pati, J. K., 2005, The Dhala Structure, Bundelkhand Craton, Central India - A New Large Paleoproterozoic Impact Structure, Meteoritics & Planetary Science, Supplement, Proceedings of 68th Annual Meeting of the Meteoritical Society, between 12-16 September in Gatlinburg, Tennessee, 40, 5092.

279. Pati, J. K., Lal, J., Prakash, K., Bhusan, R., 2008, Spatio-temporal shift of Western bank of the Ganga river Allahabad city and its implications. Journal of Indian Society of Remote Sensing, 36, 289 – 297.

280. Pedrera, A., Pérez-Peña, J. V., Galindo-Zaldívar, J., Azañón, J. M and Azor, A., 2009, Testing the sensitivity of geomorphic indices in areas of low-rate active folding (eastern Betic Cordillera, Spain). Geomorphology, 105, 218–231.

281. Penck, A., and Bruckner, E., 1909, The Alps in the Ice Age: Leipzing, Tauchnitz, 1199.

282. Peralvo, M., 2004, Influence of DEM interpolation methods in Drainage analysis, GIS in Water Resources 04, Texas, USA.

283. Perez-Pena, J.V, Azanon, J. N. and Azor, A., 2009, CalHypso: AnArc GIS extension to calculate hypsometric curves and their statistical moments. Applications to drainage basin analysis in SE Spain. Computers & Geosciences, 35, 1214-1223.

284. Philips, L. F., and Schumm, S. A., 1987, Effect of regional slope on drainage networks. Geology, 15, 813-816.

285. Pierce, K. L., 1986, Dating methods, in Active Tectonics: edited by R. E. Wallace (Wasington, D. C: National Academy Press), 195-214.

286. Pike, R. J., 1993, A bibliography of geomorphometry, with a topical key to the literature and an introduction to the numerical characterization of topographic form. U.S. Geological Survey Open-file Report, 93-262-A, 132.

287. Pirasteh, S., Tripathi, N. K., Ayazi, M.H., 2006 , Localizing Ground Water Potential Zones in Parts of Karst Pabdeh Anticline, Zagros Mountain, SouthWest Iran using Geospatial Techniques. International Journal of Geoinfomatics, 2 (2), 35-42.

288. Pirasteh, S., Tripathi, N.K., Mahmoodzadeh A., Ziaee H., 2008, Remote Sensing and GIS Techniques to Study Watershed Basin Erosion for Development Program: ZFB, Iran. International Journal of Geoinformatics, 4 (3), 59-66.

289. Pirasteh, S. and Woodbridge, K., Rizvi, S.M., 2009, Geo-information technology (GiT) and tectonic signatures: the River Karun & Dez, Zagros Orogen in south-west Iran. International Journal of Remote Sensing, 30(2), 389-404.

290. Pirasteh, S., Safari, H. O., Pradhan, B., Attarzadeh, I., 2010, Litho-morphotectonics analysis using Landsat ETM data and GIS techniques: Zagros Fold Belt (ZFB), SW Iran. International Geoinformatics Research and Development Journal, 1 (2), 28-36.

291. Pohl, C. and Van Genderen, J. L., 1998, Multisensor image fusion in remote sensing: concepts, methods and applications. International Journal of Remote Sensing, 19, 823-854.

292. Poon, J., Fraser, C.S., Chunsun, Z., Li, Z. and Gruen, A., 2005, Quality assessment of digital surface models generated from IKONOS imagery. The Photogrammetric Records, 20 (110), 162-71.

293. Price, N.J. and Cosgrove, J.W., 1990, Analysis of geological structure. Cambridge University Press, Cambridge, p502.

294. Pries, R. A., 1995, A system for large-scale image mapping and GIS data collection. Photogrammetric Engineering and Remote Sensing, 61, 503-511.

295. Prost, G. L., 1990, Recognizing thrust faults on remote sensing images. World Oil 221 (3), 39– 46.

296. Rabus, B., Eineder, M., Roth, A. and Bamler, R., 2003. The shuttle radar topography mission - a new class of digital elevation models acquired by spaceborne radar. ISPRS Journal of Photogrammetry & Remote Sensing 57 (2003) 241–262.

297. Raj, R., Bhandari, S., Maurya, D.M. and Chamyal, L.S., 2003, Geomorphic indicators of active tectonics in the Karjan river basin, Lower Narmada valley, western India. J. Geological Society of India, 62, 739-752.

298. Ramasamy, S.M., Kumanan, C.J., Selvakumar, R. and Saravanavel, J., 2011, Remote sensing revealed drainage anomalies and related tectonics of South India. Tectonophysics, 501, 41–51.

299. Ramasamy, S.M., Bakliwal, P.C., Verma, R.P., 1991, Remote sensing and river migration in western India. International Journal of Remote Sensing 12 (12), 2597–2609.

300. Ramasamy, S.M., 2006, Remote Sensing and Active Tectonics of South India. International Journal of Remote Sensing, 27 (20), 4397–4431.

301. Ramsay, L. A., Walker, R. T., and Jackson, J., 2007, Geomorphic constraints on the active tectonics of Southern Taiwan. Geophys. J. International, 170, 1357-1372.

302. Rao, C.V., Sathyanarayana, P., Jain, D.S. and Manjunath, A.S., 2007, Topographic map updation using Cartosat-1 data. Proceedings of the 2007 Annual Conference of the Remote Sensing & Photogrammetry Society, Newcastle upon Tyne, unpaginated CD-ROM, available at: www.ceg.ncl.ac. uk/rspsoc 2007 /papers.htm (accessed on 6 May, 2010).

303. Reichenbach, P., Pike, R.J., Acevedo, W. and Mark, R.K., 1993, A new landform map of Italy in computer-shaded relief. Bollettino Geodesia e Scienze Affini, 52, 22-44.

304. Reinfelds, I., Cohen T., Batten P., Brierley G., 2003, Assessment of downstream trends in channel gradient, total and specific stream power: a GIS approach. Journal of Geomorphology, 60, 403-416.

305. Rhea, S., 1989, Evidence of uplift near Charleston, South Carolina. Geology, 17, 311– 315.

306. Riley, C. and Moore, M. C. M., 1993, Digital Elevation Modeling in a study of the neotectonic geomorphology of the Sierra Nevada, southern Spain. Geomorphology, N. F. Suppl. Band, 94, 25-39.

307. Ritter, J.B., Miller, J. R., Enzel, Y., Howes, S.D., Nadon, G., Grubb, M.D., Hoover, K. A., Olsen, T., Seneau, S. L., Sack, D., Summa, C. L., Taylor, I., Tousinthiphonexay, K. C. N., Yodis, E. G., Schneider, N.P., Ritter, D.F., and Wells, S.G., 1993, Quaternary evolution of the Cedar Creek alluvial fan, Montana. Geomorphology, 8, 51-54.

308. Rockwell, T.K., Keller, E.A., Clark, M.N., and Johnson, D.L., 1984, Chronology and rates of faulting of Ventura River terraces, California. Geological Society of America Bulletin, 95, 1466-1474.

309. Rognant, L., Plan`es, J.G., Memier, M., and Chassery, J.M., 2001, Contour Lines and DEM: Generation and Extraction. C.Y. Westort (Ed.): DEM 2001, LNCS 2181, 87–97.

310. Rosgen, D.L., 1994, A classification of natural rivers, Catena, 22, 169–199.

311. Sabins, F. F., 1997, Remote Sensing: Principles and Interpretation. W.H. Freeman and Company, New York, Third Edition, p494.

312. Sadybakasov, I., 1990, Neotectonics of High Asia (in Russian): Moscow, Nauka, 176.

313. Saintot, A., Angelier, J., and Chorovicz, J., 1999, Mechanical significance of structural patterns identified by remote sensing studies in Crimea. Tectonophysics, 313, 187-218.

314. Saraf, A.K., 1999, IRS-1C-LISS-III and PAN data fusion: an approach to improve remote sensing based mapping techniques. International Journal of Remote Sensing, 20, 1929-1934.

315. Saraf, A.K., Das, J. D., Agarwal, B. and Sundaram, R.M., 1996, False topography perception phenomena and its correction. International Journal of Remote Sensing, 17, 3725-3733.

316. Sarkar, K. and Nandy, D. R., 1977, Structures and tectonics of Tripura-Mizoram area of India. Misc. Publ. No. 34, Geol. Survey of India (pt. 1), 141-148.

317. Sarkar, K. and Nandy, D. R., 1976, Structures and tectonics of Tripura- Mizoram area, India. Geological Survey of India, Miscellaneous Publication, No. 34, 141-148.

318. Satyabala, S.P., 2003, Oblique plate convergence in the Indo-Burma (Myanmar) subduction region. Pure and Applied Geophysics, 160, 1611-1650.

319. Saunders, W., 2000, Preparation of DEMs for use in environmental modelling analysis. Maidment, D., Djokic, D. (Eds.), Hydrologic and Hydraulic Modelling Support with Geographic Information Systems, ESRI Press, Redlands, CA, 29– 51.

320. Scheidegger, A. E., 1961, Mathematical models of slope development. Geological Society of America Bulletin, 72, 37-50.

321. Schmidt, K. M. and Montgomery, D.R., 1995, Limits to relief. Science, 270, 617-620.

322. Schumm, S. A., 1986, Alluvial River response to active tectonics. Studies in National Research Council (Ed.), Active Tectonics, National Academy Press, Studies in Geophysics, Washington, D. C., 80-94.

323. Schumm, S. A., Dumont, J.F., and Holbrook, J.M., 2002, Active Tectonics and alluvial rivers. Cambridge University Press, U.K., p276.

324. Schumm, S. A. and Khan, H. R., 1972, Experimental study of channel patterns. Geological Society of America, 83, 1755-1770.

325. Schumm, S.A., 1973, Geomorphic thresholds and complex response of drainage systems. Morisawa, M. (Ed.), Fluvial Geomorphology, Binghamton, New York, 299–309

326. Schumm, S.A., 1985, Patterns of alluvial rivers. Annual Review of Earth and Planetary Sciences, 13, 5 –27.

327. Seeber, L. and Gotnitz, V., 1983, River profile along the Himalayan Arc as indicators of active tectonics. Tectonophysics, 92, 335-367.

328. Sengupta, S., 1996, Geological and geophysical studies in the western part of Bengal basin, India. American association of Petroleum Geologists, 50 (5), 1001-1017.

329. Sharma, A., Tiwari, K.N. and Bhadoria, P.B.S., 2009, Measuring the Accuracy of Contour Interpolated Digital Elevation Models. J. Indian Soc. Remote Sens., 37,139–146.

330. Shettigara, V.K., 1992, A generalized component substitution technique for spatial enhancement of multispectral images using a higher resolution data set. Photogrammetric Engineering and Remote Sensing, 58, 561-567.

331. Shin, D., Lee, H. and Wonkyu, P., 2003, Stereroscopic GCP Simulation Model for the Assessment of Camera Modeling Algorithms. ISSDQ Proceedings, Hongkong, China.

332. Sikder, A.M. and Alam, M. M., 2003, 2-D modelling of the anticlinal structures and structural development of the eastern fold belt of the Bengal Basin, Bangladesh. Sedimentary Geology. 155, 209-226.

333. Small, E.E., Anderson R.S., 1995, Geomorphocally driven late Cenozoic uplift in the Sierra Nevada, California. Science, 270, 277-280.

334. Small, E.E. and Anderson R.S., 1998, Pleistocene relief production in Laramide mountain ranges, western United States. Geology, 26, 123-136.

335. Smith, G.I., and Street-Perrott, F.A., 1983, Fluvial lakes of the western United States, in Portar, S.C., ed., Late Quaternary environments of the United States: the late Pleistocene: Minneapolis, University of Minnesota Press, 190-212.

336. Sorensen, R. and Seibert, J., 2007, Effects of DEM resolution on the calculation of topographical indices: TWI and its components. Journal of Hydrology, 347, 79–89.

337. Soulakellis, N. A., Novak, I. D., Zouros, N., Lowman, P. and Yates, J., 2006, Fusing Landsat-5/TM Imagery and Shaded Relief Maps in Tectonic and Geomorphic Mapping: Lesvos Island, Greece. Photogrammetric Engineering & Remote Sensing, 72 (6) 693–700.

338. Sparling, D. R., 1967, Anomalous drainage pattern and crustal tilting in Ottawa country, Ohio. Ohio Journal of Science, 67, 378-381.

339. Stocklin, J., 1968, Structural history and tectonics of Iran: a review. American Association of Petroleum Geologists Bulletin, 52, 1229–1258.

340. Stolte, J., Liu, B., Ritsema, C.J., van den Elsen, H.G.M. and Hessel, R., 2003, Modelling water flow and sediment processes in a small gully system on the Loess Plateau in China. Catena, 54, 117-130.

341. Stolte, J., van Venrooij, B., Zhang, G., Trouwborst, K.O., Liu, G., Ritsema, C.J., and Hessel, R., 2003, Land-use induced spatial heterogeneity of soil hydraulic properties on the Loess Plateau in China. Catena, 54, 59-75.

342. Strahlar, A. N., 1952, Hypsometric (area-altitude) analysis of erosional topography. Geological Society of America Bulletin, 63, 11172-11142.

343. Sun, G., Ranson, K. J., Kharuk, V. I. and Kovacs, K., 2003, Validation of Surface Height from Shuttle Radar Topography Mission Using Shuttle Laser Altimeter. Remote Sensing of Environment, 88, 401-411.

344. Susan, R., 1993, Geomorphic observations of rivers in the Oregon coast range from a regional reconnaissance perspective. Journal of Geomorphology, 6, 135-150.

345. Takagi, M., 2005, Accuracy of Digital Terrain Model According to Spatial Resolution. In: D.Fritsch, M. Englich and M. Sester (Eds), 'IAPRS', 32 (4), ISPRS Commission IV Symposium on GIS – Between vision and applications, Stuttgart, Germany.

346. Tao, V. and Hu, Y., 2001, A Comprehensive study on the rational function model for photogrammetric processing. Photogrammetric Engg & Remote Sensing, 67(12), 1347-1357.

347. Tate, A., Mueller, K. J. and Golombek, M. P., 2002, Geometry and kinematics wrinkle ridges on lunae and soils plana Mars: implications for fault/fold growth history, Lunar and Planetary Science XXXIII.

348. Thelin, G. P. and Pike, R. J., 1991, Landforms of the conterminous United States-A digital shaded-relief portrayal, U.S.G.S. Miscellaneous Investigation Map, I-2206, scale 1: 3500000.

349. Thorson, R.M., 1989, Glacio-isostatic response of the Puget Sound area, Washington. Geological Society of America Bulletin, 101, 1163-1174.

350. Trinh, Ph. T., Lacassin, R., Tapponnier, P., Leloup, P. H. and Yem, N. T. 1993, Evidence for active strike-slip movements in Northwestern Vietnam. Terra Abstracts, Abstract Suppl. No. 1 to Terra Nova, 5, 265.

351. Tripathi, N. K. and Singh, P., 2000, Integrated GIS and remote sensing approach to map pollution in upper lake, Bhopal, India. Geocarto. International, 15 (4), 49 – 55.

352. Tripathi, N. K., Siddiqi, M. U., Gokhale, K. V. G. K., 2000, Directional morphological image transforms for lineament extraction from remotely sensed images. International Journal of Remote Sensing, 21 (17), 3281 – 3292.

353. Tripathi, N. K. and Bajpai, V. N., 1998, Remote Sensing Applications in Geosciences, Anmol Publications Pvt. Ltd., New Delhi.

354. Tronin, A. A., 2010, Satellite remote sensing in seismology. A review. Remote Sensing, 2, 124 – 150 (DOI: 10.3390/rs2010124).

355. Tronin, A. A., 2006, Remote sensing and earthquakes: A review. Physics and Chemistry of Earth, 31, 138 –142.

356. Tronin, A. A., 1996, Satellite thermal survey—a new tool for the study of seismoactive regions. International Journal of Remote Sensing, 17, 1439 –1455.

357. Tronin, A. A., Hayakawa, M., Molchanov, O. A., 2002, Thermal IR satellite data application for earthquake research in Japan and China. Journal of Geodynamics, 33, 519 – 534.

358. Tsimi, C., Ganas, A., Soulakellis, N., Kairis, O., and Valmis, S., 2007, Morphotectonics of the Psathopyrgos active fault, western Corinth Rift, Greece. International Conference of the Geological Society of Greece, Athens 24-26 May 2007.

359. USGS, 2004. http://seamless.usgs.gov/website/seamless/faq/srtmfaq.as (visited on April 2009).

360. Vaze, J., and Teng, J., 2007, Impact of DEM Resolution on Topographic Indices and Hydrological Modelling Results. In: Oxley, L. and Kulasiri, D. (ed.). MODSIM 2007 International Congress on Modelling and Simulation, Australia, December 2007, 706-712.

361. Veevers J.J., 1981, Morphotectonics of Rifted Continental Margins in Embryo (East Africa), Youth (Africa-Arabia), and Maturity (Australia). The University of Chicago Press.

362. Verma, R.K., Mukhopadhyay, M. and Ahluwalia, M.S., 1976, Seismicity, gravity, and tectonics of northeast India and northern Burma. Bulletin of the Seismological Society of America, 66 (5), 1683-1694.

363. Verma, R.K., Mukhopadhyay, M. and Nag, A.K., 1980, Seismicity and tectonics in S. China and Burma. Tectonophysics, 64, 85-96.

364. Verrios, S., Zygouri, V. and Kokkalas, S., 2004, Morphotectonic analysis in the Eliki fault zone (Gulf of Cornith, Greece). Bulletin of the Geological Society of Greece. V-XXXVI. Proc. 10th International Congress, Thessaloniki, 1706-1715.

365. Walker, R. and Jackson, J., 2002, Offset and evolution of Gowk fault, S. E. Iran: a major intra-continental strike-slip system. Journal of structural Geology, 24, 1677-1698.

366. Wang, H. and Ellis, E.C, 2005, Spatial accuracy of orthorectified IKONOS imagery and historical aerial photographs across five sites in China. International Journal of Remote Sensing, 26 (9), 1893 -1911.

367. Warner, R.F., 1971, The early Tertiary landscape of southern New England, New South Wales. Australian Geographer, 11, 242– 258.

368. Warner, R.F., 1992, Floodplain evolution in a New South Wales coastal valley Australia, spatial process variations. Geomorphology, 4, 447– 458.

369. Warren, S.D., Hohmann, M.G., Auerswald, K. and Mitasova, H., 2004, An evaluation of methods to determine slope using digital elevation data. Catena, 58, 215-233.

370. Watson, D.F., 1992, Contouring: A Guide to the Analysis and Display of Spatial Data. Pergamon, Oxford, p340.

371. Weibel, R. and Heller, M., 1991, Digital terrain modeling. In Geographical Information Systems: Principles and Applications. Edited by D.J. Maguire, M.F. Goodchild and D.W. Rhind (London: Longman), 269-297.

372. Welch, R., and Ehlers, M., 1987, Merging multiresolution SPOT HRV and Landsat TM data. Photogrammetric Engineering and Remote Sensing, 53, 301- 303.

373. Weldon, R. J., 1986, Late Cenozoic geology of Cajon Pass, implication for tectonics and sedimentation along the San Andreas fault (Ph.D Thesis). California Institute of Technology, Pasadena.

374. Weldon, R., Sieh, K., Zhu, Ch. N., Han, Y., Yang, J.W., and Robinson, S. 1994, Slip rate and recurrence interval of earthquakes on the Hong He (Red River) fault, Yunnan. PRC, Proc. IWSSH-SEA, 27 Jan–4 Feb 1994, Hanoi, 244–248.

375. Wells, S.G., Bullard, T.F., Menges, C.M., Drake, P.G., Karas, P.A., Kelson, K.I., Ritter, J.B., and Wesling, J.R., 1988, Regional variations in the tectonic geomorphology along a segmented convergent plate boundary, Pacific Coast of Costa Rica. J. Geomorphology, 1, 239-265.

376. Wharton, G., 1995, The channel-geometry method: guidelines and applications. Earth Surface Processes and Landforms, 20,649– 660.

377. Whipple, K. X., and Dunne, T., 1992, Debris flow fans in Owen Valley, California. Geological Society of America, 104, 39-43.

378. Whipple, K. X. and Tucker, G.E., 1999, Dynamics of the stream-power river incision model, Implications for height limits of mountain ranges, landscape response timescale, and research needs. Journal Geophysical Research, 104, 17,661-17,674.

379. Whipple, K.E. Kirby, E. and Brocklehurst, S.H., 1999, Geomorphic limits to climate induced increases in topographic relief. Nature, 401, 39-43.

380. Wobbe F., Gloaguen R., and Stanek K., River profile analysis for neotectonic analysis. Submitted to Computer & Geosciences.

381. Wobus, C., Whipple, K., Kirby, E., Snyder, N., Johnson, J., Spyropolou, K., Crosby B. and Sheehan, D., 2006, Tectonics from topography: Procedures, promise and pitfalls. In: Willett, S. D., N. Hovius, M. T. Brandon und D. Fisher (Hrsg.): Tectonics, climate, and landscape evolution, Geological Society of America Special Paper 398, S. Geological Society of America, 55-74.

382. Wong, A., Wu, L., Gibbons, P. B. and Faloutsos, C., 2005, Fast estimation of fractal dimension and correlation integral on stream data. Information Processing Letters, 95, 91-97.

383. Wood, J. and Fisher, P., 1993, Assessing interpolation accuracy in elevation models. IEEE Computer Graph. Appl., 13(2), 48–56.

384. Wood, J., 1994, Visualizing contour interpolation accuracy in digital elevation models. Hearnshaw, H.M., Unwin, D.J. (Eds.), Visualization in Geographical Information Systems. Wiley, Chichester, 168-180.

385. Zang, Y., 1999, A new merging method and its spectral and spatial effects. International Journal of Remote Sensing, 20, 2003-2014.

386. Zizioli D., 2008, DEM-based morphotectonics analysis of Western Ligurian Alps. Scientifica Acta, 2, (2), 44 – 47.

URL LINKS:

1. http://www.nrsc.gov.in/
2. http://glcfapp.glcf.umd.edu:8080/esdi/index.jsp
3. http://srtm.csi.cgiar.org/I
4. http://www.gdem.aster.ersdac.or.jp/search.jsp
5. http://en.wikipedia.org/wiki/Morphotectonics
6. http://books.google.co.in
7. http://forums.esri.com
8. http://www.hydroeurope.org
9. http://www.google.co.in/#sclient=psy&hl=en&biw=1366&bih=667&source=hp&q=Creating+a+Topographic+Index+&aq=&aqi=&aql=&oq=&pbx=1&fp=704c7470618df8cb
10. http://www.crwr.utexas.edu/gis/gishydro04/Introduction/Exercises/Ex4.htm
11. http://www.hydroeurope.org/jahia/webdav/site/hydroeurope/shared/Exercices/GIS%20%20Hydro%20Models/Watershed%20and%20Stream%20Network%20Delineation_Tutorial.pdf
12. http://www.crwr.utexas.edu/gis/gishydro07/Introduction/Exercises/Ex4.htm
13. http://www.google.co.in/url?sa=t&source=web&cd=7&ved=0CFUQFjAG&url=http%3A%2F%2Fciteseerx.ist.psu.edu%2Fviewdoc%2Fdownload%3Fdoi%3D10.1.1.128.8081%26rep%3Drep1%26type%3Dpdf&ei=6229Tce8OMumrAe7p6mTBg&usg=AFQjCNGEEhWe_IbkEEptm5Y1NfJTJjMoTg&sig2=6XCbCOLK3loSAqU6wD5ZNQ
14. http://ucsb.academia.edu/ReginaldArcher/Papers/363859/TERRAIN_FEATURE_XTRACTION_FROM_VARIABLE_RESOLUTION_DIGITAL_ELEVATION_MODELS
15. http://hydrology.neng.usu.edu/taudem/90info.htm
16. http://hydrology.neng.usu.edu/taudem/
17. http://www.mappingsciences.org.au/journal.htm
18. http://ucsb.academia.edu/ReginaldArcher/Papers/363859/TERRAIN_FEATURE_EXTRACTION_FROM_VARIABLE_RESOLUTION_DIGITAL_ELEVATION_MODELS
19. http://www.erdas.com/service/support/SpatialModels/Spatial_Models.aspx
20. http://gis.ess.washington.edu/data/erdas_pdfs/LPS_ATE.pdf

ANNEXURE-I

Summary of control points, tie points and error parameters for DEM generation from Cartosat-1

Rational function refinement summary for first image (612-283)

Triangulation Report with LPS

The output image x, y units: pixels

The output ground X, Y units: degrees

The output ground X, Y residual units: meters

The output ground Z and its residual units: meters

Total RMSE = 1.973

Total RMSE after processing= 0.951

Maximum no. of iterations-10

Ground coverage value- 0.00010

Table-1 Coordinates of control points

Point ID	X	Y	Z	Overlap
1	93.01	24.63	540	2
2	93.08	24.71	35	2
3	93.01	24.81	27	2
4	93.12	24.82	35	2
5	93.21	24.67	80	2
6	93.19	24.84	45	2
7	93.07	24.86	32	2
8	93.09	24.63	25	2
9	93.02	24.88	36	2
10	93.2	24.7	82	2

Table-2 Coordinates of tie points

Point ID	X	Y	Z	Overlap
1	93.01480873	24.63673738	498.3653	2
2	93.07610009	24.71087514	62.1219	2
3	93.01010096	24.80991142	70.8785	2
4	93.1210081	24.81590241	37.2111	2
5	93.20875997	24.66574772	71.07	2
6	93.19026536	24.83864214	19.2419	2
7	93.06917637	24.85889336	39.9424	2

8	93.08698222	24.63138134	10.7099	2
9	93.01896937	24.88289286	65.8939	2
10	93.20382531	24.69901256	62.2266	2
11	93.16676455	24.61851685	307.8796	2
12	93.19575179	24.81108996	49.8653	2
13	93.16223192	24.82350551	48.9048	2
14	93.1373783	24.84914292	52.3338	2
15	93.08410228	24.86434234	37.4625	2
16	93.10254312	24.76728698	18.246	2
17	93.12703898	24.70267324	267.0474	2
18	93.19715433	24.76971124	234.8141	2
19	93.21974023	24.72247135	77.2215	2
20	93.14621703	24.74077361	40.5315	2
21	93.0309189	24.78111432	80.154	2
22	93.03129901	24.82913611	46.4369	2
23	93.07607684	24.80703947	28.0043	2
24	92.97043758	24.72876365	28.2842	2
25	92.95323331	24.65051337	61.2754	2
26	93.02642064	24.67533222	582.6181	2
27	92.99132626	24.69842167	51.1893	2
28	93.06219108	24.7327923	198.464	2
29	93.00533741	24.74502351	49.5239	2
31	93.02837563	24.71567469	61.1329	2
32	92.97923337	24.6453264	45.5961	2
33	92.96534159	24.69180751	60.2769	2
34	93.01575952	24.85585994	44.8318	2
36	93.2382966	24.80434576	104.5781	2
37	93.21782262	24.85866426	16.2723	2
38	93.00789617	24.89042849	49.02	2
39	93.10291305	24.67635576	55.4846	2
40	93.13095377	24.63160914	44.3593	2
41	93.13194165	24.76899512	19.4212	2
42	93.10298958	24.82967582	97.3221	2
43	93.13084144	24.85875167	56.0288	2

44	93.10620583	24.74064568	25.7118	2
45	93.05064125	24.64633809	247.5082	2

Rational function refinement summary for Second image (612-284)

Triangulation Report with LPS

The output image x, y units: pixels

The output ground X, Y units: degrees

The output ground X, Y residual units: meters

The output ground Z and its residual units: meters

Total RMSE = 1.487

Total RMSE after processing= 0.514

Maximum no. of iterations-10

Ground coverage value- 0.00010

.

Table-3 Coordinates of control points

Point ID	X	Y	Z	Overlap
1	93.01	24.63	550	2
2	93.08	24.63	34	2
3	93.16	24.47	58	2
4	93.03	24.50	32	2
5	92.92	24.44	50	2
6	93.0	24.41	30	2
7	93.12	24.37	60	2

Table-4 Coordinates of tie points

Point ID	X	Y	Z	Overlap
1	93.01051412	24.63394395	561.0134	2
2	93.08308147	24.62875355	25.4608	2
3	93.15802034	24.46443714	73.251	2
4	93.03056556	24.5056575	20.6396	2
5	92.91683389	24.43773943	7.8937	2
6	93.00255197	24.40790515	82.5509	2
7	93.11842994	24.37156447	43.4385	2

8	92.94887781	24.67196509	49.7599	2
9	93.12945257	24.63830177	81.2858	2
10	93.13768072	24.63584533	105.8082	2
11	93.16052307	24.63448	456.5156	2
12	93.15978318	24.63177754	443.7046	2
13	93.07844314	24.64619426	32.2164	2
14	93.1984063	24.61068182	104.5223	2
15	92.97010852	24.64576949	46.3878	2
16	92.97044153	24.64414325	49.1193	2
17	93.06515965	24.62732281	75.663	2
18	93.07323765	24.62361979	58.0016	2
19	93.12581256	24.61888042	77.5995	2
20	93.18564652	24.60538975	177.8575	2
21	92.94044297	24.64511335	48.1134	2
22	92.94486861	24.64566307	47.2712	2
23	92.96640272	24.63954877	55.8927	2
24	92.96578942	24.63941572	54.9566	2
25	93.06387117	24.62405638	51.5609	2
26	93.07382974	24.61937394	52.0103	2
27	93.07185818	24.61945036	53.5627	2
28	93.0977705	24.61397367	42.3668	2
29	93.09710608	24.61288465	47.1813	2
30	93.10324474	24.61606907	45.249	2
31	93.12357238	24.61094613	62.6586	2
32	93.18553562	24.60111918	134.9805	2
33	93.18873238	24.59829826	162.0844	2
34	92.93995431	24.64238078	50.783	2
35	92.93609499	24.64184432	48.3569	2
36	92.96254334	24.63673248	50.235	2
37	92.98837719	24.6256944	67.0183	2
38	93.06202683	24.61084368	45.0712	2
39	93.12035893	24.6005567	64.6981	2
40	92.9370446	24.62734994	51.2287	2
41	92.96090035	24.61577675	48.0702	2

42	93.05796936	24.60130296	92.0507	2
43	93.15773795	24.57657175	212.8483	2
44	93.1653941	24.58036692	281.8792	2
45	93.17073898	24.57865873	209.0101	2
46	93.17420104	24.57454029	225.7082	2
47	92.93099643	24.61799488	60.5105	2
48	92.98421128	24.60640014	57.9132	2
49	92.98582213	24.60913557	70.1697	2
50	92.98716649	24.60828945	67.2617	2
51	93.04339912	24.59528023	84.5145	2
52	93.06944959	24.59213966	30.5118	2
53	93.11229229	24.5836494	53.6083	2
54	93.11767033	24.58015268	153.835	2
55	93.12373213	24.58267032	252.4768	2
56	92.93155805	24.61466359	50.0592	2
57	92.98724749	24.6037733	72.2142	2
58	93.06355349	24.58841619	92.0576	2
59	93.11507374	24.57570198	88.5792	2
60	93.17460695	24.5521571	166.9731	2
61	92.95405448	24.58857169	57.0938	2
62	92.95345622	24.58736995	56.1338	2
63	92.97811173	24.58313462	49.8279	2
64	93.05578833	24.56709002	57.9293	2
65	93.12444068	24.55331599	344.9189	2
66	93.14142379	24.55322333	481.4373	2
67	92.95365034	24.58605296	53.9423	2
68	92.95281148	24.58409865	55.1799	2
69	92.95014912	24.58207831	52.7858	2
70	92.97673284	24.57655723	52.926	2
71	92.98472367	24.57919518	56.6526	2
72	93.09020166	24.5586463	46.6346	2
73	93.16002178	24.53536889	135.2689	2
74	92.94830882	24.55873703	66.0201	2
75	93.04585998	24.54214775	31.8953	2

76	93.0708462	24.5367979	80.3897	2
77	93.07511557	24.53416813	47.0462	2
78	93.08675719	24.53132113	157.6235	2
79	93.13588975	24.52418281	525.8366	2
80	93.13414816	24.52222589	377.8163	2
81	92.91959445	24.56275092	55.4379	2
82	92.97632166	24.5504106	69.5623	2
83	93.12727636	24.52179932	458.3028	2
84	93.04385352	24.51663177	35.9739	2
85	93.15377488	24.49785894	129.1187	2
86	92.91595635	24.53610996	57.2754	2
87	92.94149886	24.53373741	48.8895	2
88	92.94234931	24.53187795	48.604	2
89	93.02669646	24.51522775	69.7003	2
90	93.08674103	24.50322656	223.4379	2
91	93.10792209	24.50029835	490.751	2
92	93.14963588	24.49213658	122.662	2
93	93.15333648	24.49310771	113.0451	2
94	93.04392048	24.50397	113.9635	2
95	93.07017435	24.50176777	68.941	2
96	92.91054479	24.52813234	72.084	2
97	93.14522047	24.47131247	147.3735	2
98	92.93507909	24.50720395	48.1339	2
99	92.96024021	24.50502431	64.475	2
100	93.05726531	24.48051081	130.0137	2
101	93.05478536	24.47675745	85.8916	2
102	93.13910366	24.46259413	216.0494	2
103	92.93200767	24.50050309	59.5147	2
104	92.96103923	24.48474897	64.5213	2
105	93.14931004	24.44708228	73.0011	2
106	93.03144479	24.46874843	91.7995	2
107	92.93349422	24.47956093	82.8588	2
108	92.89867238	24.48064549	72.1946	2
109	92.91256221	24.47894084	68.3405	2

110	93.00341603	24.46126857	103.378	2
111	93.03183887	24.45116496	54.3323	2
112	93.13837675	24.43453758	108.6212	2
113	93.0310517	24.44977783	40.4939	2
114	92.92483396	24.46120585	66.9233	2
115	93.06104597	24.43408976	135.9384	2
116	92.89848637	24.45974968	81.5534	2
117	92.93373064	24.44793513	80.9049	2
118	93.04919401	24.42385965	136.2556	2
119	93.10464063	24.41779038	528.7141	2
120	93.1051568	24.41736808	518.2949	2
121	93.13310552	24.4112765	56.7568	2
122	93.06061582	24.42112619	143.1943	2
123	92.94276758	24.43787103	76.1022	2
124	93.02439519	24.42190994	66.876	2
125	93.10291626	24.40390509	658.8948	2
126	92.91407512	24.42723354	50.4079	2
127	93.12474245	24.38675496	48.9929	2
128	93.12360041	24.38505043	50.3056	2
129	92.91222421	24.42413964	52.8664	2
130	93.04539642	24.40010322	168.297	2
131	93.0248496	24.39767355	91.6242	2
132	93.09477095	24.38275944	661.3005	2
133	93.09485249	24.3813331	678.062	2
134	93.01772272	24.39180098	41.4241	2
135	93.04766469	24.3856722	173.9183	2
136	92.98987349	24.38952669	91.8633	2

Rational function refinement summary for Second image (612-285)

Triangulation Report with LPS

The output image x, y units: pixels

The output ground X, Y units: degrees

The output ground X, Y residual units: meters

The output ground Z and its residual units: meters

Total RMSE = 1.330

Total RMSE after processing= 0.612

Maximum no. of iterations-10

Ground coverage value- 0.00010

Table-5 Coordinates of control points

Point ID	X	Y	Z	Overlap
1	93.013	24.418	35	2
2	93.022	24.236	38	2
3	93.04	24.338	50	2
4	93.124	24.375	48	2
5	93.098	24.415	757	2
6	92.922	24.442	42	2
7	92.888	24.245	76	2
8	92.883	24.214	241	2

Table-6 Coordinates of tie points

Point ID	X	Y	Z	Overlap
1	93.0124798	24.41772047	34.5254	2
2	93.02257197	24.23569811	44.6957	2
3	93.03967788	24.3375412	41.4999	2
4	93.12368131	24.37528097	41.6136	2
5	93.09868681	24.41494127	767.1649	2
6	92.9223094	24.44174476	46.6044	2
7	92.88812395	24.2450999	75.1888	2
8	92.88246742	24.21497385	236.0923	2
12	93.08232813	24.42013153	456.579	2
13	93.11774735	24.40932978	469.4098	2
14	92.97503626	24.43376061	505.1078	2
15	93.02977012	24.4257559	53.307	2
16	93.08057233	24.4147618	467.7665	2

17	93.15400147	24.39771251	569.8045	2
18	92.92247453	24.44093196	53.4576	2
19	92.92133842	24.43748431	45.7218	2
20	92.97595766	24.42067784	332.4387	2
21	92.97122708	24.41595346	430.8728	2
22	93.05175155	24.40112972	196.5822	2
23	92.91924447	24.4236095	123.2453	2
24	92.92287239	24.42166377	117.1361	2
25	93.02488707	24.39762933	55.7755	2
26	93.05068534	24.39384505	214.1476	2
27	93.08265398	24.38904615	872.185	2
29	92.89224465	24.41939923	180.7517	2
30	92.96674208	24.39172271	409.3553	2
32	93.07983364	24.3694262	450.8984	2
33	92.88872953	24.39970152	76.8401	2
34	92.99424075	24.38205805	102.5815	2
35	93.14185891	24.35141876	277.207	2
36	92.91528769	24.39413973	133.4949	2
37	92.92426168	24.38975771	246.4397	2
38	93.09152126	24.35668145	278.0992	2
39	92.88722248	24.39146524	55.4085	2
40	92.93178759	24.38361089	115.4554	2
41	92.96263336	24.37097839	597.3245	2
42	93.11762275	24.34063099	379.9156	2
43	92.89857968	24.36755884	161.694	2
44	92.97834045	24.35276651	495.3482	2
45	93.01271618	24.3506409	180.703	2
46	93.03639101	24.34556321	37.9476	2
47	93.03799472	24.34411793	65.8898	2
48	93.05388456	24.33773987	263.8096	2
49	93.1251036	24.32507614	445.5012	2
50	92.87532759	24.35918348	196.5094	2
51	92.93353736	24.34475547	568.1053	2
52	93.08444471	24.31820933	145.0986	2
53	92.9988168	24.32394772	656.4343	2
54	93.1133292	24.30569593	309.2718	2
55	92.87560109	24.34571322	147.2059	2
56	92.92721123	24.33498574	264.8018	2
57	92.93261605	24.33167722	454.0321	2
58	92.97786248	24.32606751	533.8208	2
59	93.0302312	24.31599877	40.9014	2
60	93.0294505	24.31496242	45.3827	2
61	93.0338547	24.31608533	146.7773	2
62	93.08016481	24.30728773	82.6099	2
63	93.10161222	24.30083062	522.6235	2
65	92.90276776	24.33348853	352.7836	2
66	92.94856892	24.30956068	655.148	2

67	92.9770099	24.30482597	673.0035	2
68	93.05168031	24.28432691	47.0405	2
69	93.10511905	24.276467	703.257	2
70	92.87025999	24.31759465	188.081	2
71	92.89326591	24.31177434	248.7355	2
72	92.96145313	24.29872715	524.0584	2
73	92.96689976	24.2959731	662.4302	2
75	93.05026279	24.28315268	53.4256	2
76	93.05141247	24.28151406	47.5705	2
77	93.0518766	24.27855204	45.3167	2
80	92.86406425	24.29249491	192.0655	2
81	92.89039163	24.28500821	210.4584	2
82	92.92267022	24.28324467	535.5952	2
83	92.96912173	24.27162785	669.902	2
84	92.99374946	24.26600591	142.2184	2
85	93.04150364	24.25684008	167.6854	2
86	93.09643533	24.24506064	531.2634	2
87	93.09860747	24.24702959	610.9459	2
88	92.8644148	24.28753931	175.2324	2
89	92.96481023	24.26939386	684.704	2
90	92.99239264	24.26318779	119.6115	2
91	93.04344226	24.25177254	216.2634	2
92	93.04433399	24.25130675	234.7766	2
93	93.07618444	24.24663384	450.3111	2
94	93.11487749	24.24050178	828.0912	2
95	92.8534934	24.26378487	266.3879	2
96	92.88498439	24.25943354	357.2791	2
97	92.93489528	24.24864069	374.9327	2
98	92.9564543	24.24320186	692.1039	2
99	92.97939833	24.23987153	562.1476	2
100	92.98479924	24.2369949	417.9889	2
101	93.09389797	24.21459381	706.0188	2
102	92.88110235	24.25333336	231.2013	2
103	92.95412488	24.23899091	650.3193	2
104	92.98564314	24.23095212	453.1158	2
105	93.00493954	24.23003583	322.3179	2
106	92.8547984	24.25423104	165.7772	2
107	92.87695612	24.23726875	94.6337	2
108	93.00899603	24.20848057	179.0603	2
109	93.03463636	24.20506522	387.0132	2
110	93.06467643	24.19715731	660.7486	2
111	92.86100965	24.23495614	76.4252	2
112	92.87678333	24.23291644	117.9981	2
113	92.87926656	24.23106255	146.918	2
114	92.90629681	24.22674406	85.6814	2
115	93.08231709	24.18932545	757.209	2
117	93.00176079	24.19923424	60.0633	2

118	92.84358498	24.22225021	296.6763	2
119	92.8742043	24.22073037	146.8428	2
121	92.89791106	24.19979242	158.4052	2
122	92.94366059	24.19098651	505.5185	2
123	92.95489297	24.18839856	470.8872	2
124	93.02621471	24.17473128	651.7966	2
125	92.85695046	24.20678105	169.5274	2
126	92.91741074	24.19427687	323.2973	2
127	92.94419874	24.18737967	461.8879	2
128	92.97120956	24.18172026	617.9972	2
129	93.02465416	24.17377069	645.2502	2
130	93.03691959	24.17134961	834.16	2
131	93.05557087	24.16758882	722.2274	2
132	92.89372311	24.19186527	68.8591	2
133	92.91926808	24.18561012	251.773	2
134	92.94275617	24.18330651	393.5934	2
135	92.99773565	24.16920661	284.0443	2
136	93.02157837	24.16834414	645.2729	2
137	92.86699205	24.18956213	121.9476	2
138	93.08221001	24.1485444	525.161	2

ANNEXURE – II

LIST OF PUBLICATIONS

List of publications out of this research work

1. Das, J. D., Saraf, A. K., and **Yazdana Shujat** (2010) Remote sensing technique in identifying geometry and geomorphic features of Indo-Burman frontal fold belt, *International Journal of Remote Sensing,* Vol. 31 (16), 4481-4503.

2. Das, J. D., **Yazdana Shujat** and Saraf, A. K., (2010) Spatial technologies in deriving the morphotectonic characteristics of tectonically active western Tripura region, Northeast India, *Journal of the Indian Society of Remote Sensing.* DOI: 10.1007/s12524-011-0090-6.

3. Das, J. D., **Yazdana Shujat**, Saraf, A. K., Rawat, V., and Sharma, K., (2011) Morphotectonic features and fault propagation folding of Bhuban Hills, NE India using Satellite image and DEM, (2011), *Journal of the Indian Society of Remote Sensing*. 39 (1), 73-81, DOI: 10.1007/s12524-011-0066-6.

4. **Yazdana Shujat,** Das, J. D., and Saraf, A. K., (2011) DEM generation, comparison and accuracy assessment using GIS, *Journal of Applied Geomatics,* **(submitted).**

Other publications

5. Rawat, V., Saraf, A. K., Das J. D., Sharma, K. and **Yazdana Shujat, (**2011), Anomalous land surface temperature and outgoing long-wave radiation observations prior to earthquakes in India and Romania, *Natural Hazards,* V-56, DOI 10.1007/s11069-011-9736-5.

6. Saraf, A. K., Das, J. D., Biswas, A., Rawat, V., Sharma K. and **Yazdana Shujat,** (2010), SAR Interferometry in post-seismic ground deformations detection related with 2001 Bhuj Earthquake, India, *International Journal of Remote Sensing* **(Accepted).**

7. Sharma, K., Saraf, A. K., Das, J. D., Rawat, V., and **Yazdana Shujat** (2010), SRTM and ASTER DEM characteristics of two areas from Himalayan region, *International Geoinformatics Research and Development Journal* **(Accepted).**

8. Rawat, V. Saraf, A. K., Das, J. D., Sharma K. and **Yazdana Shujat** (2010), Remote Sensing Observation of Earthquake Thermal Precursors in India and Iran, *International Journal of Applied Earth Observation and Geoinformation* **(submitted).**

ANNEXURE – III

REPRINTS OF FEW SELECTED PUBLICATIONS

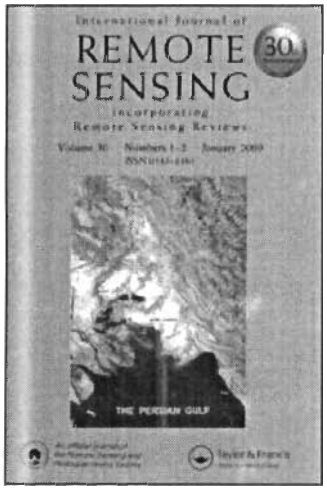

International Journal of Remote Sensing
Publication details, including instructions for authors and subscription information:
http://www.informaworld.com/smpp/title~content=t713722504

A remote sensing technique for identifying geometry and geomorphological features of the Indo-Burman frontal fold belt

J. D. Das[a]; A. K. Saraf[b]; Yazdana Shujat[b]
[a] Department of Earthquake Engineering, Indian Institute of Technology Roorkee, Uttarakhand, India [b] Department of Earth Sciences, Indian Institute of Technology Roorkee, Uttarakhand, India

Online publication date: 13 September 2010

To cite this Article Das, J. D. , Saraf, A. K. and Shujat, Yazdana(2010) 'A remote sensing technique for identifying geometry and geomorphological features of the Indo-Burman frontal fold belt', International Journal of Remote Sensing, 31: 16, 4481 — 4503
To link to this Article: DOI: 10.1080/01431160903154366
URL: http://dx.doi.org/10.1080/01431160903154366

International Journal of Remote Sensing
Vol. 31, No. 16, 20 August 2010, 4481–4503

Taylor & Francis
Taylor & Francis Group

A remote sensing technique for identifying geometry and geomorphological features of the Indo-Burman frontal fold belt

J. D. DAS†, A. K. SARAF*‡ and YAZDANA SHUJAT‡
†Department of Earthquake Engineering, Indian Institute of Technology Roorkee, Uttarakhand, India
‡Department of Earth Sciences, Indian Institute of Technology Roorkee, Uttarakhand, India

(*Received 25 February 2008; in final form 17 November 2008*)

Satellite images are capable of displaying prominently the geometry and morphology of folds, especially when these have large spatial extent. The frontal part of the Indo-Burman fold belt, falling in parts of Bangladesh and north-east India, has developed into exemplary linear N–S oriented doubly plunging folds in late Tertiary sedimentary rock sequences and are arranged in a set of alternating ridge-forming anticlines and valley-forming synclines. Formation of these folds is attributed to E–W oriented compressional tectonics resulting out of eastward subduction of the Indian plate below the Burmese plate. Fold types present in the area appear to be simple but the present fold geometrical arrangement reveal some interesting features. The 90-m SRTM-DEM (Shuttle Radar Topographic Mission–Digital Elevation Model), remote sensing techniques, principal component analysis and resolution merging were used to understand the geometry and morphology of the folds covering a large area, through comparative assessment and enhancement of the structural features. This study includes identification of: multi-folds within a visibly single entity; the overlapping nature of folds and the interrelation between anticlines; the geometry of fold noses; fault-affected fold limbs causing bulging; and anticline bifurcation and formation of elliptical and cuspate synclines; as well as recognition of exposed eroded-out folded layers of the anticline and the effect of deformation and faulting. The doubly plunging nature of the folds and higher topography at the middle latitudes of the study area could have formed due to up-arching tectonic activity.

1. Introduction

Folds on the Earth's surface are one of the most commonly and prominently occurring structural features that can be imaged by Earth-observing satellites. Geometry and morphology of the folds are prominently displayed on satellite images, especially in the case of large-scale folds. Folded rocks remain one of the most attractive subjects for structural geologists all over the world (Hobbs 1976, Davis and Reynolds 1984, Price and Cosgrove 1990). Satellite images have provided plan views and allowed understanding of the geometry and extent of the folds formed on the Earth's surface (Sabins 1987, 1997, Lillesand and Kiefer 2000, Drury 2001). Folds are such evident features that even very low resolution imaging technology can pick up regional-scale folds. Folds are formed when planar surface such as beddings are warped into a

*Corresponding author. Email: saraffes@iitr.ernet.in

International Journal of Remote Sensing
ISSN 0143-1161 print/ISSN 1366-5901 online
http://www.tandf.co.uk/journals
DOI: 10.1080/01431160903154366

curviplanar structure. The resulting geometry of folding is dependent on phases of deformation. One phase deformation would result in simple fold geometry, whereas a superimposed episode of folding often generates a complex outcrop (i.e. interference) pattern of superposed folds.

The Zagros fold-thrust belt in SW Iran, exhibiting a series of simple anticlines characterized by large open folding with widths of 10 km and lengths of 100 km or more, formed due to continental convergence between Arabia and Asia in the late Tertiary, is one of the most studied tectonic zones in the world (Stocklin 1968, Colman-Sadd 1978, Alavi 2004, McQuarrie 2004). This fold-thrust belt constitutes piles of folded and faulted rocks varying in thickness from 4 to 7 km of mainly Paleozoic and Mesozoic succession overlain by 3–5 km of Cenozoic siliciclastic carbonate rocks (Alavi 2004). The concentric folds of Zagros have been affected by detachment folds, fault propagation fold, fault bend folds, strike slip and normal faulting.

One such area showing exemplary linear N–S orientated plunging folds formed in late Tertiary sedimentary rocks occurs in parts of Bangladesh and north-east India. The folds are arranged in a set of alternating anticlines forming higher ridges and synclines forming the linear valleys, constituting the frontal fold belt of the Indo-Burman fold belt (see figures 1(*a*) and 2). These folds formed in the sedimentary wedge developed over the inclined subducting Indian Plate generating E–W trending compressional tectonics (see figure 1(*b*)); regionally the study area also remains under the influence of Himalayan orogeny and plateau tectonism in the north (see figure 1(*a*)). Folds are considerably open on the westernmost side but folding intensity increases as one moves eastward. The fold ridges also have been affected by faulting, essentially forming a fold thrust belt. Several anticlines and synclines have been delineated and studied in detail (Ganguly 1993). We have focused our studies on the westernmost part, as many interesting interplays of anticlines and synclines can be seen.

In the study area, outcrops of anticlines and synclines of different length, width and shape are exposed in what appear to be simple folds. However, some interesting geometry can be seen if these features are studied on satellite images. Several areas of interest (see figure 2) exhibiting a specific folding pattern have been selected for detailed studies and subsets were prepared using ERDAS Imagine 9.0. These fold patterns are studied here in view of their arrangement, geometry and morphology using DEM (digital elevation model), satellite images and GIS (Geographical Information System) techniques. This study also helped reveal the nature of deformation that the area has experienced. Data used for this study are Landsat ETM+ (Enhanced Thematic Mapper) images (Path-136, Rows-43, 44 and 45; dated 19 December 1999 and 7 February 2001) and 90-m SRTM-DEM (Shuttle Radar Topographic Mission–Digital Elevation Model).

2. Geology and tectonics

The study area forms part of the Neogene Surma basin, comprising a repetitive succession of arenaceous and argillaceous sediments, the thickness of which ranges from about 5.7 km to 10 km (Ganguly 1993). The sequence of sediments shows thinning upward known as rhythmites (Nandy 2001). The marine sediments are overlain by the fluvial deposits of Pliocene-Quaternary-Recent river deposits in the topographic and structural low. The depositional basin configuration is attributed to the eastward subduction of the Indian plate below the Burmese plate with the formation of an eastward inclined depositional basin (see figure 1(*b*)). A sedimentary wedge

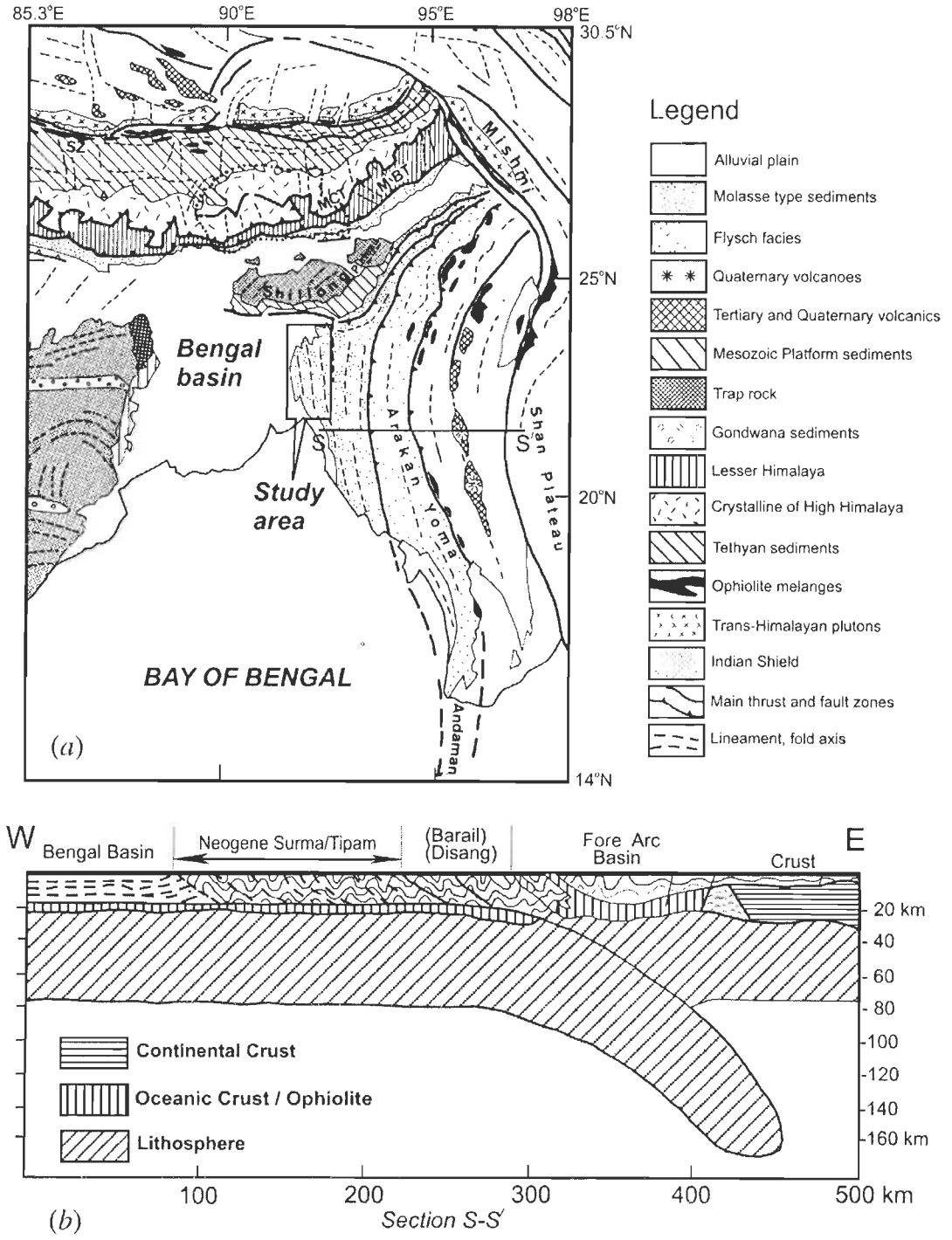

Figure 1. (*a*) Frontal part of the Indo-Burman fold belt forming the study area in the regional tectonic perspective. Source of regional tectonic set-up is Gansser (1983), reproduced with kind permission of Springer Science + Business Media. (*b*) An E–W section showing inter-relation between the tectonic plates and geological set-up (Redrawn from Das Gupta and Nandy 1995. Every effort has been made to obtain permission to reproduce this image). Neogene Surma/ Tipam comprised of mudstone, sandstone and siltstone and Barail/Disang (Oligocene-Eocene) comprised of sandstone, shale and limestone.

Figure 2. Colour-coded 90-m SRTM-DEM of the study area showing N–S trending linear fold ridges with westward curvature. Grey to red colours represent lowest to highest elevations. Hill-shade prepared from the DEM using sun azimuth 315°, sun elevation 45° and *z* factor as 0.00000956 and overlaid on the DEM. Colour codes assigned to different height ranges. ATM-ANTC—Atharamura anticline, BRM-ANTC—Baramura anticline, LGT-ANTC—Langtarat anticline, HKW—Hailakandi-west overlap, ABD—Abdullapur overlap, BRF—Baramura west limb fault, LGF—Langtarat west limb fault, BRS—Baramura south overlap, ATM—Atharamura middle, ATS—Atharamura south, LGM—Langtarat middle, LGS—Langtarat south, TBG—Tuibangadam synclines, BDN—Bandarban nose.

formed in the area and the sediments started developing folds under the active E–W oriented compressional tectonism. With the subsequent increase in E–W directed tectonic forces, folding intensity increased and the westward-lying spacious open basin accommodated all the folding activity. In fact the folds could migrate westward freely, as there was no high landmass to offer resistance to this fold movement. It is

also suggested that the base of these structures is marked by a folded detachment and fault-propagation folds grown over this (Sikder and Alam 2003).

The present architecture of the region is westerly convex N–S fold belt with maximum width of 200 km. Structurally, the area exhibits short to long linear fold ridges, sub-parallel doubly plunging, enechelon anticlinal ridges and synclinal valleys preserved mostly in thinly laminated multilayers of silt shale alternations. Amplitude of these folds is higher than their wavelengths. In general, the axes of the fold show gentle convexity towards the west in the middle part of the belt. Intensity of the folding increases eastward, thereby increasing amplitude, length and tightness of the folding (Sarkar and Nandy 1976, Ganguly 1984, 1993, Nandy 2001). The regional shape of this fold belt is wide in the north but with southward narrowing.

It is also observed that some anticlines bifurcate into two anticlinal ridges with sub-parallel axial trends, and merge again to enclose an elliptical synclinal valley (Nandy 2001), a common feature in the Chittagong (Bangladesh) hills, giving rise to flattened structural domes and basins. Reasons for formation of these types of structures may include a change in orientation of the compressional axis (Nandy 2001). In the study area, i.e. in the western part of the belt, the folds are open with distinct outcrop pattern; whereas the folds are much more compressed and also overturned to the east. The fold types present are concentric, cuspate, box-like folds with flat crests and steep limbs in the study area. The flanks of the anticlines are affected by strike, listric faulting running sub-parallel to the crest of the fold (Sarkar and Nandy 1976). The fold ridges are also segmented by cross and conjugate oblique faults (Nandy 2001).

3. Image processing

3.1 *Principal component analysis (PCA)*

The principal component analysis (PCA) technique is useful for image data compression, image enhancement, change detection and image fusion. In this process all of the information contained in an original *n*-band dataset gets compressed into fewer new bands or components. The statistical PCA process transforms a multivariate dataset of intercorrelated variables into a dataset of new uncorrelated linear combinations of the original variables. The PCA images then become linearly uncorrelated with others because these *n*-components are orthogonal. The total variance of original images is mapped into new components. The first principal component (PC1) has the greatest percentage of the total variance and succeeding components (PC2, PC3, ..., PC*n*) each contain a decreasing percentage of the total variance (Chavez *et al.* 1991, Shettigara 1992, Pohl and Van Genderen 1998, Lillesand and Kiefer 2000). In this study PCA has been carried out using ERDAS Imagine 9.0 (ERDAS Inc., Norcross, Georgia, USA) in the following steps: first all the Landsat ETM+ bands (except thermal ones) were stacked, forming an input file for PCA, and then multilayer output containing PC elements were generated. Bright and different colour coding than the FCC (false colour composite) image gives more contrast to the ridges and surrounding features.

3.2 *Image fusion*

For improved visual and automatic image interpretation multisensor data are integrated; this technique has been used successfully by Cliche *et al.* (1985), Welch and Ehlers (1987), Chavez *et al.* (1991), Pohl and Van Genderen (1998), Saraf (1999) and Zang (1999). Data fusion is the combination of multisensor data which have different

spatial, spectral and radiometric characteristics to acquire a high quality image. Low and high resolution merged images are applicable for many remote sensing applications such as geology, topographic mapping, land cover and land use mapping.

In this study image fusion techniques have been used; these preserve spectral characteristics whilst increasing spatial resolution to provide images of greater quality. First, the Landsat ETM+ FCC images were prepared using the band combination (4 to red, 3 to green and 2 to blue). We have also tested different combinations for making FCC, i.e. Landsat ETM+ bands 5, 4 and 3 and 7, 4 and 3, but it was observed that band combination 4 to red, 3 to green and 2 to blue produced best result especially for our study area. Then the Landsat ETM+ FCC and PAN (panchromatic) data were fused by employing the modified intensity hue saturation merge technique given in ERDAS Imagine 9.0 software. Bilinear interpolation resampling technique has been chosen for this purpose. Although other techniques, e.g. principal component, Brovery transform and multiplicative, for fusing multisensor data are available, it is found that the HIS (hue-intensity-saturation) technique is most suitable for the dataset used in this work. Further, the resultant fused image with higher spatial resolution was helpful in studying and interpreting fold morphology and faults, as the features could be zoomed sufficiently, allowing examination of minor details which was otherwise not possible in 30-m resolution Landsat data.

4. Geometry and geomorphology of folds

Satellite images and DEM of the study area exhibit outcrops of doubly plunging anticlines and synclines having different pattern, shape, size and arrangement. Generally, anticlines form linear higher ridges with well-defined geometry exhibiting the effect of deformational processes that the region has experienced. The top layers of the anticlinal folds have been removed due to erosional processes of natural agents exposing fold limbs and plunging noses which are identifiable on satellite images. Fold limbs belonging to either anticline or syncline are recognized based on the nature of erosional surfaces, geometrical arrangement, the nature of exposed elongated beds and the bedding arrangement pattern as displayed on satellite images (see figure 3). These remote sensing characteristics have been used for interpretation purposes. It is observed that some features such as extent, size and the bulged-out limbs of folds are better depicted on DEM than FCC. For the purpose of detailed analysis, some areas

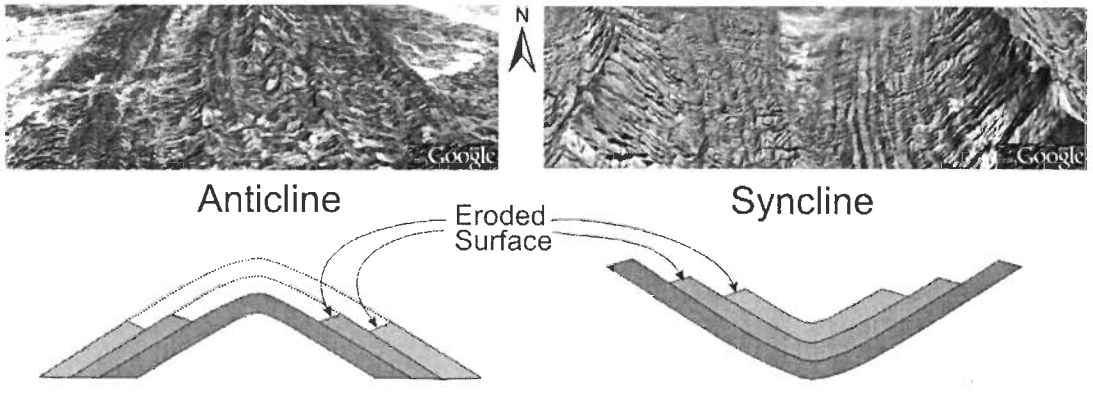

Figure 3. Arrangement of anticlinal and synclinal bedding. Upper pictures are satellite images (grabbed from Google Earth) showing the 3D perspective view of bedding arrangement in case of anticline and syncline. Nature of eroded bedding surfaces is marked in the lower sketches.

with interesting geomorphological features have been selected. Areas of interest have been picked up from 90-m SRTM-DEM, PC-FCC (FCC generated using first three PC elements of Landsat ETM+ bands) and FCC-PAN merged (FCC generated from Landsat ETM+ bands 4, 3 and 2 fused with Landsat PAN). The nature of all the features is more obvious on satellite images, allowing better visual interpretation. It is also noted that false topographic perception plays a role when we view the features on an image (Saraf *et al.* 1996) and in order to nullify this effect images were rotated suitably.

The prominent westernmost individual anticlinal ridges encountered are Baramura, Atharamura, Langtarat, etc. (moving eastward from the plains; see figure 2). All these anticlines occur partly in Bangladesh and north-east India (Tripura). The Baramura anticline is a doubly plunging anticline with curved fold axis and bulged-out western fold limbs and is westward bending in the northern part. This anticline extends for about 93.5 km with a maximum width of 245 m and the maximum bulge in the anticline occurs at latitude 28° 35′, with a water gap through which a river crosses over the anticline transversely. The westward bend in the upper part of this anticline is probably due to transverse faulting. The Atharamura and Langtarat anticlines appear as a single continuous long fold ridge with several longitudinal curves and bends with overall westward curvature. But closer examination reveals that these anticlines are constituted by three doubly plunging anticlines. However, the outer complete antclinal fold limbs provide a continuous appearance to the fold ridge. The southernmost part of the Atharamura anticline possesses a clearer exposure of plunging nose, exposing a maximum number of detectable folded layers. The Atharamura and Langtarat anticlines extend for about 200 and 150 km respectively (see figure 2).

By studying satellite images the plunging fold noses could be assessed as delineated based on geometry and bedding arrangement. These are Atharamura middle, Atharamura south (ATM and ATS of figure 2) and Langtarat middle, Langtarat south (LGM and LGS of figure 2). Several subset images from 90-m SRTM-DEM, PC-FCC and FCC-PAN merged, covering the area of upper and lower plunging noses, have been prepared (see figures 4, 5, 6 and 7). It can be seen that in all these cases the outermost sedimentary layer shows continuity, but the inner layers become rounded to form closers. These fold noses are linked through a highland bordered by sedimentary beds. DEMs of figures 4(*a*), 5(*a*) and 6(*a*) are colour-coded to make the parts more distinct. The upper plunging fold nose of the Atharamura middle part are more prominent on colour-coded DEM and FCC-PAN (see figures 4(*a*) and 4(*c*)). Although both the fold noses have same trend, slight bending (towards each other) occurred in the linked region. A similar bending and linking effect can also be seen in case of Atharamura south. In this case the lower plunging fold nose is more prominent. Although the Langtarat middle part shows quite smooth continuity of the fold, the upper and lower plunging fold noses are very prominent and distinct in all the three images (see figures 6(*a*), (*b*) and (*c*)); whereas, in the case of Langtarat south, the lower plunging fold nose is prominent.

It can be observed that the western limb of the Baramura anticline bulges out (BRF of figure 2) considerably, as shown in figure 8. Several limbs (at least four) show bulging with maximum effect on the outer limb, which could have happened due to the faulting. A gravity/growth fault along the western limb (F_L; see figure 8(*b*)) can cause such lateral bulging. Due to a westward down-throw mechanism the limbs moved away, causing the bulging effect. A substantial gap has also been created between the limbs and a linear river valley has developed along the contact of two

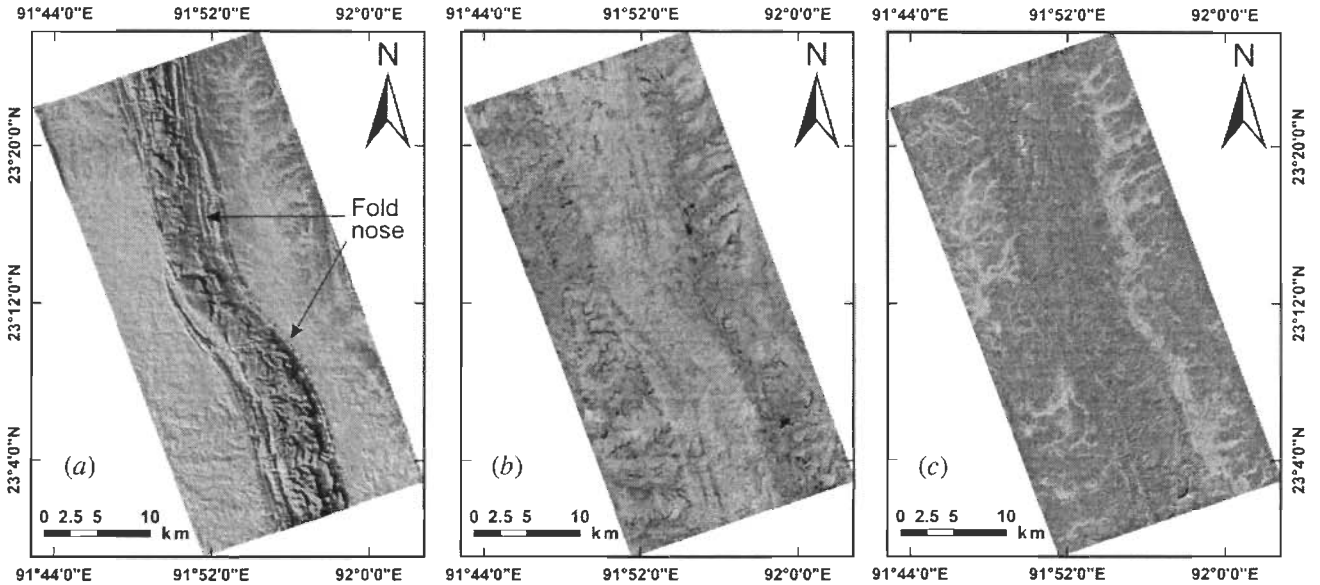

Figure 4. Plunging middle Atharamura anticline noses (ATM in figure 2). (*a*) 90-m SRTM-DEM hill-shade image of DEM prepared using sun azimuth 225° and sun elevation 20° and then colour coded; (*b*) FCC of first three principal component images obtained from Landsat ETM+ multi-band data; (*c*) fused Landsat ETM+ FCC (bands 4, 3 and 2 as red, green and blue) and Landsat PAN image.

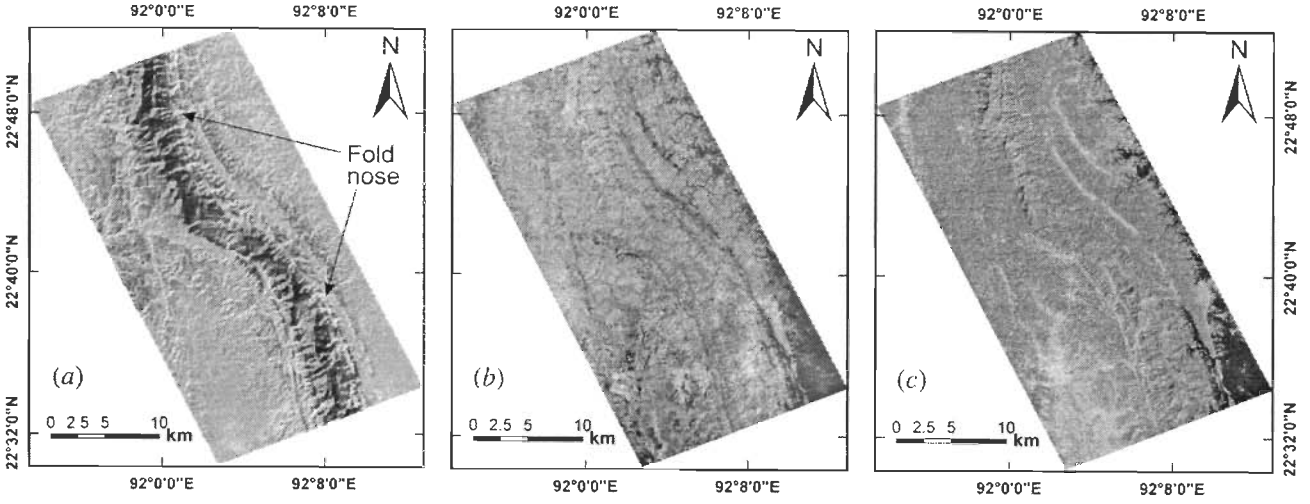

Figure 5. Plunging south Atharamura anticline noses (ATS in figure 2). (*a*) 90-m SRTM-DEM hill-shade image of DEM prepared using sun azimuth 315° and sun elevation 20° and then colour coded; (*b*) FCC of first three principal component images obtained from Landsat ETM+ multi-band data; (*c*) fused Landsat ETM+ FCC (bands 4, 3 and 2 as red, green and blue) and Landsat PAN image.

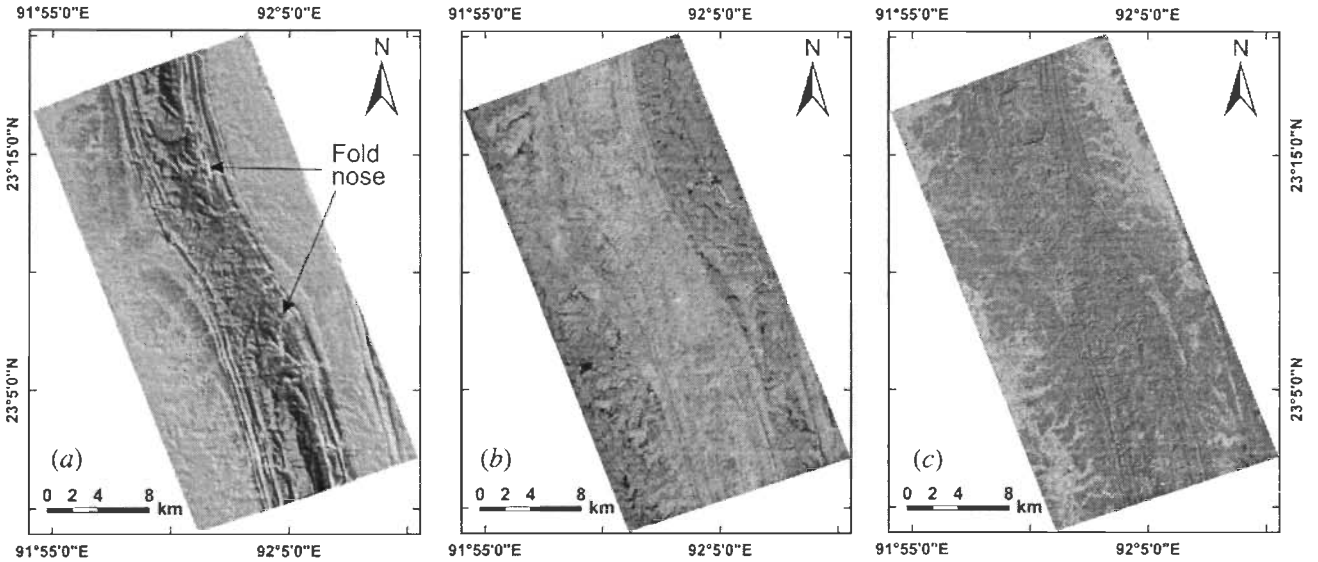

Figure 6. Plunging middle Langtarat anticline noses (LGM in figure 2). (*a*) 90-m SRTM-DEM hill-shade image of DEM prepared using sun azimuth 225° and sun elevation 20° and then colour coded; (*b*) FCC of first three principal component images obtained from Landsat ETM+ multi-band data; (*c*) fused Landsat ETM+ FCC (bands 4, 3 and 2 as red, green and blue) and Landsat PAN image.

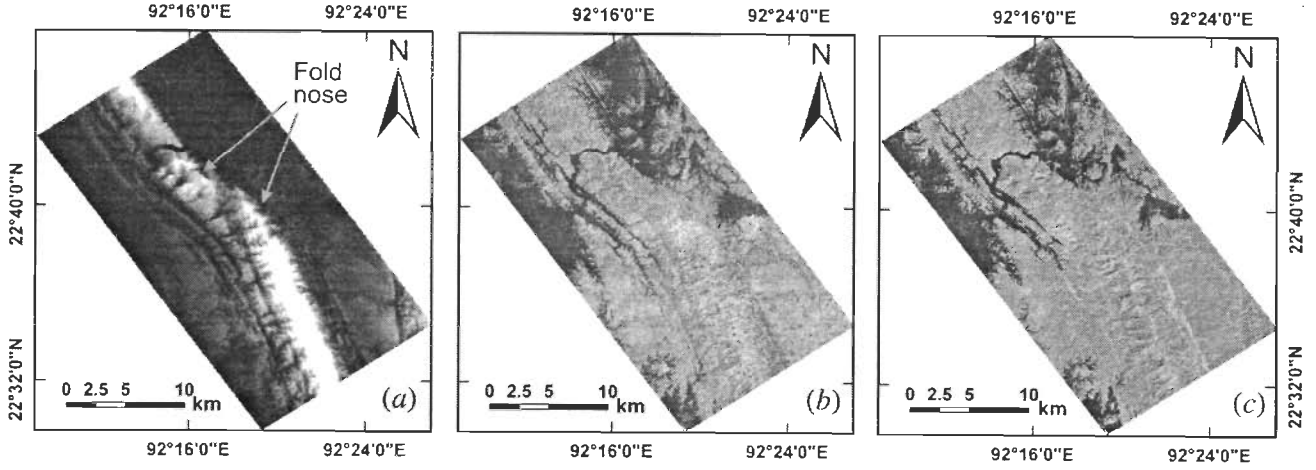

Figure 7. Plunging south Langtarat anticline noses (LGS in figure 2). (*a*) 90-m SRTM-DEM; (*b*) FCC of first three principal component images obtained from Landsat ETM+ multi-band data; (*c*) fused Landsat ETM+ FCC (bands 4, 3 and 2 as red, green and blue) and Landsat PAN image.

fold limbs. At this place the fold ridge also faulted transversely (F_T; see figure 8(*b*)), creating first a gap through which a river could cross over. These effects are seen very clearly in particular in figures 8(*b*) and 8(*c*). Another example of such fault-affected western limb and bulging can be seen in the north Langtarat anticline (see figure 9) located just east of the Baramura anticline bulge across the Atharamura anticline (LGF of figure 2). A westward bulging effect can be seen very clearly on the DEM (see figure 9(*a*)), which happened due to a similar faulting effect as described above. Several limbs are involved in this process, and were bulged out for about 9 km. It may be seen that due to this bulging the Atharamura anticline became curved westward to accommodate the expansion. These bulged-out limbs were terminated against another adjacent anticline to the north-east. This morphology is the result of faulting and further deformation.

There are several instances of en-echelon (overlapping) anticlines occurring in the study area (see figures 10, 11, 12 and 13). Intricate overlaps are seen at two places: Abdullapur (ABD) and Hailakandi west (HKW). In the overlapping part of HKW, the limbs of the upper and lower anticlines were pressed against each other so much that the limbs merged (see figure 10). The western side limbs (four) of the lower anticline show the continuity after a kink at the overlapping part. This might have been caused by reverse faulting, as marked in the figure, and subsequent movement. Meanwhile, the Baramura-south anticlinal overlap (BRS of figure 2) shows a simple contact with slight compression on the limbs of the eastern anticline (see figure 11). However, it appears that the fold contact is affected by faulting. In the case of the Abdullapur overlap three anticlines are involved (see figure 12). The fold nose of the southern anticline, Jampai anticline (JA), pressed against the middle anticline. But it may be observed that the northernmost anticline extends much farther southward, although it appears not to. The extended part of the anticline is clearly visible on the DEM (marked on figure 12(*b*)), and is displayed as eroded rounded limbs of fold nose. The eastern middle ridge however exhibits an outcrop of bedding, but it is understood that the complete geometry is not preserved (see figure 12). In another case (south of the area in figure 12) the specific arrangement of the anticlinal ridges (LNT of figure 2) gave a fork shaped appearance (see figure 13). The anticlines involved in this are Jampai anticline (JA) and Bakhan anticline (BA). In fact the JA has become faulted transversely in the area marked by F_T and shifted diagonally (see figure 13(*b*)). Meanwhile, the western anticline is an individual one, but placed closer to the JA.

An interesting feature that has developed in the study area due to specific arrangement of the anticlines (TBG of figure 2) is cuspate and elliptical geometry (see figure 14). It may be seen that the southern part of Jampai anticline (marked as JA in figure 14(*b*)) is bifurcated into two-sided limbs (EL1 and WL1) at geographical coordinates 23° 22′ N and 92° 15′ E and again reunites at 23° 07′ N and 92° 19′ E to form an elliptical syncline (about 25 km long with a maximum width of about 8.5 km, marked as ES in figure 14) occupied by harder rocks with circular exposures. Just at the lower east side of the elliptical valley the eastern limbs again bifurcate into two-sided limbs (EL2 and WL2), giving rise to a cuspate shaped syncline (about 26 km long with a maximum width of 10 km, marked as CS in figure 14). The cuspate valley is bounded by very high ridges with very steep inner slopes, which should have formed due to reverse faulting; during this process the eastern limbs upthrusted along the side of the syncline (see figures 14(*d*), 14(*e*) and 14(*f*)). The west bounding ridge of the cuspate valley extends up to a river, whereas the anticlinal limbs on the eastern side continue further south. Another minor elliptical valley bounded by the curved anticline on the west can be seen formed to the

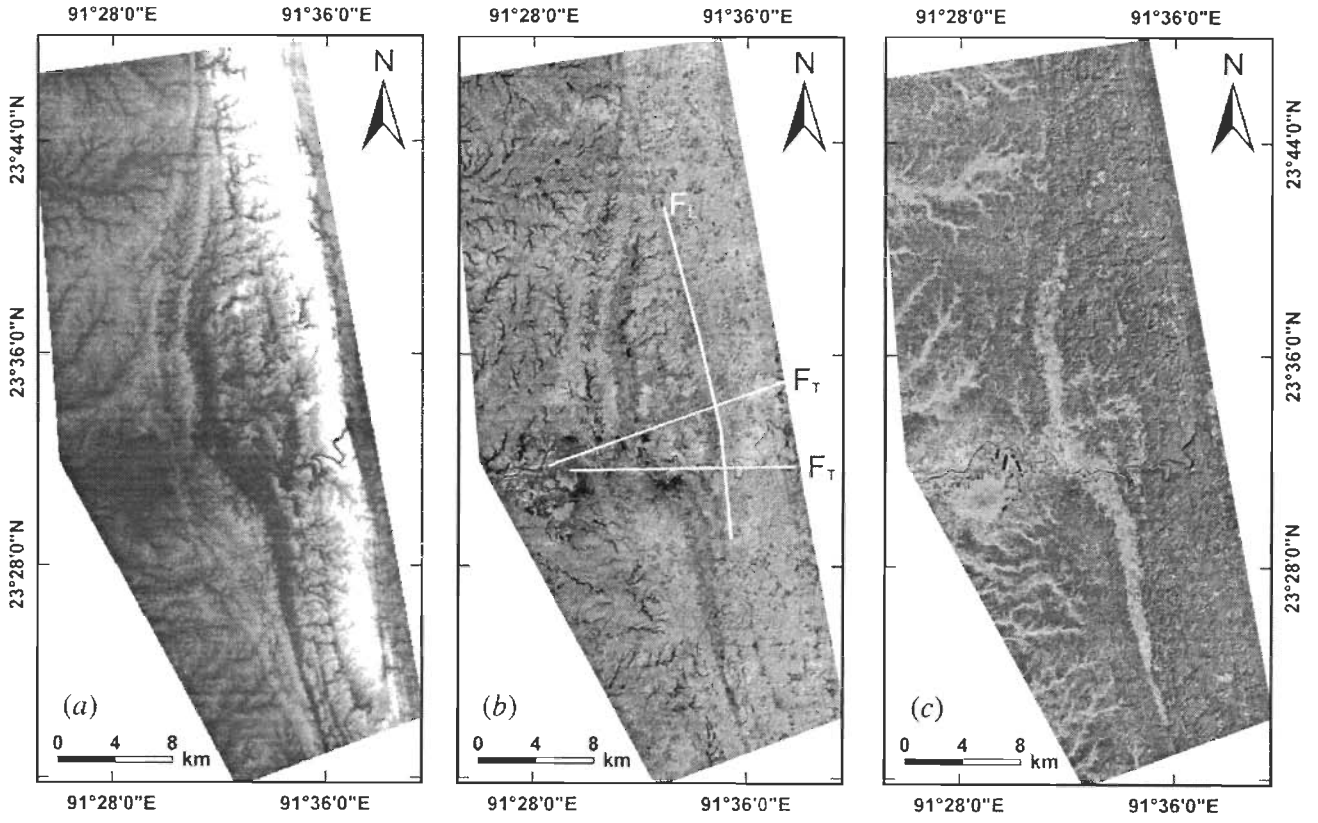

Figure 8. Faulted western limb of the Baramura anticline (BRF in figure 2). (*a*) 90-m SRTM-DEM; (*b*) FCC of first three principal component images obtained from Landsat ETM+ multi-band data; (*c*) fused Landsat ETM+ FCC (bands 4, 3 and 2 as red, green and blue) and Landsat PAN image. F_T and F_L are transverse and longitudinal faults.

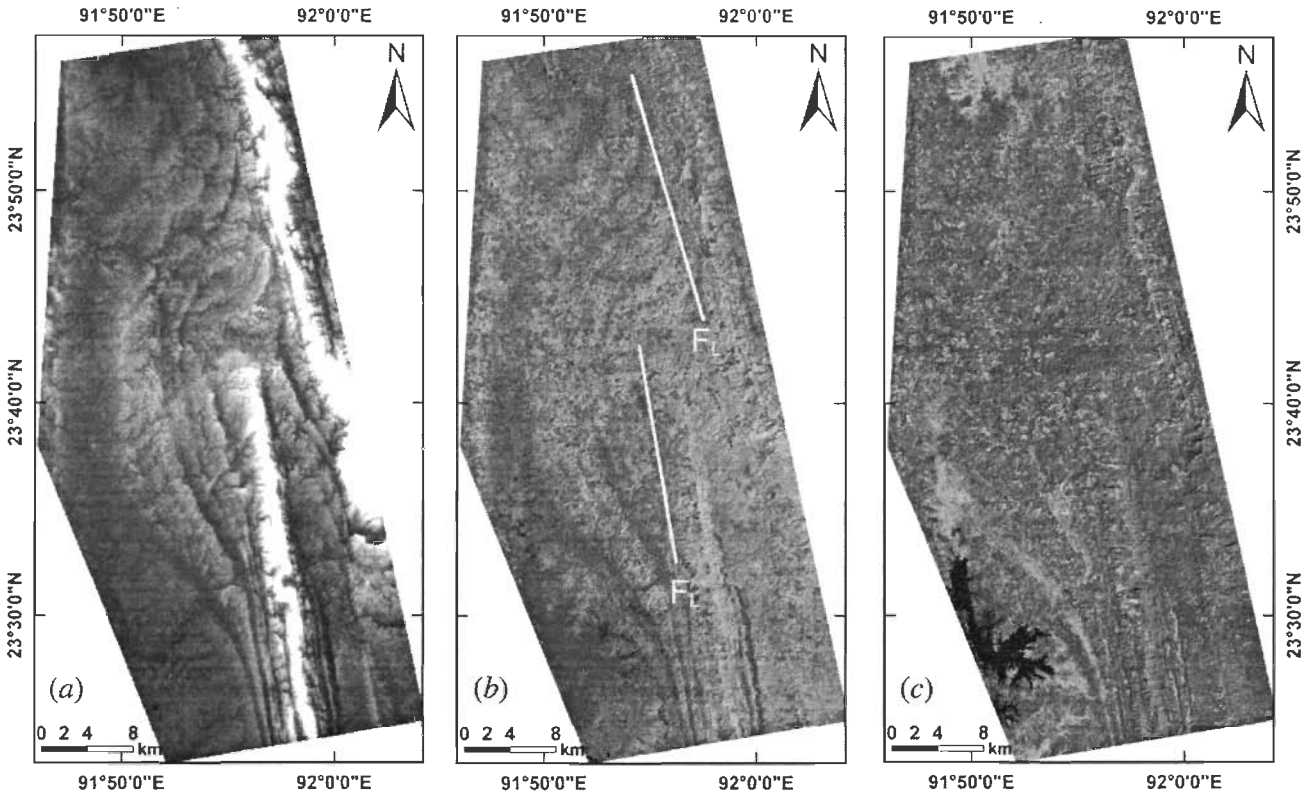

Figure 9. Faulted western limb of the Langtarat anticline (LGF in figure 2). (*a*) 90-m SRTM-DEM; (*b*) FCC of first three principal component images obtained from Landsat ETM+ multi-band data; (*c*) fused Landsat ETM+ FCC (bands 4, 3 and 2 as red, green and blue) and Landsat PAN image. F_L—longitudinal fault.

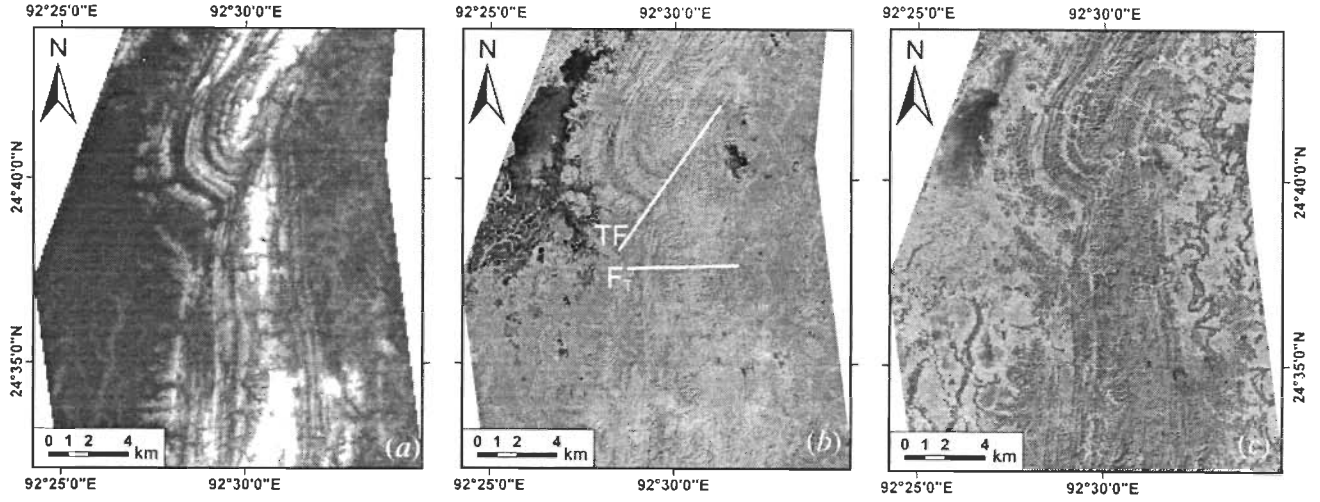

Figure 10. Overlapping anticlines in Hailakandi-west area (HKW in figure 2). (*a*) 90-m SRTM-DEM; (*b*) FCC of first three principal component images obtained from Landsat ETM+ multi-band data; (*c*) Fused Landsat ETM+ FCC (bands 4, 3 and 2 as red, green and blue) and Landsat PAN image. TF—thrust fault; F_T—transverse fault.

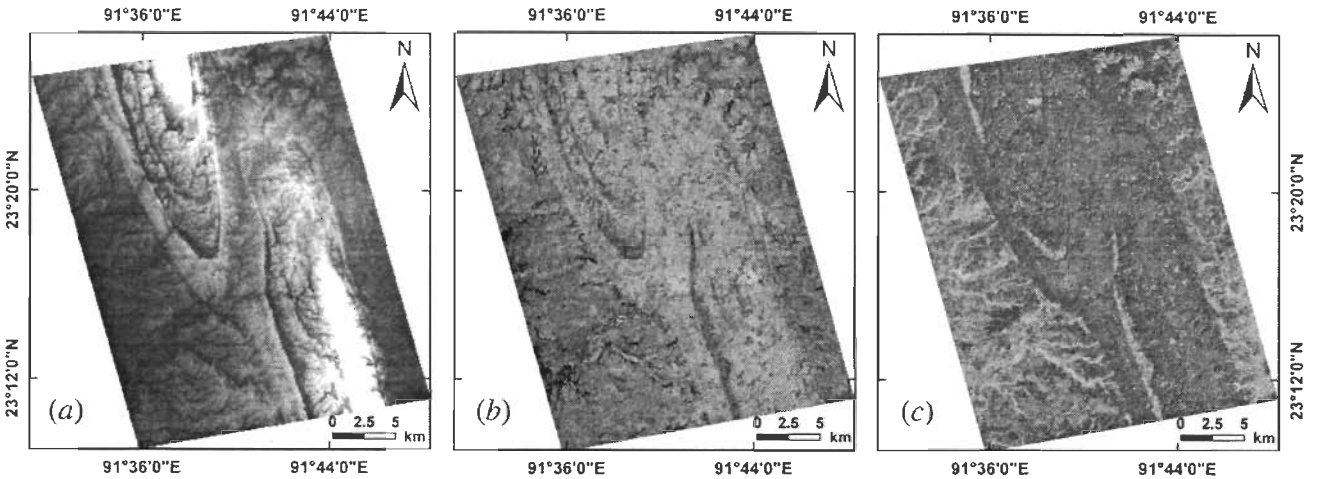

Figure 11. Overlapping anticlines in Baramura south anticline (BRS in figure 2). (*a*) 90-m SRTM-DEM; (*b*) FCC of first three principal component images obtained from Landsat ETM+ multi-band data; (*c*) fused Landsat ETM+ FCC (bands 4, 3 and 2 as red, green and blue) and Landsat PAN image.

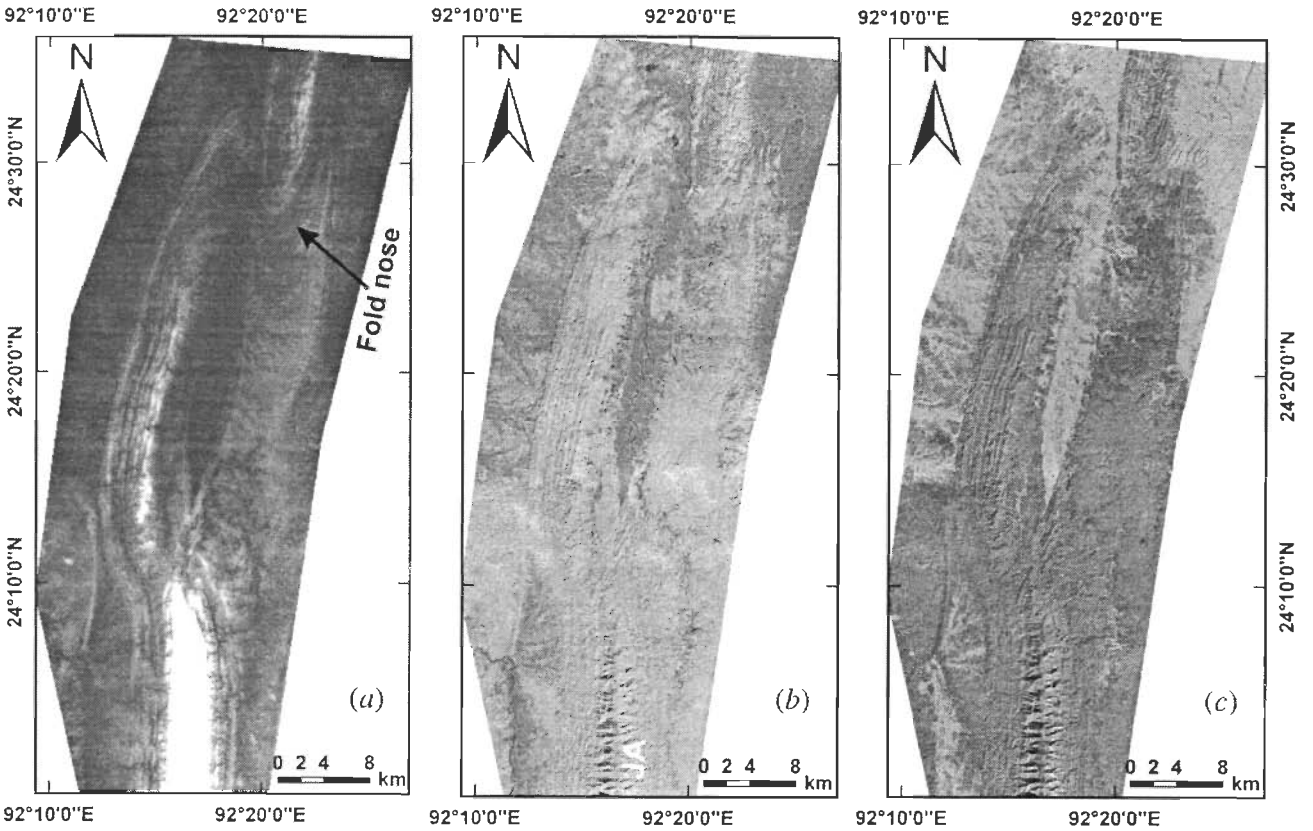

Figure 12. Overlapping and linked anticlines in Abdullapur area (ABD in figure 2). (*a*) 90-m SRTM-DEM; (*b*) FCC of first three principal component images obtained from Landsat ETM+ multi-band data; (*c*) fused Landsat ETM+ FCC (bands 4, 3 and 2 as red, green and blue) and Landsat PAN image. JA—Jampai anticline.

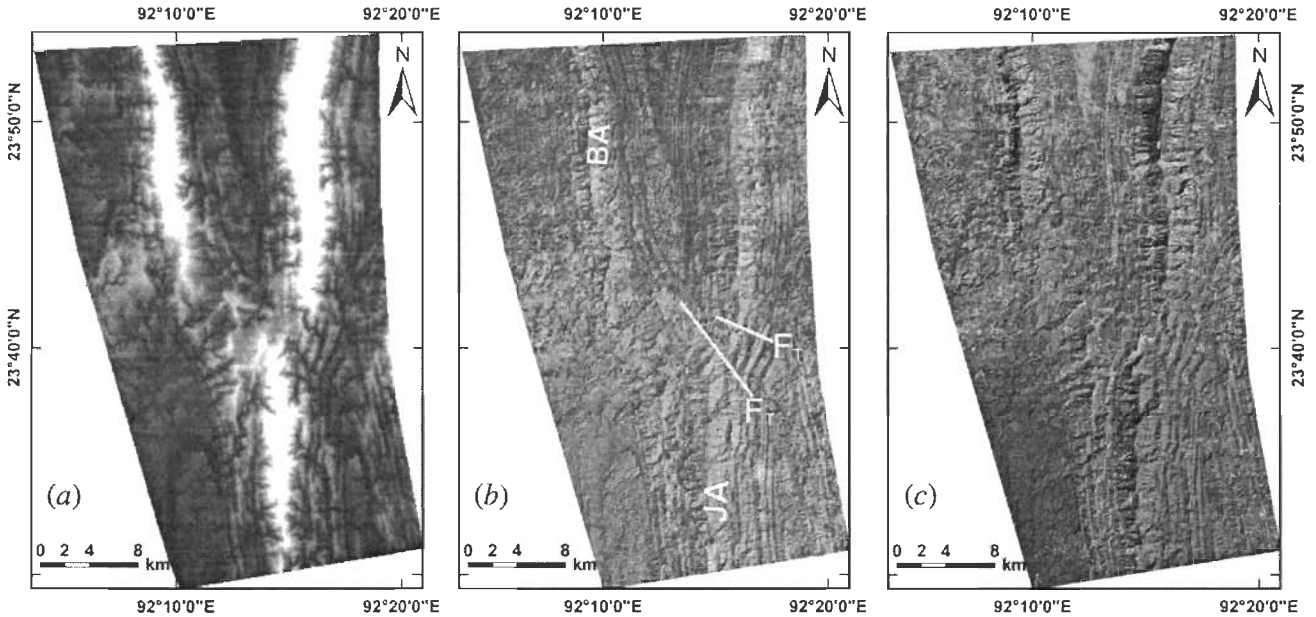

Figure 13. Anticline arrangement giving appearance of fork (LNT in figure 2). (*a*) 90-m SRTM-DEM; (*b*) FCC of first three principal component images obtained from Landsat ETM+ multi-band data; (*c*) fused Landsat ETM+ FCC (bands 4, 3 and 2 as red, green and blue) and Landsat PAN image. F_T—transverse fault. JA—Jampai anticline; BA—Bakhan anticline.

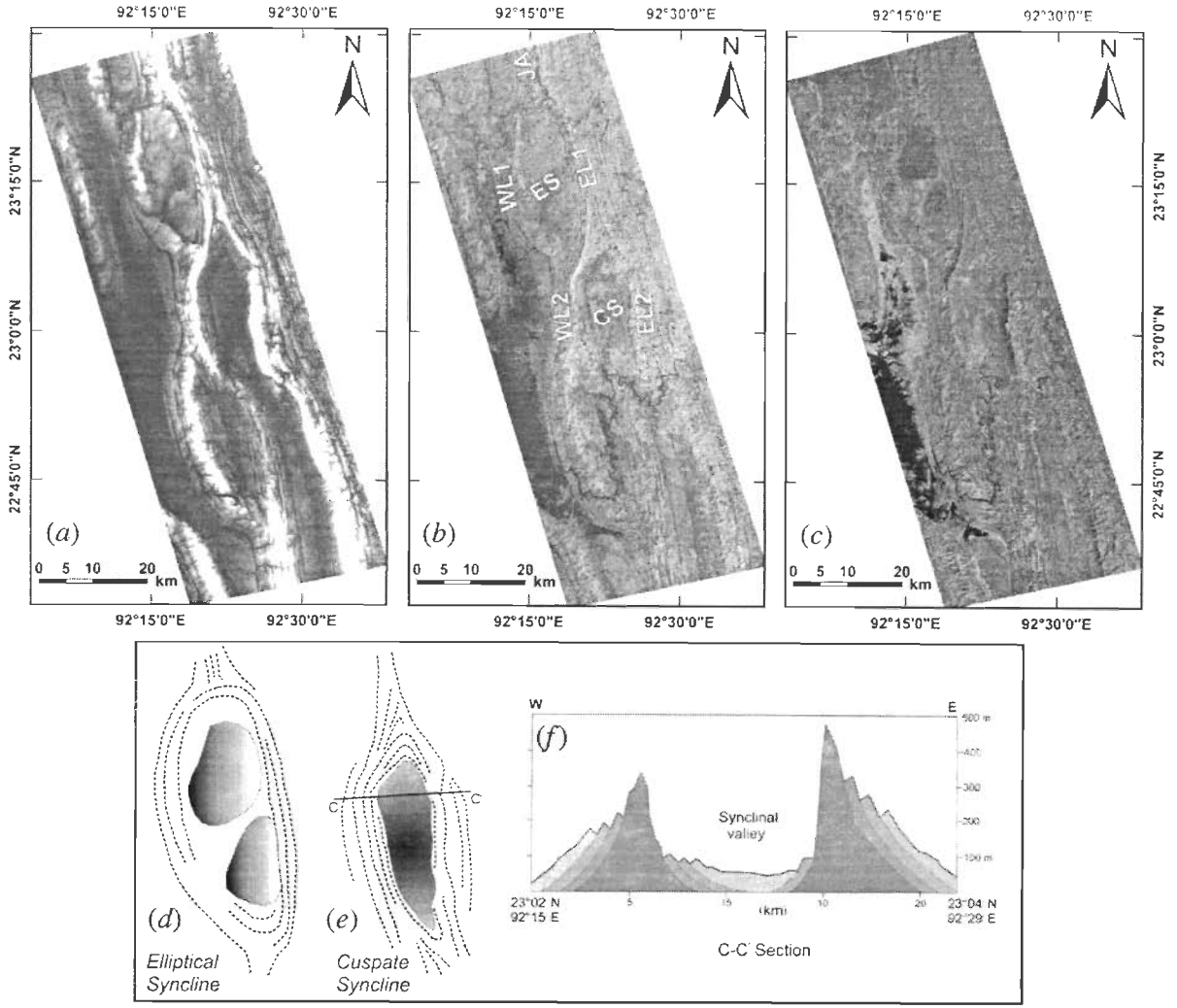

Figure 14. Anticline bifurcation, elliptical and cuspate valleys in Tuibangadam area (TBG in figure 2). (*a*) 90-m SRTM-DEM; (*b*) FCC of first three principal component images obtained from Landsat ETM+ multi-band data; (*c*) fused Landsat ETM+ FCC (bands 4, 3 and 2 as red, green and blue) and Landsat PAN image. JA—Jampai anticline; EL and WL—eastern and western limb; ES—elliptical syncline; CS—cuspate syncline. (*d*, *e* and *f*) Schematic drawing of morphological traces of the elliptical and cuspate synclines and a cross profile section along C–C′ of cuspate syncline respectively. The elevation values across the cuspate syncline are obtained through GIS profiling from 90-m SRTM-DEM.

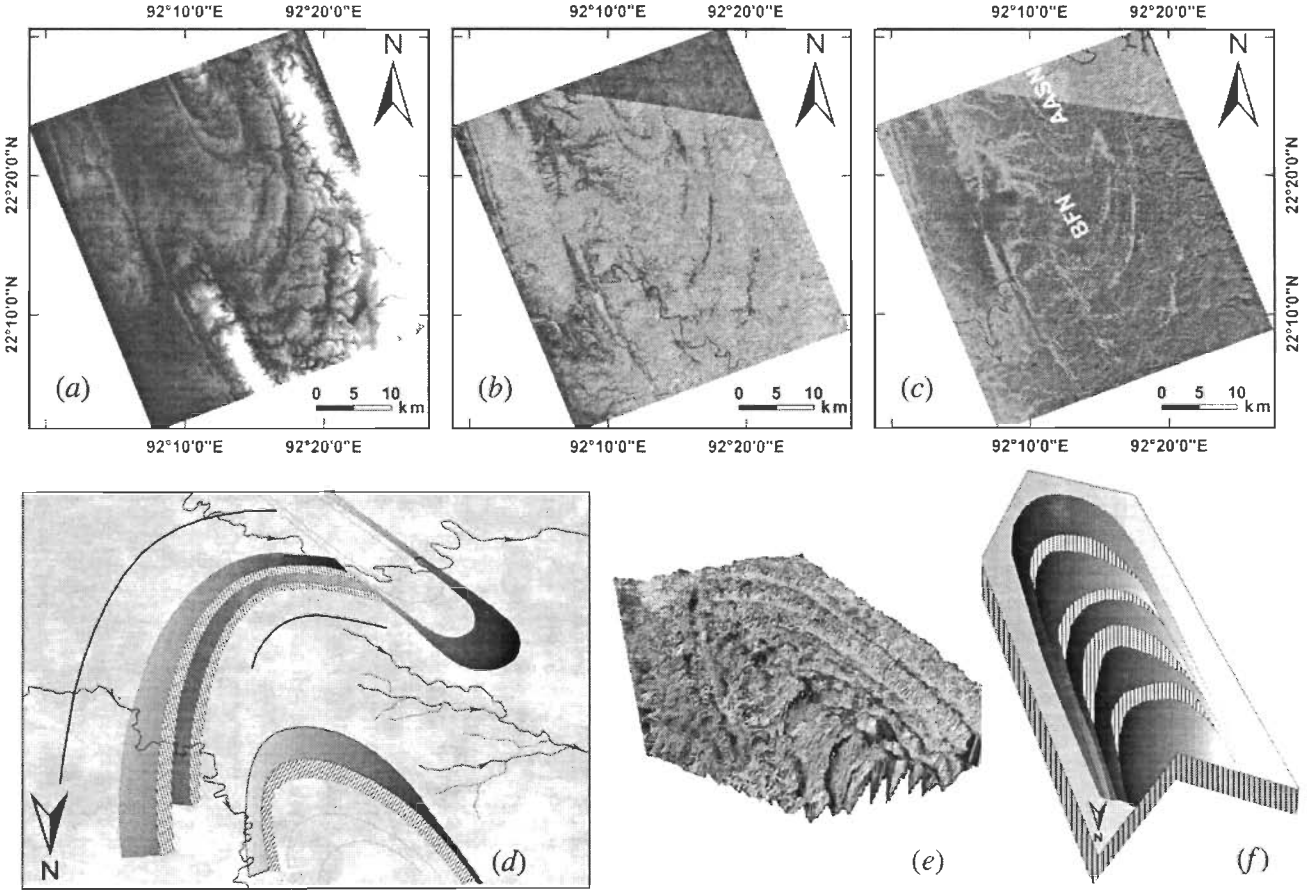

Figure 15. Plunging anticline co-noses in southernmost Atharamura anticline and Bandarban area (BDN in figure 2). (*a*) 90-m SRTM-DEM; (*b*) FCC of first three principal component images obtained from Landsat ETM+ multi-band data; (*c*) fused Landsat ETM+ FCC (bands 4, 3 and 2 as red, green and blue) and Landsat PAN image. (*d*) This sketch shows interrelation of anticlinal fold noses as in the above figure. This is prepared after rotating the image by 180° for better visualizing the morphology. (*e*) Image showing the individual plunging fold noses (rotated by 180°) which is generated by draping Landsat FCC on DEM with seven-fold exaggeration using virtual GIS. (*f*) Sketch showing the example of folded limbs as exposed. This is prepared after rotating the image by 180° for better visualizing the morphology. AASN—Atharamura anticline southern nose; BFN—Bandarban fold nose.

GANGULY, S., 1984, Tectonic evolution of the orogenic belt of Tripura. *Quarternary Journal of Geological Mining and Metal Society India*, **56**, pp. 128–137.

GANGULY, S., 1993, Stratigraphy, sedimentation and hydrocarbon prospects of Tertiary succession of Tripura and Cacher. *Indian Journal of Geology*, **65**, pp. 145–180.

GANSSER, A., 1983, *Geology of the Bhutan Himalaya* (Switzerland: Birkhauser Verlag).

HOBBS, B.E., 1976, *An Outline of Structural Geology* (New York: John Wiley & Sons).

LILLESAND, T.M. and KIEFER, R.W., 2000, *Remote Sensing and Image Interpretation* (New York: John Wiley and Sons).

MCQUARRIE, N., 2004, Crustal scale geometry of the Zagros fold–thrust belt, Iran. *Journal of Structural Geology*, **26**, pp. 519–535.

NANDY, D.R., 2001, *Geodynamics of Northeastern India and the Adjoining Region* (Kolkata: ACB Publications).

POHL, C. and VAN GENDEREN, J.L., 1998, Multisensor image fusion in remote sensing: concepts, methods and applications. *International Journal of Remote Sensing*, **19**, pp. 823–854.

PRICE, N.J. and COSGROVE, J.W., 1990, *Analysis of Geological Structure* (Cambridge: Cambridge University Press).

SABINS, F.F., 1987, *Remote Sensing: Principles and Interpretation* (New York: W.H. Freeman and Company).

SABINS, F.F., 1997, *Remote Sensing: Principles and Interpretation, 3rd edn* (New York: W.H. Freeman and Company).

SARAF, A.K., 1999, IRS-1C-LISS-III and PAN data fusion: an approach to improve remote sensing based mapping techniques. *International Journal of Remote Sensing*, **20**, pp. 1929–1934.

SARAF, A.K., DAS, J.D., AGARWAL, B. and SUNDARAM, R.M., 1996, False topography perception phenomena and its correction. *International Journal of Remote Sensing*, **17**, pp. 3725–3733.

SARKAR, K. and NANDY, D.R., 1976, Structures and tectonics of Tripura–Mizoram area, India. *Geological Survey of India, Miscellaneous Publication*, **34**, pp. 141–148.

SHETTIGARA, V.K., 1992, A generalized component substitution technique for spatial enhancement of multispectral images using a higher resolution data set. *Photogrammetric Engineering and Remote Sensing*, **58**, pp. 561–567.

SIKDER, A.M. and ALAM, M.M., 2003, 2-D modelling of the anticlinal structures and structural development of the eastern fold belt of the Bengal Basin, Bangladesh. *Sedimentary Geology*, **155**, pp. 209–226.

STOCKLIN, J., 1968, Structural history and tectonics of Iran: a review. *American Association of Petroleum Geologists Bulletin*, **52**, pp. 1229–1258.

WELCH, R. and EHLERS, M., 1987, Merging multiresolution SPOT HRV and Landsat TM data. *Photogrammetric Engineering and Remote Sensing*, **53**, pp. 301–303.

ZANG, Y., 1999, A new merging method and its spectral and spatial effects. *International Journal of Remote Sensing*, **20**, pp. 2003–2014.

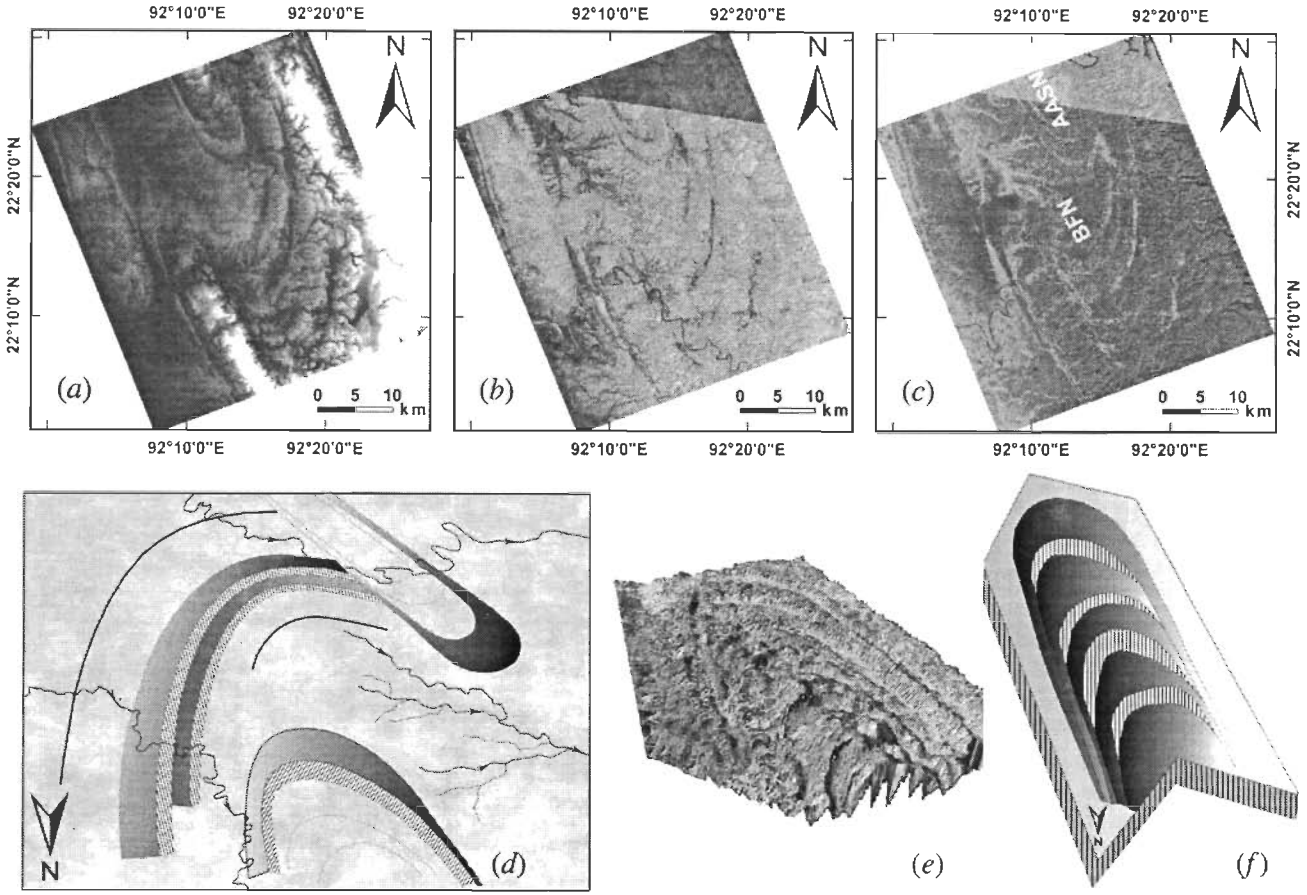

Figure 15. Plunging anticline co-noses in southernmost Atharamura anticline and Bandarban area (BDN in figure 2). (*a*) 90-m SRTM-DEM; (*b*) FCC of first three principal component images obtained from Landsat ETM+ multi-band data; (*c*) fused Landsat ETM+ FCC (bands 4, 3 and 2 as red, green and blue) and Landsat PAN image. (*d*) This sketch shows interrelation of anticlinal fold noses as in the above figure. This is prepared after rotating the image by 180° for better visualizing the morphology. (*e*) Image showing the individual plunging fold noses (rotated by 180°) which is generated by draping Landsat FCC on DEM with seven-fold exaggeration using virtual GIS. (*f*) Sketch showing the example of folded limbs as exposed. This is prepared after rotating the image by 180° for better visualizing the morphology. AASN—Atharamura anticline southern nose; BFN—Bandarban fold nose.

south-west of the cuspate valley. This specific configuration could have resulted due to fault-related folding and later stages of the deformation processes. The morphological trends of folded beds formed around the elliptical and cuspate synclines and cross profile of cuspate syncline are shown by a sketch (see figures 14(*d*), 14(*e*) and 14(*f*)). The section C-C′ across the cuspate syncline shows the transverse topography, revealing the high ridge and steep inner slopes (topographical information has been derived from a DEM using GIS profiling).

Occurrence of anticlinal plunging co-noses (BDN of figure 2) can be seen at the southernmost tip of the Atharamura anticline (AASN). In this area, referred to as Bandarban (a place in Bangladesh), one wide fold nose (marked as BFN) and three other fold noses can be seen (see figure 15). These folds are NNW–SSW trending fold ridges with one very wide fold nose which is partially preserved. The wide nose represents the early stage of an open anticline. During the later stages of deformation another anticline has developed at the core of wide anticline with slight westward axial shift. The anticlines marked as AASN and BFN are not same, as the fold axes have different fold geometry. A sketch (figure 15(*d*)) shows the morphology of the folds. This sketch has been prepared after rotating the image by 180°, so that the feature can be seen better.

Some of the plunging noses of anticlinal folds show several preserved folded limbs. From the weathered outcrop of the anticline closer to the low plunging nose, it is possible to identify on the satellite image the number of sedimentary layers that were eroded away. In case of one such anticline (marked as AASN in figure 15), having its bedding (weathered) geometry well preserved was well recorded on the satellite image (see figure 15(*e*)). In all, eight bedding layers could be identified. The nature of the some plunged folded layers is shown by a sketch which is rotated by 180° (see figure 15(*f*)). The length of this particular anticline is about 35 km, with a central width of 7.32 km and a maximum elevation of about 400 m.

5. Discussion and conclusion

This study focused on a folded terrain located farthest from the zone where the Indo-Burman plate contacts the source zone of the E–W orientated lateral tectonic forces, transforming the deposited sediments in the sedimentary basin into the N–S oriented series of anticlines and synclines. Although the folds appear to be simple to some extent, careful study revealed some significant features which could be studied with the help of satellite images and 90-m SRTM-DEM. Satellite images and DEM provided a synoptic view to understand first the overall geometry of the folded sequence. DEM produced a clearer picture of the features in some cases. The purpose of this paper was to establish how remote sensing techniques (satellite images and SRTM-DEM) could be used to understand and reveal the geometry of the folds in a particular area.

Digitally processed satellite image-based delineation and interpretation of geomorphological features formed the main basis for this study, which has revealed ground characteristics. While studying and interpreting the geomorphological features we have integrated all the information available from single band images, FCC and PCA. ETM-FCC and PCA images show more contrasting colours (e.g. the river valleys), making the appearance of the feature more prominent. Fusing of 30 m and 15 m Landsat ETM+ and PAN images enabled enlarged views of the specific features. However, it is also noted that the PCA image did not produce the expected results in all cases.

The low resolution DEM mainly exhibits a combination of bright and grey colours with very limited range, without revealing the ground characteristics. The elongated fold limbs of the study area are displayed as a very bright tone, making them stand out. However, a comparative display of DEM, ETM-FCC and PCA gives the opportunity to check their appearance in different images. In some cases (figures 2, 4, 5 and 6) hill-shade layers were also generated (in GIS) from DEM and colour-coded. During generation of hill-shade different combinations of illumination and azimuth angle have been tested and the suitable ones have been found. This was done in order to make the fold limbs more prominent.

It may be concluded that remote sensing techniques provided insight into the image characteristics of the fold patterns and were very useful in identifying and delineating several types of fold geometry. Plunging fold noses have been identified and delineated that are otherwise not apparent. The overlapping nature of anticlinal ridges could be studied using DEM and satellite images.

Remarkable western anticlinal limb bulging is found to be attributed to normal faulting and the geomorphological features of faulted anticlinal limbs are expressed well on satellite images. Further, interesting features formed in the region are elliptical and cusp shaped synclines bounded by fault affected ridges, and an anticline within the earlier wide anticline. Remarkably multi-curved geometry of the western fold ridges is attributed to the free westward fold migration, deformation of soft sediments in many phases, and longitudinal and transverse faulting. The region has, in general, higher topography in the middle latitude part and the plunging nature of folds indicates that the region has also suffered up-arching tectonic activity.

Acknowledgement

The authors are thankful to Department of Science and Technology (DST), Government of India for overall support for this work. Landsat ETM+ and PAN data are taken from Global Land Cover Facility (GLCF), University of Maryland, USA. 90-m SRTM-DEM are taken from Consortium for Spatial Information (CGIAR-CSI). Google Earth was very useful to cross-check the morphology and topography of geological features on images of high resolution.

References

ALAVI, M., 2004, Regional stratigraphy of the zagros fold-thrust belt of Iran and its proforeland evolution. *American Journal of Science*, **304**, pp. 1–20.

CHAVEZ, P.S., SIDES, S.C. and ANDERSON, J.A., 1991, Comparison of three different methods to merge multi resolution and multi spectral data: Landsat TM and SPOT panchromatic. *Photogrammetric Engineering and Remote Sensing*, **57**, pp. 295–303.

CLICHE, G., BONN, F. and TEILLET, P., 1985, Integration of the SPOT Pan channel into its multispectral mode for image sharpness enhancement. *Photogrammetric Engineering and Remote Sensing*, **51**, pp. 311–316.

COLMAN-SADD, S.P., 1978, Fold development in Zagros simply folded belt, Southwest Iran. *American Association of Petroleum Geologists Bulletin*, **62**, pp. 984–1003.

DAS GUPTA, S. and NANDY, D.R., 1995, Geological framework of the Indo-Burmese convergence margin with special reference to ophiolite emplacement. *Indian Journal of Geology*, **67**, pp. 120–125.

DAVIS, G.H. and REYNOLDS, S.J.,1984, *Structural Geology of Rocks and Regions* (New York: John Wiley and Sons).

DRURY, S.A., 2001, *Image Interpretation in Geology* (Cheltenham, UK: Nelson Thornes).

GANGULY, S., 1984, Tectonic evolution of the orogenic belt of Tripura. *Quarternary Journal of Geological Mining and Metal Society India*, **56**, pp. 128–137.

GANGULY, S., 1993, Stratigraphy, sedimentation and hydrocarbon prospects of Tertiary succession of Tripura and Cacher. *Indian Journal of Geology*, **65**, pp. 145–180.

GANSSER, A., 1983, *Geology of the Bhutan Himalaya* (Switzerland: Birkhauser Verlag).

HOBBS, B.E., 1976, *An Outline of Structural Geology* (New York: John Wiley & Sons).

LILLESAND, T.M. and KIEFER, R.W., 2000, *Remote Sensing and Image Interpretation* (New York: John Wiley and Sons).

MCQUARRIE, N., 2004, Crustal scale geometry of the Zagros fold–thrust belt, Iran. *Journal of Structural Geology*, **26**, pp. 519–535.

NANDY, D.R., 2001, *Geodynamics of Northeastern India and the Adjoining Region* (Kolkata: ACB Publications).

POHL, C. and VAN GENDEREN, J.L., 1998, Multisensor image fusion in remote sensing: concepts, methods and applications. *International Journal of Remote Sensing*, **19**, pp. 823–854.

PRICE, N.J. and COSGROVE, J.W., 1990, *Analysis of Geological Structure* (Cambridge: Cambridge University Press).

SABINS, F.F., 1987, *Remote Sensing: Principles and Interpretation* (New York: W.H. Freeman and Company).

SABINS, F.F., 1997, *Remote Sensing: Principles and Interpretation, 3rd edn* (New York: W.H. Freeman and Company).

SARAF, A.K., 1999, IRS-1C-LISS-III and PAN data fusion: an approach to improve remote sensing based mapping techniques. *International Journal of Remote Sensing*, **20**, pp. 1929–1934.

SARAF, A.K., DAS, J.D., AGARWAL, B. and SUNDARAM, R.M., 1996, False topography perception phenomena and its correction. *International Journal of Remote Sensing*, **17**, pp. 3725–3733.

SARKAR, K. and NANDY, D.R., 1976, Structures and tectonics of Tripura–Mizoram area, India. *Geological Survey of India, Miscellaneous Publication*, **34**, pp. 141–148.

SHETTIGARA, V.K., 1992, A generalized component substitution technique for spatial enhancement of multispectral images using a higher resolution data set. *Photogrammetric Engineering and Remote Sensing*, **58**, pp. 561–567.

SIKDER, A.M. and ALAM, M.M., 2003, 2-D modelling of the anticlinal structures and structural development of the eastern fold belt of the Bengal Basin, Bangladesh. *Sedimentary Geology*, **155**, pp. 209–226.

STOCKLIN, J., 1968, Structural history and tectonics of Iran: a review. *American Association of Petroleum Geologists Bulletin*, **52**, pp. 1229–1258.

WELCH, R. and EHLERS, M., 1987, Merging multiresolution SPOT HRV and Landsat TM data. *Photogrammetric Engineering and Remote Sensing*, **53**, pp. 301–303.

ZANG, Y., 1999, A new merging method and its spectral and spatial effects. *International Journal of Remote Sensing*, **20**, pp. 2003–2014.

J Indian Soc Remote Sens
DOI 10.1007/s12524-011-0066-6

RESEARCH ARTICLE

Morphotectonic Features and Fault Propagation Folding of Bhuban Hills, NE India Using Satellite Image and DEM

J. D. Das · Yazdana Shujat · A. K. Saraf · V. Rawat · K. Sharma

Received: 26 December 2009 / Accepted: 29 April 2010

Abstract Present topography of Bhuban Hills, lying in the Indo-Burman frontal fold belt of Northeastern part of India, is an aberration from a normal anticlinal morphology and exhibits several transverse and longitudinal fault affected segments resulting into distinct morphotectonic units. Six different morphotectonic units could be delineated along N-S stretch of the hill ridge. The western side of the northern most part of the hill ridge forms steep escarpment as this portion has been affected by the longitudinal faulting representing a case of fault propagation folding. The northernmost segment comprising three morphotectonic units (MU1 to MU3) is unique in the sense that this part exhibits effect of both the longitudinal and transverse faulting, uplifted narrow ridge with downthrown eastern side (MU2). Northern part of the Bhuban Hills has become curved westward due to the right lateral movement along the transverse fault TF1. The fifth morphotectonic unit (MU5) has undergone subsidence whereas, the sixth unit (MU6) exhibit bulging effect as this part experienced differential fault movements. Stream profiles, longitudinal and transverse topographic profiles extracted from contour map and Digital Elevation Model corroborated with the topographical anomalies developed over the Bhuban Hills.

Keywords Bhuban Hills · Morphotectonics · DEM · Satellite image · Faulting

J. D. Das (✉)
Department of Earthquake Engineering,
Indian Institute of Technology Roorkee,
Uttarakhand, India
e-mail: jddasfeq@iitr.ernet.in

Y. Shujat · A. K. Saraf · V. Rawat · K. Sharma
Department of Earth Sciences,
Indian Institute of Technology Roorkee,
Uttarakhand, India

Published online: 15 February 2011

Introduction

Hilly topography of any region is a manifestation of tectonic forces that operated in the region. Folding and thrusting of sedimentary sequence is responsible for resulted topography and have a great impact on rate of upliftment, rate of subsidence and landscape development (Burbank and Anderson 2001). Impulsive tectonic activity gives rise to dissected and rugged topography, which can be interpreted analyzing satellite images and Digital Elevation Model (DEM).

Bhuban anticline lies in a tectonically very active region and it is the frontal part of the Indo-Burman fold belt (Fig. 1). This fold belt is an outcome of E-W oriented compressional tectonic forces that prevailed in the region during eastward subduction of the Indian plate under the Burmese plate. Owing to this process the westerly laying sedimentary wedge got deformed into a series of N-S oriented alternating anticlines and synclines. Intensity of folding gradually increases eastward in the sedimentary sequence and are affected by several longitudinal and transverse faulting (Nandy

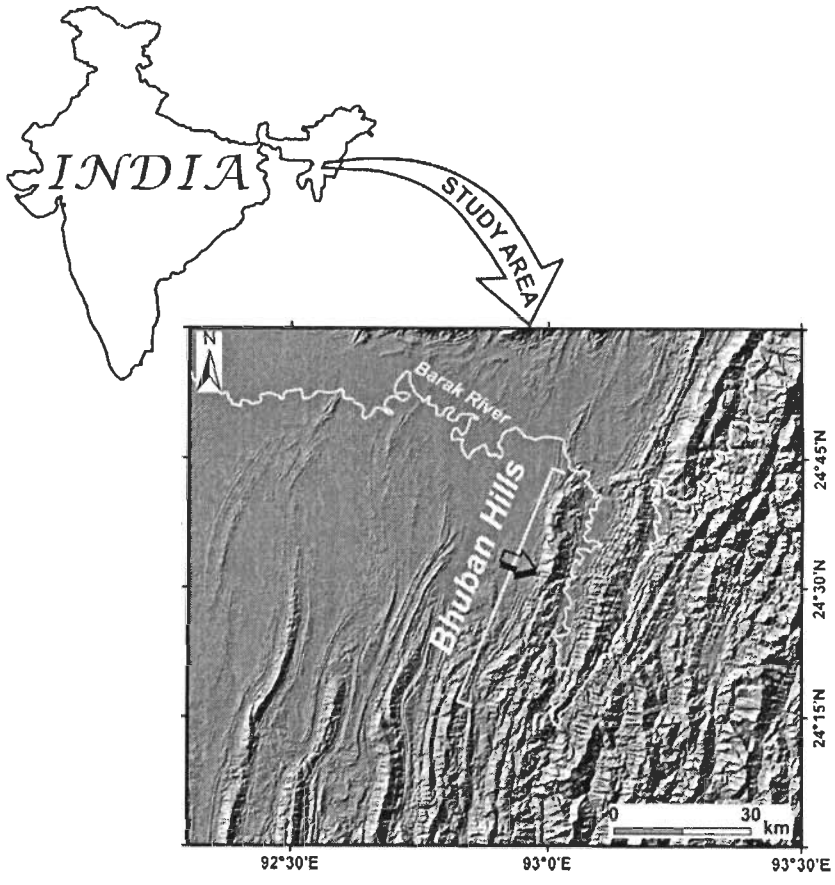

Fig. 1 Study area showing Bhuban Hills in a set up of frontal fold belt comprising several anticlines, synclines and a river valley as shown by shaded relief model of 90 m SRTM-DEM

2001). Geologically, the Bhuban Hills is made up of sandstone, shales, soft clays and mudstone of Miocene age (Das Gupta and Biswas 2000). The frontal fold belt represents an unique fold-and-thrust belts of the accretionary wedge associated with convergent margins as suggested by Chapple (1978). The structural evolution of many frontal fold belts is that of initial buckling and subsequent fault-propagation folding Davis et al. (1983) and Mitra (1990) and the frontal Indo-Burman fold belt also exhibit similar structural set up. Characteristic structural features of such belt is a basal surface of detachment with large lateral compression causing reverse faulting in the overlying sedimentary sequence as shown in Fig. 2. From characteristics of the fold belt as viewed on satellite images, it appears that folds are superposed in nature and have developed due to the combined effects of buckling and fault propagation and such effects can be observed at a few places of the frontal fold area.

Present topography and geometry of the Bhuban Hills can be seen as severely fault affected. In fact, nature of faulting is responsible for present shape of the Bhuban Hills. This hill exhibits modified and changed morphotectonic characteristics, especially the northern part of Bhuban Hills, than the normal anticlinal morphology. Most prominent presentation of the hill is westward convexity in the topography with a very steep western slope in northern part.

Data Used and Methodology

In this study, we have introduced proper blending of appropriate information from various sources like Survey of India topographic maps (1:50000), satellite image and DEM (90 m-SRTM) for extracting the morphotectonics of the Bhuban Hills. DEM has been generated by converting contours of topographic maps into a digital form and employing GIS based triangulated irregular network model. Topo-DEM was defined under the projection Coordinated Geographic System using datum WGS84 as that of SRTM DEM

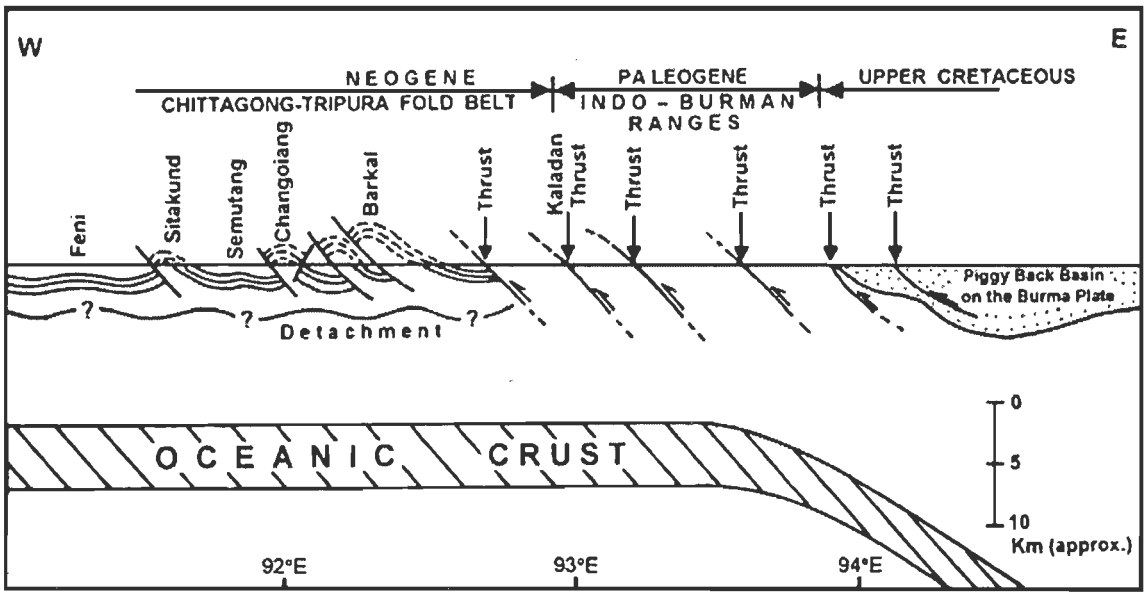

Fig. 2 Schematic structural cross-section of Bangladesh-Indo-Burman fold range showing upthrust sequence in a plate tectonic set up (source: Sikder and Alam 2003)

and checked for matching between the DEMs. Satellite image, topographic maps and SRTM-DEM have been treated in image processing software (ERDAS Imagine version 9.3) and data analysis software (ArcGIS version 9.3) for deriving morphological information, topographical and drainage profiles.

DEM provides vital information on topography characteristics through slopes, aspect and elevations beside snap shot view of the landscape features allowing better visualization and interrogation of topographic features. GIS technology provided the tools for the generation of several informative layers on slope, aspects, hill shade, and other surface parameters and extraction of quantitative information viz. elevation profiles of Bhuban Hills.

Results and Discussions

Morphotectonic Features

In the Bhuban Hills region several longitudinal and transverse faults could be demarcated and due to faulting six distinct morphotectonic units or segments (MU1 to MU6) have developed displaying unique topography (Fig. 3). North-northeasterly running linear ridges especially along western side of the northern part of Bhuban Hills is placed at very lower relief compared to the elevated ridge. Satellite image (Landsat ETM+band 5) also displays different morphotectonic units as is by shaded relief model of 90 m resolution SRTM-DEM (Fig. 3).

First unit (MU1) is the northernmost part represented by a small hill appears to have detached from the main hill due to transverse faulting (TF1) across the ridge. Morphotectonic units MU2 and MU3 are the adjacent western and eastern blocks of hills respectively. MU2 forms high linear ridge with the formation of extremely steep escarpment on the western side with westward convex topography (Fig. 4 a, b and c). Whereas, MU3 forms the eastern slope of the hill ridge but with a sudden drop in the topography as this unit suffered less upthrusting than the MU2. Bhuban Hills show very interesting slope properties and are characterized by very steep more than 80° slope mainly on the western side of MU2. The eastern side (MU3) is marked by gradually decreasing slope of about 10°–30° (Fig. 5). Western steep slope displayed by the northern part of Bhuban Hills is a direct effect of longitudinal reverse faulting. Due to which part of ridge has been uplifted in the form of a wall as can be seen in field photographs (Fig. 4 b and c). MU3 topography is considerably rugged and eastward dipping beds are exposed. Topographical features in MU2 and MU3 have developed in response to intense deformational process in this part.

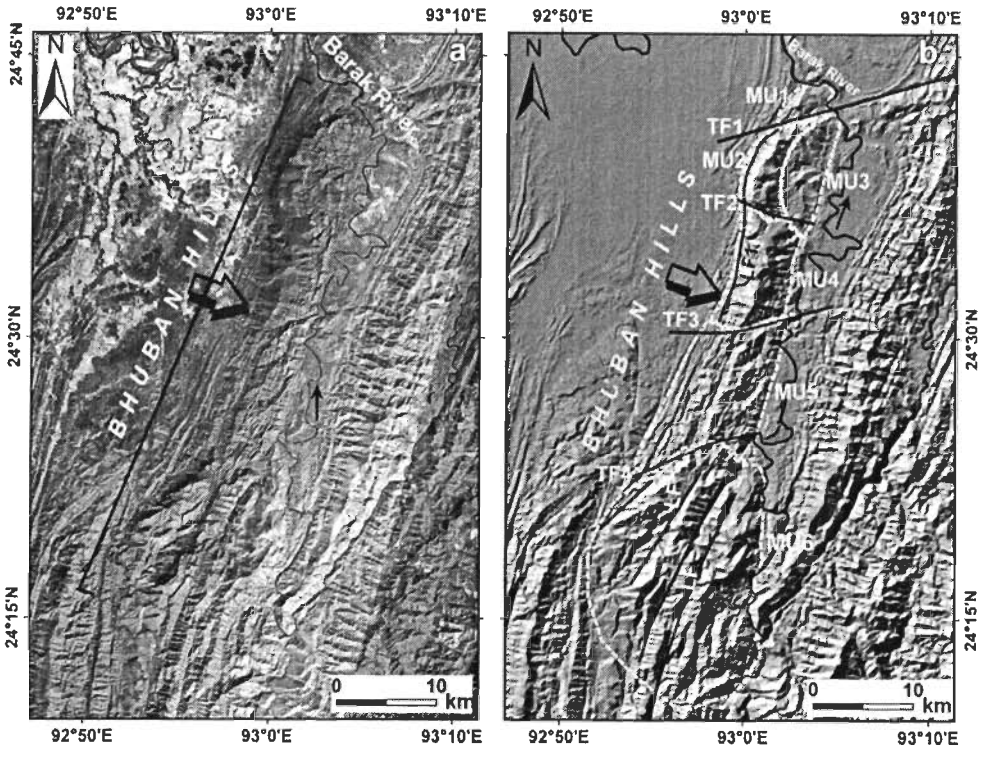

Fig. 3 Satellite image-Landsat ETM (**a**) and shaded relief model of SRTM-DEM of Bhuban Hills (**b**). Different morphotectonic units (MU1 to MU6), longitudinal (LF) and transverse (TF1 to TF4) faults of the Bhuban Hills are shown

One portion of higher ridge in MU2 formed into an easterly sloping table land with development of streams which falls suddenly on to a lower relief area on the east (Fig. 5a). Towards north of this table land a stream can be seen forming a deep cut on to the topography. Further, to the south of table land a deep erosional valley and considerably large northward slope has formed across the ridge (Fig. 5a). Prominent stream network of the eastern slope (MU3) is shown in Fig. 5b and the stream profiles of select streams (Str 1, 2 and 3) are shown in Fig. 5c, d and e. Stream profile of stream 1 developed over the table land clearly exhibit a vertical drop of about 175 m at place with latitude 24.6 N and longitude 93.03E. Other two stream profiles indicate gentle gradient as these streams now have cut deeper into the topography otherwise having steeper slopes. All the streams are ephemeral in nature but their deep cut into the topography indicate tectonic upliftment and subsequent heavy erosion.

MU2 exhibits gradual increase in altitude from north to south up to the transverse fault TF2. Also, around the fault TF2 the part of ridge has been severely dissected forming a transverse wind gap. The fourth unit (MU4) extends from 24.6° to 24.5°N showing high ridge with steeper western slope. From the nature of topographic feature it appears that this part also suffered upthrusting along a longitudinal fault on western side of the hill. Altitude of this part is higher than the first part and bounded by TF2 and TF3. Fifth unit (MU5) is bounded by two transverse faults (TF3 and TF4) and extends from 24.5°N southward with low altitude ridges formed by anticlinal limbs and appear to have suffered subsidence. MU6 has altogether different topographic expression as this part is represented by bulged out four ridges affected by low magnitude fault-propagation folding. Westernmost ridge of this unit show remarkable westward rotation. All the transverse faults as discussed above are shown in Fig. 3.

Topographic Variations

Topographic variation in the Bhuban Hills region can be assessed on the basis of topographic profiles showing elevation variation along and across the ridge. Locations and extent of the topographic profiles are shown in Fig. 6.

For the purpose of comparison these profiles have been derived digitally from contour and SRTM

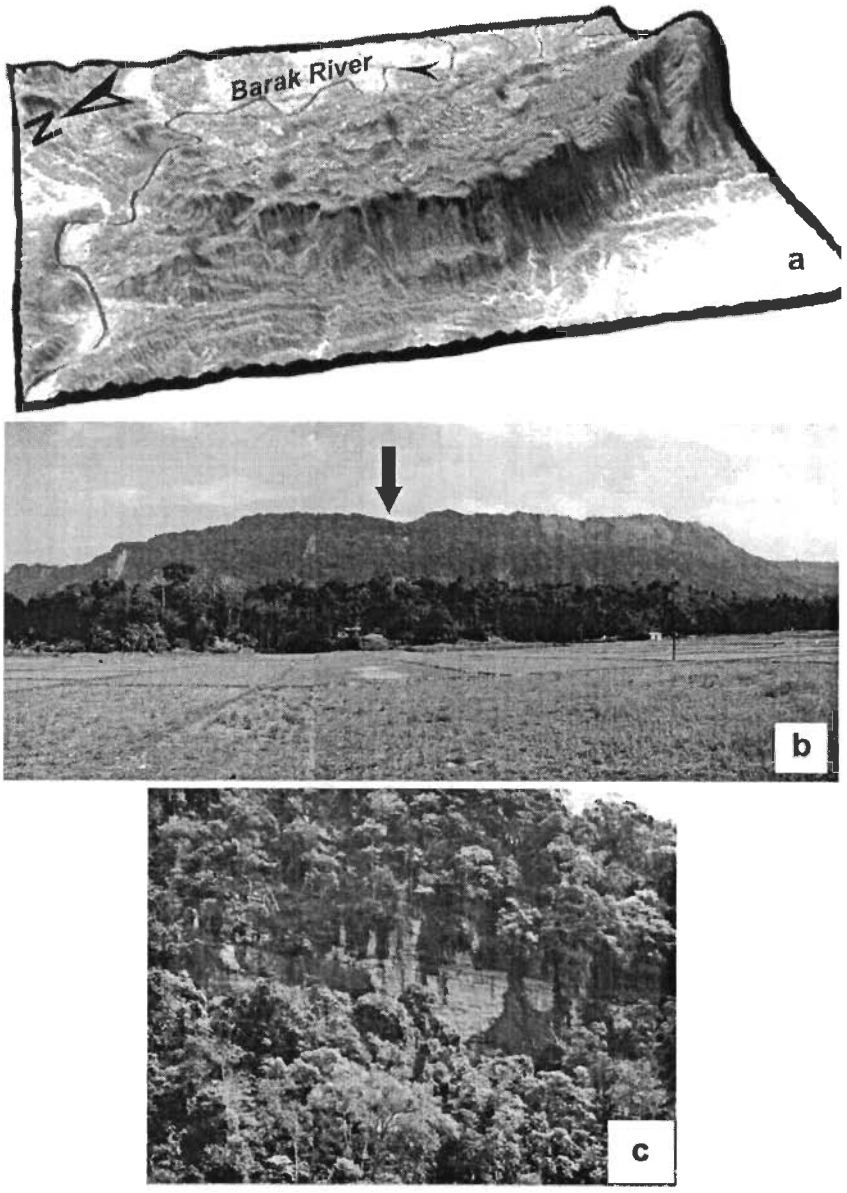

Fig. 4 Western steep slope of Bhuban Hill which is a virtual GIS image (x4 exaggeration) generated using satellite image draped on digital elevation model (**a**). Field photograph of western view of the northern Bhuban Hill (**b**). Field photograph showing exposed steep escarpment of the Bhuban Hill at a location shown by a pointer in Fig. 4b (**c**)

DEMs. These topographic profiles are actually representative of all the undulation present on the ridge and no smoothing has been carried out. As a result slight mismatch has occurred although by enlarge all the profiles are in good agreement.

Longitudinal Profile L1

This profile is following the ridge top of the Bhuban Hills (Fig. 7). Two profiles i.e. of contour and SRTM DEMs are in good agreement as these profiles are following close to each other. The profiles also show four distinct segments which are upthrust convex part (MU2), upthrust part (MU4), subsided part (MU5) and bulged out ridges part (MU6) as discussed earlier. Faulted parts of the ridge exhibit sharp drop in elevation and most remarkable drop in elevation may be observed in subsidence zone.

Transverse Profiles (TP-1 to TP-8)

These transverse profiles are taken at some intervals across the Bhuban Hills covering significant topo-

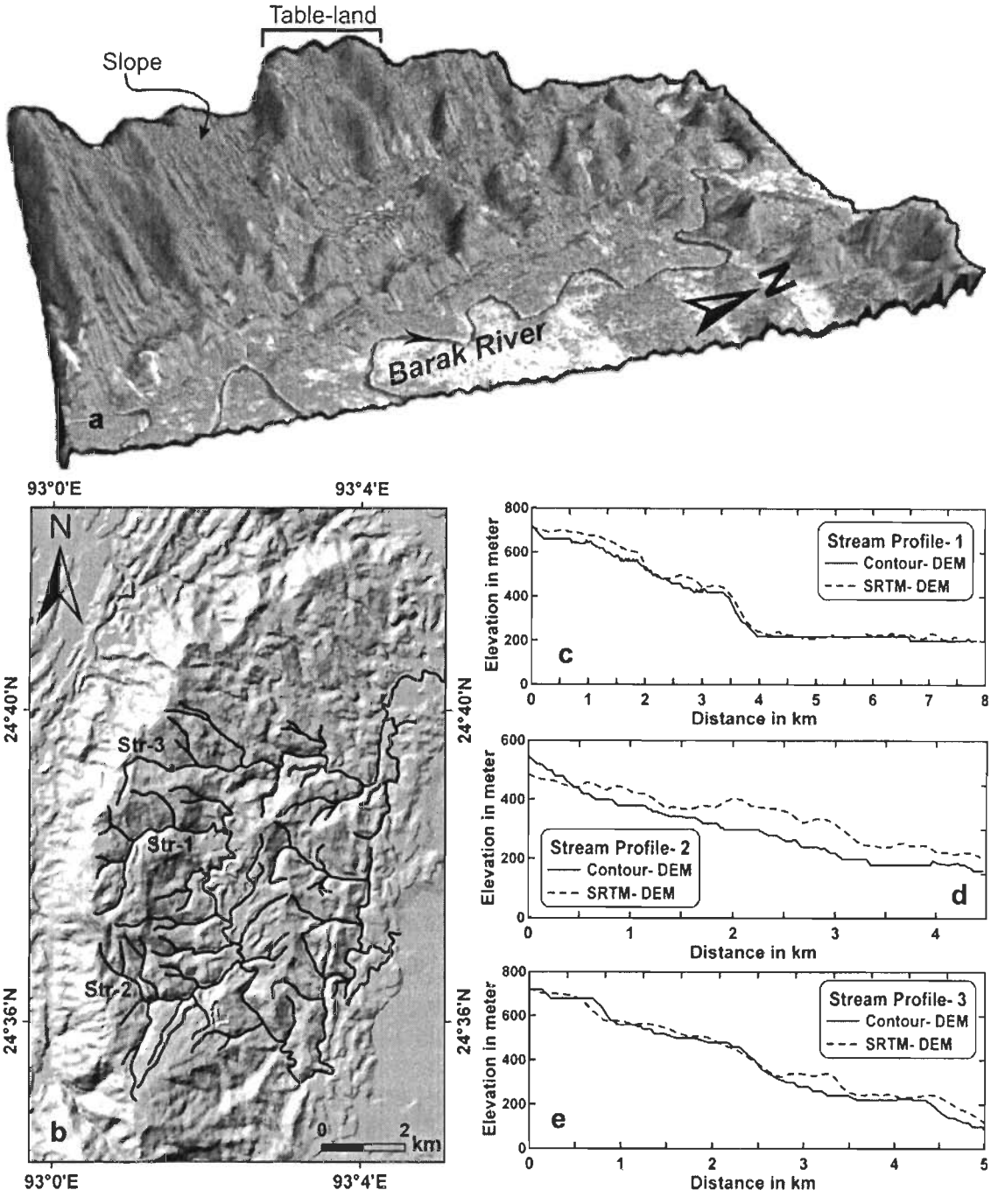

Fig. 5 Eastern view of northern Bhuban Hills showing high and low topography-a virtual GIS image (x5 exaggeration) generated using satellite image draped on digital elevation model (**a**). Main stream network in MU2-MU3 region of the eastern side of hills (**b**). Stream profiles of streams 1, 2 and 3 as shown in Fig. 5b (**c**, **d** and **e**)

graphical features and the elevation information is digitally derived from contour and SRTM-DEMs. Both the profiles in case of different transverse sections matches well as these follow close to each other (Fig. 8a–h). First transverse profile taken across the northernmost part of ridge shows two peaks having altitude more than 300 m (Fig. 8a). These ridges have been dissected due to faulting.

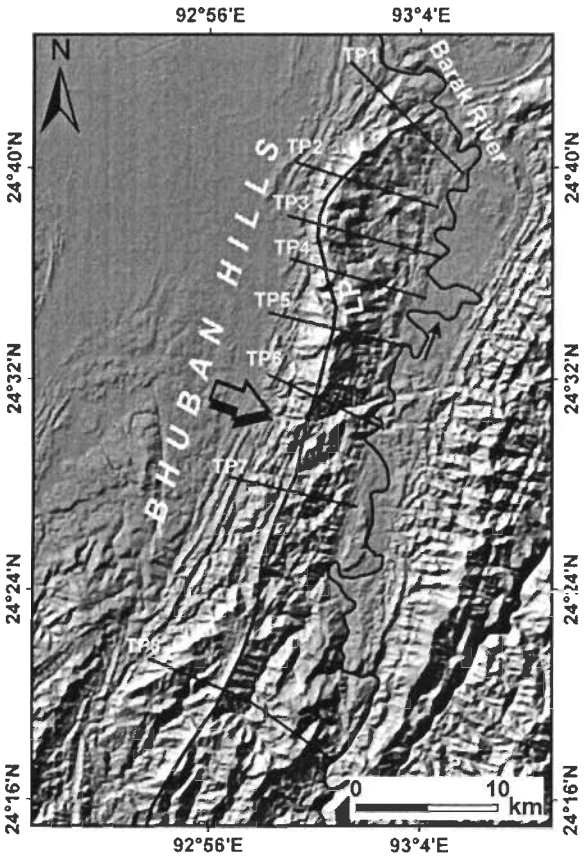

Fig. 6 Topographic profile lines of the Bhuban Hills showing a Longitudinal Profile LP and Transverse Profiles TP-1 to TP-8

The second transverse profile shows one peak of about 600 m with very steep western slope and gentle eastern slope which is due to the very steep topography of the Bhuban Hills in that part (Fig. 8b and c). This topography is the result of reverse longitudinal faulting as discussed earlier. Topography along the profile TP2 exhibit sharp peak with slightly inwardly curved western slope and moderate eastward slope whereas, the ridge is wider along the profile TP3 with steep eastern and western slopes. High topographical difference on the east side along the profile TP2 indicates differential upliftment or subsidence of that part. The third transverse profile (TP3) shows a wider ridge part having altitude more than 600 m with steep western side. Whereas, on the eastern side the topography initially show steep slope followed by a very gentle slope (Fig. 8c). Wider ridge part forms table type topography than the narrow ridge topography as the normal anticlinal ridge would have been. Both the transverse topographic profiles exhibit sudden drop in topography on the eastern side followed by gentle rugged slope. The fourth transverse profile (TP4) is showing peak of about 600 m altitude (Fig. 8d). This profile passes through northward slope formed on the ridge just south of transverse fault (TF2) which must have remained responsible for this type of slope.

Fifth transverse profile (TP5) passes across the highest region of Bhuban Hills forming wide rounded ridge top with steeper eastern and western slopes (Fig. 8e) and represented by a peak of about 1000 m. The transverse profile number six (TP6) is showing a sharp peak with elevation more than 600 m and a small peak on east side as the profile crosses a transverse fault and deep stream valley (Fig. 8f). Topographic profile (TP7) traverses through the subsided ridge part showing rugged topography with two peaks and the profile representing fold limbs by several peaks both on the eastern and western slopes (Fig. 8g). Whereas, the topographic profile (TP8) exhibit three distinct peaks (Fig. 8h) which have suffered bulging due to faulting.

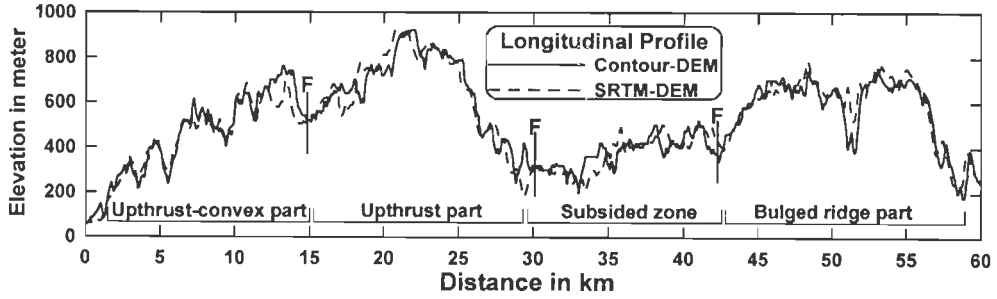

Fig. 7 Longitudinal profile of the Bhuban Hills showing different zones and fault (F) locations. Longitudinal profile location is shown in Fig. 6

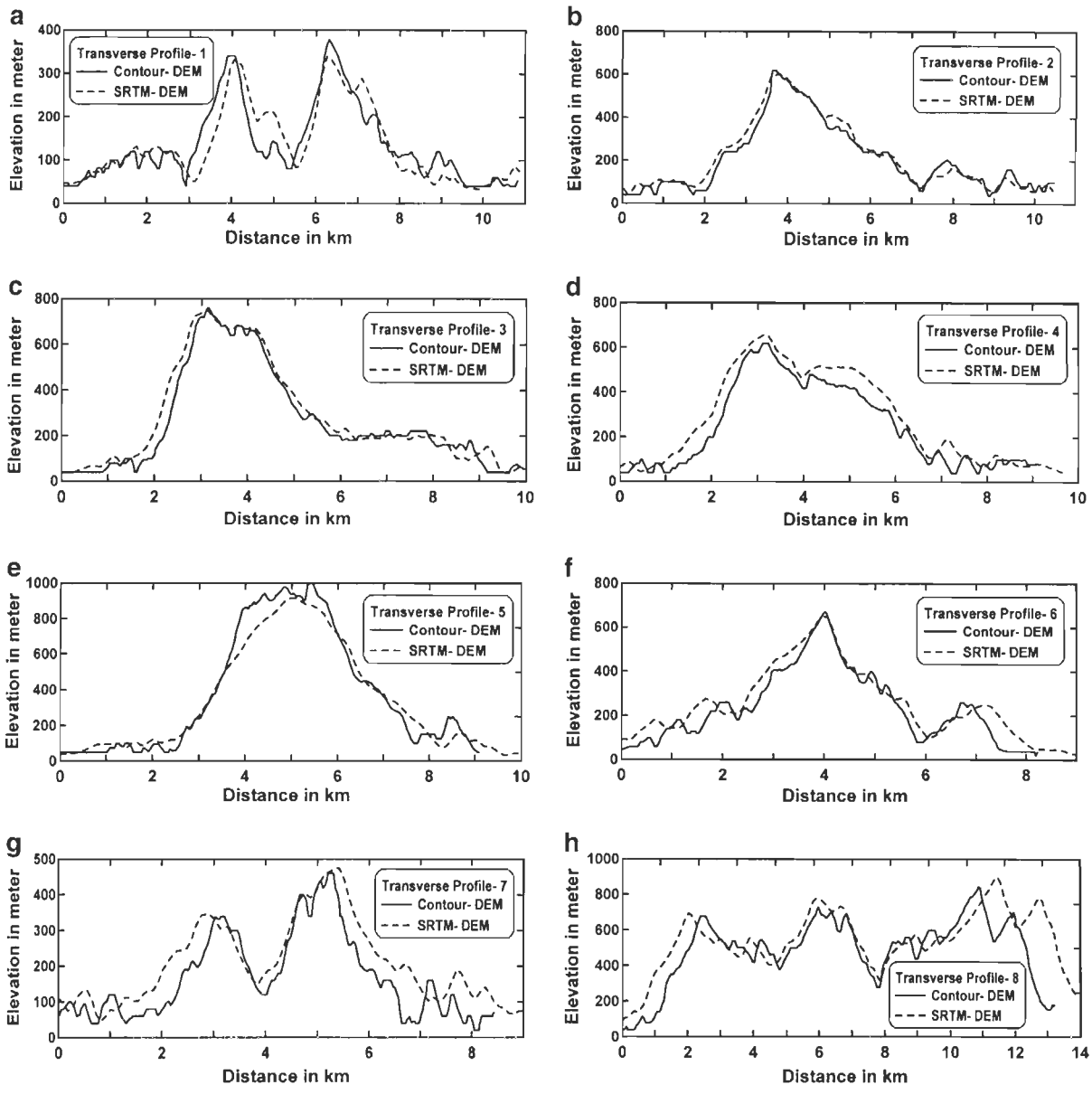

Fig. 8 **a–h** Transverse Profiles-1 to 8 from both contour and SRTM-DEM. Locations of profiles are shown in Fig. 6

Conclusions

Bhuban Hills falling in the frontal fold belt of Indo-Burman fold belt in Northeast India preserves predominantly the morphological characteristics resulted due to intense deformations. Six different morphotecontic units (MU1 to MU6) and several longitudinal and transverse faults could be identified and delineated from the small stretch of hills based on satellite images and digital elevation model.

Topography is especially different from latitude 24.5° to 24.7° for a distance of about 23 km. The western part has been affected by reverse longitudinal faulting causing upliftment of a linear zone forming higher relief and topographical difference of about 632 m and 815 m in the morphotectonic units 2 and 4 respectively. This has been resulted due to fault propagation folding. The topography of the northern most part (MU2 and MU3) of the Bhuban Hills is unique and suffered severe fault movements as

indicated by unplifted ridge part bounded by subsided eastern and western sides. In this part differential fault movement along northerly striking fault is so evident that a part of MU2 has been uplifted to greater height forming a steep slope on the eastern side against MU3.

The northern part of Bhuban Hills also exhibit westwardly curved topography due to the right lateral fault movement along the transverse fault (TF1) and longitudinal faulting along the westward side. Fifth morphotectonic unit (MU5) has experienced subsidence and bounded by transverse fault whereas the sixth unit bulged outward due to differential fault movement along the faulted ridges. Longitudinal and several transverse topographic profiles also corroborate the topographic anomalies attributed to the faulting effect.

Acknowledgements This paper is the outcome of the research work through a project (No. MoES/P.O.(Seismo)/23 (520)/SU/2005) funded by the Ministry of Earth Sciences, Govt. of India to whom authors are grateful.

References

Burbank, D. W., & Anderson, R. S. (2001). *Tectonic geomorphology* (p. 270). Oxford: Blackwell Scientific.

Chapple, W. A. (1978). Mechanics of thin-skinned fold-and-thrust belts. *Geological Society of America Bulletin, 89*, 1189–1198.

Das Gupta, A. B., & Biswas, A. K. (2000). *Geology of Assam* (p. 169). Bangalore: Geological Society of India Publication.

Davis, D., Suppe, J., & Dahlen, F. A. (1983). Mechanics of fold-andthrust belts and accretionary wedges. *Journal of Geophysical Research, 88*, 1153–1172.

Mitra, S. (1990). Fault-propagation folds: geometry, kinematic evolution and hydrocarbon traps. *American Association of Petroleum Geologists Bulletin, 74*, 921–945.

Nandy, D. R. (2001). *Geodynamics of northeastern India and the adjoining region*. Kolkata: ACB. 209p.

Sikder, A. M., & Alam, M. M. (2003). 2-D modelling of the anticlinical structures and structural development of the eastern fold belt of the Bengal basin, Bangladesh. *Sedimentary Geology, 155*, 209–226.